Photodiagnosis of Oral Malignancy using Laser-Induced Fluorescence and Diffuse Reflectance Spectroscopy

Doctoral Thesis

submitted to

Cochin University of Science and Technology

for the award of the degree of

Doctor of Philosophy

by

Rupananda Mallia J

Biophotonics Laboratory
Atmospheric Sciences Division
Centre for Earth Science Studies
Akkulam,Thiruvananthapuram-695 031
India

August 2008

DECLARATION

I hereby declare that the thesis entitled **"*Photodiagnosis of Oral Malignancy using Laser-Induced Fluorescence and Diffuse Reflectance Spectroscopy*"** is an authentic record of research work carried out by me under the supervision and guidance of **Dr. N. Subhash**, Scientist F, Biophotonics Laboratory & Head, Atmospheric Sciences Division, Centre for Earth Science Studies, Thiruvananthapuram, in the partial fulfillment of the requirement for the Ph. D degree under the Faculty Sciences, Cochin University of Science and Technology, and no part of it has previously formed the basis of the award of any degree, diploma, associateship, fellowship or any other similar title or recognition.

Rupananda Mallia J.

Thiruvananthapuram

August 2008

CESS

CENTRE FOR EARTH SCIENCE STUDIES

An Institution under the Kerala State Council for Science Technology & Environment

P.B. 7250, Akkulam, Trivandrum - 695 031, India

Tel:91-471-2511631; Fax: 91-471-2442280 *e-mail: subhashn@cessind.org*

August 28, 2008

Dr. N. Subhash
Scientist F, Biophotonics Laboratory &
Head, Atmospheric Sciences Division

CERTIFICATE

This is to certify that the thesis entitled **"*Photodiagnosis of Oral Malignancy using Laser-Induced Fluorescence and Diffuse Reflectance Spectroscopy*"** is an authentic record of the research work carried out by **Mr. Rupananda Mallia J** under my direct supervision and guidance for partial fulfillment of the requirements for the Ph. D degree of Cochin University of Science and Technology, under the Faculty of Science and no part thereof has been presented for the award for any degree in any university.

N. Subhash

"No man is an island"

Acknowledgements

It has truly been a privilege for me to work in the frame zone between laser, physics and medicine, in an area that has the potential to improve the quality of life of human beings. For the last half decade, I had really enjoyed the research work as a Ph. D student at Centre for Earth Science Studies (CESS), at its bliss. This work could not have been accomplished without the help of many people and I would like to use this opportunity to express my sincere thanks to all of them.

At the very outset, I am extremely obliged to my research guide, Dr. N. Subhash, Scientist F, Head ASD, CESS, Trivandrum for having great guidance both in all practical details and in planning and evaluation of the studies. He has made me to think out of box and put me on the research track and taught me lots of things about the fascinating field of lasers and physics by raising questions and valuable discussions. His impressive knowledge in subject made this work very comfortable and smooth throughout. I am truly grateful to him for having had this opportunity to receive the knowledge in science and warm friendship.

As part of this work it was possible to establish a Biophotonics Laboratory at this centre and this was indeed, made possible due to financial support from the Department of Science & Technology (DST), Govt of India. I express my sincere gratitude for their financial support. The Research Council (RC) of the CESS has been highly appreciative of this work and sanctioned additional funds and a project fellow through an internal project (PLAN-223), which made the research very smooth. I would like to thank all the members of the research council for their incessant and generous support and encouragement during the course of this work. I was really privileged to get selected as a Senior Research Fellow of the CSIR, New Delhi and am indeed thankful to the CSIR for the fellowship.

It has also been a thrill and fun to work in a hospital environment. The Ethics Committee of the Regional Cancer Centre (RCC) that gave approval for the clinical trials was very appreciative of the work and I am very thankful for their encouragement and valuable directions during the reviews.

Hearty encouragement from doctors of RCC requires a special attention. I am grateful to the medical doctors with whom I was associated with. I am wordless to express my gratefulness for the enthusiasm shown by Dr. Jayaprakash Madhvan, Medical Superintendent and Head of Lung and GI Tract Cancer, who has provided required facilities at RCC from the very beginning. The whole-hearted support of Dr. Paul Sebastian, Head of Surgical

Oncology Department during ex-vivo studies and clinical trials require special mention. Dr. R. Rejnish Kumar, Department of Radiation Oncology, was very kind and understanding and helped me during clinical trials, for which I am very grateful. I am also thankful to the many fruitful discussions I had with Dr. Anitha Mathews, Department of Histopathology at RCC. It has been a pleasure to work closely with these people who with their skills, enthusiasm and hard work have built up a very strong hospital for cancer treatment and research in Kerala.

I would like to express my sincere thanks to my colleague Mrs. Shiny for her unstinted cooperation during the clinical trials. I really appreciate and extend my sincere thanks to my numerous friends Mr. Prem G, Sreejith C, Shamji VR, Tiju VI, Praveen N, Aneesh V, Jiji K, Suraj, Mrs. Sreebha B, Sreeja A, who came forward as healthy volunteers and helped me to develop a healthy reference standard and all patients who gave their willingness and consent for the clinical studies, and also the various post-graduate students. The assistance of Ms. Rajeswary S, Asalatha AS, Raji U, Sanju SC, Shali SS, Smita V, Rintu MS and Durga S, Princy, Vibitha B, Anitha, who supported me during their M.Sc. project work in our laboratory, is gratefully acknowledged.

I would also like to thank the Ph. D programme review committee (CUSAT) and Dr. C. Sudha Kartha, member of the doctoral committee, for valuable suggestions and advices. Thanks are also due to Mr. Ismail, Krishnachandran and Yesudasan Paulose of the Atmospheric Sciences Division of CESS for their assistance in setting up the Biophotonics Laboratory and the technical support during the entire period. I am also expressing my thanks to the administrative staff of CESS for all the support extended. Finally, I would like to thank Dr. M. Baba, Director, CESS and Dr. B. Rajan, Director, RCC for their support and encouragement throughout the tenure of my Ph. D Programme .

Last, but not least, I express my gratitude to all my all family members, for their patience and understanding during the period of my work. As always, I believe that, with their indispensable support, everything is possible in life!

RUPANANDA MALLIA J

CESS, TRIVANDRUM

"To my beloved ones"

Table of Contents

Chapter 1

Background, Purpose and Definition of Problem

Chapter 2

Interaction of Light with Tissue: Some Basic Concepts and Background

Chapter 3

Instrumentation, Materials & Methods

Chapter 4

Discrimination of Malignant Oral Cavity Lesions using R540/ R575 Reflectance Spectral Ratio: An *Ex Vivo* Study

Chapter 5

Oxygenated Hemoglobin Diffuse Reflectance Ratio for *In Vivo* Detection of Oral Pre-cancer

Chapter 6

Clinical Studies for Early Detection of Oral Cancer using LIAF Spectral Ratio Reference Standards

Chapter 7

Grading of Oral Mucosa by Curve-fitting of Corrected Autofluorescence Spectra

Chapter 8

5-ALA Induced PpIX Fluorescence in Oral Cancer Detection *In Vivo*

Chapter 9

Diffuse Reflectance Spectral Features: An Adjunct to *In Vivo* Tongue Cancer Diagnosis by Autofluorescence

Chapter 10

"Knowledge is a journey, not a destination"

Abstract

Oral cancer represents a significant and growing concern worldwide due to its high prevalence. Current clinical procedure for detection of oral cancer involves visual inspection and ensuing biopsy guided histopathological analysis, which is considered as "gold standard". This intact procedure is subjective, time consuming, agonizing and costly. Consequently, exploration and development of new techniques for early oral cancer diagnosis assume great significance. Researchers have been trying to develop various instruments based on optical spectroscopic techniques for detection of different types of cancer during the last two decades. These optical spectroscopic techniques could facilitate non-invasive and real-time tissue characterization and help to eliminate or reduce the need for multiple biopsies and increase the cure and survival rates. However, development of an optimal cost-effective optical system with adequate sensitivity and specificity for clinical use is still a challenge.

Two non-thermal regimens of light interaction with biological tissues are mainly discussed in the present work, namely laser-induced autofluorescence (LIAF) and diffuse reflectance (DR) for detection of oral malignancy or pre-malignancy. The work described in this thesis is mainly of applied nature, focusing on the analysis of data from ex-vivo *tissue samples and extending these results to diagnose oral cancer in a clinical environment. The present work mainly aims to improve and contribute to the contemporary research on fluorescence and diffuse reflectance for tissue characterization. Towards this, a portable and compact laser-induced fluorescence and reflectance spectroscopic system (LIFRS) has been developed for point monitoring of fluorescence and diffuse reflectance spectra of oral tissues/lesions. The LIFRS system uses a 405 nm diode laser in the violet region for excitation of tissue fluorescence and a white light source (tungsten halogen lamp) for tissue DR studies.*

Both LIAF and DR studies were performed for oral cancer diagnosis, but special emphasis was given to discern between different tissue types and for early detection of the disease. The normal LIAF and DR fingerprint spectra form healthy population exhibit different characteristics with the tissue abnormality. In DR studies, a novel approach that uses oxygenated hemoglobin absorption band ratio (R545/R575) was introduced for tissue grading and early detection of cancer. This work also introduces a new criteria based on spectral ratio reference standard (SRRS) scatter plots of fluorescence intensity ratios (F500/F635, F500/F685 and F500/F705) for oral pre-cancer detection and tissue grading with excellent diagnostic accuracies, validated with the blind-tests. In addition, optimum accumu-

lation time of protoporphyrin IX (PpIX) in different healthy anatomical sites of oral cavity was also studied after exogenous application of 5-ALA, which is a precursor of PpIX. Results were then extended to the clinical level to detect tissue abnormalities in a group of patients.

Furthermore, corrected tissue fluorescence (CTF) was derived by filtering out blood absorption artifacts from LIAF spectra using DR spectra from the same location. A curve-fit analysis was carried out on these CTF's using Gaussian spectral functions (GSF). The derived GSF parameters were proven useful for diagnosing tissue abnormalities and grading of oral squamous cell carcinoma (SCC).

List of publications

The following scientific publications were brought out based on the work presented in this thesis

A. International Journals:

Rupananda Mallia, J., Subhash. N., Shiny, S.T., Anitha, M., Paul, S., and Jayaprakash. M., 2008. Diffuse reflectance spectral features: an adjunct to tongue cancer diagnosis by autofluorescence. *Applied Spectroscopy* (Manuscript prepared).

Rupananda Mallia, J., Subhash. N., Shiny, S.T., Anitha, M., Paul, S., and Jayaprakash. M., 2008. *In vivo* 5-ALA induced PpIX fluorescence kinetics of different anatomical sites of oral cavity: An application in oral cancer detection. *Laser Surg Med* (Manuscript prepared).

Rupananda Mallia, J., Shiny, S.T., Anitha, M., Paul, S., Jayaprakash. M., and Subhash. N., 2008. Grading of oral cavity squamous cell carcinoma using curve fitting of corrected autofluorescence. *Head Neck* (submitted).

Rupananda Mallia, J., Shiny, S.T., Anitha, M., Paul, S., Jayaprakash, M., and Subhash, N., 2008. Oxygenated hemoglobin diffuse reflectance ratio for *in vivo* detection of oral pre-cancer. *J Biomedi Opt,* v.13(4), pp.(041306)1-10.

Rupananda Mallia, J., Shiny, S.T., Anitha, M., Paul, S., Jayaprakash, M., and Subhash, N., 2008. Laser-induced autofluorescence spectral ratio reference standard for early discrimination of oral cancer. *Cancer, v.*112(7), pp.1503-1512.

Rupananda Mallia, J., Subhash, N., Shiny, S.T., Rejnish, K.R., Anitha, M., Jayaprakash, M., and Paul, S., 2007. Oral Pre-malignancy detection using autofluorescence spectral ratios. *Oral Oncology (S),* v.2(1), pp.259–260.

Subhash, N., Rupananda Mallia, J., Shiny, S.T., Anitha, M., Paul, S., and Jayaprakash, M., 2006. Oral cancer detection using diffuse reflectance spectral ratio R540/R575 of oxygenated hemoglobin bands. *J Biomed Optics*, v.11(1), pp.(014018)1–6.

B. Patents:

Subhash, N., Rupananda Mallia, J., Shiny, S.T., Jayaprakash, M., Anitha, M., Paul, S. A low cost device for detecting neoplastic changes in tissue, File No. 265/CHE/2006, Pub. Date 14-12-2007.

Subhash, N., Shiny, S.T., Rupananda Mallia, J., and Mini, J. Tooth caries detection by curve-

fitting of UV laser induced fluorescence emission, File No.1910/CHE/2005, Pub. Date 27-07-2007.

C. Conference Proceedings:

Rupananda Mallia, J., Shiny, S. T., Rejnish, K. R., Anitha, M., Paul, S., Jayaprakash, M., Gigi, T., and Subhash, N., 2007. Photodiagnosis of oral pre-malignancy *in vivo* using HbO_2 spectral ratios. *National Laser Symposium 2007,* Ahemadabad, Gujarat (Presented).

Rupananda Mallia, J., Shiny S. T., Rejnish, K. R., Anitha, M., Paul, S., Jayaprakash M., and Subhash, N., 2006. Diagnosis of oral cavity neoplasms with fluorescence spectroscopy. *Proceedings of Kerala Science Congress 2006*, CESS, Trivandrum, pp.458-461.

Subhash, N., Rupananda Mallia, J., Shiny, S. T., Mathew, A., Paul, S., and Jayaprakash, M., 2004. Discrimination of malignant oral cavity lesions using R540/R575 reflectance spectral ratio. *Proceedings of the International Photonics Conference 2004,* Kochi, pp.26(1-6).

D. Publications in related fields:

Shiny, S. T., Rupananda Mallia, J., Anitha, M., Paul, S., Jayaprakash, M., and Subhash, N., 2007. Autofluorescence and diffuse reflectance spectroscopy in detection of tooth enamel demineralization and remineralization. *J Biomed Opt* (Submitted).

Shiny, S. T., Rupananda Mallia, J., Mini, J., and Subhash, N., 2008. Investigation of in vitro dental erosion by optical techniques. *Lasers Med Sci*, v.23, pp.319-329,

Subhash, N., Shiny, S. T., Rupananda Mallia, and J., Mini, J., 2005. Tooth caries detection by curve fitting of laser-induced fluorescence emission: A comparative evaluation with reflectance spectroscopy. *Lasers Surg Med,* v.37, pp.320–328.

Subhash, N., Mohanan, C. N., Rupananda Mallia, J. and Muralidharan, V., 2004. Quantification of stress adaptation by laser-induced fluorescence spectroscopy of plants exposed to engine exhaust emission and drought. *Functional Plant Biology*, v.31, pp.709–719.

Subhash, N. and Rupananda Mallia, J., 2003. Changes in laser-induced chlorophyll fluorescence signatures during regeneration of kacholam and colocasia plants from water stress, Proc. IGARSS 2003, Tolouse, France, *IEEE,* pp.3293-3295.

Preface

Chapter I peeks into the history on the application of light in medical diagnostics. Also, it gives a brief introduction to different types of animal tissues, especially the epithelial tissues, where 90% of the cancer originates. The primary step in oral cancer detection and diagnosis is to record patient history and conduct a visual examination. If a suspicious lesion is identified, it is biopsied and a histopathological examination of the sample is carried out. Different types of existing adjunctive methods for screening tissue transformations and their diagnostic accuracy, as compared to gold standard, are briefly narrated in this section. Various statistical methods related to data analysis, interpretation and accuaracy testing are also describedFinally, the significance of early detection in cancer diagnosis and treatment, and the need for developing an alternate/adjunct modality is described.

An understanding of the interaction of radiation with oral mucosa and of the different types of absorption and emission processes involved is essential for the development of an optimized diagnostic system. **Chapter II** outlines the basic theory of light absorption, scattering, diffuse reflectance and fluorescence emission of tissues. Various enzymatic de-carboxylation and oxidation process of the biosynthetic Heme pathway initiated with condensation of 5-Aminolevulinic acid (5-ALA) and Succinyl co-enzyme A are presented. The selective accumulation of protoporphyrin IX (PpIX), which is a precursor of the Heme, with tissue abnormality is discussed. Further, different types of exogenous/endogenous flurophores and their absorption and emission characteristics are presented, along with details of recent studies carried out elsewhere in similar tissue types.

Recent advances in fiber optics, light sources, detectors and computer-controlled instrumentation have stimulated unprecedented growth in the development of photonic technologies for a wide variety of diagnostic applications. The use of noninvasive optical techniques for early detection of pre-cancer is a rapidly emerging area in the field of biophotonics. Among the various non-invasive optical techniques, those relying on tissue fluorescence and diffuse reflectance are most promising in the diagnosis of epithelial pre-cancers. **Chapter III** details configuration of a compact, fast and versatile laser-induced fluorescence and reflectance spectroscopy system (LIFRS) for near real-time cancer diagnosis. Alongside, data acquisition, processing and analytical techniques using LIFRS are presented. The section also describes the ethical issues, clinical study protocol and patient inclusion/ exclusion criteria. Different techniques used in data processing and analysis are also elaborated in this section.

Chapter IV explains the development of a simple, low-cost and non-invasive modality with potential for detection and distinguishing different grades of oral cancer using DR spectroscopy. The *ex vivo* diffuse reflectance spectra in the 400-600 nm region is measured from surgically excised oral tissues with the LIFRS system. Reflectance spectral intensity

was found higher in malignant tissues and show dips at 542 and 577 nm owing to absorption from oxygenated hemoglobin (HbO_2) present in the tissues. Measurements carried out on surgically excised malignant and adjoining normal mucosa showed that these absorption features are more prominent in neoplastic tissues owing to increased microvasculature and blood content. It is observed that the reflectance intensity ratio of hemoglobin bands, R545/R575, from malignant sites are lower than that of normal sites and varied according to the grade of malignancy. The diffuse reflectance intensity ratio R545/R575 of the hemoglobin bands appears to be a useful tool to discriminate between malignant and normal lesions of the oral mucosa in a clinical setting.

In **Chapter V**, the applicability of R545/R575 ratio for differentiating various tissue types in a clinical setting. Towards this, clinical studies were conducted in 29 patients to detect oral pre-cancer is presented. Site-specific normal spectra were derived from a group of 36 healthy volunteers for comparison with those of patients. *In-vivo* diffuse reflectance spectra from 14 anatomical sites of the oral cavity of healthy volunteers were recorded on a miniature fiber-optic spectrometer with white light excitation. In contrast to the *ex vivo* results, the R545/R575 ratio was lowest for healthy tissues and appeared to increase with the grade of malignancy. Scatter plot of the R545/R575 ratio was used for discerning diverse tissue types. As compared to scatter plots that use the mean diffuse reflectance ratio from all anatomical sites, those using site-specific data showed improved sensitivity and specificity for early diagnosis and grading of oral cancer. In the case of buccal mucosa, very good sensitivity and specificity were obtained to distinguish different grades of oral cancer using the R545/R575 ratio scatter plot.

Chapter VI presents a spectral reference standard developed to discriminate malignant squamous cell carcinoma (SCC) from pre-malignant dysplasia and hyperplasia using the spectral data of healthy population as control. Towards this, LIAF emission spectra were recorded in the 420-720 nm spectral range from the oral cavity of 35 healthy volunteers and 44 patients. Histopathological analysis of the biopsy samples showed that oral mucosa adjacent to malignant sites in patients are not usually normal, but showed varying degrees of epithelial dysplasia and hyperplasia. Three spectral ratio reference standard (SRRS) scatter plots of the fluorescence spectral intensity ratios F500/F635, F500/F705 and F500/F685 were created to differentiate normal mucosa from hyperplasia, hyperplasia from dysplasia, and dysplasia from SCC using data obtained from 40 sites in 20 patients and 11 sites in 35 healthy volunteers. The classification sensitivity and specificity of the SRRS was blind-tested to diagnose oral malignancy on a different subject group.

Autofluorescence emission from normal tissues of the oral cavity consists of a broad band centered at 500 nm with a shoulder peak around 550 nm, whereas in malignant samples additional peaks were seen around 435, 630 and 680 nm. The exact peak position of the constituent bands and their relative contribution in the overall corrected LIAF spectrum was determined by curve-fitting using Gaussian spectral functions and the resultsare presented in **Chapter VII**. Corrected spectra were derived by filtering out the HbO_2 absorption

anomalies in the LIAF spectra, by division with the corresponding DR spectra. Fluorescence intensity ratios, F500/F635 and F500/F685, derived from the raw spectral intensities, curve-fitted peak intensities and Gaussian curve areas were higher for normal tissues as compared to malignant tissues and tend to decrease for increasing grades of malignancy. Differences were also noticed in the curve-fitted parameters such as the peak center, Gaussian curve area and bandwidth (FWHM) with tissue transformation. It was seen that the curve-fitted amplitude and area ratios, F500/F630 and F500/F680, were more sensitive to tissue transformation as compared to the raw LIAF ratio. Finally, the curve-fitted spectral characteristics were used to discriminate pre-malignant dysplastic lesions from SCC, dysplastic lesions from hyperplastic and hyperplastic from normal mucosa using the SRRS criteria and the results are compared with those derived from the raw spectral data.

The uptake of 5-ALA by oral tissues was studied by monitoring the LIAF spectral changes over different periods of time and the results are presented in **Chapter VIII**. 5-ALA was applied topically on the different anatomical sites of the oral cavity of healthy volunteers and the spectral intensities of ALA induced porphyrin peaks were studied and optimal time for accumulation for PpIX were determined for each of these sites. The results were then used for detection of malignancy in a patient population. In order to check the efficacy of the technique, porphyrin fluorescence intensities at 635, 685 and 705 nm were determined from the LIF spectra normalized at 500 nm. The LIF intensity (F635, F685, F705) of patients were determined in a clinical environment and compared with the corresponding spectral data without 5-ALA.

Chapter IX presents a comparative study on the performance of LIAF and DR in tongue cancer detection. Even though, both the methodologies have comparable sensitivities and specificities, cost-effectiveness gives diffuse reflectance modality an edge over LIAF technique. Also, from the available results, it is seen that the DR methodology has the potential to diagnose tongue pre-cancer while techniques based on tissue autofluorescence and 5-ALA induced PpIX fluorescence have low specificity owing to the presence of porphyrin peaks in healthy tissues.

Chapter X is the executive conclusion section, which discusses the virtues of the developed techniques and this doctoral work, its future perspectives in cancer detection, limitations of the techniques used and some suggestions on prospective studies. The section also critiques the diagnostic accuracies of LIAF and DR modalities by comparing with the results of different international research groups, to verify their status in the contemporary optical techniques for early detection of malignancy.

Abbreviations and Acronyms

ALA	*δ- or 5-Aminolevulinic acid*
AUC	*Area Under Curve*
CCD	*Charge Coupled Device*
DRS	*Diffuse Reflectance Spectroscopy*
DST	*Dorsal Side of Tongue*
CTF	*Corrected Tissue Fluorescence*
ESS	*Elastic Scattering Spectroscopy*
FAD	*Flavin Adenine Dinucleotide*
GSP/F	*Gaussian Spectral Parameters/Functions*
Hb	*Deoxygenated Hemoglobin*
HbO_2	*Oxygenated Hemoglobin*
HpD	*Haematoporphyrin Derivative*
IC	*Internal Conversion*
IR	*Infrared*
ISC	*Inter System Crossing*
LIAFS	*Laser-Induced Auto Fluorescence Spectroscopy*
LIFRS	*Laser-Induced Fluorescence and Reflectance System*
LST	*Lateral Side of Tongue*
MDSCC	*Moderateley Differentiated SCC*
MPDSCC	*Moderate to Poorly Differentiated SCC*

MWDSCC	*Moderate to Well Differentiated SCC*
NADH	*The reduced form of NAD+*
NPV	*Negative Predictive Value*
PDD	*Photo Dynamic Detection*
PDSCC	*Poorly Differentiated SCC*
PDT	*Photo Dynamic Therapy*
PpIX	*Protoporphyrin IX*
PPV	*Positive Predictive Value*
ROC	*Receiver Operator Characteristics*
RSS	*Raman Scattering Spectroscopy*
SCC	*Squamous Cell Carcinoma*
SRRS	*Spectral Ratio Reference Standards*
UV	*Ultraviolet*
VBL	*Vermillion Border of Lip*
VIS	*Visible*
WDSCC	*Well Differntiated SCC*

Chapter 1

Background, Purpose and Definition of Problem

Background, Purpose and Definition of Problem 1

1. 1 Introduction

1.1.1 Light in Medicine - A Brief Background

Light is everywhere in the world and color is such an everyday phenomenon that we usually don't give any serious consideration to its effects. But colors can produce surprising effects and it carries information from our surroundings to our eyes and brains. Yet, light and its interaction with matter is intresting as well as perplexing when we perceive it more closely and deeply. Light is essential for all forms of life within the biosphere and it is the ambient sunlight which supports photosynthesis in plants and many photochemical and photobiological reactions in the human body.

Sun light had been used in ancient cultures like Egypt, Greece, China and India in the treatment of various diseases (Spikes, 1985; Epstein, 1990). The use of light with some dyes is described in the sacred Atharvaveda (1400 BC) to improve the efficacy of the phototherapy for the repigmentation of the skin (Fitzpatrick and Pathak, 1959). Heliotherapy, a therapy wherein the full body is exposed to the sun was first used by Greeks about 3000 years ago. By 19th century, phototherapy was developed as a branch of sceience with marked contributions from Neils Finsen, who is kown as the father of the modern phototherpy. He received the Nobel prize for his work, in treating cutaneous tuberculosis with near ultra violet (UV) and UV light exposure (Finsen, 1901).

The lasers, since its invention in the early sixtees, were shown to have properties useful for medical applications (Katzir, 1993; Boulnois, 1986). It yields monochromatic, non-ionizing light, which can target and be absorbed by specific bio-molecules, leaving other molecules more or less unaffected. This results in selective, specific and comparatively harmless interactions between the light and medium, which is of importance from a clinical view point. Laser light being monochromatic and coherent can easily be focused into spots of different sizes, thus providing variable probing areas and power densities. This in combination with its minimally invasive character and flexibility, provided by the use of optical fibers, resulted in lasers soon being recognized as a potential option both for therapy and diagnostics of cardiovascular diseases and tumors.

The treatment modalities using light exposure have two branches, viz. phototherapy, photochemotherapy or phtodynamic therapy (PCT or PDT). Phototherapy solely depends on the light of different wavelengths and intensities. Photochemotherapy is a chemically enhanced phototherapy, ie. it involves a exogenous agent, which sensitize tissue, followed by irradiation with light of proper wavelength. Advancements in laser technology and optics resulted in new lasers with differenrt wavelengths that to more medical diagnostic

applications like cancer detection. This thesis is mainly focused on the diagnostic application of light also known as photo dynamic diagnosis (PDD), for cancer detection rather than its theraputic use. The motoivation for this thesis work are:

a) To reduce moratalities due to cancer, by innovationg new criterias based on optical techniques which have enormous potential in the biomedical field.

b) To reduce the need for removal of tissues for histological analysis by using the spectral features of the tissue in question, thereby reducing patient morbidity and psychological discomfort to claustrophobic patients, by accurate and early detection of the disease.

c) To identify most malignant lesion site for the biopsy using different optical spectroscopic techniques, which could greatly improve the survival and curing rates.

1.1.2 Cancer - A Growing Health Concern

Cancer is a disease that affects millions of people across the globe and the number of cancer patients are on the rise. The term "malignancy or cancer" can be defined as a disease associated with the uncontrolled proliferation of cells, which are capable of invading surrounding normal cells and spreading cancerous foci at different and distant sites of the body and consequently disrupting the organs function. In India, oral and cervical cancers are two of the prominent forms of cancer affecting the squamous epithelial tissues.India accounts for a third of the world burden of oral cancer. It is estimated that in 2002 there were 274,000 new cases of oral cancer and fatality due to this disease is on the increase globally, out of which the Indian contribution is 85,000 and 46,000 respectively (Forlay et al., 2007; Parking et al., 2002).

The causes of the oral cancer are numerous. Most of the patients with oral cancer have a history of heavy smoking, most often combined with the frequent use of alcoholic drinks, especially strong liquors. Another major causative factor affecting the Indian population is the excessive and permanent use of Pan Masala, Gutka and chewing of beetle leaves with pan, tobacco and calcium chloride (Shetty et al., 1999). About 85% of these people with history of these habits suffer from oral cancer, which arise from the squamous epithelium layer, known as squamous cell carcinomas (SCC) of the tissue. The oral mucosa that gets exposed to tobacco and alcohol abuse is therefore at risk of developing pre-malignant lesions and invasive tumours (Wingo et al., 1995).

SCC involves cell growth changes on the superficial tissues of the oral region, the epithelium. Nearly 85% of all oral cancers are categorised as SCC (Boring et al., 1994). A chronic (long-term) mouth ulcer that does not heal, a lesion attached to deeper tissues, oral mucosal lesions etc., are all suspectable pre-SCCs. During the process of cancer formation, multiple areas of the oral mucosa undergo carcinogenic changes. It is seen that 28% of the

patients diagnosed with SCC of the oral mucosa develops a primary tumour within the next ten years.

The outcomes of most cancer patients are poor in terms of survival. The reason is that the tumors are often diagnosed and treated too late, only after the symptoms appear, which means in the latter stages. At this stage, many tumors have already grown large or metastasized into other parts of the body and their treatment/management could be very limited in their effectiveness. Treatment of small tumours without regional metastases gives higher survival rates, better functional and a esthetic results and a lower morbidity than in the case of advanced tumours. Early treatment strongly improves the survival rates and results in a lower morbidity because treatment at a less invasive stage is more successful and therefore, is of great clinical importance (Hyde and Hopper, 1999; Silverman, 1988). Early detection is related to the disease mortality: 5-yr survival rate is 81% for early stages of oral cancer while it is 30% for late-stage disease (Carvalho et al., 2005). Further, the 5-yr survival rate has remained dismal with little improvement over the last 30 yr (<50%), mainly due to the fact that a significant proportion of these cancers have already metastasized to regional or distant structures at the time of diagnosis (Ries et al., 1997; Johnson et al., 1995; Blair and Callendar, 1994).

Oral pre-malignant lesions with increasing degrees of dyspasia/atypia (mild, moderate and severe) that appear clinically as leukoplakia (white patches) and erythroplakia (velvety red patches) are believed to be the pre-cursors of oral cavity SCC. Oral erythroplakias and leukoplakias have chances of *ca.* 90% and 10%, respectively, for conversion into malignancy (Shafer and Waldron 1975; Suarez et al., 1998).

As with all cancers, the prospects of curability are better when the malignancy is detected in an early stage and oral cancer has vast potential for prevention as pre-malignant leisons can be detected early and it responds well to surgery and radiation therapy. However, about 70% of these tumors are diagnoised in advance stages due to the lack of awareness among the public on need for early diagnosis and availability of easy screening techniques. Therefore, early detection of cancer is the key to fight against this dreadful and fatal disease and regular screening of apparently healthy people is very rewarding because it permits diagnosis before development of symptoms.

1.1.3 Need for an Adjunctive Non-invasive Detection Technique

The detection of neoplastic changes in the oral cavity is usually made by visual examination and recognition by experienced clinicians. However, even for the experienced clinicians, it is not easy to distinguish between normal and pre-malignant oral mucosa. Hence, some of these lesions often go unnoticed and tend to get diagnosed in an advanced stage. Once the patient or a dentist notices a lesion, they are not sure whether the lesion is benign or pre-malignant. Only a biopsy can provide the final diagnosis. Visual inspection doesn't permit one to identify the microscopic epithelial alterations and it is a difficult task

even for the experienced eye to determine the most malignant location for a biopsy. Often, oral mucosa with inflammation or irritation could resemble pre-malignant conditions and this makes visual identification more challenging. Pre-malignancies are characterized by increased nuclear/cytoplasmic ratio, which is assessed by histopathology, following a painful biopsy. The imperative drawback of this procedure is that the biopsy results are not always representative for the complete lesion. An oral lesion can contain local pre-malignant changes at one position, while it can still be benign/malignant at a position only a few millimeters away.

In other words,. biopsy from one location of the lesion is not representative of the entire lesion. This often results in under diagnosis or usually leads to the numerous random biopsies if the oral oncologist is not convinced that a lesion is benign. These multiple biopsies can result in severe discomfort for the patient. Further, multiple stage sample preparation and analysis is time consuming and increase pathological costs. Stress therefore should be given on prevention of the disease by early detection and fast detection. This, in turn, necessitates development of adjunctive diagnostic tools to facilitate non-invasive and real-time screening of oral pre-malignant lesions.

1.1.4 Objectives of the Study

Various optical spectroscopy techniques have been getting greater acceptance in recent years owing to their non-invasive nature of tissue characterization. Numerous, published data show the potential of optical spectroscopy to differentiate between normal mucosa and abnormal lesions of the oral cavity. Diagnostic techniques based on optical spectroscopy have the potential to understand the biochemical and morphogical properties of tissues. In particular, these techniques are fast, non-invasive and quantative. In cancer diagnostics development, the potential of spectroscopic technique is not yet fully explored for *in vivo* detection of malignant superficial tumors and/or characterization (grading) of tissues. The hypothesis of present work is that these optical techniques will help to discern between different tissue types, viz. benign from pre-malignant lesions, pre-malignant from SCC of the oral cavity with good sensitivity and specificity.

This thesis work mainly aims at enhancing the sensitivity and specificity of the fluorescence and diffuse reflectance spectroscopy techniques for tissue characterization, especailly for the early differentiation of malignant and pre-malignant lesions of the oral cavity. As part of this work, the applicability of autofluorescence and 5-Aminolevulinic acid (5-ALA) enhanced PpIX fluorescence were studied along with the changes in the diffuse reflectance spectral features, with special emphasis on early detection and tissue grading. In the present study, tissue autofluorescence from the tissues of healthy population is used as normal and compared with the abnormal lesions of patients, since patient contra lateral tissues and lesion adjacent tissues are not always normal. The major objectives of the study are:

1) In-house development of a point monitoring system for sequential measurement of fluorescence and diffuse reflectance spectra from the same location.

2) Testing and calibration of the developed system in an *ex-vivo* environment i.e. analysis of autofluorescence and diffuse reflectance spectral signals of surgically excised tissues for identifying signatures representing cancerous and non-cancerous tissues.

3) Modification of the optical instrument for clinical studies based on the results of e*x vivo* findings and to conduct clinical trials at the Regional Cancer Centre (RCC) in patient/ healthy population and correlation with histopathological results.

4) Study the influence of anatomical location and individual characteristics on the autofluorescence and diffuse reflectance spectra of oral mucosa.

5) Study the uptake of 5-ALA at different anatomical sites of oral cavity and evaluate its effectiveness in enhancing the detection sensitivities via-a-vis autofluorescence in patients.

6) Validation of optical system and reference database.

1.2 Histology & Histopathology

1.2.1 Introduction

Histology is the microscopic study of cells, tissues, and organs. Also known as 'microscope anatomy', it has two basic classes: 1) *normal histology* - the study of normal tissues, and 2) *pathologic histology* - the study of diseased tissue. Pathologies is literally the study (logos) of suffering (pathos). More specifically it is devoted to the study of the structural (morphologic) and functional changes in cells, tissues and organs that underlie disease. Traditionally, the study of pathology is divided into those dealing with the basic reaction of the cells and tissues to abnormal stimuli that underlie all diseases. The latter examines the specific responses of specialized organs and tissues to more or less well-defined stimuli. By the use of molecular, microbiologic, immunologic, and morphologic techniques, pathology attempts to explain the whys and wherefores of the signs and symptoms manifested by patients.

Pathologically,malignancies are diagnosed according to the pattern of cellular growth and deviations of individual cells from their normal form (morphologic changes) and they are named according to the cells and tissues from which they arise. Morphologic changes refer to structural alterations in cells or tisues that are either characteristic of the disease or diagnostic of the etiologic process. The practice of diagnostic pathology is dedicated to identifying the nature of progression of disease by studying morphologic changes in tissue. Pathologists involved with the detection and treatment of malignancies must possess knowledge of these things in order to understand the anatomy and classification of tissues

and tumors. In this section, a review of the basic types of epithelial tissue, their locations, and the terms used to describe these normal and abnormal tissues, is attempted.

1.2.2 Basic Tissue Types

There are four basic types of tissues: 1) epithelial tissues, 2) connective tissues (blood, bone, cartilage), 3) muscle tissues, and 4) nerve tissues. Each tissue type is designed to perform a specific function. For instance, connective tissues serves to bind together other tissue forms to a supporting framework, of many organs. Whereas, muscular tissues are designed to cause the movements of the skelton and other internal organs by contractions. The nerve tissues conduct nerve impulses, muscle tissues are contractile, and epithelial tissues cover body parts. Tissues differ in several ways: 1) according to the size, shape, and arrangement of their cells; 2) according to the kind of intercellular substance; and 3) according to location and function. In this thesis, we are dealing with epithelial tissues, which are the starting points of the process of carcinogenesis in oral cavity. We are interested in the types of normal oral epithelial tissues for the main reason that 90% of oral cancers orginate from the squamous epithelial layer, namely SCC.

1.2.2.1 Epithelial Tissues

Epithelial tissue covers or lines all body surfaces inside and outside the body (Fig. 1.1). Examples of epithelial tissue are the skin and the mucosa and serosa that line the body cavities and internal organs, such as intestines, urinary bladder, uterus, etc. In some cases, epithelial tissue extends into deeper tissue layers to form glands, such as mucus-secreting glands. Epithelial cells are tightly packed together in thin sheets and have very little intercellular material between them. The thickness of the epithelium layer is approximately 200 μm. Securing the epithelium to the underlying connective tissue is a membrane called the *basement membrane*. Epithelial tissues receive nourishment from nutrients that diffuse from blood vessels in the underlying connective tissue. Dead and injured epithelial cells are constantly being replaced by new cells.

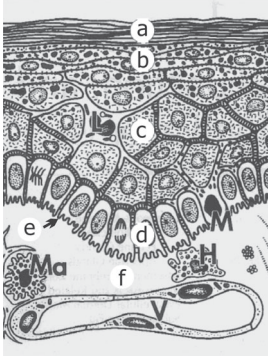

Fig. 1.1 Cartoon of human epithelium with its component **(a)** keratin layer (stratum corneum) **(b)**, **(c)** and **(d)** epithelial cells **(e)** basement membrane **(f)** mesenchyme (Adopted from Wang et al.,1999).

Epithelial tissues always have a free surface exposed to the outside (e.g. skin) or to an open space internally (e.g. the uterus, oral cavity tissues). Epithelial tissue is concerned with protection, secretion, absorption, and filtration. For example, the surface layer of the skin, the *epidermis,* has tightly packed epithelial cells and protects the body from the elements; epithelial cells in glands secrete various liquids; epithelial cells in the small intestine absorb nutrients into

the bloodstream, and so on. The term *carcinoma* is reserved for malignant growth arising from epithelial cells.

1.2.2.2 Different Types of Epithelial Tissues

Epithelial tissues may be of single layers or several cell layers thick, as shown in (Fig. 1.2). Epithelial tissue is classified into subtypes, according to the shape, arrangement, and function of cells. For instance, an epithelial membrane composed of single layers of cell is called *simple*; those several cell layers thick are called stratified. Thin, flat epithelial cells are called *squamous* (e.g. plate like); cube-like cells are called *cuboidal*; and tall, column-like cells are called *columnar.*

Simple squamous epithelium is composed of a single layer of thin, flattened cells closely fitted together. It is found on the surface of the skin (*epidermis*). Some substances easily pass through simple squamous epithelia.

Simple cuboidal epithelium is composed of a single layer of lightly packed cube-shaped cells. It covers the ovaries, lines a portion of the kidney tubules, and lines the ducts of such glands and organs as the thyroid gland, salivary glands, liver and pancreas.

Simple columnar epithelium is composed of tall, slender cells. These elongated cells are found lining the intestine, the gallbladder, the fallopian tubes, and some of the respiratory passages. Scattered among the columnar cells are cells called goblet cells, which secrete mucus onto the surface of the tissue.

Pseudo stratified columnar epithelium is so named because it seems to be arranged in several layers, when in reality it is but a single layer thick. As shown in Fig. 1.2, all cells adhere to a basement membrane, but not all of them reach the surface, thus accounting for

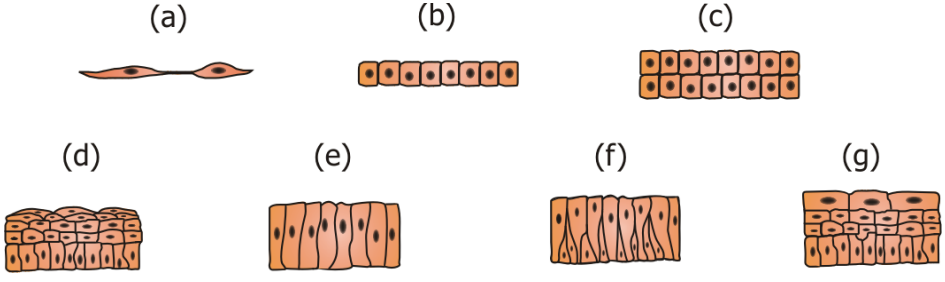

Fig. 1.2 Different epithelial tissue types of human body **(a)** simple squamous **(b)** simple cuboidal **(c)** stratified cuboidal **(d)** stratified squamous **(e)** simple columnar **(f)** pseudo stratified columnar **(g)** transitional.

the "false" appearance. This tissue lines most of the respiratory passages (e.g., the trachea, the bronchi, and the nasal cavity), and contains both ciliated cells and goblet cells. Ciliated cells have microscopic hair-like structures extending from the free surface; constantly moving, the hairs sweep debris laden mucus toward the throat.

Stratified epithelium consists of many layers of simple squamous of cells, with flater upper surface layers of cells. Among the various types of stratified epithelium are:

Stratified squamous keratinized epithelium that consists of flattened, dead, dry cells, composing the epidermis of the skin and *Stratified squamous non-keratinized epithelium* is composed of living cell linings. Other types of epithelium are *Transitional epithelium* that consists of flexible, pliable cells capable of stretching and contraction and *Glandular epithelium* found in glands. Table 1.1 lists properties of various epithelial cells and organ or site in which they found.

1.2.3 Clinical Presentation of Tumors

A "new growth" of the body's own cells, a proliferation of cells no longer under normal physiologic control is termed as tumors or neoplasms. Oral tumors can develop anywhere in the oral cavity. Some tumors are benign (non-cancerous), some may be pre-cancerous (a condition that may become cancerous), while others may be cancerous.

1.2.3.1 Benign Tumors and Hyperplasia

Benign neoplasms are typically localized tumors (lumps or masses) that, if removed, do not recur. Even if they are not removed, they are not capable of destroying adjacent organs or spreading out to other parts of the body. They are usually separated from the surrounding tissue by a capsule or connective tissues.

However, hyperplasia can be defined as an increase in the number of cells in an organ or tissue, usually resulting in increased volume of the organ or tissue and may be triggered by external stimulus. Hyperplasia can be physiologic or pathologic. Hormonal hyperplasia, which increases the functional capacity of a tissue when needed and compensatory hyperplasia, which increases tissue mass after damage or partial resection, are physiologic hyperplasias. Most forms of the pathologic hyperplasia are caused by excessive hormonal stimulation or growth factors acting on target cells. Although these forms of hyperplasia are abnormal, the process remains controlled, because hyperplasia regresses if the hormonal stimulation is eliminated. Hyperplasia is also an important response of tissue cells in reapir/ healing of wounds/ inflammations. Under such situations, growth factors are responsible for the hyperplasia. All those mentioned above are said to be benign hyperplasia. Howerer pathologic hyperplasia, stimulated by growth factors, constitutes a fertile soil in which cancerous proliferation may eventually arise. Hyperplasia that is associated with viral infections due to pappilomavirus and oral mucosal lesions such as luekoplakia and erythoplakia are at an increased risk of developing oral cancer.

Table 1.1 Features of various epithelial cells in a nut shell

TYPE	STRUCTURE	SITES
SIMPLE EPITHELIUM	One cell layer thick with all the cells attach directly to the basement membrane	
Simple squamous	One layer of flattened and tightly bound cells	Skin
Simple cuboidal	One layer of tightly bound, cube-shaped cells	Thyroid and Salivary glands, liver, pancreas
Simple columnar	One layer of tightly bound unciliated, tall shaped cells	Intestine, Gallbladder, Fallopian tubes
STRATIFIRD EPITHELIUM	Two or more cell layers flaked over one other and only the deepest layer in contact with the basement membrane	
Stratified squamous, keratinized	Many layer thick cells in outer layers are dead , flat and contain keratin	Nails , hair, dead cells
Stratified squamous non keratinized	Many layers thick , layers are flat and alive with keratin	Oral cavity, Esophagus, Vvagina
OTHER EPITHELIUM	Cell layers vary from single to many	
Pseudo stratified columnar	One layer of cells of varying heights all attached to the base membarance	Trachea, Bronchi, Nasal cavity
Transitional	Multiple layers of cuboidal and rounded cells during relaxation of the tissue and flat shape during the streching	Urinary bladder

1.2.3.2 Dysplasias/Atypias

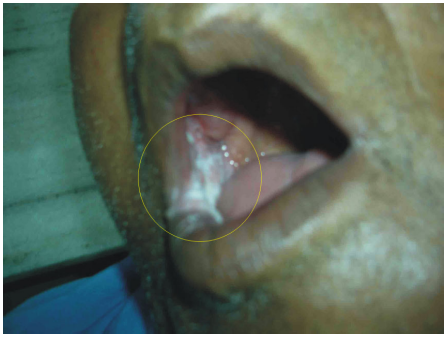

Fig. 1.3 Moderately differentiated squamous cell carcinoma (MDSCC) observed in the buccal mucosa of a 62 year old patient.

Dysplasias or Atypias are encountered principally in the stratified squamous epithelia, and links with nuclear abnormalities of epithelial cells. Pathological term "Atypical" represents proliferation of cells. In a diagnosis, the use of the term atypical is a vague warning to the physician that the pathologist is worried about something, but not worried enough to say that the patient has cancer. It finds its best use as a term to describe the phenomenon in which epithelium proliferates and develops the microscopic appearance of neoplastic tissue, but otherwise tends to "behave itself" and continues to line body surfaces without actually invading them, as a true malignant neoplasm would do. Pathologically these atypias and dysplasias are graded as mild, moderatre and severe. The development of epithelial pre-cancers are initiated with transformation of cells, which give rise to changes in nuclear shape, size, density and overall thickening of the epithelial layer (Evan GI and Voudden, 2001; Shafer WG and Waldron CA, 1975). These dysplasias are characterized by a constellation of changes that include a loss in the uniformity of the individual cells as well as a loss in their architectural orientation. Dyspastic tissues also exhibit considerable variation in size and shape (Pleomorphism). It may be convenient (but not totally accurate) to consider these atypias/dysplasias as a "pre-cancer" or an incipient cancer. Oral epithelial dysplasias are pre-cancerous lesions found in the oral cavity that appear clinically as erythroplakia and leukoplakia, with their chances of conversion to malignancy being ca. 90% and 10%, respectively (Boone et al., 1997).

1.2.3.3 High Risk Lesions

Erythroplakia: It is a descriptive clinical term for any red macular lesion affecting the oral mucosa, which cannot be given a specific clinical diagnosis. Erythroplakia may manifest as a homogeneous red maculae, a mixed macular red and white lesion, or as a red lesion with superimposed white granular spots. The chances of these lesions characterized clinically as erythroplakia to be malignant is well over 10%.

Leukoplakia: It is a descriptive term for a white lesion in the oral mucosa that cannot be attributed to any other clinically definable lesion. Along with the erythroplakia, leukoplakia is belived to be the precursors of SCC (Suarez et al.,1998). The rate of malignant transformation of leukoplakia cannot be predicted accurately, but it is important to acknowledge up to 90% of all pre-cancerous lesions appear as leukoplakia.

1.2.3.4 Malignant Carcinomas

Malignant neoplasms of any squamous epithelial cell orgin, d of the body is termed a squamous cell carcinoma (SCC). SCC constitutes 85% oral cavity malignancy (Wingo et al., 1995). Verrucous carcinoma, a form of SCC that comprises 5% of all diagnosed oral cancers, can spread deeply into surrounding tissue requiring surgical removal with a wide margin of surrounding tissue. In the early stages, cancer is present only in the lining layer of cells and this type of cancer is known as carcinoma in situ (CIS, Fig. 1.3). When the cancer spreads beyond cell lining, it is called invasive SCC (Fig. 1.4). Carcinogenesis is a multi-step process that usually arises in the epithelium (Alberts et al., 2002). Thus, malignancy is expressed by 1) Local invasion, in which the malignant tumor breaks the extra cellular matrix; 2) Metastasis, in which cells from the malignant tumor seed out to other parts of the body and then grow into tumors themselves; and/or 3) Para neoplastic syndromes, in which the neoplasm secretes metabolic poisons or inappropriately large amounts of hormones that cause problems with functions of various body systems.

1.2.3.5 Metastasis

Metastasis is an active process in multi-stage carcinogenesis, where malignant tissues invade the surrounding tissues and transfer the disease from primary site to a secondary part not directly connected with it via blood circulation. Fig. 1.4 shows the progression of normal to invasive tumor and its metastasis.

1.2.4 Etiology of Cancer

1.2.4.1 Etiology or Causes

There are two major classess of etillogic factors: Intrinsic or genitic, and acquired (e.g., chemical, physical and bilogical). Major factors causing oral malignancies are linked to life

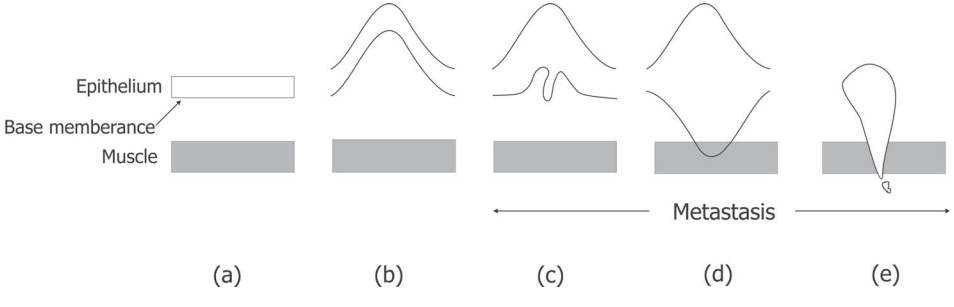

Fig. 1.4 Process of carcinogenesis **(a)** normal squamous epithelium **(b)** carcinoma in situ **(c)** and **(d)** tumor invasion **(e)** metastasis-spreading of cancer to distant parts via blood stream.

style and generally appear in the middle aged groups (55±15). The established lifestyle risk factors for oral cancers are:

- smoking- cigarettes, cigars, pipers and bidies
- tobacco chewing - betel quid, pan, ghutka and pan masala
- high alcohol consumption (synergistic with tobacco)

Oral cancer remains one of the most disfiguring and debilitating cancer of all of the malignancies. In our studies all the subjects have history of above listed habits alone or in combination. Knowledge or discovery of the primary cause remains the backbone to fight against this dreadful disease i.e., disease diagnosis, understanding of disease; and treatment development.

1.2.4.2 Prevention

The proverb "Stitch in time saves nine" suits well to this context. Primary prevention of oral cancer means to change/stop the behaviors known to be associated with oral cancer, like smoking, tobacco chewing and alcohol consumption. Whereas, early detection of potentially malignant lesions by effective screening modalities assume secondary importance. This helps in effectively avoiding chances of spreading to the secondary sites, by metastasis and enhances curability.

To provide timely treatment of oral cancer, oral healthcare providers must understand and detect the disease, in its premature stages. Fig. 1.5 shows the conventional oral cancer detection algorithm. Since the essence of malignancy escapes full understanding, prevention must be equated with early detection. Primary prevention strategies coupled with early detection measures may have greater impact in reducing morbidity and mortality associated with oral cancer. The optimal management of oral cancer requires a "team effort" from the healthcare providers to clinicians. Oral healthcare providers, especially dentists, can be expected to be called upon to identify suspicious lesions, if any, in the oral cavity of their patients. Early, active participation in developing preventive and therapeutic strategies, in implementing the plan, and in education and rehabilitation is paramount in addressing the quality of life issues. Thus, the role of a general dentist is very important in the early detection of oral soft tissue lesions in the head and neck area. Appropriate diagnostic procedures must be implemented as a matter of course in the evaluation of any lesion not responding to usual therapy in 1-2 weeks and when a malignancy is suspected. To safeguard and advance the welfare of the patient, whenever the diagnosis is in doubt, the clinician has the obligation to initiate consultation with or referral to a respective peer or specialist with special skills, knowledge and experience.

1.2.5 Diagnosis

1.2.5.1 Histopathology

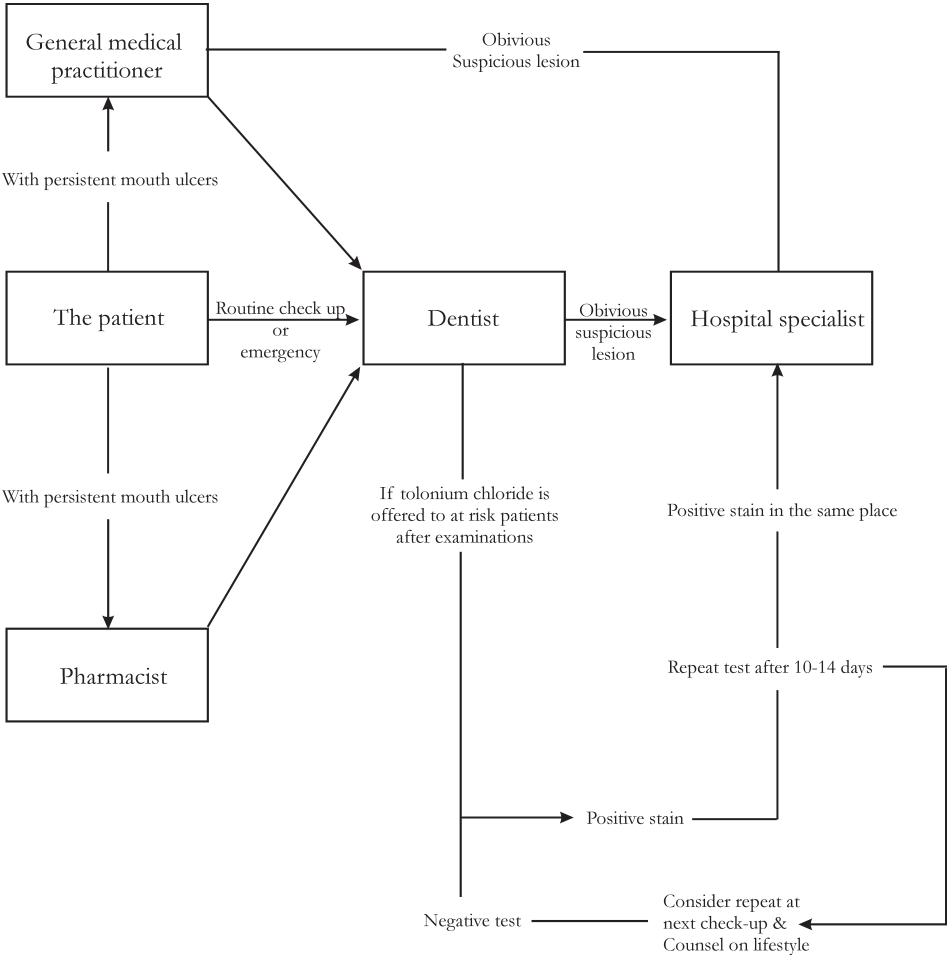

Fig. 1.5 Oral cancer detection algorithm.

There are striking similarities among the lesions affecting oral tissues. It is essential in the differential diagnostic process to consider all possibilities before making a definitive diagnosis. In some instances, a history of pathogenesis aided by radiographic characteristics and laboratory profiling may confirm with the clinical impression. However, many medical conditions, including all cases of cancer, must be diagnosed by removing a sample of tissue from the patient and sending it to a pathologist for examination. This process of tissue removal for microscopic studies is known as biopsy (a Greek-derived word that may be loosely translated as *view of the living*) and histopathology followed by biopsy remains the *gold standard* for diagnoising pre-malignant oral lesions. A biopsy may be either excisional or incisional. An excisional biopsy is the technique of choice when a lesion is relatively small and the lesion is excised in its entirety. Whereas, an incisional biopsy is indicated when a lesion is large. In some instances, when clinician is not sure which part of the lesion is most abnormal, several specimens may have to be taken for adequate microscopic evaluation,

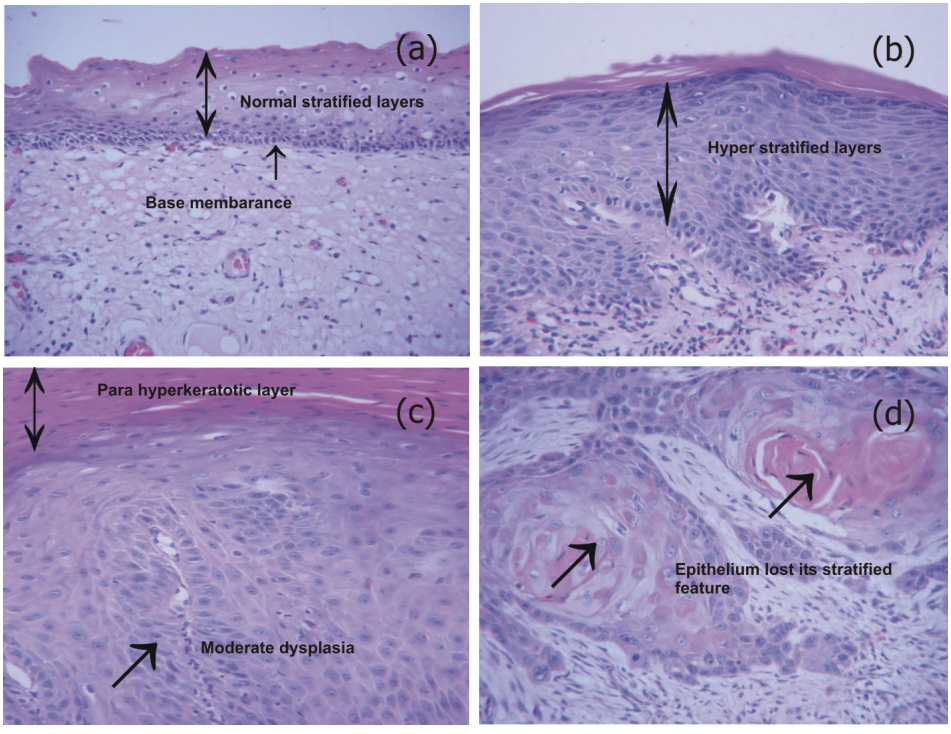

Fig. 1.6 Histological images of different type tissues **(a)** normal squamous epithelium **(b)** hyperplastic epithelium **(c)** dysplastic epithelium with hyperplasia **(d)** dysplastic epithelium with hyperplasia and hyperkeratosis and **(e)** well differentiated squamous cell carcinoma (WDSCC).

termed as random multiple biopsies. The goal of an oral biopsy is to provide an accurate pathological representation of the tissue in question. There are many biopsy methods available such as punch biopsy, needle biopsy, brush biopsy and scalpel biosy. In this *in vivo* study on patients, punch biopsy was performed for tissue removal. After the specimen is removed from the patient, it is fixed in formalin for hardening and from such frozen tissues histologic slides are prepared. Briefly, the preparation of these slides involve dehydration with various chemicals, embedding with paraffin, micro sectioning using microtome and mounting on thin glass plates and staining using different dyes for revealing cellular components. Such prepared histologic sections are examined by experienced histopathologists under microscope for the tissue characterization.

Fig. 1.6 represents histological microscopic images of different squanous epithelial tissues of the oral cavity, viz. normal, hyperplastic, dysplastic, and SCC. As can be seen from the figure, normal oral mucosa is covered by a squamous epithelium, composed of several cell layers with flattened cells in the superficial layers. In hyperplastic mucosa number of such layers are much higher than in normal, while in dysplastic epithelium, the layered structure is partly lost and the cell nuclei become irregular and enlarged; starting from the deepest lying cell layers, and getting more superficial with increasing grades of dysplasia. In SCC, the layered structure is totally lost. However, in the case of CIS, the base membrance is intact and this prevents access to vascular channels, and hence metastasis.

1.2.5.2 Diagnostic Accuracies

1.2.5.2.1 Sensitivity and Specificity

Sensitivity and specificity represent two operating characteristics that indicate the accuracy of a diagnostic method i.e., its ability to correctly identify the condition of interest (Pretty and Gerrardo, 2004a, b). In our study, they indicate the ability of different spectral criteria in discriminating the normal tissues from benign, benign from pre-malignant, pre-malignant from malignant. When results of a diagnostic procedure are compared with gold standard there could be four possibilities.

True Positive (TP), whereby the procedure results indicate that the person has disease, and this assessment is confirmed by the gold standard. False Positive (FP), whereby the procedure results indicate that the person has disease, but gold standard indicates that the disease is absent. True Negative (TN), whereby the procedure results indicate that the person has no disease, which is in agreement with the gold standard. False Negative (FN), whereby the procedure results shows that the person has no disease, which is not in agreement with the gold standard.

The sensitivity of a diagnosing method is the percentage of diseased who are correctly diseased, and can be expressed as (TP/TP+FN). Thus a procedure with 100% sensitivity will identify every diseased individual as diseased. Whereas, specificity of the same procedure is the percentage of disease-free individuals who are detected correctly and expressed as

(TN/TN+FP). An ideal diagnosing system should be highly sensitive and specific, but for many diagnostic procedures these two characteristics are inversely related and increase in one is often associated with the reduction of other.

An alternate method to calcualte these diagnostic accuaracies is by dividing diagnostic outcomes with the corresponding gold standard results. For example, the sensitivity can be expressed by the ratio (diagnostic abnormal/gold standard abnormal)% and the specificity can be represnted as the ratio (diagnostic normal/ gold standard normal)%.

1.2.5.2.2 Positive and Negative Predictive Values

By quantifying the sensitivity of a diagnostic procedure it is possible to determine an operating characteristic of that procedure that establishes if a patient has the disease in question. Determination of the specificity allows assessment of another operating characteristic of the procedure that determines if the patient does not have the disease. Sensitivity and specificity are relatively independent of the prevalence of a disease (the pretest probability that an individual patient has the disease), and therefore these parameters are generally stable for the same procedure administered in different study populations. In other words, sensitivity and specificity are inherent properties of the test. They are useful for comparing procedures and for deciding which test to use in a particular clinical setting.

Sensitivity and specificity do not aid in interpreting the result of a particular procedure for an individual patient; they do not help in ruling in or ruling out the disease once the results of the test are known, and so they have no predictive value. To answer these more practical questions, the predictive values of the diagnostic procedure must be determined. The predictive values are easily derived from the contingency similar to sensitivity and specificity as described in (Table 1.2). The positive predictive value (PPV) is the likelihood that the patient actually has the disease, given a positive test result and can be expressed as (TP/TP+FP). The negative predictive value (NPV) is the likelihood that the patient does not have the disease should the procedure result be negative and can be calculated from the expression (TN/TN+FN) . Whereas, the values for sensitivity and specificity depend only on the operating characteristics of the procedure itself, the PPV and NPV vary according to the prevalence of the disease. Thus, predictive values cannot be quoted without prior knowledge of disease prevalence in the population from which the estimates are being derived. PPV and NPV are not qualities of the procedure itself; rather, they are functions of both the characteristics of the procedure and the environment in which it is being used. In other words, the accuracy of PPV and NPV values would be lower in general population and when the same screening procedures are applied to high risk populations, they are highly effective in identifying those with the disease or condition of interest.

1.2.6.2.3 ROC Curve Analysis

The diagnostic performance or the accuracy of a test to discern between diseased cases from normal or conditions of interest is evaluated using receiver operating characteristic

(ROC) analysis (Zweig and Campbell, 1993; Griner et al., 1981). When one considers the diagnostic test in a mixed population, one with disease and other without, a perfect separation between the two categories is essential. However, the distribution of the test results will overlap. In a ROC the sensitivity is plotted against (1-specificity) for different cut-off points. The ROC is advantageous because it allow the user to take a good decision on the effectiveness of differnt diagnostic methods without constraining him to single values of sensitivity and specificity, which largely depends on the threshold value chosen (Metz, 1978). Each point on the ROC plot represents a sensitivity/specificity pair corresponding to a particular decision threshold and one can easily predict best methodology from the area under the curve. A test with perfect discrimination (without any overlap the two distributions) has a ROC plot that passes through the upper left corner from thelower left corner to the upper right corner (100% sensitivity, 100% specificity). Whereas, a straight line from lower left corner to the upper right corner represents a procedure in which the two distributions overlap completely. The more accurately a methodology or technique sepearates two data types, the corresponding area under ROC curve (ROC-AUC) approximates to 1.0. Therefore, closer the ROC curve is to the upper left corner of the plot, the higher is the overall accuracy of the test. In other words, higher the ROC-AUC greater will be the total diagnostic accuracy of the method.

1.2.5.3 Different Existing Adjunctive Methods in Oral Cancer Detection

Various adjunctive methods can help the clinician to screen the suspicious lesion for cancer during the visual examination procedure which could help to locate the most abnormal site of the lesion for a biopsy.

Table 1.2 A 2 x 2 contingency table illustrating the outcomes of a comparison between a diagnostic procedure and gold standard and the use of these values to calculate Sensitivity,Specificity,negative and positive predictive values

		Gold Standard results		
		Positive	Negative	Total
Diagnostic Procedure results	Positive	True Positive (TP)	False Positive (FP)	TP+FP
	Negative	False Negative (FN)	True Negative (TN)	FN+TN
	Total	TP+FN	FP+TN	FN+TN+FP+TP

Auxillary Imaging Modalities: Various imaging modalities play a vital role in the treatment, planning and progress monitoring in post therapeutic treatment. Imaging methods like MRI, CT and PET are common practices for treated and cured patients to have imaging scans in an effort to catch any relapse early on. All these modalities showed similar diagnostic accuracies between 75% to 94.2% for detection of oral SCC of (Araki et al., 1997; Wiener et al., 2005) and the accuracy for detection of SCC is significantly high when all the imaging modalities were used together (Ng et al., 2005; Yen et al., 2005). However, the disadvantages of these diagnostic imaging modalities are their limitation to accurately differentiate different types of pathology, high costs and the regulatory requirements of these machines.

Visual Inspection using Acetic acid (VIA) and Chemi-luminescence: Neoplastic epithelial cells tend to have altered nuclear-cytoplasmic ratio. Dehydration with acetic acid highlights this higher nuclear density and imparts an "acetowhite" appearance to tissues. Therefore, by applying acetic acid to the suspicious tissue, the abnormal tissues turn white and normal tissues remain as such.

This phenomenon can be further amplified by replacing conventional lighting with diffuse blue-white chemiluminescent illumination. A chemi-luminescent illumination system (ViziLite™) to examine the oral mucosa is available commercially. The technique is painless, easy to learn and may ultimately identify suspicious lesions missed during visual inspection under incandescent overhead and halogen dental illumination. Epithelium with an altered nuclear-cytoplasmic ratio reflects the diffuse, low-level, blue-white chemi-luminescent light and the lesions become clinically discernible and appear "acetowhite". These bright white lesions are sharply demarcated from the adjacent, normal epithelium, which takes on a blue hue. Large-scale studies, however are required to further refine issues related to the sensitivity and specificity of the technology in correlation with the clinical, cytological and histological features of oral epithelial lesions. This strategy has been shown to increase the detection of biopsy proven epithelial dysplasia and malignancy of the cervix and lower genital tract when compared with naked eye or magnified visualization under incandescent or halogen projected lighting.

VILI (Visual Inspection using Lugol's Iodine): It is also known as Schiller's test. By the application of Lugol's Iodine to the suspicious tissues, normal tissue turns brown while the abnormal tissues will turn to saffron yellow. This colour change takes place due to differences in glycogen content in normal and abnormal tissues. Iodine is glycophilic and is taken up bynomal tissues which makes them dark.

Toluidine blue staining (TBS) test: Toluidine blue staining is considered to be a fast, minimally invasive, patient-accepted and sensitive test that has been in use for over thirty years in identifying early oral SCC and high-grade dysplasias (Patton, 2003). However, the detection of low-grade (mild/moderate) oral dysplasia has been less consistent, since significant portion of such lesions less readily stain with toluidine blue. Eventhough studies by Epstein et al., 2003 indicated that toluidine blue is more sensitive than clinical examination

in high risk patients, with sensitivity of 96.7% and specificity of 90.9%, the sensitivity and specificity reported by Onfore et al (2001) were much lower in distinguishing low grade dysplasias. Therefore, during the clinical examination of a suspicious lesion, a clinician makes use of toluidine blue dye for confirmation of a minimally invasive SCC prior to biopsy.

Oral brush biopsy: This is another new way to test for oral cancer before biopsy and is beginning to be used by dental professionals. The oral brush biopsy can be a fast, effective and minimally invasive screning procedure. Here, a dentist uses a small brush to gather cell samples of a suspicious area. The oral brush biopsy procedure is simple, involves very little or no pain or bleeding, and requires no topical or local anesthetic. Firm pressure with a circular brush is applied to the suspicious area. The brush is then rotated five to ten times, causing some pinpoint bleeding or light abrasion. The cellular material picked up by the brush is transferred to a bar-coded glass slide, preserved, and dried. At the laboratory, a computer-aided scanner (Oral CDx) helps to identify and display individual cells which may be malignant. If suspect cells are identified by the computer, a pathologist then examines the identified cells to determine the final diagnosis. Eventhough Oral CDx technique may bridge the gap between clinical inspection and histological evaluation of questionable oral lesions, the specificity and accuracy values are inconsistent (Svirsky et al., 2002).

1.3 Conclusions

Exploration of the possibilities with new techniques in the biomedical field is always challenging. For the last few decades mankind have been developing and using various techniques to diagnose the dreadful disease of cancer in its early stages. Eventhough, many diagnostic modalities are present in oral caner screening, their sensitivity or specificities are relatively low, which make them less effective diagnostic tools. Gold standard histopathology, on the other side is an invasive time consuming process causing discomfort to the patient. Hence, early non-invasive, real-time diagnosis and treatment of pre-malignant and malignant lesions assume great significance in reducing patient morbidity and mortality.

More recently, the limitations of diagnostic pathology and tissue morphology for diagnosing diseases have become increasingly evident, and now encompass other auxilliary approches for analyzing such disease states. In this context, if applied successfully, optical spectroscopy has immense potential to represent the improtant forward step towards advances in diagnostic and theraputic mecical applications. For the devolopment of such optimized optical systems, there is a need to understand the interaction of light with complex matter, such as biological tissues. The next chapter, throws light on different optical spectroscopic aspects and basic concepts of light tissue interaction.

Chapter 2

Interaction of Light with Tissue: Some Basic Concepts and Background

Interaction of Light with Tissue: Some Basic Concepts and Background

2

2.1 Introduction

The two fundamental processes that can occur when light propagates through a tissue are scattering and absorption and these processes are strongly wavelength dependent. High energy electromagnetic radiation, such as gamma rays and X-rays, are not scattered to a great extent, but rather propagates through the tissue in straight trajectories. The transmitted radiation is altered due to absorption, which varies with tissue type. When light is absorbed, high-energy photons lead to bond breaking and ionization of molecules, which in turn is potentially carcinogenic. Low energy radiation such as IR or Microwave, on the other hand, induces excitation of rotational and vibrational energy levels in the molecules, leading to a temperature increase.

The light-tissue interactions in the diagnostics approach must in contrast be non-destructive; meaning a resonant light absorption that is below the threshold required to stimulate chemical and thermal reactions. Light radiation in the visible region are the ideal choice to achieve the above conditions. The key factors for tissue diagnostics are instead light scattering and emission processes. By analyzing the features of the scattered and re-emitted light in terms of wavelength, temporal and spatial/angular distributions, indirect information on tissue characteristics can be gained. There exists a variety of potential methods, either based on resonant light absorption followed by re-emission, such as laser-induced autofluorescence (LIAF),or non-resonant inelastic scattering in conjunction with Raman spectroscopy, elastic scattering, diffuse reflectance(DR) spectroscopy, absorption spectroscopy and time resolved transmittance.

As compared to X-ray diagnostics and usage of ionizing radiation, the spectral techniques are risk free and gives instantaneous information on the nature of disease in a highly sensitive manner, in real-time, without the need for tissue removal. Further, these systems can be automated for easy use by less skilled personnel and is adaptable for field applications where mass screening can be carried out on a large number of patients.

In contrast to the current clinical practices described in chapter 1, optical spectroscopy can provide non-invasive and real-time information which is free from artifacts that may arise due to cutting, freezing and staining of tissue. Fluorescence spectroscopy, Raman spectroscopy, diffuse reflectance spectroscopy and light-scattering are emerging new-generation techniques in the diagnosis of all kinds of malignancies. Among these techniques, the potential of LIAF and DR is immense and yet, is not fully explored for detection of pre-cancerous lesions. Tissue fluorescence with ultraviolet-visible (UV-VIS) excitation can effectively probe multiple biochemical constituents that are present in the normal and malignant tissues. However, cost-effective, simple and compact features of reflectance

spectroscopy system make it attractive in biological tissue characterization. In this study, we have used visible laser light at 405 nm for fluorescence studies and a conventional tungsten halogen lamp as white light for diffuse reflectance studies.

2.2 Light

Nearly all objects in the universe emit, reflect and/or transmit light, with the hypothetical exception of dark matter. The distribution of this light along the electromagnetic spectrum (called the spectrum of the object) is determined by the composition of the object. Electromagnetic spectrum consists of wavelengths in the 10^{-13} to 10^{5} m range. The visible light encompasses a narrow band of nearly 400 nm, which can be viewed and distinguished by the human eye. Table 2.1 depicts the wavelength regions of the visible spectrum and Fig. 2.1 shows the entire electromagnetic spectrum. The wavelength of the light is inversely proportional to the energy (E) of the incident photons

$$= hc/E \qquad [2.1]$$

$$= h/\nu \qquad [2.2]$$

Where 'h' is the Plank's constant, 'c' is the velocity of light and 'ν' is the frequency of the incident photon.

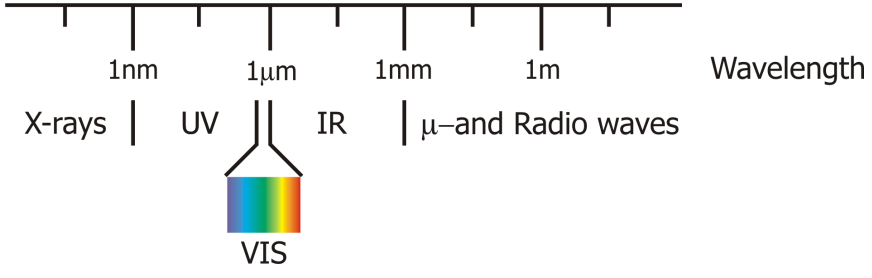

Fig. 2.1 Entire electromagnetic spectrum.

2.3 Optical Spectroscopy

The disadvantages of traditional biopsy form a strong clinical rationale for developing other non-invasive and real-time diagnostic techniques to improve the detection of early pre-malignant changes in the oral mucosa. One of these techniques under investigation is optical spectroscopy, often referred to as "Optical Biopsy". Although it is an inaccurate term,

Table 2.1 Wavelength range of different colours in visible range of EM spectrum

Colour	Wavelength range (nm)
Violet	400-455
Blue	455-492
Green	492-577
Yellow	577-597
Orange	597-622
Red	622-780

perhaps an oxymoron term, since "biopsy" refers specifically to tissue removal, whereas implication "optical" indicates that tissue is not removed. Nonetheless, the term represents a form of optical measurement, generally by using optical spectroscopy to diagnosis in situ or in vivo tissue abnormalities in real-time.

Optical spectroscopy allows non-invasive physical and chemical characterization of biological tissues. In this technique the tissue under scrutiny is illuminated with a UV or visible laser source. Consistent differences in spectroscopic signatures are seen in malignant versus benign tissue samples. This methodology helps to eliminate or reduce the need for surgical biopsy and allow treatment to take place before a cancer is well established or spreading. As compared to X-ray diagnostics and the usage of ionizing radiation, optical spectroscopic techniques are risk free and give information on the invasive nature of the disease in a fast and highly sensitive manner without the need for tissue removal. The use of ionizing radiation comprises the risk of cancer induction as well. Further, cost of such optical non-ionizing imaging or spectroscopy systems are comparitively low and such

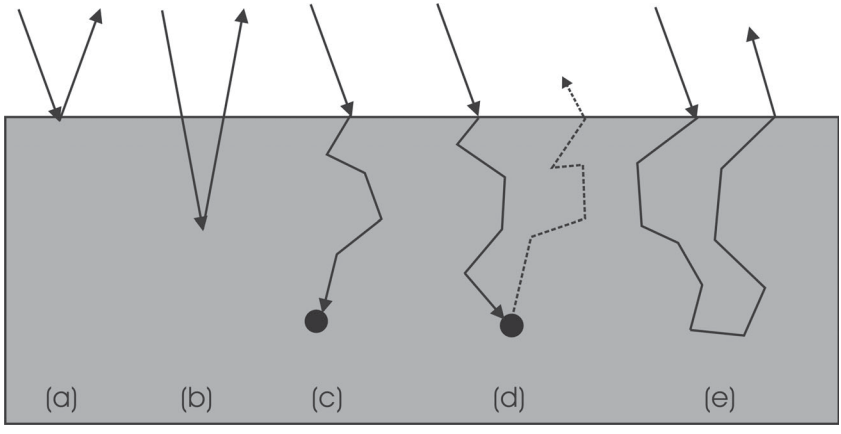

Fig. 2.2 Different types of interaction of light with tissue **(a)** reflection **(b)** back scattering **(c)** Absorption **(d)** fluorescence/Raman scattering **(e)** diffuse Reflectance. Black dotts shown are either tissue chromophore, flurophore or a scatterer.

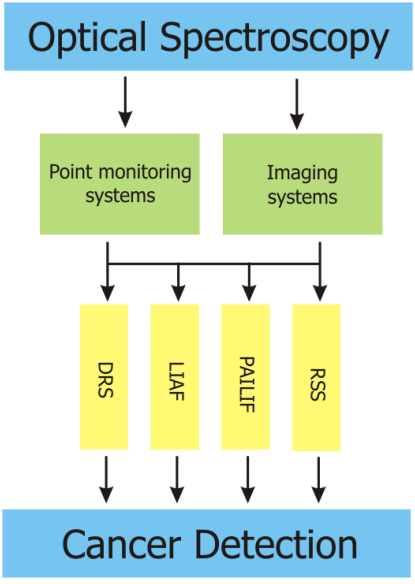

Fig. 2.3 Algoritham showing optical spectroscopic applications in cancer detection using point-monitoring, imaging, diffuse reflectance spectroscopy(DRS),laser-induced autofluorescence spectroscopy (LIAFS), photosensitizer assisted laser-induced fluorescence (PALIF) and Raman scattering spectroscopy (RSS).

quantitative techniques, which may provide several advantages over commonly used techniques, are currently under investigation world-wide for detection of cancer. The structural and chemical composition of cells and tissues strongly influence their optical features and therefore, alterations in the optical characteristics may indicate the presence of diseased tissue. Optical spectroscopy also facilitates early detection of cancerous tissues in humans by providing additional physiological information (as compared to X-ray, ultrasound or MRI) on tissue oxygenation levels, total hemoglobin, water and lipid content that helps to improve the contrast between normal, benign and malignant.

Fig. 2.2 represents the variety of processes that occur when an optical photon is incident on the epithelial tissue surface. Case "a" represents simple reflection (Fresnel) from the tissue surface, while "b" stands for elastic backscattering from cellular and structrual components of the tissue. Absorption of light photon by cellular components is an other possibility shown in the case "c". Fluorescence and Raman scattering are two of the most relevent inelastic processes shown by case "d"; while, case "e" represents diffuse refectance where majority of photons undergo numerous scattering and absorption events before being emitted.

Table 2.2 Various tissue absorbers with their absorption maxima

Tissue Absorbers	Description	Absorption maxima (nm)
Water	Pigment	760, 900, 1250, 1400 etc.
Oxygenated Haemoglobin	Protein complex	410-420, 542, 575
Deoxygenated Haemoglobin	Protein complex	430, 550, 750
Urocanic acid	Pigment	260-280
Bilirubin	Pigment	460
β-carotene	Pigment	480
Melanin	Pigment	UV-VIS

In this way, biochemical and structural/ morphological information of tissue can be gained by measuring absorption, fluorescence, diffuse reflectance and Raman scattering (Fig. 2.3). Each of these spectroscopic technique has separate physical basis and all have the potential to become an adjuvant method to conventional cancer detection methods. Among these optical techniques, the present study focuses on fluorescence emission (both autofluorescence and photosensitizer assisted laser-induced fluorescence) and diffuse reflectance of tissues for cancer diagnosis.

2.3.1 Absorption

When the energy of an incoming photon corresponds to the energy gap between the electronic states of a molecule or chromophore, it gets absorbed. The probability of light absorbtion is strongly dependent on the absorption coeficient (μ_a) of the chromophore. Absolute values of absorption coefficents for typical tissues lie in the range, 10^{2} - 10^{4} cm^{-1} (Tuchin V, 2007). The main chromophores in most of the bilogical tissues are water (H_2O), melanin and oxy and deoxy hemoglobin (Hb and HbO_2). Fig. 2.4 shows the wavelength dependance of the absorption coefficent and Table 2.2, the absorption peaks of some of the important tissue chromophores.

Between approximateley 200 nm and 1300nm, the absorption due to water is very low. At visibile wavelengths up to 600nm, the absorption coefficent is less than $1mm^{-1}$ (Charlota

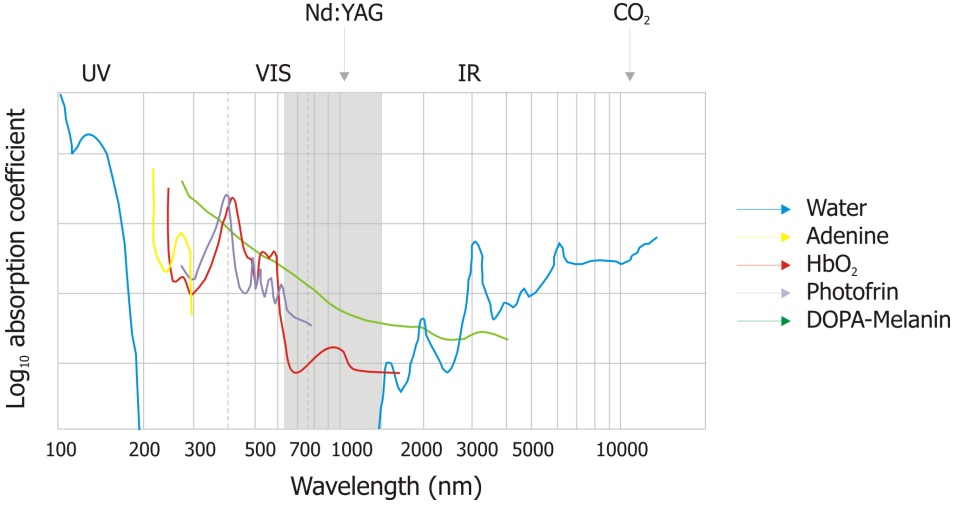

Fig. 2.4 Absorption coefficents of major chromophores in a biological tissue is depicted versuses the wavelength (Adopted from Boulnois et al., 1986).

Eker, 1999), and above 950nm, water starts dominating absorption. In the UV and IR spectral region, light is readily absorbed by water and this accounts for the small contribution of scattering and the inability of radiation to penetrate deep into tissue beyond one or two cell layer of the tissue(Tuchin V, 2007). Light in the 600-1300 region, which is often referred to as the optical therapeutic window of tissue, is used for many diagnostic and therapeutic purposes, as it offers better penetration depth. This spectral range also has minimum blood absorption, where scattering prevails over absorption and maximum penetration of 8-10 nm takes place in the biological tissue. Also at longer wavelengths, absorption increases with intensity of the reflected radiation escalating to 35-70% of the total incident light due to backscattering (Tuchin V, 2007). However, light in this region heats up the tissue, there by causing hyperthermic effect, which could be good for therapeutic applications, but not as a diagnostic tool.

In the UV region, the major absorbers are proteins and aminoacids. Eventhough UV radiation can cause therapeutic effects for certain skin diseases, these radiations are not recommended as they can cause pathological effects of immuno-suppression, mutation, and hence, skin–cancer (Young et al., 1997; Setlow et al., 1993). Nonetheless, short-wave VIS light penetrates typical tissues as deep as 0.5 to 2.5 mm, where the scattering and absorption are equally dominant with the intensity of radiation increasing to 15-40% of the incident radiation one has the additional opportunity to study these two phenomenon simaltaneously (Tuchin V, 2007). In this region, the dominant absorber is oxygenated hemoglobin having strong absorption at 420, 545 and 575 nm. Therefore, this absorption gets affected by changes in blood content and oxygenation that are known to be associated

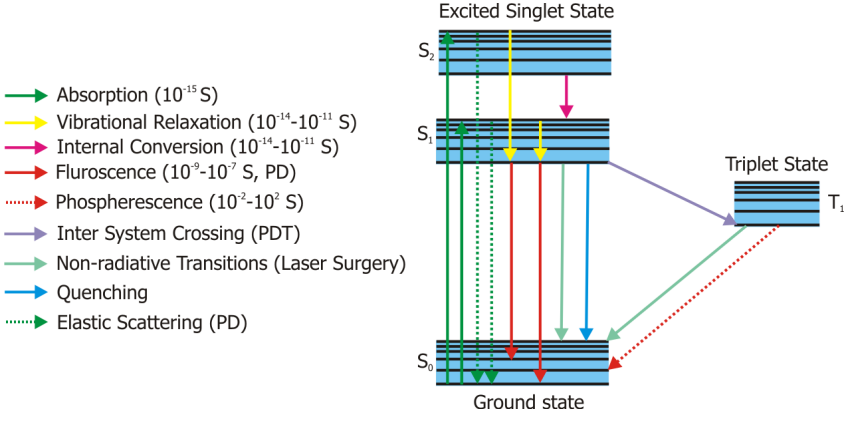

Fig. 2.5 Jablonski energy level diagram showing the various decay paths of an excited state molecule.

with cancer due to altered tissue metabolism and, in some cases, neovascularization. However, absorption due to melanin, adenine and photofrin are very feeble as compared to oxygenated hemoglobin. In this work, the absorption features of HbO_2 has been used the first time for detecting tissue abnormality, characterization and early cancer diagnosis (See Chapter 4 and Chapter 5).

2.3.2 Fluorescence

2.3.2.1 Historical Overview

Fluorescence is the property of a material to emit radiation of higher wavelength on absorption of light at shorter wavelength. This phenomenon of was discovered by Stokes in 1852, who observed this type of emission in fluorite. He found that when illuminated with UV light, some samples emitted radiation at a longer wavelength. This discovery was not considered to be of any importance for a long time. It was not until the beginning of 20^{th} century that the potential of fluorescence for medical applications was investigated. In 1911, Stubel reported that all animal tissues emitted fluorescent light, when exposed to UV radiation. The fluorescence was observed by the unaided eye and classified according to the color.

2.3.2.2 Physical Basis of Fluorescence

Fluorescence involves absorption of a photon by a molecule and the subsequent emission of another fluorescent photon. Molecules that release their excess energy by emitting fluorescence light are called flurophores. Such molecules are usually rigid and are frequently characterized by the presence of a series of alternating single and double bonds. The electronic state of a molecule can be described by the Jablonski energy diagram (Fig. 2.5). In this diagram, the electronic states of molecules are divided into vibrational states, which in turn are divided in rotational sublevels.

The absorption bands of most fluorescing molecules are very broad. This is due to the many rotational levels, partially overlapping each other due to the strong interaction between nearby molecules, causing a varying external field for each molecule. The lowest energy state of a molecule is represented by its ground state, called singlet state (S_0), and for this state all the electron spins are paired, means no unpaired electron spins exist. While triplet states (T) for most molecules, are unstable excited states, characterized by two unpaired electron spins. If an incoming photon has an energy that corresponds to the energy difference between an excited state and the ground state of the molecule, it can be absorbed. When a molecule in its ground state absorbs a photon with sufficient energy, the molecule will get excited to a higher singlet state. Fig 2.5 shows an excitation from the ground state S_0 to the S_2 state. Since excited states are unstable, the molecule relaxes down to the lower level S_1, by internal collision, which is a non-radiative process. The de-excitation to the S_0 level can also occur though internal collisions. A rapid relaxation to the lowest rotational-

vibrational level of excited state will follow a process called *Internal Conversion* (IC).

Alternatively, it can result in the emission of a fluorescence photon. The relaxation can take place to any vibrational level of S_0 also. Hence, the total fluorescence from the molecule will not be sharp peaks at one distinct wavelength, but a broader distribution. Since some energy was lost in the non-radiative relaxations, the fluorescence will have a lower energy and thus, a longer wavelength than the incoming excitation photon. From the excited state S_1, a transition can also take place to a triplet state (T_1), even though this is a spin forbidden transition. Transitions from the triplet state can also be spin–forbidden, and it will take a relatively long time before the molecule relaxes. Again, the relaxation can occur through internal conversion or by emission of a photon through a process called *phosphorescence.* This has a lifetime in the microsecond to second range, while fluorescence life times are in the nanosecond range.

The shape of fluorescence spectrum will reflect the transition probability to the lower electronic state. The difference in wavelength between excitation and emission light allows one to easily separate the evoked fluorescence light from the reflected excitation light, which is generally much higher in intensity. Continuous excitation of the flurophore causesntinuous emission of fluorescent light; unless the flurophore can be destroyed by excitation (photo bleaching). The average time a molecule stays in the excited state is called the fluorescence life time,t given by equation [2.3],

$$1/\tau=1/\tau_0+\Sigma K \qquad [2.3]$$

where "K" is the Boltzmann's constant. ΣK is the sum of all process competing with fluorescence and lifetime τ_0, is the intrinsic lifetime. At any finite temperature, the molecules will be distributed among the energy levels available to them because of thermal agitation. The exact distribution will depends on the temperature (T) and the separation between the energy levels (ΔE) in the energy ladder. At a given temperature, the number of molecules in an upper energy level (n_{upper}) relative to that in a lower level (n_{lower}) is given by Boltzmann distribution as,

$$n_{upper} / n_{lower} = \exp^{(-\Delta E/KT)} \qquad [2.4]$$

When an electromagnetic radiation is applied to a molecule, it is just as likely to cause transition from a higher to a lower energy state, as it is to cause transitions from a lower to a higher energy level. Consequently, net absorption or transition to a higher energy level can occur only if the difference between the populations of the energy levels concerned is significant, as given by equation [2.4].

As illustrated Fig. 2.5 the photon energy gained by the molecule may undergo a number of processes in addition to fluorescence, which may also be utilized for diagnostic

and therapeutic purposes. For example, since singlet states are short-lived this energy is also re-emitted as elastic scattering that could be utilized for photodiagnosis. Alternatively, after relaxing to the lowest singlet state (S_1), the molecule may undergo intersystem crossing to a triplet state (T_1) and contribute to photochemical reactions causing selctive destruction of abnormal tissues by a process known as Photo Dynamic Therapy (PDT, See section 2.4). Also, the heat energy from non-radiative decay causes the temperature to increase, which is utilized in laser surgical applications.

2.3.3 Autofluorescence and Endogenous Tissue Fluorophores

Tissue Autofluorescence (AF) is the fluorescence of the tissues when no chemical substances have been applied and it is the natural (auto)fluorescence of the tissue . Under UV and near UV-VIS light irradiation all mammalian tissues emit fluorescence from various fluorophores in tissue with a broad distribution in the longer wavelength region. This fluorescence is referred to as autofluorescence, or endogenous fluorescence. The spectrum is also influenced by the optical properties of tissue. Strong absorbers may decrease the overall intensity of the fluorescence spectrum, without changing its shape by absorbing the excitation light (Gillenwater et al., 1998a). Haemoglobin is such an absorber which can also absorb fluorescence light at certain wavelengths and this alters the appearance of the recorded fluorescence spectrum producing dips in the spectrum and the illusive presence of false peaks (Rokhar et al., 1995).The tissue fluorescence spectra are very complex, and the

Table 2.3 Different tissue fluorophores with their excitation and emission maxima

Tissue Fluorophores	Description	Excitation maxima(nm)	Emission maxima (nm)
NADH	Co-enzyme	290, 340, 350, 365	440, 450, 455, 460
NADPH	Co-enzyme	336	464
FAD, Flavins	Co-enzymes	450	515, 535
Collagen	Strucural protein	270, 325, 330, 335	380, 390-405, 395, 400, 405
Collagen cross-links	Strucural proteins	370	460-490
Elastin	Strucural protein	290, 325, 350, 360	340, 400, 420, 460
Elastin cross-links	Strucural proteins	390-420, 400, 420-460	500, 500-540
Tryptophan	Amino acid	280, 295	350, 340-350, 345
Tyrosine	Amino acid	275	300, 340
Phenylalanine	Amino acid	260	280
Phospholipids	Lipids	436	540, 560
Ceroid	Lipids	340-395	430-460, 540
Keratin(dry)	Fibrous protein	365, 370, 375	430, 460
Pyridoxine	Vitamin	332	400
Porphyrins	Porphyrins	405, 400-450, 630	635, 690, 705
Lipofuscin	Pigment	340-395	430-460, 540
Eosinophils	Blood cells	370, 500	440,550

contributions from the different flurophores can not usually be separated, but can be identified by their emission peaks.

2.3.3.1 Detection Principle

When photon from a laser source impinges on normal tissue surface, it penetrates and gets absorbed by various tissue flurophores and these absorbed flurophores re-emit light in the form of a "finger print" autofluorescence spectra (Fig. 2.6). During tissue transformation towards abnormality, variations are observed in the "fingerprint" fluorescence spectra. Carcinogenic processes produce alterations not only at the cellular level but also in the structural tissue composition and this gets reflected in autofluorescence spectral shape and intensity. Usually, alterations in the concentration of these flurophores take place prior to major structural tissue changes, and this makes LIAF very sensitive to early tissue transformation.

Various aspects of the autofluorescence that can be studied are fluorescence intensity, spectral shape and lifetime. The fluorescence spectral shape can be studied by different methods; studying variations at different emission wavelengths by changing the excitation wavelength is one possibility. This method yields fluorescence spectra as a superposition of fluorescence emission of all the flurophores present within the tissue volume probed. Variations in the fluorescence lifetime can be detected utilizing fast detectors, capable of recording the fluorescence intensity as a function of time. All these approaches can give information on the composition of the flurophores, and changes due to the microenvironment.

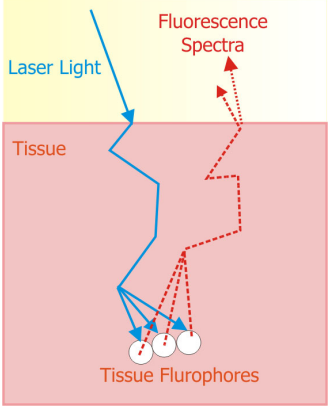

Fig 2.6 Fluorescence detection principle

Autoflurophores which are also known as endogenous flurophores include amino acids, enzymes and co-enzymes, vitamins, lipids and porphyrins. Much research had been done to investigate these autoflurophores using various techniques such as excitation and emission matrices (Mahadevan et al., 1993; Rava et al., 1991; Richards-kortum et al., 1991) and time-resolved fluorescence spectroscopy (Anderson-Engels., 1991). The endogenous flurophores that are speculated to play a vital role in transfo-rmations that occur with carcin-ogenesis are amino acids, tryptophan,and tyrosine; structural proteins like collagen, and elastin; co-enzymes like NADH, FAD and porphyrins, and the emission from these flurophores are strongly wavelength dependent. Table 2.3 depicts the excitation wavelengths and emission maxima of different tissue flurophores and Fig. 2.7 shows the absorption and emission spectra of dominant tissue flurophores.

Nicotinamide adenine dinucleotide (NADH) is located 80% in the mitochondria of cells and rest in the cytosol, which plays an important role in the metabolism of the cell, by acting as a co-enzyme in the citric acid cycle (Richards-kortum and Sevick-muraca, 1996; Richards-kortum et al., 1987). Much attention has been given to NADH for distinguishing between different lesions, in particular between pre-malignant and benign lesions. As abnormal mucosa is associated with variation in the metabolism rate, the NADH concentration might be different as compared to normal tissue. Consequently, the autofluoresc-ence in blue region has been reported to be lower in abnormal tissues (DaCoasta et al., 2003; Ramanujam, 2000).

Collagen and elastin are fibrous proteins rich in connective tissues and tissue stroma. Collagen and elastin form the connective tissue layer and can be decomposed by processes associated with disease, in particular for pre-malignant lesions. This could reflect in lower autofluorescence intensity (Gillenwater et al., 1998b; Richards-kortum and Sevick-muraca, 1996). Epithelial thickening may shield the collagen and elastin fluorescence from the deeper layers.

Tryptophan is an amino acid found in mitochondrial proteins (Andersons- Engels and Wilson, 1992). It contributes to the tissue fluorescence when only excited with the light below 300 nm. The other main endogenous flurophores are tissue co-enzymes like flavins and FAD (Drezek et al.,

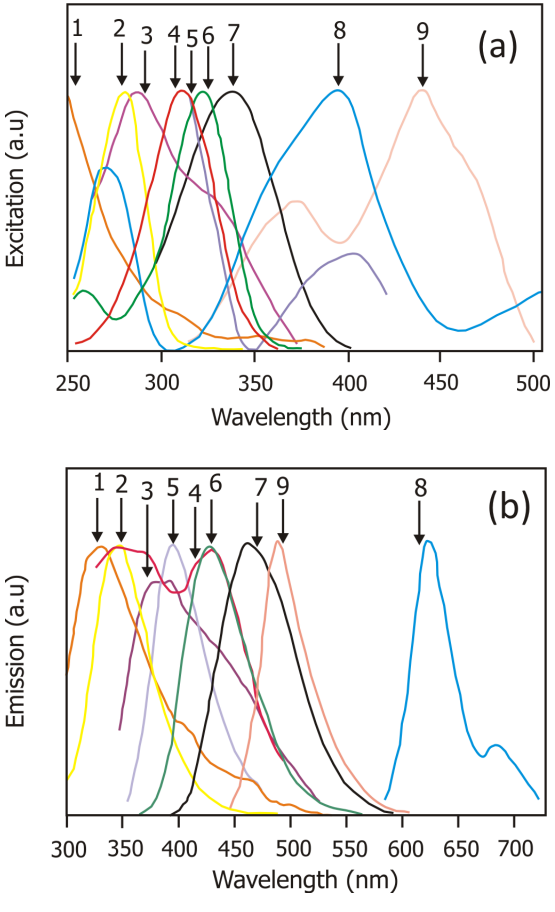

Fig. 2.7 Spectral characteristics of different flurophores existing in organisms **(a)** absorption **(b)** emission. 1- Collagen, 2- Tryptophan, 3- Elastin, 4- Pyridoksamino-5-phospate, 5-pyrodixine, 6- 4-pyridoxic acid, 7- NADH, 8- PpIX, 9- FAD (Adopted from Bottiroli et al., 1995).

2001; Benson et al., 1979; Chance and schooner, 1966), *Lipofuscin* (Tsuchida et al., 1987). Main excitation and emission peaks of various native tissue flurophores extracted from the following references (Stamatas et al., 2006; Niedorf et al.,2005; Da Costa et al., 2003; Finlay et al., 2003; Teuchner et al., 2003; Kollias et al., 2002a; Gillies et al., 2000; Ramanujam et al., 2000; Kollias et al., 1998; Young et al., 1997; Richards-Kortum et al., 1996; Sterenborg et al.,1994; Rava et al., 1991; Kozikowski et al.,1984) are listed in Table 2.3.

Protoporphyrin (PpIX) is an endogenous porphyrin that is associated with tissue alterations and malignancy. This porphyrin gets selectively accumalted in abnormal tissue due to a break in the heam cycle. Therefore, the relatively narrow porphyrin fluorescence peaks from PpIX could be informative about the condition of the mucosa under investigation. The selective accumaltion of these porphyrins in abnormal tissue is best understood from the pathway of heme biosynthesis.

2.3.3.2 Heam Cycle

All mammalian nucleated cells can synthesize heme for their aerobic energy needs, which takes place partly in the mitochondria (M) and partly in the cytosol (C)(Bottomley and Muller-Eberhard, 1988). The first step of the normal enzymatic heme biosynthetic pathway is naturally initiated with the condensation of glycine and succinyl-coenzyme A

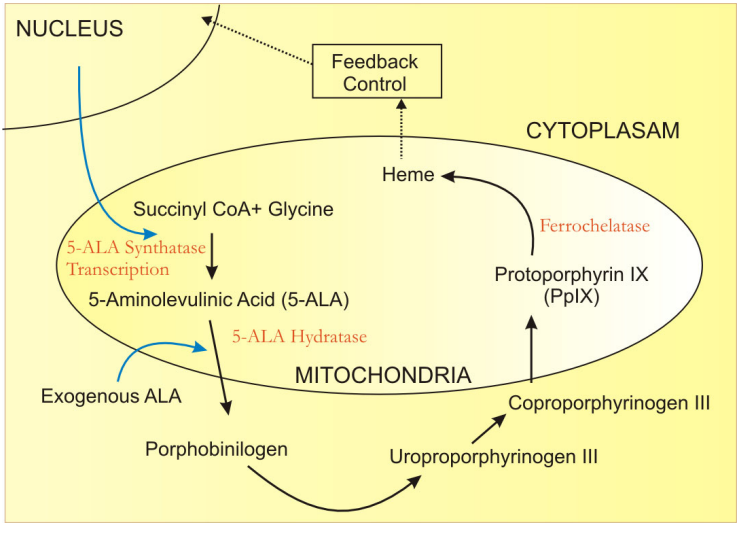

Fig. 2.8 Biosynthetic Heme pathway and conversion to PpIX.

(CoA), catalysed by *5-aminolevulinic acid-synthase (ALA-S)* located in the inner mitochondrial membrane, which is considered to have a regulatory function on the biosynthesis of heme. As can be seen from the Fig. 2.8, second step involves the formation of coprpporphyrinogen III, which is a cytosolic process. In this particular step, two molecules of 5-ALA enters into cytosol from mitrochondria to form porphobinilogen, in the presence of *5-ALA dehydratase* as enzyme. Porphobinilogen, which is the precursor of the pyrolle ring undergo a biochemical reaction in the presence of *deaminase* and *isomerase* as enyme to form uroporphyrinogen III. Decarboxylation, catalyzed by *uroporphyrinogen carboxylase* uroporphyrinogen III to coproporhyrinogen III. Finally, in the third step, when the reaction re-enters the mitochondria, the coproporphyrinogen III get converted to protoporphyrin IX (PpIX), after decarboxylative and oxidative processes in the presence of molecular oxygen.

In normal tissue, the last step has a rate-limiting function, which is the incorporation of Fe^{2+} into PpIX by the enzyme ferrochelatase. All enzymatic steps in the process are irreversible. The heme thus produced is then coupled to various proteins and forms the conjugated proteins, viz. hemoglobin, myoglobin, cytochrome C, and catalyses and peroxidises. There is a negative feedback in the system on the enzyme ALA-S by the final product heme at several stages and there is an action directly on the final protein product.

However, in abnormal pre-malignant and malignant lesions, due to the lack of activity of the enzyme ferrochelatase (EI- Sharabasy et al., 1992; Hillegersberg et al., 1992; Leibovici

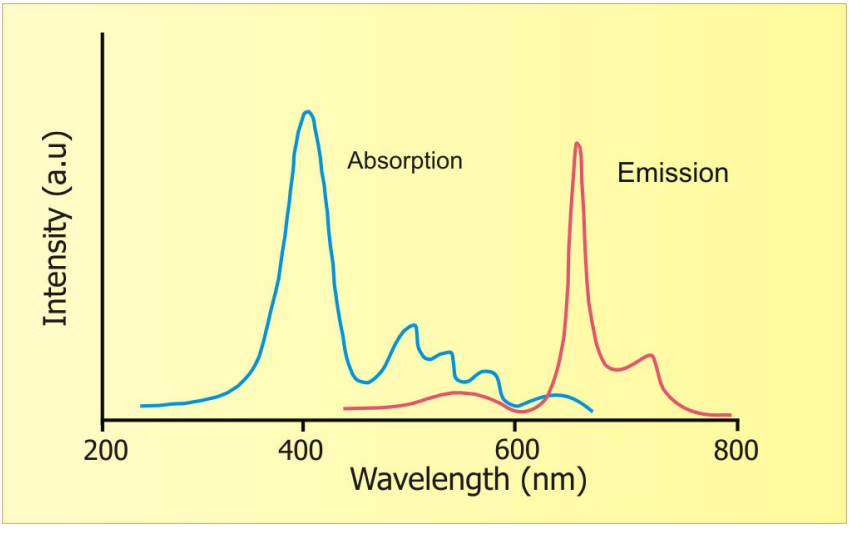

Fig. 2.9 PpIX Absorption and emission and absorption spectra with their constituent peaks.

et al., 1988; Dailey and Smith, 1984), the production of heme is hindered and the enzyme catalyzing third step of the pathway - deaminase, exhibits an increased activity (Hinnen et al., 1998; Leibovici et al., 1988). This results in the selective accumulation of PpIX (Heyerdahl et al., 1997; Regula et al., 1995) and its pre-cursors Coproporphyrinogen III and Uroporphyrinogen III (Moesta et al., 2001). Thus, by tracking the fluorescence emission from the PpIX and its pre-cursors, the abnormalities in tissues can be monitored, following illumination with a suitable laser light tuned to the absorption peak of the PpIX. Fig. 2.9 shows the absorption and emission spectra of PpIX with the prominent absorption peak located at 405 nm and the fluorescence emission Charecterized by dual peaks at 635 and 705 nm.

2.3.3.3 LIAF in Cancer Diagnosis: Current Status and Trends

The feasibility for tumour demarcation in certain clinical specialties were carried out using LIAF spectra (Andersson-Engels, 1992). Many researchers have investigated laser-induced autofluorescence (LIAF) from tissues in the head and neck region and in various other organs, like bronchus, colon, cervix and esophagus for developing a non-invasive screening methodology for early diagnosis of cancer (Park et al., 2008; de Veld et al., 2004; Wu et al., 2003; Lin et al., 2001; Eker et al., 2001; Gillies et al., 2000; Qu et al., 2000; Betz et al., 1999; Wagnieres et al., 1998; Schantz et al., 1998; Richards-Kortum and Sevick-Muraca 1996; Ramanujam et al., 1994; Schomacker et al., 1992). Studies carried out in human tissue resected at surgery or biopsy from patients with cancer affecting different organs, such as uterus (Majumdar et al., 1996), breast (Mohanty et al., 2001; Majumdar et al., 1999; Jain et al., 1998; Gupta et al., 1997) and oral cavity (Majumdar et al., 1998, 1999; Roy et al., 1995) have shown that autofluorescence spectroscopy can provide good discrimination between cancerous and non-cancerous tissues.

Tissue fluorescence signatures are of significance, because spectral changes reflect changes in metabolic activity and communication between the epithelium and stroma. During the process of carcinogenesis, alterations occur in morphohistological characteristics and physiochemical compositions of the fluorophores, such as elastin, collagen and NADH present in human tissue thereby making LIAF spectral features sensitive to the tissue alterations (Richards-Kortum and Sevick-Muraca, 1996; Drezek et al., 2001). Savage et al (1995) had used different intensity ratios including red-blue ratios at various excitation wavelengths to differentiate malignant and normal lateral tongue.

Different excitation wavelengths or light sources were used to maximise emission from the tissue fluorophors. Excitation at 375 nm from a xenon lamp was utilised by Sterenborg et al (1994) for autofluorescence imaging of skin cancer. In an *in vivo* study of oral and skin SCC in hamsters it was observed that transformation from normal to pre-malignant or malignant grade is accompanied by an increase in the red/orange fluorescence intensity ratio (Van der Breggen et al., 1996). The results obtained demonstrated the potential of autofluorescence ratio to differentiate between normal and CIS in the cheek pouch during

the early stages of growth. The autofluorescence spectra of oral mucosa were studied in detail (Ingrams et al., 1997) and optimal excitation wavelengths were identified for *in vivo* detection of oral neoplasia (Heintzelman et al., 2000). Noninvasive diagnosis of cancer based on fluorescence spectroscopy and native tissue autofluorescence was also carried out in oral cavity (Gillenwater et al., 1998a) and aero digestive tract (Gillenwater et al., 1998b).

Recently, Svistun et al (2004) have observed maximum contrast in characterization of freshly resected oral tissues by observing autofluorescence spectra at 530 nm by illumination at 400 nm with a xenon lamp. Tissue fluorescence was viewed on a SLR Canon camera with a 100-mm micro lens and a broad band (60 nm) filter. The sensitivity of 91% and specificity of 86% obtained for discrimination of normal tissue from neoplasia compares favourably with the sensitivity of 75% and specificity of 43% obtained with white light illumination. This study demonstrated that oral cavity fluorescence can be viewed in real-time by human eye. Subsequently, Lane et al (2006) developed a simple, cost-effective handheld device that allows the clinician to discriminate malignant tissue by direct visualization of tissue fluorescence. Clinical trials on 44 patients with this system gave a sensitivity of 98% and a specificity of 100% in discriminating normal mucosa from severe dysplasia/carcinoma in situ (CIS) or invasive carcinoma.

A clinical trial using a Xenon lamp based fluorospectrometer with 330 nm excitation showed that the ratio of the area under the autofluorescence emission peaks at 460 and 380 nm decreased as the tissue transformed to oral submucal fibrosis from normal mucosa, but failed to distinguish normal mucosa from epithelial dysplasia and hyperkeratosis (Tsai et al., 2003). Partial least squares and artificial neural network (PLS-ANN) classifications were used in conjunction with autofluorescence spectroscopy to characterize oral lesions and discriminate pre-malignant and malignant tissues from benign tissues in patients and a sensitivity of 81%, specificity of 96% and positive predictive value of 88% were obtained (Wang et al., 2003). deVeld et al (2004) have also carried out a clinical study for classification of benign, dysplastic and malignant oral lesions using autofluorescence spectroscopy

Fluorescence from cervical lesions have been monitored in vitro and in vivo for investigating the pre-cancerous stage of cervical cancer known as cervical intraepithelial neoplasia (CIN) by various research groups (af Klinteberg, 1997; Ramanujam et al., 1996; Mahadevan et al., 1993). Photo detection of cervical intraepithelial neoplasia using 5-ALA induced porphyrin fluorescence was carried out by Hillemans et al (2000). The classification of CIN encompasses both dysplasia and carcinoma in situ (CIS). These studies were directed towards both the *in vivo* autofluorescence and ALA induced fluorescence spectral characteristics from normal and CIN, in combination with routine colposcopy and histopathological examination of biopsies. Ramanujam (2000) has given a review of application of fluorescence spectroscopy for detection of neoplastic and non-neoplastic cervical tissues. Kennedy et al (1992) had used the endogenously accumulated PpIX as a natural photosensitizer for phtotherapy of cancers.

2.4 Exogenous Flurophores and Tumor Marking Substances

The ability to detect lesions by LIAF can be further enhanced by the use of exogenous fluorophores or fluorescent tumour markers or photosensitizers. Tumour marking substances can be used both as an aid for characterization of various diseases and in treatments, especially related to oncology. When such substances are applied, it will selectively accumulate in malignant tissues within a certain time period. The abnormalities can then be detected from tissue fluorescence, when illuminated with UV and near UV-VIS light, the process often known as photodynamic detection (PDD). When the accumulated flurophore is irradiated at higher energies with appropriate laser light, a photochemical reaction is triggered leading to selective cell destruction or necrosis by a process known PDT. Most exogenous flurophores currently being evaluated as contrast agents for cancer detection are photosensitizers that can be used for PDT. The commonly used photosensitizers include hematoporphyrin derivative (HpD), pheophorbide-a, meso-tetra-hydroxy-nphenyl-chlorine (mTHPC), benzoporphyrin derivative (BPD), and a mixture of different kinds of porphyrins, chlorines and phthalocyanines.

Porphyrins have a structure similar to the heme molecule of hemoglobin (Fig. 2.10). Their photosensitizing properties and tumour selective accumulation of HpD were investigated in the first half of the last century, and had been used for fluorescence PDD and PDT in many studies later(Dougherty et al., 1992; Daniell and Hill, 1991; Lipson et al., 1961; Figge and Weiland, 1948). These porphyrin compounds have strong absorption characteristics in the blue spectral region around 400nm (the Soret band), or up to the highest Q-band at 635 nm, resulting in fluorescence between 625-710 nm (Bonnett et al., 1989). The fluorescence is characterised by a dual peaked emission in the red-wavelength region, at about 635 and 705nm. These agents accumulate in malignant or pre-malignant lesions to a higher degree than in healthy tissue, and their fluorescence will add features to recorded fluorescence spectra. This signal contributes to the difference in fluorescence spectra recorded from deceased and normal tissue and helps in demarcating the diseased lesions from the normal surrounding tissue.

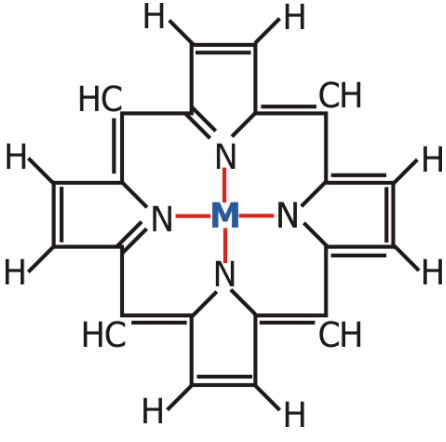

However, the main disadvantage of porphyrin compounds is their low rate of clearance from the body which causes long-

Fig. 2.10 Porphyrin ring structure, here M represents the incoprated metalic ion. During the formation of formation of Heme molecule Fe^{2+} ion is incoparated.

lasting tissue phototoxicity (Kennedy et al., 1992). Therefore, the evaluation of other tumour markers and photosensitizers becomes an interesting topic of research. A variety of compounds including anionic lipophilic photosensitizers and cationic photo sensitizers have been investigated in search for the ideal photosensitizer.

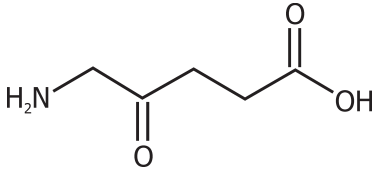

Fig. 2.11 Chemical structure of 5-ALA.

An ideal phtosemnsitizer should have following properties a) high degree of selective accumulation in malignant tissue b) good tissue penetration c) ability of self destruction through photobleaching. Many new products are being regularly discovered, though very few have made it to clinical trials and even fewer are readily available commercially. In the present study, we deal only with the 5-ALA induced porphyrin fluorescence for PDD of oral cavity carcinomas.

2.4.1 5-ALA Induced Protoporphyrin in Abnormal Tissues

One of the most promising photosensitizer that is available today is 5-ALA or δ-ALA (also known as ALA), which is a 5-carbon, straight chain amino acid (Fig. 2.11). It is chemically stable around and below a pH of 5, but can react irreversiblywithseveral condensation products at higher pH (Novo et al., 1996). ALA is a naturally occurring compound that does not fluoresce by itself but its transformation product PpIX, via Heme cycle fluoresces strongly. When ALA is supplied in excess, the negative feedback is bypassed and the capacity of ferrochelatase is exceeded as explained earlier. Porphobilinogen deaminase (PBGD) has shown to exhibit an increased activity and ferrochelatase a reduced activity (Kondo et al., 1993) in malignant tissue resulting a relative selective accumulation of porphyrins(Heyerdahl et al., 1997). On the other hand, PpIX has a natural "clearance mode" by its subsequent transformation to heme in normal tissues. It was Ghadially et al (1963) who suggested the use of non-photosensitising 5-ALA to induce photoactive PpIX. In 1999, ALA was approved in the USA for PDT of skin cancers and actinic keratosis. During recent years, d-Aminolevulinic acid (ALA) has become widely used as photosensitizer. The advantages of using ALA over the other photosensitizers PDD are:

1) Shorter duration of photo-sensitization: ALA induced PpIX is cleared from tissue within 24 hours after administration as compared to other photosensitizers such as HpD or Photofrin which persist in tissue for up to two months causing prolonged photo sensitivity.

2) Easy administration: ALA gets easily dissolved in water and in a lage number of solvents and emulsions. So, it can be administered either systemically (oral, I.V and intra dermal) or topically. Topical application targets only the treatment area and reduces systemic photo-sensitivity and side effects. Cutaneous lesions are easily sensitized with topical preparations; other tumor locations need systemic sensitization.

3) High selectivity: ALA induced PpIX fluorescence has shown sensitivity a of 95-100% and specificity of about 50-60% for oral cancer diagnosis.

4) Possibility of repeated treatments: ALA is an endogenous substance associated with low toxicity even when given in excess. The topical application of ALA induces PpIX fluorescence and photo sensitization, which remain localized to the site of application.

5) Short accumulation time: Maximum built up of PpIX occurs in about 3-4 hours after administration, but accumulated quantity of PpIX declines to zero over the next 24 hours due to metabolisation to heme by other routes.

6) Follow up treatment by PDT: Since PpIX gets selectively accumulated in cancerous cells, following photodiagnosis the patients could be treated by PDT using a strong light or laser source at 635 nm.

The disadvantages of using ALA are limited. In very few cases when high dosages were given, there were reports of nausea and vomiting. There were also reports of rise in liver enzymes and total bilirubin in some patients. ALA is a hydrophilic molecule that does not easily penetrate intact skin. The keratin layer of the skin is the main barrier for ALA when topically applied (Suhonen et al., 1999; Williams and Barry, 1992; Landmann, 1988; Menton and Eisen, 1971). For cutaneous lesions, however, this layer is usually damaged; resulting in an increased penetration of ALA and thus an enhanced selective accumulation of PpIX.

2.4.1.1 ALA Induced PpIX Fluorescence in Cancer Diagnosis Current Status and Trends

Many research groups have successfully used ALA as tumour marker on the skin (Hewett et al., 2001) and in the bladder (Riedl et al., 2001; Wang et al., 1999) and in the cervix (Bogaards et al., 2002a,b), and to a limited extend in the GI tract (McKechnie et al., 1998a,b). 5-ALA induced fluorescence has also been used in patients for diagnosis of cancer in various locations, such as the lung and bladder with promising results (Filbeck et al., 1999; Baumgartner et al., 1996; Kriegmair et al., 1996). A detailed review of the application of fluorescence diagnosis using both autofluorescence and ALA fluorescence have been published (Prosst and Gahlen, 2002). Betz et al (2002) has carried out an assessment of the advantages of ALA induced fluorescence and autofluorescence over visual inspection for diagnosing oral cancer.Areas with hypertrophic tissue and inflammatory diseases were investigated and normal tissue types, including buccal mucosa, tongue and skin were also studied by ALA induced fluorescence (Svanberg and Svanberg, 1999; Wang et al., 1999; Svanberg et al., 1994).

Fluorescence diagnosis of superficial cancer using ALA has been developed both as point-monitoring and multi-colour fluorescence imaging (Svanberg et al., 1998, Harris et al, 1995; Andersson-Engels et al., 1994). Treatment of oral leukoplakia was also carried out with the help of 5-ALA in some patients (Kubler et al., 1998). Detection of SCC of the oral cavity by imaging 5-ALA induced PpIX fluorescence was made by Leunig et al (1996).

Charoenbanpachon et al (2003) has developed a means to accelerate topical ALA-induced PpIX fluorescence with DMBA cheek pouch carcinogenesis produced dysplasia in hamsters.

Scott et al (2000) has used red to green fluorescence ratio imaging technique that showed good contrast enhancement between normal and cancerous lesions after topical application of 5-ALA. Zheng et al (2002) has developed a digitized endoscopic imaging system to classify normal, carcinoma in situ (CIS) and invasive SCC of oral cavity using red-to-blue fluorescence imaging ratios after topical application of 0.5% of ALA . In the case of brain tumours and other diseases 5-ALA based PDD and PDT has also been studied clinically (Friesen et al., 2002; Kennedy et al., 1996).

2.5 Diffuse Reflection Spectroscopy (DRS)

2.5.1 Physical Basis of Diffuse Reflectance

Diffuse reflectance (DR) technique involves detection and analysis of a portion of the incident light that undergoes multiple elastic scattering owing to inhomogeneities in the refractive index of tissue components (Fig. 2.12). The theory of diffuse reflection has been studied in detail by many authors (Wendlandt and Hencht, 1966; Kortum, 1969). When an inhomogeneous material is illuminated, some of the impinging radiation penetrates the sample and some is reflected from the surface. The portion that penetrates the sample undergoes scattering at a large number of points in its path. The fraction of radiation that comes back out of the sample is called diffusely reflected component. The returning reflection of the directional incoming radiation flux is scattered in many directions due to uneven, broken, bumpy boundary surfaces, where the coarseness is of the same order of magnitude as the wavelength. In contrast, direct or specular reflection occurs when the roughness of the boundary is small in comparison with the wavelength of the reflected radiation. Recent results have shown that tissue back scattering is altered as the size of the nucleus increases and the nuclear texture becomes coarser (Perelmann et al., 1998).

The probability that photons reach a certain depth in the tissue before they are reflected back and detected is highly dependent on the source-detector geometry; indicating that the effective volume of the tissue visited by the detected photons depends on the specific arrangement of the source and detector fibers in the probe, in addition to the tissue optical properties (Jayachandran et al., 2007; Godavarty et al., 2004;

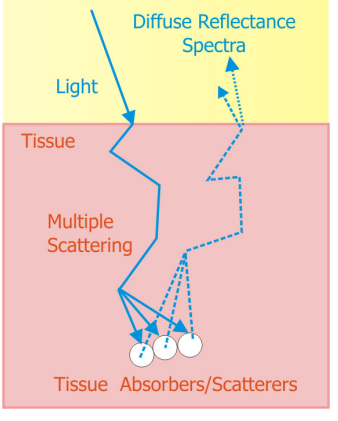

Fig. 2.12 Diffuse reflectance after multiple scattering and absrption from various tissue components at macrolevel.

Utzinger et al., 2001). By illuminating the tissue with continuous-wave white light from an optical fiber, and collecting the emanating light at various distances using several other fibers, the optical properties of tissue absorption and scattering coefficients can be calculated (Nicholas et al., 1997; Weersink et al., 1997; Farrell et al., 1992). According to the law of reflection which applies in this case, the angle of the incident and reflected rays form the same angle with the normal in reference to the reflecting surface at the point of incidence. Fig. 2.13 shows the different geometries of the illumination and collection fibers that are possible.

Fiber-optic probes that selectively collect DR light from the epithelium and underlying stroma improve *in vivo* diagnostic performance as reflectance features unique to each layer could be measured. DRS is capable of providing information on changes that occur during tissue transformation and fiber-optic probe designs that selectively collect light from the

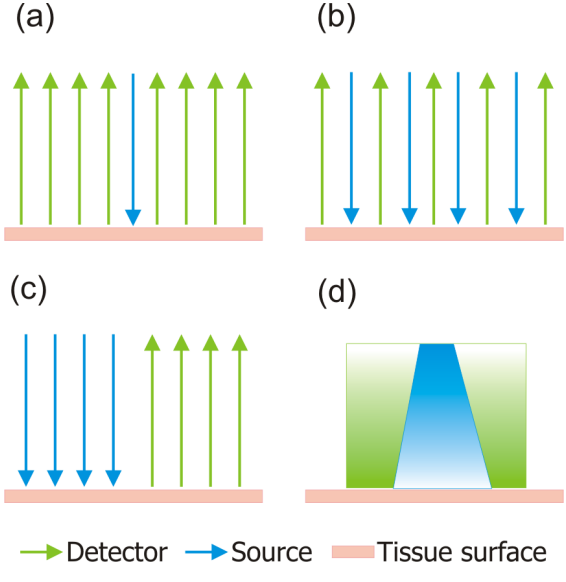

Fig. 2.13 Different measurement geometries **(a)*** single point illumination and sequential/simultaneous multiple point collection using optical fibers **(b)** sequential multiple point illumination and multiple point collection **(c)** simultaneous multiple point illumination and simultaneous multiple point collection using optical fibers **(d)** area illumination and area detection using an expanded beam of excitation source and a CCD camera. *This geometry is used in our study.

epithelium and the stroma are necessary to exploit the diagnostic signatures specific to these layers. Thus, DRS is a promising technology for detection of epithelial precancer of sites such as intestine, oral cavity and cervix which are generally described as a two-layer media consisting of a thin epithelium on top of an underlying stroma. The various aspects related to absorption have been discussed in earlier sections and the upcoming section elucidates various aspects of light scattering, which plays a vital role in DR of tissues.

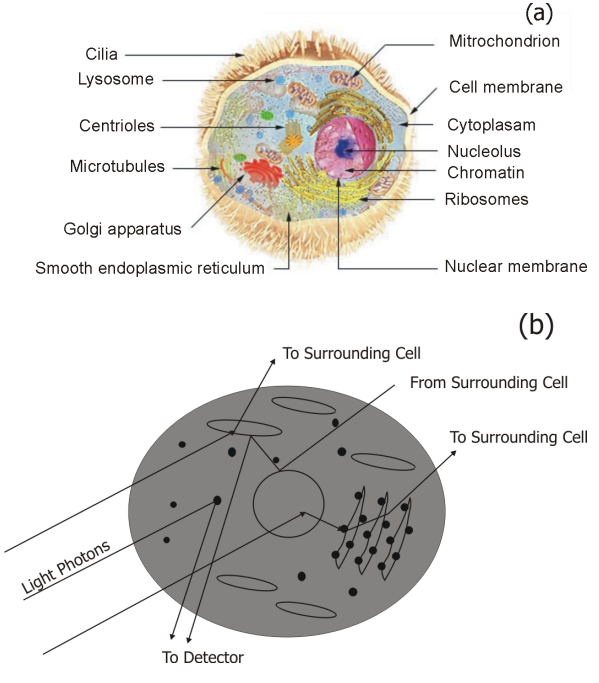

Fig. 2.14 **(a)** Major organelles and inclusion of a cell **(b)** scattering of light photons by various denser organelles like nucleous at the micro level. This occurs because of the gradient in refractive index, resulting from differences in densities and compositions of sub-cellular structures viz. nuclei, mitrochondria and other cellular oraganelles.

2.5.2 Scattering

Many biological tissues are anisotrophic (Tuchin VV, 1994, 1993; Mueller and Sliney, 1989). Light interaction within a multilayer and multicomponent skin is a very complicated process (Anderson and Parrish, 1982). Biological tissues are optically inhomogeneous with an absorbing media whose average refractive index is higher than that of air. This leads to partial Fresnel reflection of light radiation at the tissue-air interface, while the remaining part that enters into tissue undergoes multiple scattering and absorption. The light propogation within a tissue depends on the scattering and absorption properties of its components (Fig. 2. 14a).

Tissue contains many light scattering particles, such as cell nuclei and organelles and light scattering is basically affected by tissue morphology, such as nuclear size distribution, epithelial thickness and collagen content, all of which changes with cancer development (Mourant et al., 2003, 2000; Drezek et al., 2003). Healthy epithelial tissues often consist of well-organized layers (Fig. 1.6) with en face diameter of 10-20μm, quite uniform in size (Tuchin VV, 2007). During transformation, cells proliferate and appear with an enlarge nuclei when stained and enlarged nuclei are primary indicators of cancer and dysplasia in human tissues (Backman et al., 1999).

Where as absorption depends on the biomolecules in the tissue, scattering is due to spatial variation in the refractive index of larger macroscopic structures. The macroscopic average refractive index of most tissues lies in the 1.38-1.41 range at 633nm (Beuthan et al., 1996; Tearney et al., 1995, Bolin et al., 1989). Wavelength dependence of the scattering properties of tissues not only changes the total autofluorescence intensity by multiple reflections within the tissue, but also the spectral shape. Since the distribution of scatterers within the tissue is not known, these artifacts cannot be completely removed from the autofluorescence spectra. Fig. 2. 14b depicts the scattering of the light photons by various cell components and Table 2.4 provides the values of refractive index of various cellular components at 500 nm.

Histopathologists indentify tissue alterations by looking microscopically on the nuclear size of the cells and their statrified cellular distributions. Hence, changes in the nuclei of epithelial cells are important indicators of pre-invasive cancer. The fact that these changes alter the scattering properties of the epithelium indicates that epithelial scattering contains significant diagnostic information. Thus, isolation of epithelial scattering is likely to prove invaluable in correlating optical signatures with the corresponding tissue histopathology, and in assessment of the sensitivity and specificity of optical technologies targeting non-invasive detection of pre-cancerous changes.

2.5.3 DRS in Cancer Diagnosis Current Status and Trends

Among new quantitative optical techniques, DRS is one of the simplest and most cost-effective methods for understanding biological tissue characteristics (Volynskaya et al., 2008; Niedorf et al., 2005; Irving and Stephen 2004; Finlay, 2003; Feld, 1999; Palmer et al., 2002; Nicholas et al., 1997; Mahadevan-Jansen and Richards–Kortum, 1996). The application of RSS has been quite useful for characterization of small tissue samples and different cell layers with high sensitivity and specificity, but its application in a clinical environment is still very difficult (Bakker et al., 2000; Mahadevan-Jensen and Richards-Kortum, 1996). On the other hand, the potential for using DR spectroscopic techniques is greater because elastic interactions are much stronger than inelastic interactions. Several researchers have used diffuse reflectance spectroscopy to study biological tissues and in tissue characterization (Mirabal et al., 2002; Nordstorm et al., 2001; Koenig et al., 1998; Farell et al., 1992). Many of the instruments developed and tested both *in vitro* and *in vivo*, show promise to increase both sensitivity and specificity, e.g. tomography (Li et al., 2003; Jiang et al., 2002; Hebden et al., 2001, Pogue et al., 2001), multi-spectral transillumination optical imaging (Pifferi et al., 2003; Grosenick et al., 2003; Fatini et al., 1998), and functional spectroscopic techniques (Cerussi et al., 2002; Tromberg et al., 2000, 1997; Shah et al., 2001).

DRS techniques involves detection and analysis of a portion of the incident light that undergoes multiple elastic scattering owing to inhomogeneities in the refractive index of the tissue. The contrast between normal and abnormal tissue types in all these techniques relies on differences in the optical properties, i.e. in the reduced scattering and absorption

coefficients. For example, tumor absorption contrast could be associated with an increase in the blood volume and increase in the oxygenation consumption (Thompson and Tatman, 1998; Beauvoit et al., 1994). Tissue absorption in the UV and visible region is dominated by hemoglobin, with the oxygenated and deoxygenated forms having different absorption spectral features (van Zijlstra et al., 1991)

Trimodal spectroscopy using fluorescence, reflectance and light scattering was used by Georgakoudi et al (2001) individually and in combination, for evaluating low and high grade dysplasia in patients with Barrett's esophagus. They found that reflectance and light scattering spectroscopy provide morphologic information on tissue architecture and epithelial cell nuclei. Zonios et al (1999) used analytical diffusion model for diffuse reflectance data from human adenomatous colon polyps to fit an analytical model and found that differences can be attributed to hemoglobin concentration and effective scatterer size.

Elastic light scattering spectroscopy with polarized illumination/detection that reduces contribution from hemoglobin absorption was used by Sokolov et al (1999) to characterize *in vitro* cervical biopsies and *in vivo* oral cavity mucosa. Utizinger et al (2001) has investigated the slope of reflectance spectral features between 530 and 585 nm at different source-detector separations for *in vivo* characterization of ovarian cancer and found that reflectance spectral slopes between 510 and 530 nm gets strongly affected by oxy- and deoxy-hemoglobin absorption and provides useful discriminatory information. The diffuse reflectance spectrum shows characteristic hemoglobin absorption valleys at 430, 542 and 577 nm on excitation with white light and it is reported that hemoglobin content is more pronounced in malignant and premalignant lesions owing to increased microvasculature (Zonios et al.,

Table 2.4 List of approximate values for optical index of refraction of different cellular components (adopted from Irving and Stephen, 2004; Bolin et al., 1989; Tuchin V, 2007)

Cellular components	Wavelength (nm)	Index of refraction (n)
Water	*500*	*~ 1.33*
Extra cellular fluid	*500*	*~ 1.34-1.35*
Intra-cellular fluid	*500*	*~ 1.35-1.36*
Proteins	*500*	*~ 1.40*
DNA	*500*	*~ 1.44*
Bi-lipid membrane	*500*	*~ 1.46*
Mealnin	*500*	*~ 1.65*
Cytosol	*633*	*~1.38*
Membrane structures	*633*	*~1.48*
Dermis	*337, 577, 633*	*~1.50*
Epidermis	*337, 577, 633*	*~1.40*

1999). Further, these oxy- and deoxy- hemoglobin bands, seen in both normal and malignant tissues, have been utilized to extract intrinsic tissue fluorescence that is free from artefacts induced by tissue scattering and absorption (Georgakoudi et al., 2002). Many researchers have explored the use of reflectance to correct the tissue fluorescence spectral data and for understanding the effect of changes in oxygenation and tissue perfusion (Diamond et al., 2003; Muller et al., 2001; Zang et al., 2000; Coremans et al., 1997). The complimentary nature of diffuse reflectance and autofluorescence its application to correct distortions in the measured autofluorescence of oral mucosa was investigated by de Veld et al (2005a).

Numerous optical models and systems developed based on this technique have shown potential to discriminate malignancy with good sensitivity and specificity. Diffuse reflectance spectroscopy is a promising technology for detection of epithelial pre-cancers. The diffuse reflectance between 350and 750 nm affected by nuclear-to-cytoplasmic ratio was used by Mourant et al (1995) to distinguish malignant from non-malignant sites in the bladder with a sensitivity of 100% and a specificity of 97%. Ge et al (1998) used an algorithm that utilized intensities at the absorption peaks of oxy- and deoxy- haemoglobin to distinguish neoplastic from non neoplastic sites in colonic tissue and reported a sensitivity of 86% and specificity of 84%. Reflectance spectroscopy was used to detect Barrett's oesophagus with an agreement of 71% for diagnosis by four different pathologists (Feld, 1998).

Even though malignant lesions of the oral cavity could be reliably distinguished from healthy mucosa, correct classification by Principal Component Analysis (PCA) of benign from dysplastic and cancerous tissue types was difficult due to the low overall specificity of 77% and sensitivity of 69%. Very recently, a comparative study of PCA with Monte Carlo inverse model was carried out for diagnosis of oral and breast cancer using DR spectroscopy in the UV-VIS region (Skala et al., 2007; Zhu et al., 2006). The diagnosis of breast cancer carried out by Bigio et al (2000) based on elastic scattering spectroscopy (ESS) has yielded sensitivities of 69% and 58% and specificities of 85% and 93% for breast tissues and sentinel nodes, respectively, using artificial neural networks (ANN).

Using pattern recognition techniques such as multivariate discriminant analysis, the same group developed algorithms to classify ESS spectra as premalignant or benign for Barret's oesophagus (Lovat et al., 2006). When the same data set was analyzed using hierarchical cluster analysis (HCA) the corresponding sensitivities and specificities were 67%, 91% and 79%, 77%, respectively. Preliminary ESS studies on gastrointestinal tissue involving colon, rectum and stomach by Mourant et al (1996) have shown the potential of using the area under absorption dips, spectral slope from 435 to 440 nm and signal ratios in the near-UV and red spectral regions to discriminate various tissue types. In a similar study using ESS and PCA, Anjan Dhar et al (2006) differntiated different colonic pathologies by applying linear discriminant analysis to the spectra and acheived a sensitivity of 85% and specificity of 88% in distinguishing colonic dysplasia from colitis.

Collecting photons that scatter only in the epithelium and do not penetrate into the

stroma is a challenging but non-trivial problem. Depth resolution is clinically important since spatial localization of information obtained during *in vivo* measurement aids in interpretation of tissue spectra. This is particularly important when multilayered tissues are being investigated. If different layers are selectively targeted, spectral information unique to each layer can reveal various aspects of dysplastic progression thereby increasing the diagnostic potential of optical spectroscopy. Recent computational and experimental studies analyzing the influence of fiber-optic probe design parameters on depth sensitivity have focused mainly on fluorescence measurements. Therefore, fiber-optic probe design plays a crucial role in obtaining depth-resolved spectroscopic information. Amelink et al (2004) used differential path-length spectroscopy (DPS) based on diffuse reflectance to determine the local capillary oxygenation, blood volume fraction, blood vessel size and wavelength dependence of the scattering coefficient *in vivo*. DPS also gives information on the local tissue content, the average micro-vessel diameter, and β-carotene concentration and the scatter slope (van Veen, 2005). Since all these parameters may be related to local morphological and physiological changes occurring during malignant transformations, the study could establish DPS as a tool to discriminate pre-malignant lesions from normal mucosa.

2.6 Conclusion

DRS, LIAF and 5-ALA induced fluorescence spectroscopy are potential tools for photodiagnosis of cancer that can be used separately or in conjunction for tissue characterization, as in the case of trimodal technique. Based on the developments in optical spectroscopy techniques, a compact, non-invasive, near real-time optical point-monitoring system was designed and developed for early detection of oral pre-malignancies. The next chapter depicts the details the system developed for *in vivo* and *ex vivo* measurments, alongwith various ethical issues, study protocol, and different methods of data analysis and interpretation.

Chapter 3

Instrumentation, Materials & Methods

Instrumentation, Materials & Methods

3

3.1 Introduction

Recent advances in fiber optics, light sources, detectors and computer-controlled instrumentation have stimulated unprecedented growth in the development of photonic technologies for a wide variety of diagnostic applications. The use of non-invasive optical techniques for detection of tissue abnormal conditions is a rapidly emerging area in the field of biophotonics. Among the most promising approaches to screen and diagnose epithelial cancers are those that rely on quantitative measurements of tissue fluorescence and diffuse reflectance.

All biological tissues emit fluorescence when excited by UV or near UV or VIS light. It is reported that early cancerous tissues have a different autofluorescence emission spectrum than healthy tissues (Hung et al, 1991). Although modifications of the autofluorescence spectra originate in the structure of tissues or in metabolic processes, the reasons for these changes during early stages of tumor growth remain controversial and have been widely studied. They can be sorted into two broad categories: biochemical effects and architectural effects. The variations in Heam production also influence the spectral shape of tissue autofluorescence and diffuse reflectance. Therefore, the use of autofluorescence and diffuse reflectance spectral techniques still remains a pragmatic approach for tissue characterization.

The intensity difference of autofluorescence between normal and tumour tissue has been exploited for PDD, particularly for detection of early lung tumours (Majumdar et al., 2003; Mayinger et al., 2003; Lam et al., 1993; Hung et al., 1991). Various techniques have been established recently that combine multiple excitation and/or detection wavelengths with intensity ratios to discriminate the tissue autofluorescence from the fluorescence of externally administered fluorescent markers, thereby improving tumour demarcation (Anderson-Engels et al., 1997; Leunig, 1996). An important advantage of intensity ratio is that it minimizes the influence of variations in the excitation and detection geometry and enhances the contrast between tumour and adjacent normal tissue. Changes in the intensity of PpIX emission after application of ALA and their ratios have also been utilized to screen cancers affecting various organs that are easily accessible.

Further, it is known that cancerous tissues exhibit increased microvasculature and blood content and low hemoglobin oxygenation due to disturbed metabolism (Jain, 1988; Vaupel, 1996). Alterations in nuclear size distribution, epithelial thickness and collagen content during early stages of cancer development in epithelial tissues also contribute to alterations in the diffuse reflectance spectra (de Veld et al., 2005b; Zonios et al., 1999). The availability of efficient, compact light sources and delivery systems has provided impetus for the application of fluorescence-based diagnostic techniques (Profio and Balchum, 1985).

3.2 Point Monitoring Systems

The last decade have seen an impetus research and productivity in the tissue optics especially, in the field of tissue monitoring research for diagnostic purposes. Frequently, these non-invasive optical biopsy systems are point-monitoring and imaging systems. Point-monitoring systems perform spectral measurement from a small point or area (usually as small as the dia. of the excitation fiber) of the sample using an optical fiber probe having excitation and pick up fibers to guide and to collect light. The light collected from the samples, are very weak, especially fluorescence. The measurement of such "cool" fluorescence light can be achieved by using detection systems coupled with sensitive CCD cameras and proper filtering systems. It is important to note that in clinical studies using ESS or DRS to date, the methodology is point monitoring rather than imaging modality.

In order to facilitate simultaneous point monitoring of fluorescence and diffuse reflectance characteristics in a clinical environment, we have built a laser-induced fluorescence and reflectance spectroscopy (LIFRS) system that has the ability to measure reflectance and faint fluorescence spectral signals. As mentioned before, the binding thread of all this study is the use of optical spectroscopy with the LIFRS that has been built in-house to perform all spectral measurements in one go.

3.3 Development of LIFRS System for Detection of Oral Cancer

The LIFRS system designed and built for point monitoring of tissue fluorescence and diffuse reflectance is shown in Fig. 3.1. A tungsten-halogen lamp (Ocean Optics Inc., USA, Model: LS-1-LL) is used as the white light source for reflectance measurements; whereas a nitrogen laser (Laser Science Inc., USA, Model: VSL-337, 30 kW peak power, 120μJ pulse energy) pumped dye laser (Laser Science Inc., USA, Model: DUO-110, 40uJ) emitting at 405 nm provides the excitation beam for laser-induced fluorescence (LIAF) studies. The N_2 laser was operated at a repetition rate of 7Hz and the output energy was focused on to the fiber tip with the help of the Hyrax fiber-optic focusing assembly (Laser ScienceInc., USA, Model: 337702). The two light sources could be alternatively switched on/off for recording of the fluorescence and diffuse reflectance from the same sampling location. These two light sources were connected to the two legs of a bifurcated optical fiber (Ocean Optics Inc., USA, BIF 200 UV-VIS) whose third leg guides the radiation to a 3 meter long, reflection probe (Ocean Optics Inc., USA, ZR400-5 VIS-NIR) that is terminated in a stainless steel ferrule of 15 cm length and 6 mm dia. (Fig. 3.2, 3.4).

This reflection probe consists of an illumination fiber at the centre and six pick-up fibers, all of 400μ dia. for collection and transmission of fluorescence/reflectance from the tissue to a miniature fiber-optic spectrometer (Ocean Optics Inc., USA, Model: USB2000-FL). Fig. 3.3 represents the optical geometry of collection and illumination fibers, adopted in this work. During fluorescence stud-ies, the light emission from the tissue passes through a long-wavelength pass filter (Schott GG420) fitted in the in-line filter holder (Ocean Optics

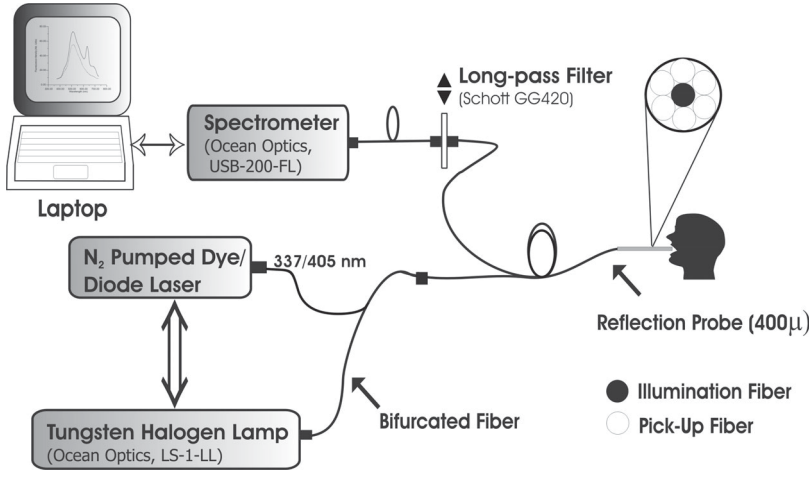

Fig. 3.1 Schematic of the LIFRS system and system developed for cancer diagnosis.

Inc., USA, FHS-UV), which blocks the back scattered excitation laser light from reaching the spectrome-ter. The spectrometer is conn-ected to the USB port of a laptop computer for control of spectral acquisition and data storage. The LIAF and DR spectrum were recorded in the 420-720nm spectral range with a resolution of 8 nm on the 2048-element linear silicon CCD array of the spectrometer with the help of the OOI Base32 software provided by Ocean Optics.

The stainless steel ferrule at the probe tip enables sterilization before and after use in boiling water. A flexible 10 mm long, black PVC sleeve was inserted at the probe tip to avoid ambient light from entering the detection system (Fig. 3.2). The separation between the probe tip and the sample was optimized (by observing the output

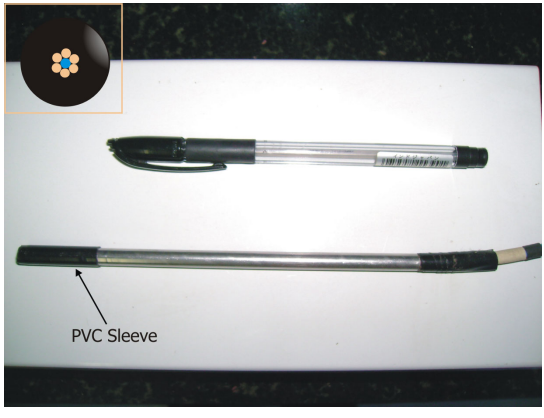

Fig. 3.2 Stainless extreme of the reflection measuring probe inserted with PVC sleeve. In subset 6-around-1 close geom-etry to ensure the highest fluorescence yield, optimized over-lapping of excitation and emission areas, of the reflection probe is exhibited.

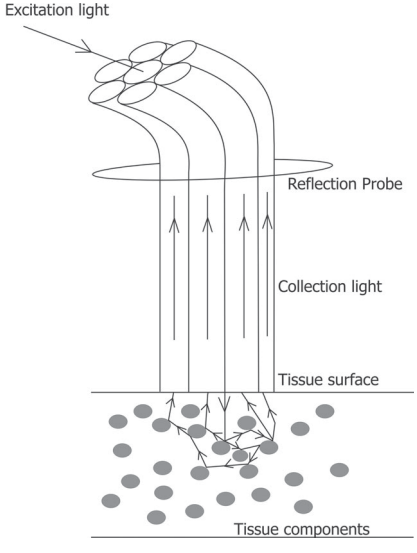

Fig. 3.3 The optical geometry of the delivery and collection fibers of the probe.

signal) to a distance of 3.5mm; wherein the excitation beam completely overlaps with the collection area. At this distance the total circular tissue area irradiated by the illumination fiber is approximately <5 mm^2 (for an illumination radius of 1.25 mm). The PVC sleeve is discarded after spectral measurements in each patient to provide extra hygiene. During spectral measurements the average out put power at the illumination fiber tip is measured and maintained at 1±.05mW using a optical power meter (Ophir, Israel, Model: Nova) with a suitable photodiode head (Ophir, Israel, Model: PD300). Total light dose on tissue during the spectral measurement is measured in J/cm^2, which is the product of the fluence rate and the illumination time [3.1].

Light dose (J/cm^2)= Fluence rate (W/cm^2) x Illumination time (Sec) [3.1]

In the present study the laser light dose incident on the tissue during each measurement period was 0.2 J/cm^2 and this radiation dose was very low to cause any tissue damage.

3.3.1 Compact LIFRS System for Clinical Studies

The main drawback of the LIFRS system shown in Fig. 3.1 when used with a nitrogen laser pumped dye laser was the large footprint of the system

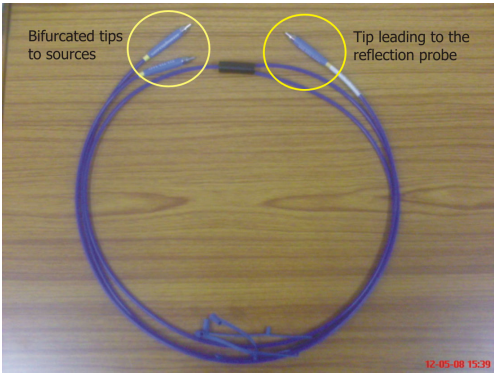

Fig. 3.4 Bifurcated fiber (200 µ dia.) cable was used for guidance light of laser and tungsten-halogen sources to tissue. Bifurcated tips were connected to the Laser and tungsten halogen lamp, while the rest is connected to one of the tip from the reflection probe.

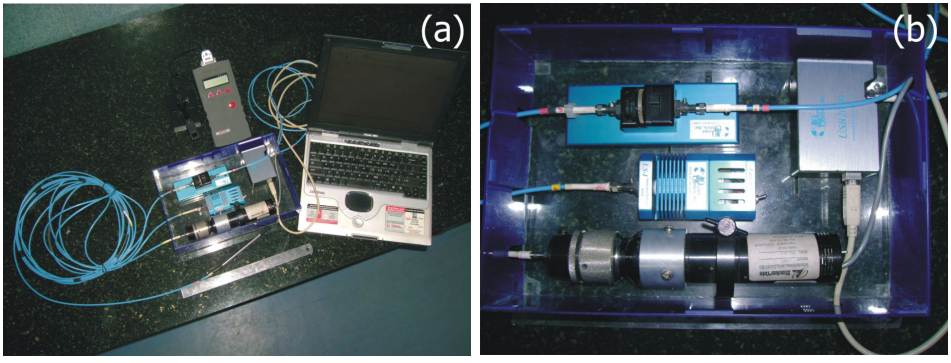

Fig. 3.5 **(a)** The compact diode laser based LIFRS optic fiber system developed for clinical studies of oral cancer **(b)** closer view of the central unit of the portable LIFRS, with diode laser at the bottom, spectrometer to the right top, in-line filter holder at top and tungsten halogen lamp positioned at centre of an acrylic box of dimensions 12 x 8 x 3 inches.

and the low output power available for excitation of fluorescence, which affected the signal to noise ratio of the detection system (Fig. 3.6). Hence, the nitrogen pumped dye laser was replaced with a 405 nm violet diode laser (Stocker Yale Inc., Canada, Model:TEC-XXX-404S-50-SF) with a CW power of 50 mW. This laser can also be operated in the pulsed mode up to a repetition rate of 10 kHz, although we used the system in CW mode. The entire system including the laser, tungsten halogen lamp, the inline filter holder and the miniature spectrometer was enclosed in a rectangular box of dimensions 12 x 8 x 3 inches made of acrylic sheet. The fiber optic cables and power supply chords were taken out through slots made in the box. These cables could be easily detached and refitted, without the need for realignment, to get the required power levels at the fiber tip. Fig. 3.5a shows the portable LIFRS system and Fig. 3.5 b, a birds-eye-view of the central unit.

3.3.2 Choice of Light Source and Wavelength

Both coherent lasers and filtered non-coherent light sources can be utilized for the diagnostic purposes. However, high monochromaticity, coherence and intensity of lasers coupled with their low divergence permits one to choose them for fluorescence measurement applications that require matching of excitation wavelength with the tissue flurophore being studied. Since, most of the work presented in this thesis work relate to fluorescence emissions from PpIX, which is selectively accumulated in the abnormal tissues, a diode laser emitting at 405 nm, which matches with the strongest absorption band of PpIX, is used. The excitation of abnormal tissues with this wavelength emission peaks at 635 and 705 nm (Fig. 2.10, Chapter 2). For diffuse reflect-ance tissue studies, a tungsten halogen lamp is used as the white light source, since it is cheaper as compared to other lamps like Xenon flash lamps and mercury arc lamps, which need additional filters to remove unwanted peaks present in

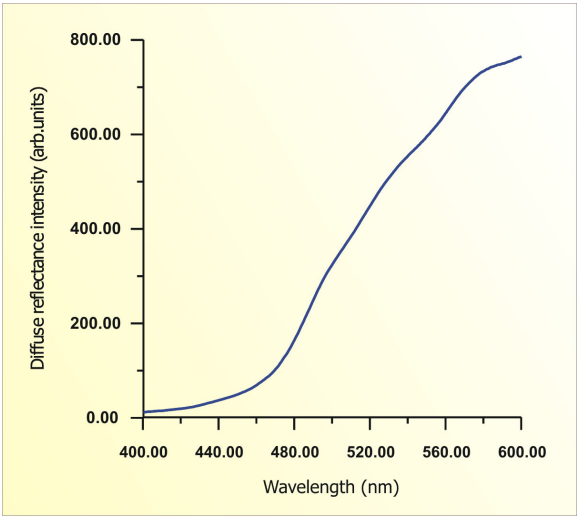

Fig. 3.6 Tungsten halogen lamp spectra recorded in 400-600 nm wavelength region, from a ground glass plate.

their emission. However, tungsten halogen lamps are free from such peaks in the entire visible spectral region (Fig. 3.6).

3.4 Data Acquisition and Analysis

3.4.1 Data Collection Using OOI Base32 Software

The probe is sterilized before use and the optical fiber light couplers are aligned to provide a Gaussian beam profile at the fiber tip. Before each set of measurement the laser power at the fiber tip was monitored using a laser power meter. The fluorescence and diffuse reflectance spectra were recorded from selected sites of the tissue by point monitoring. Mild pressure was applied to the PVC sheath covering the probe tip to avoid target movement and to avoid room light from entering into the detection system. Fig. 3.7 is a screen shot of the fluorescence spectra recorded using the OOI Base 32 program with the eightfluorescence spectra recorded from a lesion of the same patient flaked over one other. The OOI Base32 software was configured to record the spectra, averaged for 40 pulses, with a boxcar width of 8-10 nm and an integration time of 100ms.

3.4.2 Corrected Autofluorescence

Eight sequentially recorded LIAF and DR spectra from the same tissue location are manually selected and averaged. A simple model is adopted to obtain a first order

approximation of corrected autofluorescence as used by de veld et al (2005a), by dividing LIAF spectra with the corresponding DR spectra of the same tissue site. The model can be explained as follows:

For diffused light, the total diffuse reflectance $R_d(\lambda)$ and recorded autofluorescence $F_r(\lambda)$, can be expressed as a fraction of the total incident flux, which is related to the tissue absorption coefficient $\mu_a(\lambda)$ by

$$R_d(\lambda) = {}_e\text{-}\mu_a(\lambda)\langle l\rangle_{r,\lambda} \qquad [3.2]$$

$$F_r(\lambda) = {}_e\text{-}\mu_a(\lambda)\langle l\rangle_{f,\lambda} \qquad [3.3]$$

Where $\langle l\rangle_{r,\lambda}$ and $\langle l\rangle_{f,\lambda}$ are expected mean pathlength travelled by DR and LIAF photons in the tissue. All these variables are wavelength-dependent. For any given wavelength, there will be a difference in mean expected pathlengths for DR and LIAF light.

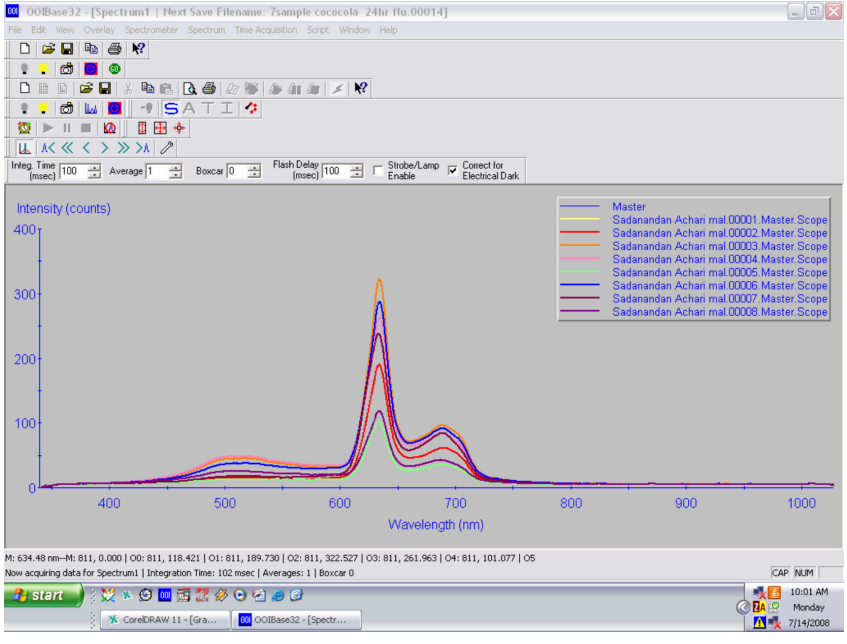

Fig. 3.7 Screen shot of the OOI Base 32 program showing eight measurements from the lesion of a patient.

Therefore, one can write

$$\langle I \rangle_{f,\lambda} = k(\lambda).\langle I \rangle_{r,\lambda} \quad [3.4]$$

Where $k(\lambda)$ depends on the tissue under investigation. Therefore, corrected autofluorescence can be expressed as

$$F_c(\lambda) = F_r(\lambda)/R_d(\lambda) = F_r(\lambda)/R_d(\lambda)^{k(\lambda)} \quad [3.5]$$

$k(\lambda)$ is defined as the ratio between the pathlengths for fluorescence and diffuse reflectance light, and is independent of wavelength. In this simple model homogeneous distribution of scatterers and fluorophores is assumed with constant absorption coefficient at all locations, which depends on wavelength of the photons. However in reality, this is not exactly the same case due to the inhomogeneous distribution of the scatterers. Nonetheless, based on the results (see chapter 7) this simplification was enough to remove or smoothen the absorption dips without affecting the florescence spectra.

3.4.3 Curve Fitting of LIAF

In order to determine the peak positions of constituent bands and their relative contributions to the overall emission, the corrected LIAF spectra were analyzed by curve-fitting using Gaussian spectral functions (Microcal Origin, Ver. 6.0)(Details are given in Chapter 7). The curve-fitting program uses the Marquardt-Levenberg algorithm that finds the true absolute minimum value of the sum of squared deviations (the value of c^2) by an iterative process. The correlation coefficient (r^2) and (c^2)values determine the quality of fit (Subhash and Mohanan, 1997; Subhash et al., 2005). The number of peaks chosen should be minimized for obtaining a best fit of the spectra, as evidenced from the values of r^2 (closest to unity) and low c^2 values. The curve fitted parameters like the peak amplitude, peak center shift, FWHM width of the peak, and the Gaussian curve area were utilized to understand tissue progression or transformation.

3.5 Laboratory Evaluation of LIFRS instrument

Prior to using the LIFRS system for clinical trials, the device was tested in the laboratory by measuring the autofluorescence, 5-ALA-induced PpIX fluorescence and diffuse reflectance spectra of *ex vivo* tissues of the oral cavity immediately following surgery (without fixing or immersion in any solvent). In this study the tissue removed from the margin area was used as control (Subhash et al., 2006). The LIF spectral intensity and curve area ratios of the different bands were used to discriminate malignant from normal tissue and to classify oral cavity cancer according to their grade. Further, the uptake of ALA by different tissues of the oral cavity was studied from the intensity of the porphyrin bands after topical application of 5-ALA on the tissues. The fluorescence intensity ratios of the emission bands as well as the diffuse reflectance ratio of the oxygenated hemoglobin absorption peaks were used in the grading of SCC.

3.6 Clinical Trials

3.6.1 Ethical Clearance for the Study

A protocol for clinical trials was prepared for screening of oral cancer using tissue autofluorescence, diffuse reflectance and 5-ALA (5-aminolevulinic acid) induced protoporphyrinIX (PpIX) fluorescence. The study involved measurements to diagnose oral cavity cancer by carrying out measurements from malignant and adjoining normal tissues, followed by histopathological analysis of the biopsies taken from the measurement sites for correlation. After obtaining the permission of the Ethics Committee (S. No. HEC/02-2005/14, dt. 14/02/05), approval from the Drug Controller, Government of India, was obtained to use 5-ALA (Medac, Germany) in patients as part of these trials. Patients who present themselves at the OP clinic were considered for enrollment in the trial.

3.6.2 Eligibility Criteria for the Subjects

Following Inclusion and exclusion criteria was followed for selecting patients for the spectral measurements.

- Patients attending OP clinic for oral cancer screening and treatment
- Consent patients above 18 years
- Able to read, understand and sign informed consent
- No previous treatment for cancer with radiation
- No application of any medication orally for at least 4 weeks
- The patient should be free from any other serious disease

3.6.3 Human Oral Anatomy

The oral cavity of is unique in structure. The surface of the oral cavity is a mucous membrane. Its structure varies in an apparent adaptation to the function of different regions of the oral cavity. On the basis of these functional criteria, the oral mucosa may be divided in to three major types (1) Masticatory mucosa like gingiva and hard palate (2) Lining or reflecting mucosa (inner lip, buccal mucosa, lower and upper alveolus, floor of the mouth, transition to floor of mouth, softpalate (3) specialized mucosa (dorsum and lateral side of tongue (DST, LST). Fig. 3.8 sketches the 13 anatomical sites of human oral cavity selected for spectral measurements. For descriptive purposes the oral mucosa may be divided into the keratinized and non-keratinized areas. The masticatory areas and vermillion border of lip (VBL) belong to keratinized type while lining mucosa and specialized mucosa belongs to non-keratinized type.

3.6.4 Conduct of Clinical Trials

The enrolled patients and their bystanders were explained in detail about the modalities of the study and its intent. Written informed consent of the patient was obtained before initiation of any measurement. Trials have been carried out in 50 patients (Fig. 3.9) and from 13 anatomical oral cavity sites of 36 healthy volunteers. Before initiation of measurements, the participants were given a mouthwash with 0.9% saline solution to reduce the effects of recently consumed food.

An experienced clinician specialized in the head and neck cancer selected patients suitable lesions and adjoining sites for spectral studies and recorded its visual imprint. Patients received no incentives for participating in this clinical studies. Most of the patients studied had prolonged smoking, pan chewing and/or alcholic consumption habits, whereas, healthy volunteers were free from such habits and had maintained good oral health or hygiene on visual examination. After spectral measurements biosy samples were taken and fixed in 10% formalin solution and sent for histopathological analysis. Histology slides were prepared from fixed tissues and classified by an experienced pathologist who was blinded to spectral results. After classification, the spectral data were correlated with pathological findings. In the case of healthy volunteers, classification was based on visual impression.

3.6.4.1 5-ALA Induced Fluorescence Studies

5-ALA solution at a concentration of 0.4% was prepared by mixing 40 mg of 5-ALA (Medac, Germany) in 100 ml of distilled water. This solution was used as a gargle or mouth wash (topical application) in the oral cavity of patients selected for the study for different time periods (10, 15 and 20 min.), following autofluorescence and diffuse reflectance

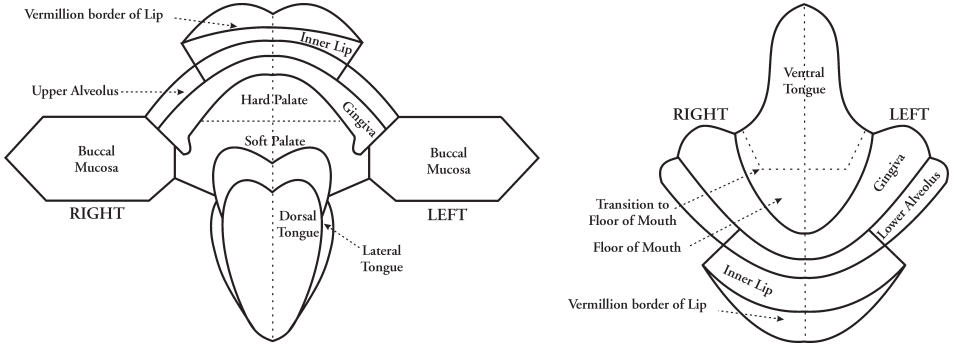

Fig. 3.8 Sketch of 13 anatomical sites of human oral cavity selected for LIAF and DR spectral measurements using LIFRS.

measurements.. Temporal spectral studies were carried out and the entire measurements of fluorescence emission procedure was repeated at different concentrations(0.2%, 0.3% and 0.5%) of ALA.

During *ex vivo* studies, topical application of 5-ALA cream prepared by mixing 30 parts of emulsifying cetylstearyl alcohol (Type A), 35 parts of thick viscous paraffin and 35 parts of white Vaseline with the requisite amount of 5-ALA was used.

3.6.5 Blinded and Follow-up Studies

To check the validity of the criteria developed using LIAF and DR spectroscopy a blind test was also carried out on patients at the RCC with clinically low/high risk oral lesions (leukoplakia and erythroplakia). The tissue types were then classified with the help of the criteria developed based on LIAF spectral ratios, and then interrogated with pathological results. Based on this, the sensitivity, specificity, PPV and NPV of the spectral criteria developed were determined.

3.6.6 Tissue Grading

As described in chapter I, 90% of the oral cancers develope in the squamous epithelial tissues. A pathologist grades these tissues according to the variations in nuclear size and

Fig. 3.9 Conduct of clinical trials using the LIFRS system at the OP Clinic of RCC, Trivandrum. The Fig. 1.3 (See chapter 1) is a zoom in to the buccal lesion of the same patient being examined by point monitoring.

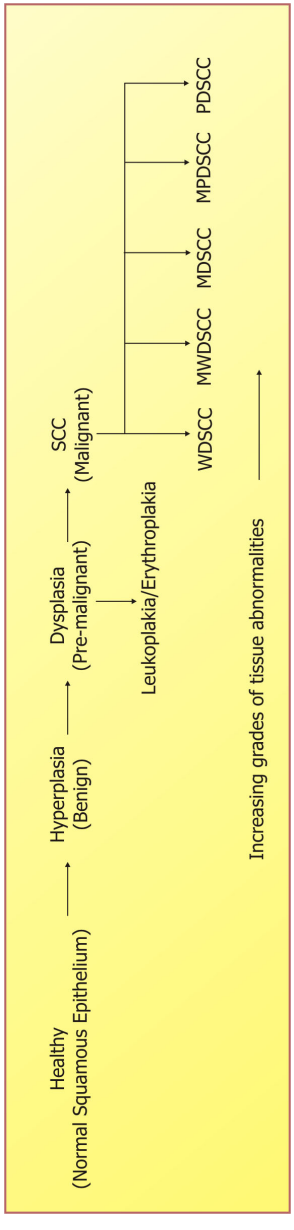

Fig. 3.10 Different conditions of the squamous epithelium with increasing grades of tissue abnormality.

stratified cell structure. In this study, different tissue type are graded using the following terms in an increasing order of tissue abnormality (Fig. 3.10). Epithelial tissues from the healthy volunteers are graded as normal squamous epithelium. The hyperplastic tissues were termed as benign tissues. Clinically observed leukoplakias and erythroplakias, which are pathologically pre-malignant tissues, are grouped as dysplastic. Then again, malignant lesions are usually graded from well to poorly differentiated. Different grades of SCC tissues such as, well differentiated SCC (WDSCC), moderate to well differentiated SCC (MWDSCC), moderately differentiated SCC (MDSCC), moderate to poorly differentiated SCC (MPDSCC) and poorly differentiated SCC (PDSCC), are grouped as malignant.

3.7 Conclusion

As per the objective an optical biopsy system known as "LIFRS" has been developed to facilitate point monitoring of oral cancer and the instrument was tested in the laboratory through *ex vivo* spectral studies on surgically excised tissues. Based on these *ex vivo* results a detail study protocol and procedure was evolved for *in vivo* clinical studies. Results of these *ex vivo* and clinical trials studies are exclusively narrated in the forthcoming chapters.

Chapter 4

Discrimination of Malignant Oral Cavity Lesions using R540/R575 Reflectance Spectral Ratio: An *Ex Vivo Study*

This work is published in:

Journal of Biomedical Opics (SPIE) **11**(1):014018 (1-6), 2006.

Discrimination of Malignant Oral Ccavity Lesions using R540/R575 Reflectance Spectral Ratio: An *Ex Vivo* Study

4

4.1 Introduction

A low-cost, fast and non-invasive method for early diagnosis of oral mucosa based on the analysis of diffuse reflectance spectral signatures is presented. The *ex vivo* diffuse reflectance spectra in the 400-600 nm region is measured from surgically removed oral cavity lesions. Reflectance spectra shows dips at 542 and 577 nm owing to absorption from oxygenated hemoglobin (HbO_2). In this study, we explore the potential of using the diffuse reflectance spectral ratio (R540/R575) of the oxygenated hemoglobin absorption bands for detection of oral cavity SCC.

4.2 Study Materials and Protocol

Tissue samples from different anatomical sites of oral cavity, like the tongue, lower alveolus and buccal mucosa were brought to the laboratory for examination from the Regional Cancer Centre (RCC), Trivandrum, immediately after surgery without fixing in any solvent.

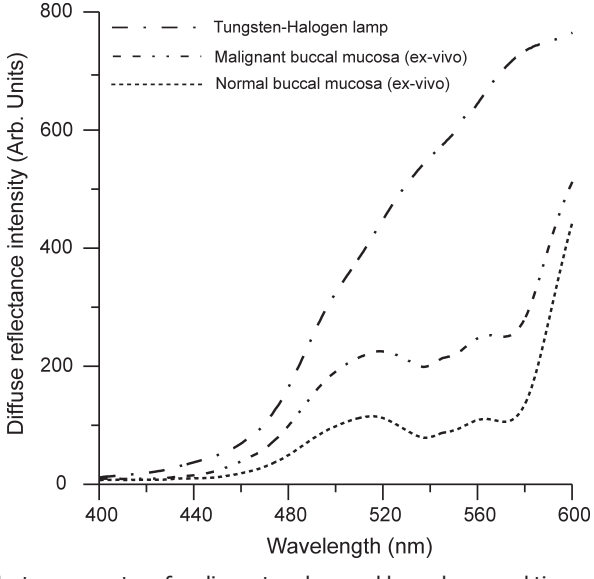

Fig. 4.1 Mean reflectance spectra of malignant and normal buccal mucosal tissues superimposed on the diffusely scattered light from a tungsten-halogen lamp for comparison.

All the measurements were carried out within 90 minutes of surgery. The dimension of the excised tissues was of the order of 1-2 cm in length, 1-1.5cm in breadth and 0.5-1cm in thickness. The tissue removed from the margin areas adjacent to the lesion were also studied, with the intention of using these as control. The lesions removed from different patients had varying grades of SCC and belonged to different parts of the oral cavity. For comparison with normal mucosal tissues, *in vivo* reflectance spectra from the oral cavity of consenting volunteers were used. This study included six surgically excised samples from lesions and six apparently normal samples from the adjoining lesion. Prior to spectral measurements, tissue samples were washed with saline solution and dried on tissue paper and after the measurements the tissue samples were fixed in 10% formalin and sent for histological correlation.

4.3 Results

The diffuse reflectance spectra depends on tissue morphology, constitution and surface features. Fig. 4.1 shows the mean of 10 measurements of the *ex vivo* diffuse reflectance spectra of the excised lesion from the buccal mucosa of a patient, pathological confirmed as moderate to well differentiated SCC and of an adjoining normal (margin) area. Averaged reflectance spectrum from the diffuse reflectance spectrum of the tungsten halogen lamp, with ground glass plate as scatterer, are also shown in (Fig. 4.1) for comparison. In all our measurements, the reflectance spectral intensity from malignant lesion was always found to be greater than that of normal mucosa. Notable differences were observed in the short wavelength region where the broad hemoglobin (Hb) absorption valley around 420 nm is prominent. Secondary dips in reflectance spectra at 542 and 577 nm owing to absorption from oxygenated hemoglobin (HbO_2) bands are evident in both normal and malignant lesions. As compared to normal lesions, the absorption at 542 and 577 nm bands are more prominent in malignant lesions, indicative of increased Hb presence and microvascular volume.

The reflectance intensity ratio R540/R575 was determined from the recorded spectra of normal and malignant lesions of 6 different patients who had undergone surgical intervention. In order to account for the broad nature of the peaks and sample to sample variation in peak position owing to absorption differences between lesions, the average reflectance intensity over ±5nm interval at the absorption maxima was used to determine the ratio.

Mean R540/R575 ratio, with their standard deviation, are shown in Table 4.1, for normal and malignant tissue samples from various sites of the oral cavity. Irrespective of tissue location, the mean R540/575 ratio was always found to be lower for malignant lesions as compared to the adjoining normal lesion. Significant changes were also noticed in the diffuse reflectance ratio according to the stage of malignancy. In the case of ulcerating and infiltrating, moderate to poorly defined SCC of the tongue, which is the highest grade of SCC studied, the decrease in the diffuse reflectance ratio from 0.94 to 0.82 was found to be maximum (14.63%), whereas in the case of a patient with buccal mucosa pathologically

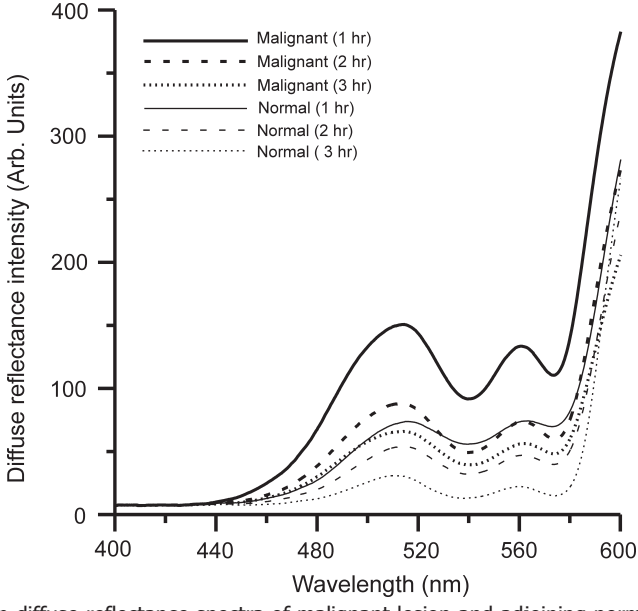

Fig. 4.2 Mean diffuse reflectance spectra of malignant lesion and adjoining normal tissue from the tongue diagnosed as moderate to poorly differentiated SCC. These spectra were recorded after 1, 2, and 3 hours of surgical excision.

Table 4.1 The mean reflectance spectral intensity ratio R540/R575 of surgically excised oral lesions from patients with different stages of oral cavity SCC.

Age (yr)/Sex	Site	Tissue type	N	Mean R545/R575	Varation (%)
48/M	Tongue	Normal	10	0.94±0.07	12.77
		MPDSCC	10	0.82±0.02	
40/M	Tongue	Normal	10	0.81±0.04	11.11
		MDSCC	5	0.72±0.01	
69/M	Lower alveolus	Normal	6	0.79±0.03	10.13
		MDSCC	8	0.71±0.02	
49/F	Tongue	Normal	6	0.81±0.02	9.88
		MDSCC	6	0.73±0.02	
42/M	Buccal mucosa	Normal	10	0.82±0.01	8.54
		MWDSCC	10	0.75±0.01	

SCC-Squamous cell carcinoma; **MPDSCC** - Moderate to poorly differentiated SCC; **MWDSCC** - Moderate to well differentiate SCC; **MDSCC** - Moderately differentiate SCC; **N** - the number of measurements.

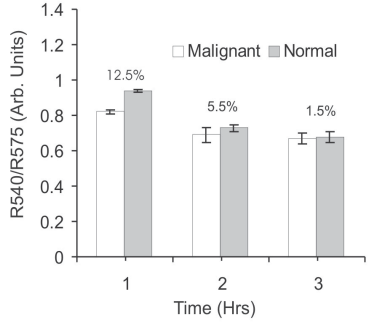

Fig. 4.3 Mean R540/575 ratio of surgically excised malignant lesion of the tongue and its adjoining normal lesion. The percentage decrease in ratio with respect to the normal lesion and standard deviation for each ratio are shown over the histogram bar.

diagnosed as moderate to well defined SCC, the change was minimal (9.33%) from 0.82 to 0.75. Thus, the R540/R575 ratio derived from the oxygenated hemoglobin band absorption appears to be a useful parameter in the grading of SCC of the oral cavity.

The temporal profile of *ex vivo* diffuse reflectance spectra is shown in Fig. 4.2 for tongue lesion. The overall *ex vivo* diffuse reflectance spectral intensity and absorption band intensities at 540 and 575 nm in both normal and malignant tissues were found to decrease gradually during the 3 hour measurement period owing to tissue degradation. During this period, the percentage variation in R540/R575 ratio between the normal and malignant lesions also decreased from 12.5% to 1.5% (Fig. 4.3) thereby demonstrating the need to carry out *ex vivo* diffuse reflectance spectra measurements within the shortest possible time for maximum tissue discrimination.

4.4 Discussion

Tumor or cancerous tissues are known to exhibit increased microvasculature and hence, increased blood content (Jain, 1988). They often have abnormally low Hb oxygenation owing to the disturbed metabolism (Vaupel, 1996). Zonios et al (1999) observed in the case of adenomatous colon polyps an increase in hemoglobin (Hb) concentration, a larger average effective scatter size and a smaller average scatter density but without any significant change in Hb oxygenation. By use of morphometry and vascular casting, they observed that pre-cancerous tissues are characterized by increased microvascular volume. Our results are in agreement with these observations as the malignant tissues exhibit increased absorption at the oxygenated hemoglobin bands and overall enhancement in spectral intensities with concomitant decrease in the R540/R575 reflectance ratio.

Palmer et al (2002) had observed that the reflectance intensities at 415, 540 and 570 nm remained relatively constant over a 90-minute time period. However, in the case of malignant tissues, the decrease of ex *vivo* reflectance intensity at 540 and 575 nm in 120 mins, was 46.2% and 46.7%, respectively. They also reported that the diffuse reflectance of both *ex vivo* and *in vivo* tissues are similar at 500 nm and decreases at longer wavelengths due to tissue de-oxygenation and changes in tissue scattering. Our measurements (Fig.

4.1) also show similarity in reflectance intensity profile in *ex vivo* malignant tissues up to 500 nm and around 600 nm. But, the temporal variations in reflectance intensity (Fig. 4.2) are prominent in the 500-580 nm region where the oxygenated Hb bands are absorbing, whereas at around 600 nm the changes are minimal between normal and malignant tissues. This increase in tissue absorbance is due to increase in hemoglobin absorption and hemoglobin deoxygenation brought about by cell lysing that increases the amount of blood content in tissues (Palmer et al., 2002).

4.5 Conclusions

Studies carried out on surgically excised tissue samples have shown that decrease in the diffuse reflectance intensity ratio R540/R575 of HbO_2 bands at 542 and 577 nm can be used to discriminate between malignant and normal lesions and in determining thegrade of malignancy. Since the normal tissue samples used for comparison were from the tumor margin areas, there is every possibility that some parts of these tissues could also be malignant. Moreover, the *in vivo* diffuse reflectance spectra from the buccal mucosa of healthy volunteers show the absence of the oxygenated hemoglobin bands (Fig. 4.1). Hence, under *in vivo* conditions the changes in the reflectance ratio between normal malignant lesions could be much more pronounced.

Pre-cancerous condition is usually characterized by cellular proliferation, microvasculature and hence, increased volume occupied by cells in tissue. Since visible light penetration is limited to the top one-half millimeter or the mucosal layer, where pre-cancerous changes occur, the diffuse reflectance ratio of oxygenated Hb bands could help in early detection of changes to the mucosal layer. Moreover, since the *ex vivo* and *in vivo* tissues have similar diffuse reflectance spectral features between 400 to 600 nm, the *ex vivo* measurements within a reasonable time frame has the advantage of reproducing clinically relevant *in vivo* conditions. In addition, the oxygenated hemoglobin reflectance ratio technique presented here appears to have the potential for the *in vivo* detection of oral and cervical cancer, and superficial tumors of internal organs, as well. Next section explains an elaborative *in vivo* study using the same technique in an clinical environment.

Chapter 5

Oxygenated Hemoglobin Diffuse Reflectance Ratio for *In Vivo* Detection of oral Pre-cancer

This work is published in:

JB0 (SPIE) **13**(4):041306 (1-10), 2008

Oxygenated Hemoglobin Diffuse Reflectance Ratio for *In Vivo* Detection of Oral Pre-cancer

5

5.1 Introduction

In this clinical trial, we utilize the R545/R575 ratio of oxygenated hemoglobin absorption bands in the DR spectra that were foundto vary with the grade of malignancy under ex vivo conditions, for early detection and grading of oral malignancy in a clinical environment. This chapter presents the results of clinical trials conducted in cancer patients to detect oral pre-cancer using this ratio. For a comparison, in-vivo DR spectra from different anatomical sites of the oral cavity of healthy volunteers were recorded. The R545/R575 ratio was lowest for healthy tissues and appeared to increase with the grade of malignancy. Scatter plot of the R545/R575 ratio was then generated to discriminate different grades of cancer.

5.2 Study Materials and Protocol

The study subjects included 36 healthy volunteers with no clinically observable lesions or inflammatory conditions in their oral cavity and 29 patients with clinically suspicious lesions of diverse grades in their oral cavity. The patients were within the age group of 32-83 years with an average age of 62 years whereas the volunteers were in the 23-28 age group with an average age of 25 years. Reflectance measurements were taken from each of the selected suspicious lesionsand margin areas approximately 1 cm within the lesion boundary with in a 6 mm dia. area (dia. of the probe). In some subjects, measurements were not possible from the margin areas as the lesion had spread all over, whereas in some patients multi-lesions suitable for measurement were present.

Before initiation of measurements, the patients and volunteers were directed to hold 0.9% saline solution for 2-3 minutes to reduce the effects of recently consumed food. After *in vivo* DRS measurements, biopsy specimens were taken from the centre of 6 mm dia area of the lesion/tissue. Since the laser beam illuminates only a small area (1.5 mm in dia.) of the lesion, multiple biopsies were not taken. The spectral ratio (R545/R575) of different patients are then compared with pathological results. Independent Student's t-test was performed on the (R545/R575) ratio between different tissue categories and the predictive values determined were used to determine the statistical significance of the method in differentiating mucosal variations.

5.3 Results

5.3.1 DRS of Healthy Population

Histopathological analysis of the biopsy samples from adjoining areas of malignant

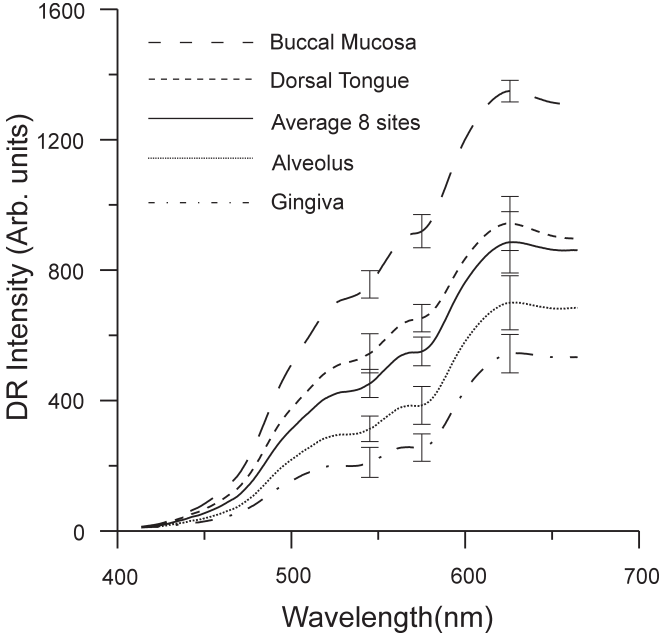

Fig. 5.1 Mean DR spectra from dorsal side of tongue, buccal mucosa, alveolus and gingiva, compared with the average spectra from the other eight sites of the oral cavity. All spectra represent the mean of 10 measurements each in 36 volunteers. The error bars relate to the standard deviations at 545, 575 and 622 nm (maximum intensity in the DR spectra) for different sites.

oral mucosa in patients often show varying degrees of epithelial dysplasia and hyperplasia. Hence, there is every possibility that utilization of the (R545/R575) ratios with respect to these adjoining lesions as control could lead to reduced sensitivities and specificities in diagnosis. In order to overcome this, DR spectral measurements were carried out from 14 different anatomical sites of the oral cavity of healthy volunteers, viz., the right and left buccal mucosa, the gingiva, the upper and lower alveolus, the floor of mouth, the hard and soft plate, the dorsal tongue, the lateral border tongue, the ventral tongue, the inner lip, the vermillion border of lip and the transition of tongue (Fig. 3.1, chapter 3).

The DR spectra of healthy volunteers show dips due to oxygenated hemoglobin absorption at 420, 545 and 575 nm. Fig. 5.1 shows the variation of the mean diffuse reflectance spectra from different sites. The DRS from gingiva and alveolus mucosa show lower reflectance intensities whereas spectra from buccal and dorsal tongue have maximum reflectance. Since the spectral features of right and left buccal mucosa and upper and lower alveolus are similar, these have been grouped and their mean spectra

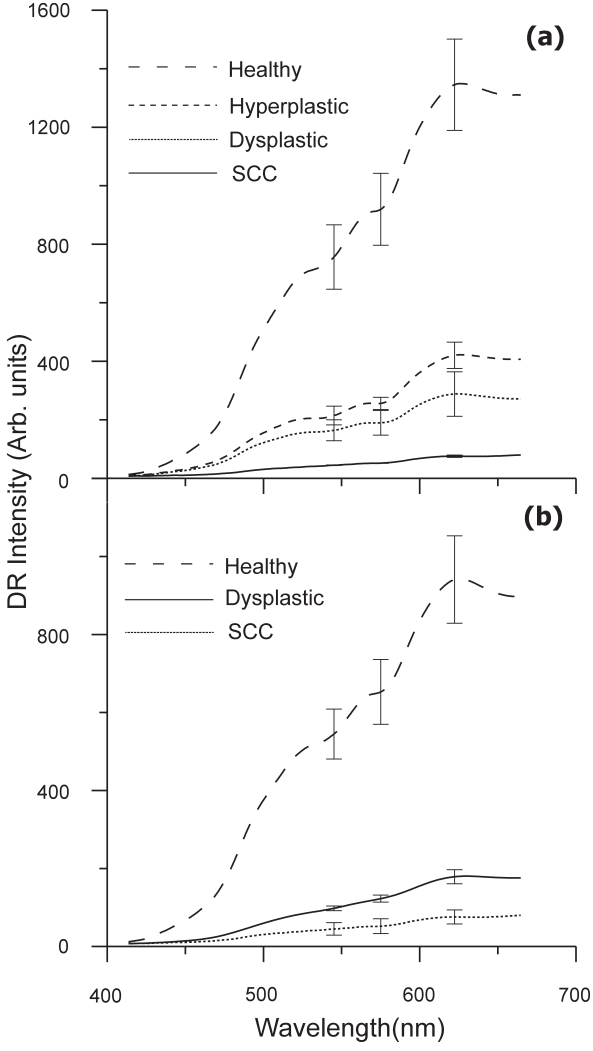

Fig. 5.2 Average DR spectra of patients grouped according to varying grades from a) buccal mucosa (SCC-12 sites, dysplasia-3 sites and hyperplasia-7 sites) of 13 patients and b) dorsal tongue (SCC-7 sites and dysplasia-3 sites) of 6 patients. The healthy spectra represents site-specific mean of 10 measurements in 36 volunteers. The error bars relate to the standard deviations at 545, 575 and 622 nm (maximum of the DR spectra) for different tissue types.

are shown in (Fig. 5.1). The average spectra from all the other 8 anatomical sites that had similar features were grouped together and shown separately.

5.3.2 DRS of Patient Population

We have observed substantial variation in the *in vivo* DR spectral intensities between SCC, dysplasia, hyperplasia and healthy mucosa. Fig. 5.2a shows the mean diffuse reflectance spectra from buccal squamous epithelium of healthy volunteers and from 22 sites in 13 patients with varying grades of malignancy, whereas Fig. 5.2b represents the spectra at 10 sites from the dorsal tongue of 6 patients and the corresponding site-specific healthy tissue spectra. As compared to healthy volunteer spectra, the oxygenated hemoglobin absorption dips at 545 and 575 nm were less prominent in cancerous lesions. The diffuse reflectance of malignant and premalignant lesions is lower owing to increased

Table 5.1 Diffuse reflectance ratio R545/R575 from 48 sites in 29 patients and their histopathological, visual and spectral impressions

Patient No	Site	Visual Impression	Histology	R545/R575	Healthy R545/R575	Spectral impression
1	Buccal Mucosa	Growth	Hyperplasia	0.79	0.758	Hyperplasia
	Buccal Mucosa	Normal	Hyperplasia	0.788	0.758	Hyperplasia
2	Dorsal tongue	Proliferative/ulcerative	SCC	0.865	0.788	SCC
	Dorsal tongue	Normal	SCC	0.867	0.788	SCC
3	Floor of mouth	Proliferative growth	SCC	0.902	0.780	SCC
	Floor of mouth	Normal	Hyperplasia	0.803	0.780	Hyperplasia
4	Lover Alveolus	Ulcerous proliferative lesion	SCC	0.903	0.770	SCC
	Lover Alveolus	Normal	SCC	0.856	0.770	SCC
5	Buccal Mucosa	Large growth	SCC	0.864	0.755	SCC
6	Buccal Mucosa	Verrucous lesions	SCC	0.837	0.755	Dysplasia
	Buccal Mucosa	Normal	Hyperplasia	0.780	0.755	Hyperplasia
7	Upper Alveolus	Ulcero proliferative lesion	SCC	0.876	0.770	Dysplasia
	Upper Alveolus	Normal	Hyperplasia	0.797	0.770	Hyperplasia
8	Buccal Mucosa	Verrucous Leukoplakia	Hyperplasia	0.800	0.755	Hyperplasia
9	Dorsal tongue	Ulcero proliferative growth	SCC	0.876	0.770	SCC
10	Lover Alveolus	Ulcero proliferative growth	Dysplasia	0.812	0.770	Dysplasia
	Lover Alveolus	Normal	Hyperplasia	0.781	0.770	Hyperplasia
11	Buccal Mucosa	Leukoplakia	Dysplasia	0.814	0.755	Dysplasia
12	Dorsal tongue	Leukoplakia	SCC	0.874	0.770	SCC
13	Buccal Mucosa	Leukoplakia	Dysplasia	0.832	0.755	Dysplasia
	Buccal Mucosa	Normal	Hyperplasia	0.815	0.755	Dysplasia
14	Dorsal tongue	Verrucous Leukoplakia	Dysplasia	0.844	0.770	Dysplasia
	Dorsal tongue	Normal	Dysplasia	0.822	0.770	Dysplasia
15	Buccal Mucosa	Leukoplakia	SCC	0.899	0.755	SCC

Table 5.1 (Continued)

Patient No	Site	Visual Impression	Histology	R545/R575	Healthy R545/R575	Spectral Impression
16	Dorsal tongue	Proliferative growth	SCC	0.855	0.770	Dysplasia
	Dorsal tongue	Normal	Dysplasia	0.815	0.770	Dysplasia
17	Floor of Mouth	Ulcero proliferative lesion	SCC	0.871	0.770	SCC
	Floor of mouth	Normal	Hyperplasia	0.836	0.770	Dysplasia
18	Buccal Mucossa	Verrucous Carcinoma	SCC	0.865	0.755	SCC
	Buccal Mucossa	Verrucous Carcinoma	SCC	0.859	0.755	SCC
	Buccal Mucossa	Verrucous Carcinoma	SCC	0.859	0.755	SCC
19	Dorsal tongue	Plaque like lesion	SCC	0.856	0.770	SCC
	Dorsal tongue	Normal	SCC	0.859	0.770	SCC
20	Buccal Mucosa	Ulcero proliferative growth	SCC	0.867	0.755	SCC
	Buccal Mucosa	Normal	Hyperplasia	0.761	0.755	Normal
21	Floor of Mouth	Verrucous growth	Dysplasia	0.837	0.770	SCC
22	Lateral Tongue	Superficial Growth	SCC	0.885	0.770	SCC
23	Hard Palate	Proliferative growth	SCC	0.952	0.770	SCC
24	Buccal Mucosa	Proliferative growth	SCC	0.920	0.755	SCC
25	Buccal Mucosa	Leukoplakia	Dysplasia	0.820	0.755	Dysplasia
26	Ventral Tongue	Ulcero proliferative growth	Dysplasia	0.812	0.770	Dysplasia
27	Buccal Mucosa	Ulcero proliferative growth	SCC	0.878	0.755	Dysplasia
	Buccal Mucosa	Normal	Hyperplasia	0.795	0.755	Hyperplasia
28	Lover Alveolus	Ulcero proliferative growth	SCC	0.814	0.770	SCC
	Floor of Mouth	Ulcero proliferative growth	SCC	0.854	0.770	SCC
29	Buccal Mucossa	Ulcero proliferative growth	SCC	0.856	0.755	SCC
	Buccal Mucossa	Ulcero proliferative growth	SCC	0.860	0.755	SCC
	Inner lip	Ulcero proliferative growth	SCC	0.850	0.770	SCC

absorption associated with tissue vascularity and other inhomogeneities, and varies according to the grade of malignancy.

5.3.3 Oxygenated Hemoglobin Absorption Ratio R545/R575

The mean diffuse reflectance spectral intensity ratio (R545/R575) with respect to the oxygenated hemoglobin absorption dips at 545 and 575 nm was calculated at different anatomical sites in healthy volunteers. The ratio has a minimum (0.75) at the vermillion border of the lip and a maximum (0.79) at the gingival mucosa, with an average of 0.782 when all anatomical sites are considered. Table 5.1 gives the mean R545/R575 ratio in 29 patients having diverse tissue characteristics, compared with the site-specific ratio of healthy volunteers. The results of histopathological examination, visual impression by the clinician and spectral impression based on scatter plots of R545/R575 ratio are also presented in Table 5.1.

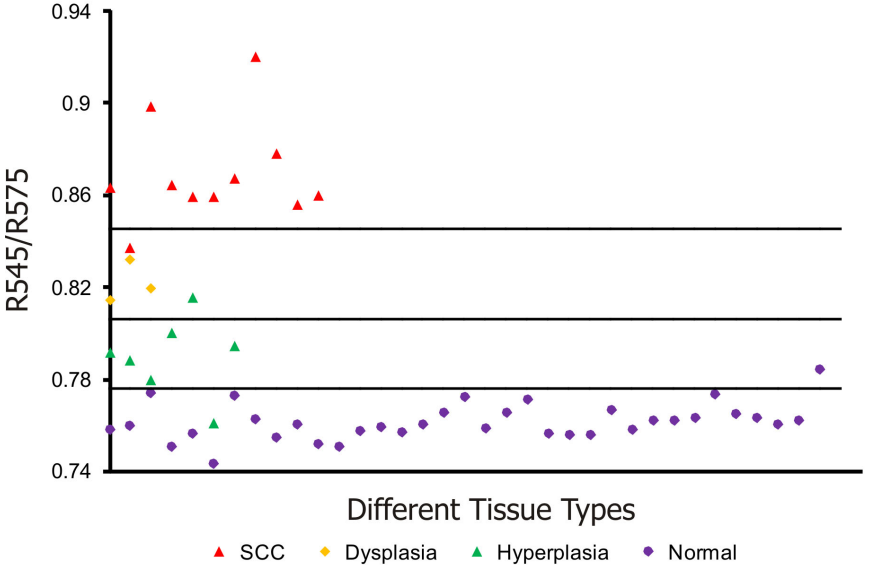

Fig. 5.3 Site-specific DR spectral ratio scatter plots discriminating different grades of cancer from 21 buccal mucosal sites in 12 patients and 36 healthy volunteers.

For ease of comparison, we have grouped the oral mucosa into four categories. The first category consists of healthy volunteer epithelium that is designated as normal; whereas, the second, third and fourth categories comprise of hyperplastic, dysplastic (pre-cancer) and SCC (malignant), respectively. Table 5.2 shows the mean R545/R575 ratio of healthy volunteer tissues and patient mucosa from all sites listed in Table 5.1, regrouped into the above three distinct categories. The R545/R575 ratio is lowest for normal and its increasing trend with higher grades of cancer points to the distinct possibility of using this ratio for tissue classification.

5.3.4 Tissue Classification using R545/R575 Scatter Plots

Histological diagnosis	Population (n)	R545/R575
Normal (healthy)	35	0.782±0.009
Hyperplasia	11	0.795±0.020
Dysplasia	10	0.822±0.012
Squamous Cell Carcinoma (SCC)	28	0.871±0.023

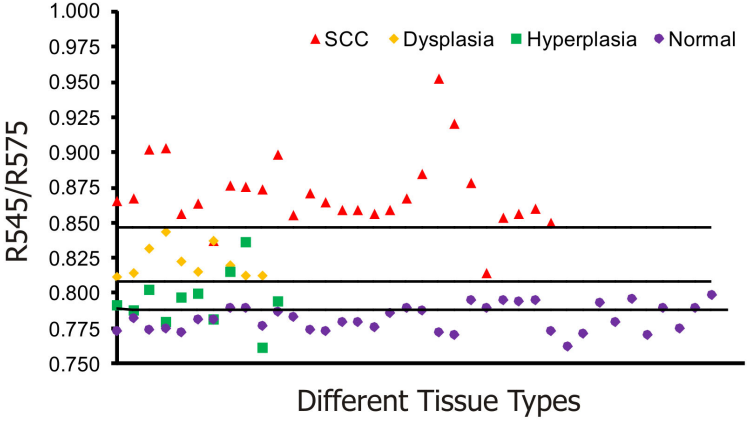

Fig. 5.4 Combined DR spectral ratio scatter plot discriminating different grades of cancer from 48 sites in 29 patients compared with the mean normal values in 36 healthy volunteers.

Fig. 5.3 shows the scatter plot of R545/R575 ratio for discriminating hyperplastic, dysplastic and malignant tissues of the buccal mucosa in 13 patients using site-specific healthy volunteer ratios as normal. Owing to the limited number of patients studied having cancers affecting these sites, the sensitivities and specificities shown may not be representative. Therefore, the mean spectral intensity ratio R545/R575 from all the 48 sites studied, comprising hyperplasia, dysplasia and SCC, for the complete set of 29 patients is plotted in Fig. 5.4 along with the corresponding mean data from 36 healthy volunteers. Discrimination lines are drawn between the normal (average of all anatomical sites) and hyperplasic, hyperplastic and dysplastic, dysplastic and SCC, at values that correspond to the average ratio value of the respective groups. The classification sensitivity and specificity in discriminating each of these categories were determined based on the discrimination threshold values, by validation with the gold standard, viz. histopathological results of biopsy taken from DRS measurement sites.

For example, the cut-off line discriminating the normal from hyperplastic was drawn at 0.789 that corresponds to the mean of the healthy volunteer R545/R575 ratio (0.782) and that of the hyperplastic mucosa ratio (0.795) of patients. Similarly, the other two cut-off lines discriminating hyperplasia with dysplasia and dysplasia with SCC were drawn at their respective mean values and each ratio is assigned a spectral impression based on their position in the scatter plot (Table 5.1).

5.4 Discussion

The mean diffuse reflectance spectra from the epithelial tissues of healthy volunteers and hyperplastic, dysplastic and SCC lesions of patients show distinctive features that relate to their unique oxygenated hemoglobin absorption and scattering properties. The decrease in diffuse reflectance intensity of abnormal mucosa may be explained by increased absorption at the thickened epithelium and local architectural changes at the cellular and sub-cellular levels, including changes in the nuclear-to-cytoplasmic ratio of the epithelial cells, stromal properties and neovascularization, which in turn affects the elastic scattering properties of the tissue (Backman et al., 2000; van Starven et al., 2000).

As observed by Lovat et al (2006) and Amelink et al (2004) we also have noticed that oxygenated hemoglobin absorption dips at 545 and 575 nm are more prominent in healthy volunteers and these dips become less pronounced in dysplastic and are minimal in SCC (Figs. 5.2 a, b). The aforesaid decrease could be explained on the basis of the bio-synthetic Heme pathway (See Fig. 2.8). In the normal biosynthesis of heme, ALA is produced from the condensation of glycine and succinyl-coenzyme A (CoA), catalysed by 5-aminolevulinic acid-synthase (ALA-S), which is located in the inner mitochondrial membrane and is considered to have a regulatory function on the biosynthesis of heme. Several bio-chemical steps involving decarboxylations and oxidations then occur when the molecule re-enters the mitochondria, where the protoporphyrinogen is finally oxidised to protoporphyrin IX (PpIX). The last step has a rate-limiting function, which is the incorporation of Fe^{2+} into PpIX by the enzyme ferrochelatase (See chapter 2, session 2.3.3.2). The limited activity of ferrochelatase in abnormal tissue hinders the conversion of PpIX to heme, which in turn limits the formation of oxygenated hemoglobin and the associated absorption at 545 and 575 nm.

The mean diffuse reflectance ratio (R545/R575) of healthy volunteers was always found to be lower as compared to that from malignant and pre-cancerous sites of patients (Table 5.2). The increase in the value of this ratio points to the grade of malignancy. As the oral mucosal tissues transform from normal to hyperplastic, from hyperplastic to dysplastic and from dysplastic to SCC, the ratio values increase respectively by 1.63, 4.86 and 10.21%.

Sensitivity and specificity (Iain and Gearardo, 2004) of diagnosis were determined using the cut-off lines in scatter plots (Figs. 5.3 and 5.4). Table 5.3 lists the mean sensitivity and specificity of discriminating normal tissues from hyperplastic, hyperplastic from dysplastic and dysplastic from SCC lesions for all the measured sites in 29 patients and specifically of the 21 buccal sites in 13 patients. The improvement in sensitivities and specificities owing to the use of the site-specific R5454/R575 ratios in the scatter plots is marked. In the case of buccal tissues, the sensitivity and specificity for discrimination of hyperplastic tissues from normal gets enhanced from the all-site value of 72% and

77%, respectively to 86% and 97%, with a positive predictive value of 0.86 and negative predictive value of 0.97. However, for discriminating pre-cancerous dysplastic buccal mucosa from hyperplastic tissues, a sensitivity of 100% and specificity of 86% was achieved, with a positive predictive value of 0.75 and a negative predictive value of 1. On the other hand, dysplastic buccal lesions were distinguishable from SCC with a sensitivity of 96% and specificity of 100%, with a corresponding positive predictive value of 1 and negative predictive value of 0.75. The low independent Student's t-test values ($p<0.005$) signifies the relevance of using scatter plots to discriminate different grades of oral mucosa.

In comparison, using trimodal spectroscopy, which is a combination of fluorescence, reflectance and light scattering techniques, Muller et al (2003) had achieved a sensitivity of 64% and specificity of 90% for distinguishing pre-cancerous dysplastic tissues from malignant oral mucosa. During bladder cancer diagnosis with diffuse reflectance, Koenig et al (1998) achieved a sensitivity of 91% and specificity of 60% for distinguishing 9 malignant and 2 dysplastic lesions using an algorithm based on the total amount of blood in tissue. Using different pattern recognition tools on diffuse reflectance spectra, a sensitivity 89% and specificity of 75% was achieved by Ge et al (1998) for identifying colonic dysplasia from hyperplasia. In comparison, Zhu et al (2006) has obtained a sensitivity and specificity of 80% for discriminating malignant and non-malignant breast tissues using both Monte Carlo inverse model and PCA algorithm.

Spectral impression given in Table 5.1 for each site was assigned based on the spectral ratios in the scatter plot (Fig 5.4). Most of the lesions from the margin areas

Table 5.3 Diagnostic accuracies for discriminating different tissue types in a group of 29 patients and results of independent Student t-test analysis of DR spectral ratio R545/ R575

Diagnostic Accuracies	Normal Vs Hyperplasia		Hyperplasia Vs Dysplasia		Dysplasia Vs SCC	
	Average	Buccal	Average	Buccal	Average	Buccal
Sensitivity (%)	72	86	100	100	96	96
Specificity (%)	77	97	82	86	100	100
PPV	0.50	0.86	0.83	0.75	1.00	1.00
NPV	0.90	0.97	1.00	1.00	0.91	0.75
p	<0.005	<0.001	<0.005	<0.01	<0.0005	<0.005

p - Level of statistical significance

that appeared clinically as normal had spectral impressions of dysplasia or hyperplasia. The accuracy of the spectral impressions could be ascertained from the matching histopathological findings in majority of the cases. Further, using these scatter plots, it was possible to accurately categorize the lesion that appeared as ulcerative proliferate growth for the clinicians as SCC, in the case of patient #4, 17, 20, 28, 29 and as dysplasia, in the case of patient #10, 26.

Clinically, leukoplakias are treated as low-risk white patches, which are generally identified histopathologically as lesions linked to hyperkeratosis and hyperplasia, with or without dysplasia. The hyperkeratotic lesion appears white to the clinicians due to the thickened keratin layer, which hinders the light from entering deeper into the tissue and also increases light scattering. Since, hyperkeratosis is often associated with dysplastic and malignant lesions; it is very difficult for the clinicians to decide whether the lesions are malignant, pre-malignant or benign. In two cases (patients #12 and 15, in Table 5.1), tissues with visual impression of leukoplakia were found to be SCC on histological analysis and also with the spectral impression based on R545/R575 scatter plot. Further, in one case where the pathological examination was not able to classify the tissue correctly as SCC (patient # 4 in Table 5.1), it was histologically classified as highly suspicious SCC; but later confirmed as SCC, considering the opinion of the clinician. Such lesions were also classified correctly by the scatter plot algorithm as SCC. Thus, the spectral methodology developed appear to be valid for grading of oral cancer and could act as an adjunct to clinicians in tissue differentiation or speedy diagnosis in a clinical environment for appropriate treatment or surgery.

5.5 Conclusions

The results of the study demonstrate that information provided by non-invasive DR spectroscopy has excellent potential to diagnose oral cancer in its early stages. Information regarding tissue transformation can be obtained *in vivo* with the help of oxygenated hemoglobin spectral ratio, R545/R575, which has the ability to discriminate pre-cancerous dysplastic buccal lesions from hyperplastic tissues with a sensitivity of 100 % and specificity of 86% when site-specific values were used. The DR technique could also discriminate hyperplastic buccal sites from normal with a sensitivity of 86% and specificity of 97%. Further, from the available results, it is seen that the DR methodology has the potential to diagnose tongue pre-cancer where techniques based on tissue autofluorescence have low specificity owing to the presence of porphyrin peaks in healthy tissues (Rupanand et al., 2008; de Veld et al., 2003; Rupananda et al., 2007) (See chapters 6 and 9 for details). Since the DR spectroscopic technique is cost-effective and relatively fast, this modality has the potential to be employed in oral cancer screening programs through community centers and as a tool for biopsy guidance or precise delineation of lesion margins during surgical interventions.

Chapter 6

Clinical Studies for Early Detection of Oral Cancer using LIAF Spectral Ratio Reference Standards

This work is published in:

Cancer (Wiley-BlackWell) **112**(7):1503-1512, 2008 &

Oral Oncology S (Elsevier) 2(1):250-260, 2007.

Clinical Studies for Early Detection of Oral Cancer using LIAF Spectral Ratio Reference Standard

6

6.1 Introduction

Laser-induced autofluorescence (LIAF) is an emerging non-invasive technique in the biomedical field, especially for detection of cancers. Primary objective of this clinical study was to develop a spectral reference standard to discriminate oral malignant squamous cell carcinoma (SCC) from dysplasia and hyperplasia. Towards this, LIAF emission spectra from oral mucosa were recorded in the 420-720 nm spectral range on a miniature fiber optic spectrometer, from 14 anatomical sites of healthy volunteers and 91 sites of patients, with excitation at 404 nm from a diode laser. Histopathological analysis of the biopsy samples showed that oral mucosa adjoining malignant sites in patients are not usually normal, but showed varying degrees of epithelial dysplasia and hyperplasia. Therefore, instead of using LIAF data from apparently normal lesions of patients as control, we have used spectral data values of the oral mucosa of healthy volunteers as control. The broad autofluorescence emission at 500 nm is characteristic of oral mucosa whereas in SCC and dysplastic oral lesions, a new peak is seen at 685 nm in addition to the previously reported peaks at 635 and 705 nm due to protoporphyrin IX emission. In order to facilitate grading of oral cavity cancer, spectral ratio reference standard (SRRS) scatter plots were generated to differentiate the normal mucosa from hyperplasia, hyperplasia from dysplasia, and dysplasia from SCC using the mean fluorescence spectral intensity ratios (F500/F635, F500/705 and F500/F685) measured from 40 sites in 20 patients and 11 sites in 35 healthy volunteers. The sensitivity and specificity of the SRRS to detect tissue transformations are then evaluated. Eventually, the spectral reference database generated was blind-tested on 21 sites in a subject group of 17 patients to check the validity of the methodology developed for early diagnosis of oral cancer. This chapter presents the modality used in the development of the SRRS criteria using LIAF spectral ratios and its application to discriminate mucosal variations and to screen early stages of tissue progression towards malignancy.

6.2 Study Materials and Protocol

The study subjects included 35 healthy volunteers with no clinically observable lesions or inflammatory conditions in their oral cavity and 44 patients having clinically high-risk lesions in their oral cavity. Ninety one sites from which measurements were taken included both suspicious lesions and adjoining mucosa. Apparently healthy tissues adjacent to the lesion (approximately 1cm within the lesion boundary). In some subjects, measurements were not possible from the adjacent mucosa as the lesion had spread all over, while in some patients multi-lesions were observed. In order to develop a site specific database, fluorescence spectra recorded from the oral cavity of healthy volunteer ats 14 different anatomicallocations, viz., the right and left buccal mucosa, the gingiva, the upper and lower alveolus, the floor of

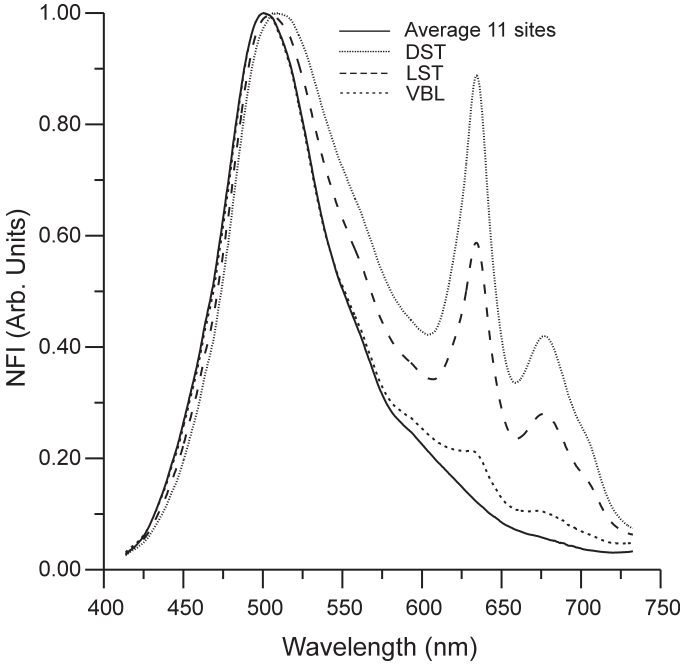

Fig. 6.1 Mean LIAF spectra from dorsal side of tongue (DST), lateral side of tongue (LST) and vermillion border of the lip (VBL) normalized to the autofluorescence peak intensity at 500 nm and compared with the average spectra from all other eleven sites of the oral cavity. DST, LST and VBL spectra represent the mean of 15 measurements each in 35 volunteers, while the average normal spectra relate to the mean of 15 measurements each at 11 sites in 35 volunteers.

mouth, the hard and soft plate, the dorsal tongue, the lateral border tongue, the ventral tongue, the inner lip, the vermillion border of lip and the transition of tongue shown in Fig. 5.1(See chapter 3, Fig.3.8) were used. The LIAF spectra from 11 sites except the vermillion border of lip, the dorsal and the lateral sides of tongue showed similar spectral characteristics with a broad peak at 500 nm. The mean LIAF from 11 sites is plotted along with the spectra recorded from the other three sites that showed dissimilar behavior in Fig. 6.1. Owing to the presence of strong emissions at 635, 685 and 705 nm (as in cancerous lesions) at the vermillion border of lip, the dorsal and the lateral sides of tongue as in cancerous lesions, these three sites were excluded and the total sites available for the study were limited to 61 from 37 patients. Out of these 61 sites, spectral ratios from 40 sites in 20 patients were used for the development of the spectral ratio reference standard (SRRS), while the data from the remaining 21 sites in 17 patients were used for the blind test to validate the reference standard developed.

Before initiation of measurements, the patients/volunteers were directed to hold 0.9% saline solution in their mouth for 2 minutes to reduce the effects of recently consumed food. The detailed study protocol is given in chpter 3(see section 3.6). After completion of *in vivo* LIAF spectral measurements from suspicious sites and the adjoining tissues selected visually by the clinician, biopsy was taken from the measurement sites and sent for histopathological analysis after fixing in 10% formalin solution. After classification, spectroscopic data were correlated with the histopathological findings. Independent Student's t-test was performed on all the three fluorescence intensity ratios, viz. F500/F635, F500/F685 and F500/F705 between different tissue categories, to determine the statistical significance of the fluorescence ratio method in differentiating mucosal variations.

6.3 Results

6.3.1 LIAF Spectral Features

In vivo LIAF spectra were measured from 40 sites of the oral cavity in 20 patients. The broad autofluorescence peak at 500 nm seen in the LIAF spectra is characteristic of all epithelial tissues. In addition, two peaks around 635 and 705 nm due to PpIX emission were observed in SCC and dysplastic tissues. Fig. 6.2 shows the mean *in vivo* LIAF spectra of different tissue types, normalized to the intensity of the autofluorescence peak to enable comparison of spectral intensity variations. In lesions pathologically diagnosed as SCC, the peak at 635 nm is very prominent as compared to dysplastic tissues and an additional peak around 685 nm is observed with the 705 nm peak appearing as a shoulder. Nevertheless, the 705 nm peak is less prominent in the spectra from dysplastic tissues and the 685 nm peak appears broadened. In hyperplastic tissues, the 705 nm peak is absent and the intensity of the 635 peak is further reduced. Conversely, these three peaks are absent in the 11 anatomical sites of healthy volunteer mucosa, except at the dorsal tongue, the lateral tongue and vermillion border of lip. Further, it was noticed that for the dorsal and lateral tongue, these peaks were as intense as that of the abnormal sites (Fig. 6.1). As regards the autofluorescence peak at 500 nm, a notable broadening and red shift *ca.* 20 nm is observed in SCC and dysplastic tissues.

6.3.2 LIAF Intensity Ratios

The average fluorescence intensity ratios (F500/F635, F500/F685 and F500/F705) determined from the autofluorescence spectra of different mucosal types in 20 patients along with the results of histopathological examination, visual impression and spectral impressions for each site studied are given in Table 6.1. In most of the cases, surrounding tissues from which control measurements were taken in patients were histopathologically found to show varying degrees dysplasia or hyperplasia. Therefore, to avoid erroneous diagnosis, the data from these apparently normal adjoining tissues of patients were excluded and the mean F500/F630, F500/F705 and F500/F685 ratios from the 11 anatomical locations of the oral cavity of healthy population that have similar spectral features used for comparison.

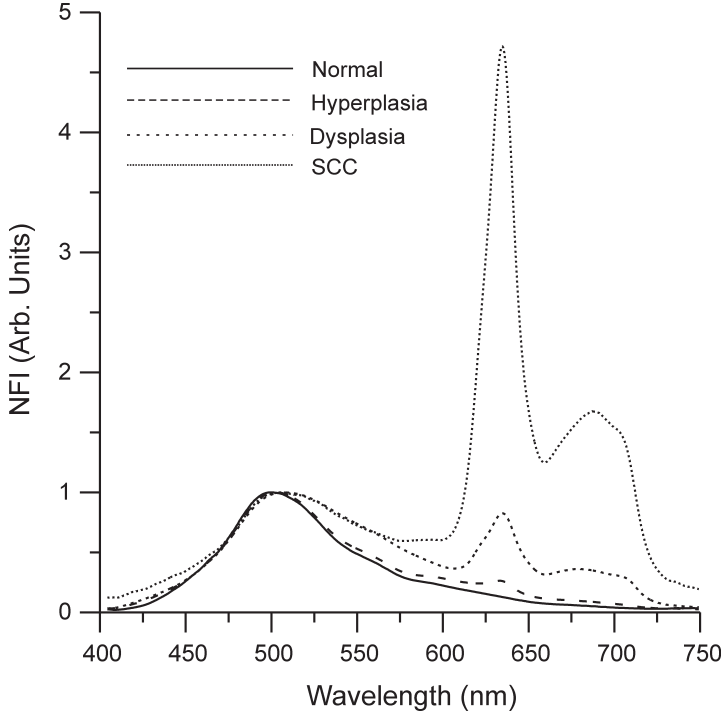

Fig. 6.2 LIAF emission from different types of oral mucosa from 40 sites of 20 patients and the mean spectra from 11 sites in 35 healthy volunteers, normalized to autofluorescence emission at 500nm. Normal spectra represent the average of 35x15x11 measurements, whereas hyperplasia and dysplasia relate to 9x15 measurements and the SCC spectra is of 18x15 measurements.

The oral mucosa is grouped into four categories; the first group consisted of healthy epithelium of volunteers, which is called as normal. The second, third and fourth categories comprised of hyperplastic, dysplastic (pre-malignant) and SCC (malignant), respectively. Table 6.2 shows the mean ratios of healthy mucosa from volunteer population with their standard deviations and the mean ratios of the patients listed in Table 6.1 regrouped into the above three distinct categories for comparison. All the three ratios show a decreasing trend with increasing malignancy, with the lowest values for SCC and the highest for normal. The F500/F685 ratio shows a maximum variation of 45% between normal and hyperplastic tissues and 68% between hyperplastic and dysplastic tissues, while the F500/F705 ratio has a variation of 75% for discrimination between dysplastic and SCC. Nevertheless, owing to the lower standard deviations and prominence of the 500 and 635 nm peaks, the F500/F635 ratio appears to be more reliable for grading of cancer.

6.3.3 Spectral Ratio Reference Standard (SRRS) for Tissue Characterization

The standard reference scatter plots are drawn using the three spectral intensity ratios F500/F635, F500/F705 and F500/F685 from 40 sites in 20 patients, comprising hyperplasia, dysplasia and SCC, and the corresponding mean data from 35 healthy volunteers. Fig. 6.3(a-c) shows the standard reference scatter plots for the three autofluorescence intensity ratios, which discriminates normal, hyperplastic, dysplastic and malignant tissues from one another. Discrimination lines were drawn between the normal and hyperplastic, hyperplastic and dysplastic, dysplastic and malignant at values that correspond to the average ratio values of the respective groups. The classification sensitivity and specificity in discriminating each of these categories were determined based on the discrimination threshold values, by validation with the gold standard, viz. histopathological results of biopsy specimens taken from LIAF measurement sites.

For example, in the case of healthy volunteers, the average F500/F635, F500/F685 and F500/F705 ratio values were 8.00, 33.68 and 27.61, respectively. The cut-off lines for discriminating the normal from hyperplastic were drawn at values corresponding to the mean of the healthy volunteer ratios and those from the hyperplastic mucosa (6.16, 21.57

Table 6.1 Fluorescence intensity ratio F500/F635, F500/F705 and F500/F685 of patients included in the SRRS and corresponding histopathologic, visual and spectral impressions

P#	Site	Histological Impression	Visual Impression	F500/F635	Spectral Impression	F500/F705	Spectral Impression	F500/F685	Spectral Impression
1	Buccal	Dysplasia	H L	2.20	Dysplasia	6.10	Dysplasia	5.10	SCC
	Buccal	Hyperplasia	Normal	5.23	Hyperplasia	16.46	Hyperplasia	11.68	Hyperplasia
2	Buccal	Dysplasia	Erythroplakia	2.17	Dysplasia	4.47	SCC	3.48	Dysplasia
	Buccal	Dysplasia	Normal	3.85	Dysplasia	9.05	Dysplasia	5.96	Dysplasia
3	Buccal	HSSCC	PG	0.34	SCC	1.05	SCC	0.75	SCC
	Buccal	Dysplasia	Normal	3.48	Dysplasia	6.88	Dysplasia	4.72	Dysplasia
4	Buccal	Dysplasia	Growth	1.49	SCC	2.82	SCC	2.28	SCC
5	Alveolus	SCC	UL	0.97	SCC	2.02	SCC	1.71	SCC
	Alveolus	Hyperplasia	Normal	5.85	Hyperplasia	20.00	Hyperplasia	14.21	Hyperplasia
6	FOM	SCC	PG	0.76	SCC	1.88	SCC	1.49	SCC
	FOM	Hyperplasia	Normal	5.33	Hyperplasia	16.68	Hyperplasia	11.95	Hyperplasia
7	Alveolus	SCC	PL	0.65	SCC	1.68	SCC	1.33	SCC
	Alveolus	Dysplasia	Normal	2.52	Dysplasia	6.94	Dysplasia	5.24	Dysplasia
8	Buccal	SCC	Growth	0.16	SCC	0.54	SCC	0.41	SCC
	Buccal	SCC	VL	1.45	SCC	3.77	SCC	2.88	SCC
9	Buccal	Hyperplasia	Normal	6.30	Hyperplasia	24.56	Normal	16.49	Hyperplasia
10	Alveolus	HSSCC	UPL	1.39	SCC	2.11	SCC	1.87	SCC
	Alveolus	Hyperplasia	Normal	8.05	Normal	36.94	Normal	24.62	Normal

Table 6.1 (Continued)

P#	Site	Histological Impression	Visual Impression	F500/F635	Spectral Impression	F500/F705	Spectral Impression	F500/F685	Spectral Impression
11	Buccal	Dysplasia	VLP	3.25	Dysplasia	12.45	Dysplasia	5.55	Dysplasia
	Buccal	Normal	Normal	7.04	Hyperplasia	34.17	Normal	21.46	Hyperplasia
12	Buccal	SCC	Leukoplakia	3.10	Dysplasia	5.91	Dysplasia	5.01	Dysplasia
	Buccal	Hyperplasia	Normal	6.99	Hyperplasia	18.01	Hyperplasia	13.95	Hyperplasia
13	Buccal	Dysplasia	Leukoplakia	3.23	Dysplasia	11.30	Dysplasia	6.26	Dysplasia
	Buccal	Hyperplasia	Normal	5.86	Hyperplasia	25.31	Normal	16.11	Hyperplasia
14	Alveolus	SCC	UPL	1.03	SCC	2.95	SCC	2.37	SCC
	Alveolus	Normal	Normal	7.33	Normal	33.30	Normal	20.68	Hyperplasia
15	Buccal	SCC	VL	0.38	SCC	1.45	SCC	1.10	SCC
	Buccal	Normal	Normal	9.02	Normal	43.92	Normal	26.53	Normal
16	Buccal	SCC	UPL	1.32	SCC	4.01	SCC	3.36	Dysplasia
	Buccal	Normal	Normal	6.92	Hyperplasia	24.20	Hyperplasia	16.84	Hyperplasia
17	Buccal	SCC	PG	1.32	SCC	2.83	SCC	2.25	SCC
	Buccal	Hyperplasia	Normal	4.93	Hyperplasia	12.03	Hyperplasia	10.10	Dysplasia
18	Buccal	SCC	UPL	0.13	SCC	0.45	SCC	0.41	SCC
	Buccal	Hyperplasia	Normal	6.99	Hyperplasia	18.9	Hyperplasia	13.95	Hyperplasia
19	Alveolus	SCC	UPL	0.26	SCC	0.92	SCC	0.58	SCC
	Alveolus	Dysplasia	Normal	2.26	Dysplasia	5.84	Dysplasia	3.76	Dysplasia
20	FOM	SCC	PG	0.24	SCC	0.79	SCC	0.71	SCC
	Buccal	SCC	Leukoplakia	0.45	SCC	1.56	SCC	1.24	SCC
	Buccal	SCC	PG	0.27	SCC	0.88	SCC	0.78	SCC
	Inner lip	SCC	PG	0.17	SCC	0.56	SCC	0.49	SCC

P#: Patient Number; **FOM:** Floor of mouth; **HL:** Homogeneous leukoplakia; **PG:** Proliferative growth; **UL:** Ulcerative lesion; **PL:** Proliferative lesion; **VL:** Verrucous lesion; **UPL:** Ulcerative proliferate lesion; **VLP:** Verrucous leukoplakia; **SCC:** Squamous Cell Carcinoma; **HSSCC:** Highly suspicious SCC.

and 15.1, respectively) of patients.

6.4 Discussion

6.4.1 LIAF Spectral Features

Many research groups have reported that the broad autofluorescence around 500 nm is due to emission from endogenous fluorophores, like NADH, FAD, colla-gen, elastin and amino acids, and the emissions at 635 and 705 nm as due to enhanced PpIX presence in the malignant tissues (Li and Xie, 2005; Huang et al., 2004;Da Costa et al., 2001; Moesta et al., 2001). In addition to these peaks, a prominent peak was noticed around 685 nm between

the PpIX emission peaks in SCC tissues. In dysplastic tissues, this peak is not very promin-ent as in SCC, but its pres-ence contributes effectively to broaden the 705 nm peak. It was noticed that the 685 nm peak is absent in healthy volunteer tissues and in contra lateral mucosa of patients and hence, cannot be attributed to chlorophyll fluorescence from leafy vegetables or from recently consumed food items as proposed earlier (de Veld et al., 2003). High performance liquid chromatograms of tumor and normal colorectal tissues have shown the presence of a higher concentration of corproporphyrinIII in malignant tissues (Moesta et al., 2001). In the same study, peaks at 630 and 685 nm were observed when corpro-porphyrinIII dissolved in methanol was excited with 505 nm light. It can thus be concluded that the peak observed at 685 nm, especially in SCC and dysplastic tissues, could be due to the accumulation of endogenous fluorophore corpropo-rphyrinIII, which is a precursor of PpIX in the heme synthesis, in malignant tissues.

6.4.2 SRRS using Healthy Population

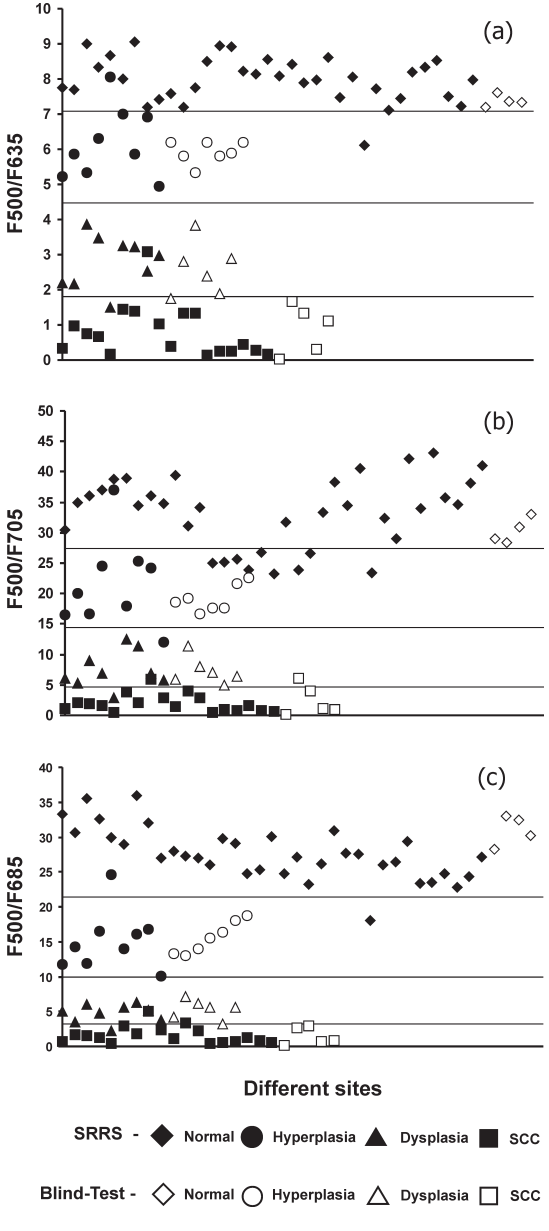

Fig. 6.3 Spectral ratio reference standard (SRRS) developed from 35 healthy population and 40 sites in 20 patients for fluorescence intensity ratios **(a)** F500/F635 **(b)** F500/F705 **(c)** F500/F685. The solid symbols represent SRRS while the hollow symbols relate to the blind test results at 21 sites in 17 patients.

Table 6.2 Mean autofluorescence spectral ratios in healthy population and patients categorized according to different grades

Histological diagnosis	Population (n)	F500/F635	F500/F705	F500/F685
Normal (healthy)	35	8.00±0.66	33.08±5.71	27.61±3.74
Hyperplasia	9	6.16±1.00 (23)	21.57±7.26 (35)	15.10±4.26 (45)
Dysplasia	9	2.78±0.80 (55)	7.61±3.17 (65)	4.82±1.33 (68)
SCC	18	0.80±0.74 (71)	1.96±1.46 (75)	1.60±1.20 (67)

SCC: Squamous cell carcinoma.
The % value given in parenthesis denotes the change with respect to the next lower grade.

In a study on classification of oral leukoplakia using artificial neural network, Van et al (2000) observed that spectroscopic changes occur not only at the center and border of lesions, but also in the surroundings, where no abnormalities are clinically visible. Therefore, in cases where the adjoining tissues of patients havve varying degrees of epithelial dysplasia, only lower values of specificity and sensitivity can be expected and in such cases, one has to depend on measurements from the contra lateral normal sites. In many patients enrolled in our study, the lesion spread was often large and it was not possible to identify a suitable adjoining/contra lateral muccosa for control measurements. In addition, there is no evidence to assume that the contra lateral mucosa is normal in patients.

Most of the patients who participated in this study had smoking, chewing or alcohol consumption habits that could affect the adjoining and contra lateral tissue structure. As compared to the mean spectral ratios of healthy population given in Table 6.2, the adjoining mucosa of patients # 11, 14, 15 and 16, shown in Table 6.1 and identified visually and pathologically as normal, were having lower ratios signifying hyperplasia. Slaughter et al (1953) reported that long-term influence of carcinogens like tobacco, smoke and alcohol on the oral mucosa leads to 'field cancerization' and influence diagnosis. Hence, measurements from these four sites were excluded in the development of the reference database. Further, the dependence of using the adjoining mucosa as control as earlier studies was overcome by use of site-specific database of healthy population (Table 6.1).

de Veld et al (2003) had conducted an extensive study on 97 healthy volunteers to understand the autofluorescence characteristics from thirteen different anatomical sites of the oral cavity wherein they observed that the 635 nm porphyrin emission arises only from the dorsal side of the tongue and the vermillion border of lip. They reported that all anatomical locations, excluding these two sites are interchangeable for diagnosis of malignant lesions using tissue autofluorescence. The present study has shown that the fluorescence spectra from lateral tongue also has an emission peak at 635 nm (Fig. 6.1) while all the other sites having similar spectral features as reported by de Veld et al (2003). Further, it

Table 6.3 Sensitivity and specificity of SRRS in discriminating different tissue types in 20 patients and results of blind-test validation in 17 patients. PPV and NPV values are shown along with sensitivity and specificity respectively in paranthesis.

A. SRRS test-results

LIAF Ratios	Normal Vs Hyperplasia		Hyperplasia Vs Dysplasia		Dysplasia Vs SCC	
	Sensitivity % (PPV)	Specificity % (NPV)	Sensitivity % (PPV)	Specificity % (NPV)	Sensitivity % (PPV)	Specificity % (NPV)
F500/F635	89 (0.89)	97 (0.97)	100 (1)	100 (1)	94 (0.94)	89 (0.89)
F500/F685	89 (0.89)	97 (0.97)	100 (1)	100 (1)	89 (0.94)	88 (0.78)
F500/F705	89 (0.47)	74 (0.96)	100 (0.9)	89 (1)	94(0.94)	89(0.88)
Over all	89 (0.75)	89 (0.97)	100 (0.97)	96 (1)	92 (0.94)	86 (0.85)

B. Blind test-results

LIAF Ratios	Normal Vs Hyperplasia		Hyperplasia Vs Dysplasia		Dysplasia Vs SCC	
	Sensitivity % (PPV)	Specificity % (NPV)	Sensitivity % (PPV)	Specificity % (NPV)	Sensitivity % (PPV)	Specificity % (NPV)
F500/F635	100 (1)	100 (1)	100 (1)	100 (1)	100 (0.83)	83 (1)
F500/F685	100 (1)	100 (1)	100 (1)	100 (1)	83 (1)	100 (0.83)
F500/F705	100 (1)	100 (1)	100 (1)	100 (1)	80 (0.80)	83 (0.83)
Over all	100 (1)	100 (1)	100 (1)	100 (1)	88 (0.88)	89 (0.89)

SCC-Squamous Cell Carcinoma.

Independent Student's t-test, $p<0.0005$ for each discrimination group.

was observed that the peaks at 685 and 705 nm, in particular at the dorsal and lateral sides of the tongue, were less intense in the vermillion border of lip. The inclusion of the ratio values from these three anatomical locations in SRRS was found to affect the sensitivity and specificity of diagnosis. Therefore, the SRRS developed can only be used to discriminate oral cancer at anatomical locations other than the vermillion border of the lip, dorsal tongue and lateral border of tongue, for which a separate spectral reference database would be required.

The diagnostic accuracies, sensitivity, specificity, PPV and NPV of measurement were also determined by validation with the gold standard, viz., histopathological results of biopsy from LIAF measurement sites. Cut-off values in the reference scatter plots Fig. 6.4(a-c) of the autofluorescence intensity ratios (F500/F635, F500/F685 and F500/F705) were used in the determination of true positives (TP), false positives (FP), true negatives (TN) and false negatives (FN) using which diagnostic accuaracies were calculated, as described in the chapter 1 (See section 1.2.5.2). Advantage of using PPV and NPV along with sensitivity and

specificity is also briefly described in this section.

For the F500/ F635 ratio, by selecting cut-off at the mean (7.08) of normal and hyperplastic values, a sensitivity and specificity of 89% and 97%, respectively, was obtained to discriminate normal from hyperplastic mucosa with a PPV of 0.89 and NPV of 0.97. In the same plot, cut-off drawn at 1.79 discriminates pre-malignant dysplastic tissues from malignant SCC with a sensitivity of 94% and specificity of 89%, with a PPV of 0.94 and NPV of 0.89. Using the information provided by the three reference plots, an overall sensitivity and specificity of 89% was achieved, with a PPV and NPV of 0.75 and 0.97 respectively, in distinguishing normal from hyperplasia. On the other hand, dysplasia could be discriminated from hyperplasias with a sensitivity, specificity, PPV and NPV of 100%, 96%, 0.97 and 1 respectively. Table 6.3 illustrates the independent and overall sensitivities and specificities obtained for differentiating the four different types of mucosal variations using the F500/ F635, F500/F685 and F500/F705 ratio SRRS plots, with their student t-test values (p). All the three ratios used in differentiating various tissue categories have very low independent student t-test values $p<0.00005$, authenticating the significance of using the standard reference healthy population data values to identify hyperplastic tissues from dysplastic and dysplastic from SCC.

It may be noted that the fluorescence measurements were confined to a circular area of 6 mm in diameter at the selected site and the average of fifteen measurements represent the spectra of each site. However, the biopsy samples (approximately, 2 mm in dia.) for histopathology were taken only from a portion within the measurement area. An oral lesion can be malignant at one site, while it can be pre-malignant at another site, a few millimeters away. When entire lesions were illuminated with the violet laser light, intense red fluorescence was occasionally seen emanating from different parts of the malignant lesions, indicating that lesion intra sites differ in abnormality. This could be the reason for the lower sensitivities and specificities reported for distinguishing dysplasias from SCC, when the average values of 10 measurements were used for spectral representation (Table 6.3). This urges the use of a fluorescence imaging system for investigating larger lesions and for discriminating early stages of oral cancer using LIAF spectral ratios, with improved diagnostic in specificity and sensitivity, although at a higher costs.

Spectral impressions given in Table 6.1 depend on the position of the spectral ratios in the SRRS plots. Although the lesions from the margin areas were seen clinically as normal, the spectral impressions based on reference scatter plots have identified these sites as dysplastic or hyperplastic, and the spectral diagnosis matches well with histopathological findings in most cases. Further, using these standard plots it was possible to accurately categorize the lesions that appeared as ulcerative proliferate growth for clinicians, but identified histopathologically as SCC. It was noticed that in most cases, clinical examinations are capable to identify lesions as normal or abnormal, but were unable to classify them viz. as hyperplasia, dysplasia or SCC. In comparison, the SRRS of the three spectral ratios showed better sensitivities and specificities for discrimination of different mucosal variations.

Table 6.4 Spectral ratios F500/F635, F500/F705 and F500/F685 used in the SRRS blind-test validation with their histopathologica and visual l impressions

P#	Site	Histopathology	Visual Impression	F500/F635	F500/F705	F500/F685
1	Alveolus	Dysplasia	UPG	1.74	5.90	4.19
	Alveolus	Hyperplasia	Normal	6.20	18.62	13.30
2	Buccal	Dysplasia	Leukoplakia	2.80	11.43	7.12
3	Buccal	SCC	Verrucous lesion	0.04	0.14	0.12
4	Inner lip	SCC	Verrucous lesion	1.70	6.12	2.64
	Inner lip	Dysplasia	Normal	3.83	8.05	6.18
5	Buccal	SCC	U P G	1.32	4.01	3.00
	Buccal	Hyperplasia	Normal	5.81	19.29	13.07
6	Floor of mouth	Dysplasia	Verrucous growth	2.40	7.00	5.64
7	Hard palate	SCC	Proliferate growth	0.29	1.06	0.65
8	Buccal	Dysplasia	Leukoplakia	1.90	4.97	3.22
9	Ventral tongue	SCC	UPL	1.12	1.02	0.82
	Ventral tongue	Dysplasia	Normal	2.90	6.34	5.56
10	Buccal	Hyperplasia	Normal	5.34	16.65	14.00
	Buccal	Hyperplasia	Normal	6.20	17.6	15.5
11	Buccal	Hyperplasia	HL	5.80	17.62	16.30
12	Inner lip	Hyperplasia	HL	5.90	21.60	18.00
13	Gingiva	Hyperplasia	Ulcer	6.20	22.60	18.70
14	Buccal	Normal	Normal	7.20	29.20	28.20
15	Buccal	Normal	Normal	7.60	28.33	33.00
16	Buccal	Normal	Normal	7.35	31.00	32.45
17	Buccal	Normal	Normal	7.32	33.00	30.23

P#: Patient Number; **HL:** Homogeneous leukoplakia; **UPG:** Ulcerative proliferate growth; **UPL:** Ulcerative proliferate lesion; **SCC:** Squamous Cell Carcinoma.

Clinically, leukoplakias are treated as low/high-risk lesions, which are generally identified histopathologically as hyperplasias, with or without mild to moderate dysplasias. In addition, the reference scatter plots discriminated SCC sites that were misclassified clinically as leukoplakias, in two cases (Patient #12 and 19 in Table 6.1). Further, in some cases, even pathological examination was not able to classify the samples correctly as SCC (Patient # 3 and 10 in Table 1). These cases were classified as highly suspicious SCC (HSSCC), but generally confirmed as SCC, after taking into consideration the opinion of the clinician. The SRRS developed was also able to classify such cases correctly.

6.4.3 Validation of SRRS for Tissue Discrimination

In order to test the reliability of the SRRS, a blind-test was carried out in a different subject group of 17 patients. Table 4 shows the site location, histopathological and visual impressions and the values of the three spectral ratios. For validation, the three spectral ratios belonging 21 sites in patients were inserted in the SRRS developed (Fig. 6.3 a-c) and the results were correlated with histopathological findings. The sensitivity specificity values obtained for blind-test indiscriminating different tissue types are given in Table 6.4. It can be seen that the SRRS discriminates normal mucosa from hyperplastic, and hyperplastic from dysplastic mucosa, with 100% sensitivity and specificity(with a PPV and NPV value of 1). An overall sensitivity of 88% and specificity of 89% was achieved in discriminating five SCC lesions from six dysplastic tissues, with a PPV of 0.88 and a NPV of 0.89 respectively. In addition, the ulcerated lesion observed clinically as hyperplasia (Patient #10) was identified correctly, in agreement with the gold standard.

Zheng et al (2002) has used scatter plots of the red-blue intensity ratio to differentiate benign tissues (consisting of hyperplasia and inflammation) from malignant oral tissues (comprising dysplasia, SCC and CIS) with a sensitivity and specificity of 92 and 93%, respectively. In contrast, the SRRS scatter plots of the F500/F635, F500/F685 and F500/F705 ratios could simultaneously differentiate mucosal variations such as hyperplasia, dysplasia and SCC from normal with improved sensitivities and specificities. All the three ratios were found to provide 100% sensitivity and specificity for early discrimination of tissue transformation from hyperplasia to dysplasia. The sensitivity and specificity given in Table 6.3 for blind-tests were also higher than earlier reports (Gillenwater et al., 1998a; Zheng et al., 2002; af Klitenberg et al., 1997) and were obtained without the use of ALA or any other exogenous photosensitizer. Out of the three SRRS developed, the one based on F500/F685 ratio gave 100% sensitivity and specificity for discrimination of various tissue types.

6.5 Conclusions

Non-invasive *in vivo* LIAF diagnostic modality described in this paper provides important spectroscopic information that helps to understand the tissue progression towards malignancy, without the use of an exogenous photosensitizer. The SRRS scatter plots developed shows

improved sensitivity and specificity as compared to the clinical impressions and matches well with the gold standard. This suggests that the methodology developed could act as an adjunct to the clinicians for early discrimination of oral dysplasias and hyperplasias. Among the three ratios studied, the F500/F685 ratio was found to be more suited and show great potential as a non-invasive tool to understand tissue progression from normal to pre-malignant and from pre-malignant to malignant with good sensitivity and specificity. The results of this study confirm that the distinction between the normal and diseased tissues within a patient is difficult and could lead to false classification or low specificities, as in most of the cases tissues surrounding the lesion show varying degrees of dysplasia.

There is a need to extend clinical trials to other sites of the oral cavity that were excluded from this study and to explore the possibilities for detection of high risk lesions like erythroplakia and sub-mucosal fibrosis (SMF) and to differentiate between different grades of SCC based on tissue autofluorescence. Since the LIAF spectrum could be gathered and analyzed in a short time (2-3 mins.), the SRRS developed could be employed as a tool for biopsy guidance and could act as an adjunct to the surgeons for fast and precise delineation of lesion margins during surgical interventions.

Chapter 7

Grading of Oral Mucosa by Curve-fitting of Corrected Autofluorescence Spectra

This work is submitted to:

Head and Neck (Wiley-Blackwell), 2008.

Grading of Oral Mucosa by Curve-fitting of Corrected Autofluorescence Spectra

7

7.1 Introduction

This study evaluates the advantages of correcting the recorded LIAF spectra, oxygenated hemoglobin (HbO_2) absorption, and then analyzing the same by curve-fitting using Gaussian spectral functions for discrimination early stages of oral cancer. Grading of oral mucosa is carried out in this*ex vivo* study in fourteen surgically excised tissue samples from different anatomical sites of oral cavity, while clinical studies were carried out at 30 sites in 15 patients. Corrected LIAF spectra were derived by filtering out HbO_2 absorption characteristics from LIAF spectra, by division with the corresponding DR spectra. The exact peak positions of the constituent bands and their relative contributions in the LIAF spectrum were also determined by curve-fitting. Withthis technique, it was possible to determine differences in parameters like the peak center, Gaussian amplitude, Gaussian curve area and bandwidth (FWHM) of the constituent peaks for different tissue types. The results of a comparative evaluation of these ratios with those derived from raw LIAF spectral data, both under *ex vivo* and *in vivo* environments, are presented.

7.2 Study Materials

7.2.1 Study Protocol and Tissues/Subjects

Surgically excised tissues from different anatomical sites of oral cavity, like the ventral tongue, buccal mucosa, hard palate and lower alveolus, were included in the *ex-vivo* study. The tissue samples were brought to the laboratory from Regional Cancer Center (RCC), Trivandrum, immediately after surgery without fixing in any solvent. Prior to the *ex vivo* LIAF and DR measurements, tissues were washed with saline solution and air dried on tissue paper. All the measurements were initiated within 90 minutes of surgery. The size of the excised tissues were 1-2 cm in length, 1-1.5 cm in breadth and 0.5-1 cm in thickness. *Ex vivo* study consisted of 14 tissues of pathologically confirmed normal (n=7), well differentiated SCC (WDSCC, n=3), moderately differentiated SCC (MDSCC, n=3) and poorly differentiated SCC (PDSCC, n=1) tissues.

The *in vivo* study included and 15 patients, with measurements taken from 30 suspicious sites, having clinically low/high-risk lesions in their oral cavity. These sites were pathologically confirmed as dysplatic (n=7), WDSCC (n=4), MDSCC (n=5) and PDSCC (n=6) lesions. The control values recorded earlier on 35 healthyvolunteers and presented in chapter 6 were used in this study

The control fluorescence and DR spectra relate to measurements from the oral cavity of healthy volunteers at 14 different anatomical locations (See chapter 3). However, owing

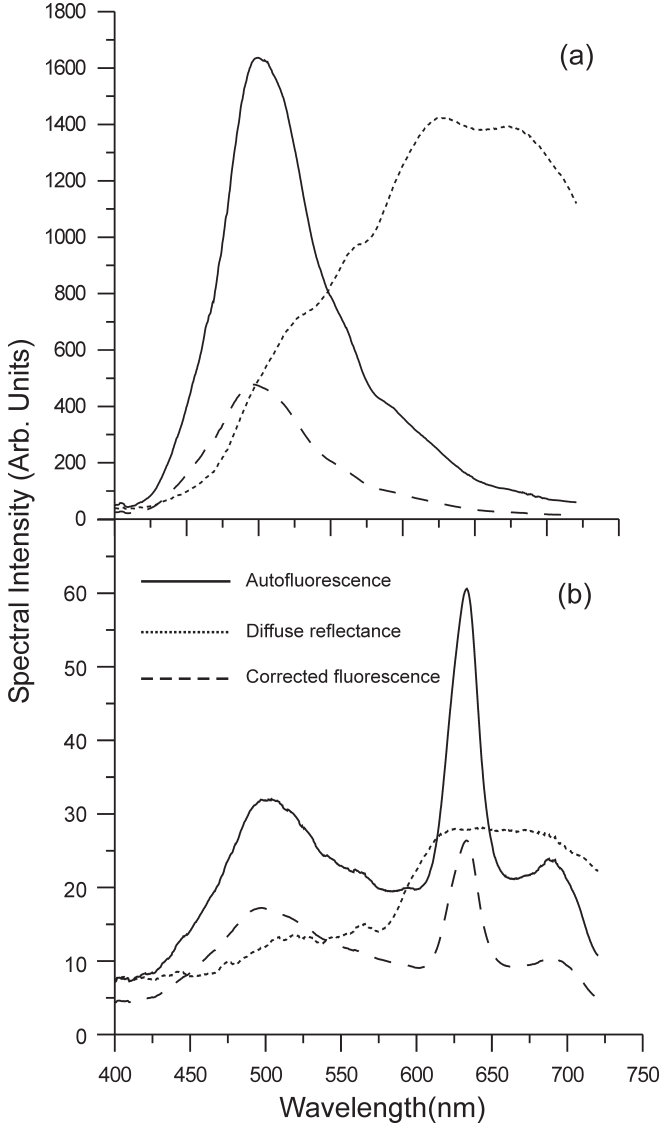

Fig. 7.1 Average *ex vivo* autofluorescence from the excised tissue of a patient and the corresponding intrinsic fluorescence spectra derived for (X=0.3), from **(a)** normal **(b)** MDSCC buccal mucosa.

to the presence of broademissions at 635, 685 and 705 nm at the vermillion border of lip, the dorsal and the lateral sides of tongue, as seen in cancerous lesions, these 3 sites were excluded from the study (see chapter 6). After classification, spectroscopic data were correlated with the histopathological findings. Independent Student's t-test was performed on the Gaussian amplitude and area ratios, F500/F630 and F500/F680, to assess the statistical significance of the fluorescence ratios in discerning different types of mucosal variations.

7.2.2 Data Processing

Prior to measurements, the background spectrum was taken and the OOI Base32 software was configured to automatically subtract the same during each measurement. Ten sets of LIAF and DR spectral measurements were taken from each sample/lesion in the 400-720 nm spectral window and the mean value was used in data analysis. Various refining models have been used by different groups to recover intrinsic autofluorescence spectra from the recorded fluorescence spectra (Diamond et al., 2003; Muller et al., 2001). We have used a first order approximation of intrinsic autofluorescence spectra by dividing autofluorescence with the diffuse reflectance spectra from the same tissue site, as given by de Veld et al (2005a):

$$F_i(\lambda) = F_r(\lambda)/R_d(\lambda)^{k(\lambda)} \qquad [7.1]$$

where, $F_i(I)$ is the corrected autofluorescence from the flurophores, $F_r(\lambda)$ is the recorded autofluorescence, $R_d(\lambda)$ is total diffuse reflectance and $k(\lambda)$ is a variable power depending on the tissue under investigation (See chapter 3, session 3.4.2). We have observed that the HbO_2 absorption artefacts depend on the lesion type and shows marked variations at sites such as the tongue, gingiva, alveolus and buccal mucosa. Hence, various values between 0.20-0.45 were chosen for the variable power (k) to smoothen the absorption dips. It was noticed that while applying this correction, the overall fluorescence intensity gets reduced by *ca* .50% for k=0.25. Figs. 7.1(a, b) represent the *in vivo* LIAF spectra and the derived corrected fluorescence spectra of normal and malignant buccal mucosa for k=0.30.

7.3 Results

7.3.1 LIAF Spectral Features

7.3.1.1 Ex-vivo Studies

Ex-vivo fluorescence measurements were carried out on surgically excised tissues from the malignant and margin areas of the oral cavity. We have grouped the oral mucosa into four categories, as per histopathology. The first group consisted of the adjoining tissues that were treated as normal, while the second, third and fourth categories comprised of WDSCC, MDSCC and PDSCC, respectively, with increasing grade. Fig. 7.2a represents the

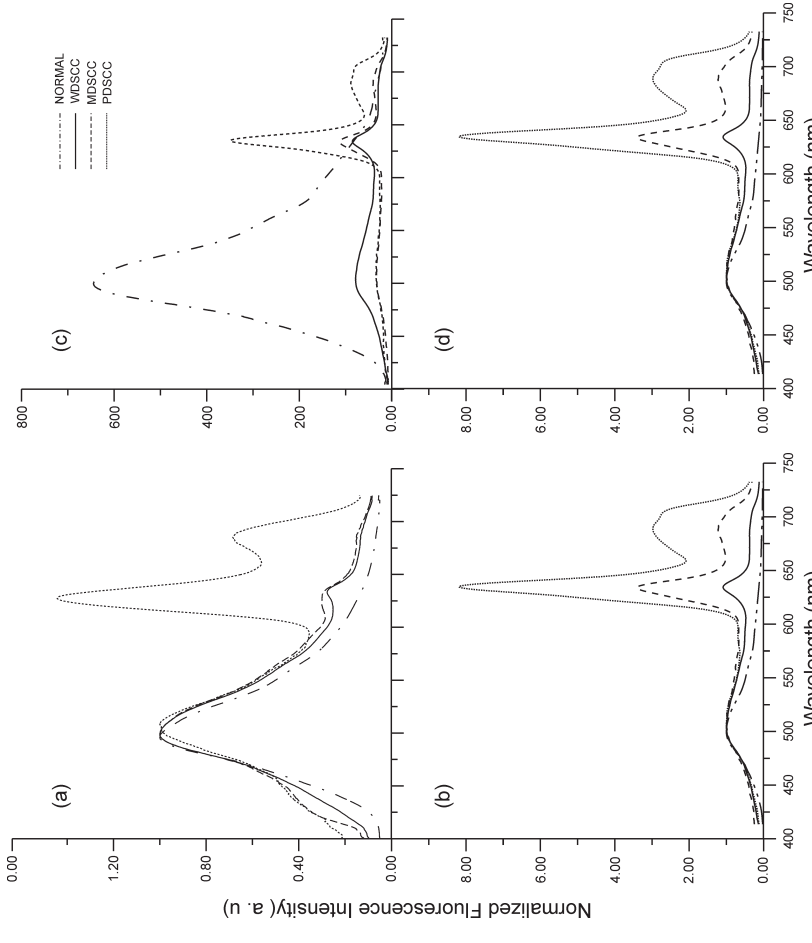

Fig. 7.2 Average LIAF spectra of different types of oral mucosa **(a)** absolute *ex vivo* **(b)** *ex vivo* spectra normalized to the intensity at 500 nm **(c)** absolute *in vivo* and **(d)** *in vivo* spectra normalized to the intensity at 500 nm. *Ex vivo* normal spectra are from margin buccal, ventral tongue and alveolus areas of the lesions, whereas *in vivo* normal spectra relate to average of 11 anatomical sites other than DST, LST and VBL of healthy volunteers (mean of 10 measurements from each tissue type).

mean *ex vivo* LIAF spectra of normal and cancerous oral mucosa and Fig. 7.2b, after normalization to the intensity of the autofluorescence peak at 500 nm. The malignant tissues exhibit two peaks centred *ca.* 630 and 680 nm, and a third peak *ca.* 440 nm in MDSCC and PDSCC that appears as a shoulder to the autofluorescence peak. Absorption anomalies due to (HbO_2) that appear as dips at 545 and 575 nm in the LIAF of both malignant and normal tissues were corrected using equation (1), with the help of the mean DR spectra recorded from the same tissue location.

As compared to normal tissues, malignant tissues exhibit lower fluorescence intensities at 500 nm and also a red-shift that increases with the grade of malignancy (Fig. 7.2b). The increase in fluorescence intensity at 630 and 680 nm with increasing grades of malignancy is plotted in Fig. 7. 3a.

7.3.1.2 Clinical In Vivo *Studies*

As seen in *ex vivo* tissues, the autofluorescence peak from *in vivo* normal mucosa appears at 500 nm (Fig. 7.2c). But, in malignant mucosa the peaks seen at 630 and 680 nm appeare red-shifted about 5 nm to 635 and 685 nm (Fig. 7.2d). However, for the sake of simplicity these would continue to be designated as 630 and 680 nm peaks. The peak observed earlier *ca.* 440 nm was absent in all grades of malignant lesions, but, a broad peak *ca.* 700 nm was observed in PDSCC lesions which was absent in *ex vivo* tissues. As an be seen from Figs. 7.2d and 7.3b, intensity of peaks in the 600-720 nm spectral region is greater in the *in vivo* spectra and the spectral intensity variation between different grades of cancer is higher as compared to the *ex vivo* spectra.

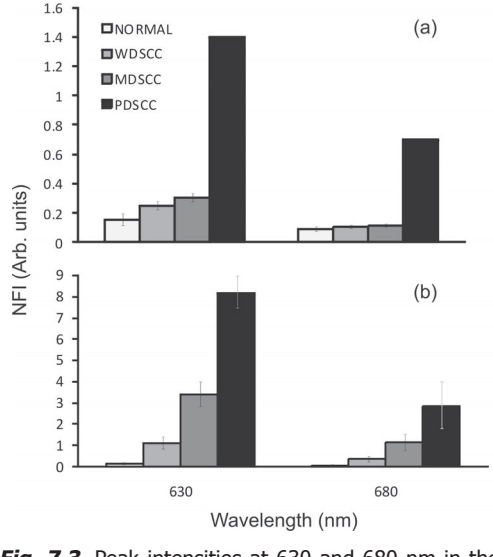

Fig. 7.3 Peak intensities at 630 and 680 nm in the 500 nm-normalized LIAF spectra for normal and different grades of oral SCC **(a)** *ex vivo* **(b)** *in vivo*, with their standard deviations.

7.3.2 Curve-fit Analysis

The corrected LIAF spectra from surgically excised tissues, normal tissues of volunteers and malignant tissues of patients recorded during clinical trials were analyzed by curve-fitting. It was observed that two Gaussian peaks were enough to fit the normal tissue spectrum, while five peaks were

Table 7.1 Gaussian curve-fitted parameters of the mean intrinsic *ex vivo* LIAF spectra for different tissue types.

Tissue Types	Peak center (nm)	FWHM (nm)	Gaussian Area	Gaussian Amplitude	r^2	χ^2
NORMAL (n=7)	496.4 ± 0.3 544.1 ± 1.3	60.7 ± 3.2 116.4 ± 4.2	12568 ± 1345 10684 ± 1123	165 ± 23 73.2 ± 14.5	0.99	13.24
WDSCC (n=3)	435.7 ± 0.2 497.8 ± 0.6 549.3 ± 1.3 632.4 ± 1.1 680.3 ± 0.3	39.6 ± 1.8 54.2 ± 1.2 96.8 ± 1.5 23.1 ± 1.0 47.7 ± 2.2	485 ± 37 2686 ± 185 2820 ± 212 243 ± 29 230 ± 16	9.8 ± 1.2 39.5 ± 2.4 23.2 ± 4.3 8.4 ± 0.11 3.8 ± 0.13	0.99	0.21
MDSCC (n=3)	437.6 ± 0.3 498.2 ± 0.8 548.6 ± 4.3 630.1 ± 1.5 680.1 ± 0.4	37.0 ± 2.3 54.1 ± 0.8 96.8 ± 1.9 27.0 ± 0.7 37.8 ± 1.0	287 ± 42 1473 ± 153 1584 ± 193 327 ± 17 198 ± 18	6.2 ± 0.2 21.7 ± 3.8 13.0 ± 1.0 9.6 ± 0.30 4.16 ± 0.5	0.99	0.21
PDSCC (n=1)	444.10 502.78 552.65 628.05 679.18	52.09 48.99 68.29 25.59 38.86	182.57 461.68 296.22 413.29 279.9	2.79 7.51 3.46 12.88 5.75	0.99	0.05

FWHM - Full width at half maximum; χ^2 - Absolute minimum value of the sum of squared deviations; r^2 - Correlation coefficient; **WDSCC** - Well differentiated squamous cell carcinoma; **MDSCC** - Moderately differentiated squamous cell carcinoma; **PDSCC** - Poorly differentiated squamous cell carcinoma.

required to obtain optimal values for the correlation coefficient r^2 (close to 1) and χ^2 in malignant tissues. Tables 7.1 and 7.2 show the center, amplitude, width (FWHM) and Gaussian curve area of the deconvoluted peaks in the LIAF spectra, respectively under *ex vivo* and *in vivo* situations, along with their r^2 and χ^2 values of fitting. For *in vivo* clinical studies, the categorization has been extended to 5 grades to include dysplastic and hyperplastic tissues.

7.3.2.1 Ex-vivo Studies

Fig. 7.4(a, b) shows the curve-fitted *ex vivo* LIAF spectrum of normal buccal tissues and MDSCC lesions, with their deconvoluted constituent bands. Normal tissue spectra were fitted with two peaks centered at 496.4 and 544.1 nm, while all classes of malignant tissues required three additional peaks centered around 435, 630 and 680 nm for a good fit(r^2 = 0.99). As the tissue transforms from normal to the highest grade of malignancy PDSCC,

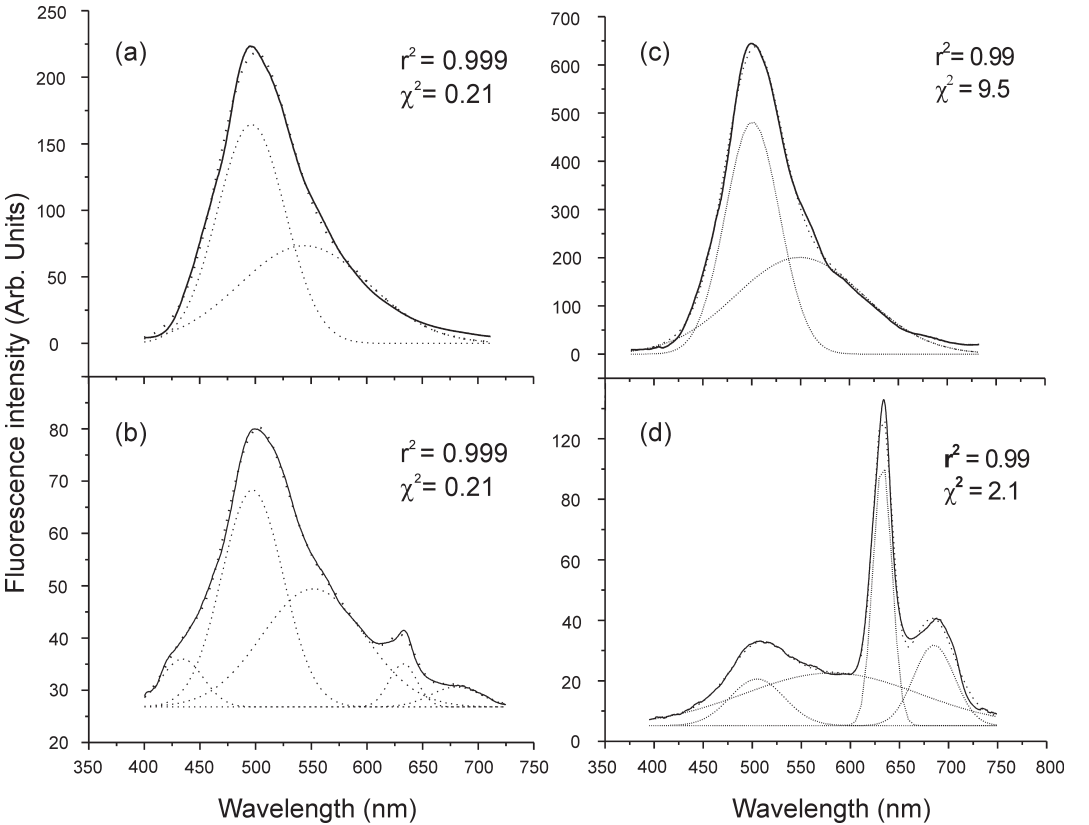

Fig. 7.4 The curve-fitted intrinsic mean LIAF spectrum showing constituents bands from **(a)** *ex vivo* normal buccal mucosa **(b)** *ex vivo* MDSCC of buccal mucosa **(c)** *in vivo* normal buccal mucosa **(d)** *in vivo* MDSCC of buccal mucosa. The dots on the LIAF spectrum relate to the data points. The solid line is the curve-fitted line, whereas the dotted lines show the constituent bands.

Table 7.2 Gaussian curve-fitted parameters of the mean intrinsic in vivo LIAF spectra for different tissue types

Tissue Type	Peak center (nm)	FWHM (nm)	Gaussian Area	Gaussian Amplitude	r^2	χ^2
NORMAL (n=36)	500.7 ± 0.6	55.5 ± 1.2	33583 ± 3248	482 ± 24	0.99	9.5
	549.0 ± 0.5	131.1 ± 0.5	32991 ± 2234	200 ± 16		
HYPERPLASTIC (n=8)	501.0 ± 0.2	53.7 ± 3.2	20455 ± 3872	305 ± 32	0.99	13.9
	549.0 ± 0.5	129.6 ± 2.3	28408 ± 1923	163 ± 17		
Dysplastic (n=7)	508.0 ± 0.6	65.3 ± 2.4	10027 ± 1945	150 ± 34	0.99	17.1
	587.3 ± 0.4	164.7 ± 3.5	12358 ± 2784	152 ± 14		
	633.7 ± 0.1	21.1 ± 0.4	1722 ± 236	26.2 ± 4.7		
	682.7 ± 0.2	55.0 ± 2.1	1185 ± 156	15.8 ± 1.2		
WDSCC (n=4)	508.8 ± 0.3	72.5 ± 0.5	6042 ± 1278	27.1 ± 3.5	0.99	20.5
	589.5 ± 0.4	181.8 ± 1.2	2779 ± 124	66.1 ± 7.5		
	634.3 ± 0.1	17.0 ± 3.3	2065 ± 237	51.6 ± 6.4		
	685.3 ± 1.0	43.7 ± 0.2	1961 ± 218	17.6 ± 1.2		
MDSCC (n=5)	507.2 ± 1.2	72.3 ± 0.1	1071 ± 105	15.5 ± 1.7	0.99	21.4
	599.6 ± 4.3	178.9 ± 3.4	2893 ± 145	17.4 ± 2.3		
	634.8 ± 0.6	19.1 ± 1.3	3099 ± 164	87.6 ± 6.5		
	685.8 ± 1.4	41.6 ± 0.5	2393 ± 191	26.7 ± 4.5		
PDSCC (n=6)	510.1 ± 1.2	73. 7 ± 0.3	1132 ± 55	14.0 ± 1.8	0.99	31.4
	621.3 ± 5.2	194.1 ± 3.6	2654 ± 83	298 ± 34		
	634.9 ± 1.1	19.1 ± 1.5	45593 ± 5425	1898 ± 233		
	685.3 ± 1.3	36. 6 ± 1.7	31007 ± 6347	682 ± 49		
	705.2 ± 2.3	17.4 ± 2.4	9644 ± 1056	451 ± 33		

FWHM - Full width at half maximum; χ^2 - Absolute minimum value of the sum of squared deviations; r^2 - Correlation coefficient; **WDSCC** - Well differentiated squamous cell carcinoma; **MDSCC** - Moderately differentiated squamous cell carcinoma; **PDSCC** - Poorly differentiated squamous cell carcinoma.

the 496.4 nm peak shifts about 6 nm and the 544.1 nm peak by about 8 nm towards the red region, whereas the 435.7 nm peak observed only in malignant tissues shifts by about 9 nm as the grade of malignancy changes from WDSCC to PDSCC. Another notable feature was the change in bandwidth of constituent peaks with malignancy. During tissue transformation from normal to PDSCC, the width (FWHM) of the 496.4 and 544.1 nm bands reduces respectively by about 8 and 68 nm. The 435.7 nm peak that appears in malignant tissues broadens from 39.6 to 52 nm and the 685 nm band narrows by 10 nm from 48 to 38 nm as the grade of cancer changes from WDSCC to PDSCC. In addition, the Gaussian curve area under different peaks showed substantial variation with increasing grades of the malignancy. Gaussian area of the 496.4 and 544.1 nm peaks decreased remarkably from 12568 to 461 and from 10684 to 296, respectively, during this transformation while the area under 630 and 680 nm peaks increased respectively by 70% and 22% for PDSCC tissue as compared to WDSCC. A large variation of about 98% was observed in Gaussian amplitudes of 496.4 and 544.1 nm bands during tissue transformation from normal to PDSCC, while the amplitude variations between WDSCC and PDSCC were 85% and 63%, respectively.

7.3.2.2 Clinical In Vivo *Studies*

As observed in the case of *ex vivo* studies, the accurate fitting of the healthy corrected fluorescence spectra was possible with two peaks at 500.7 and 549 nm Fig. 7.4 (c, d). WDSCC and MDSCC spectra gave good fitting accuracy with four peaks, whereas in PDSCC an additional fifth peak was observed at 705.2 nm. As seen in excised tissues, a red shift of 8 nm was observed in WDSCC lesions with respect to healthy mucosa, while the corresponding shift in PDSCC lesions was 10 nm. However, as compared to *ex vivo* findings, the 549 nm peak shows significant red-shifts of 40 and 50 nm respectively for WDSCC and MDSCC lesions and a higher shift of 72 nm for PDSCC lesions. The Gaussian curve area and amplitude of 500.5 nm peak was found to decrease with malignancy, while at higher grades of malignancy, the curve-fitted area and amplitudes of the 634.3 and 685.3 nm peaks showed an increasing trend, as observed under *ex vivo* conditions.

7.3.3 Raw and Curve-fitted LIAF Ratios

The fluorescence ratios F500/F630 and F500/F680 were determined from derived from the peak-fitted amplitude, area and raw spectral intensities and its variation for three different grades of oral cancer under *ex vivo* and five grades of cancer under *in vivo* conditions and the values are given in Table 7.3. It can be seen that the ratios derived from *in vivo* corrected fluorescence spectra follow a trend similar to that of the *ex vivo* ratios. Under *in vivo* conditions, a variation of 73% and 76% was observed, respectively in the raw F500/F630 and F500/F680 ratios, as the grade of malignancy changed from WDSCC to PDSCC, while the corresponding Gaussian curve area ratios showed a higher variation of 82% and 84%, respectively. In comparison, the Gaussian amplitude ratio F500/F630 was found to decreased by 86% from 0.52 to 0.074 and the F500/F680 ratio by 87%, from 1.54 to 0.20, as tissue transformed from WDSCC to PDSCC. Fig 7.6 shows variations in mean F500/F630 and

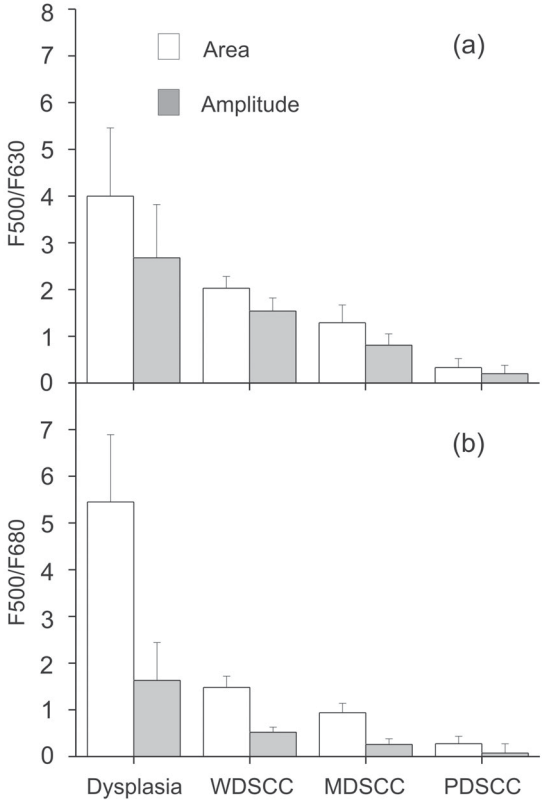

Fig. 7.5 Variations of **(a)** F500/F630 **(b)** F500/F680 Gaussian amplitude and area ratios for different abnormal tissues with their standard deviations *in vivo*.

F500/F680 area and amplitude ratios of different abnormal tissues viz. dysplasia, WDSCC, MDSCC and PDSCC.

7.4. Discussion

7.4.1 Comparison of *Ex vivo* and *In vivo* Spectral Features

The broad autofluorescence emission at *ca.* 500 nm, also known as the blue peak, appeares due to the prescence ofendogenous flurophores, such as NADH, FAD, collagen, elastin and amino acids with in the tissue (Drezek et al., 2001; Richards-kortum and Sevick muraca, 1996). As reported earlier (Da Costa et al., 2003; Ramanujam, 2000; Richards-kortum and Sevick muraca, 1996), the intensity of the blue peak is lower in malignant

lesions as compared to normal. Further, the intensity of this peak decreases with increasing grades of the malignancy under both *ex vivo* and *in vivo* conditions (Figs. 7.2(a, c)). In contrast, the LIAF intensities in the red spectral region (600-710 nm) were found to increase for abnormal tiss-ues as compared to normal tissues. In malignant tissues, besides the PpIX emission peak at 635 nm (Li and Xie, 2005; Huang et al., 2004; de Veld et al., 2004), we have noticed a new peak at 680 nm. However, in *ex vivo* malignant tissues, the 705nm peak is not as promin-ent as under *in vivo* conditions, but its contribution in the overall LIAF spectra was found to broaden the 680 nm peak. The reason for the appearence of this particular band and its its intensity varia-tions already discussed and expalined in chapter 6 (See section 6.4.1). During *in vivo* measurements, the contribution of 705 nm peak is marked, particularly in PDSCC lesions, whereas under *ex vivo* conditions only a broadening of the 685 nm peak is seen.

With respect to MDSCC lesions, PDSCC *ex vivo* lesions show an increase of *ca*. 5 times in fluorescence intensity at 630 nm and *ca.* 7 times in fluorescence intensity at 680 nm (Fig. 7.3a). However, the increase in fluorescence intensity at both 680and 630 nm under *in vivo* condition is *ca.* 2 times only. Nevertheless, the intensity increase between other grades is more prominent at 635 nm in both *ex vivo* and *in vivo* (Fig. 7.3b). As compared to *the in vivo* spectra, during *ex vivo* studies an additional peak was observed at 435 nm in malignant tissues, which could be attributed due to new flurophores created during the process of tissue degradation. Further, under *in vivo* environment variations at both 630 and 680 nm are more marked and these can be used to distinguish different tissue types. The spectral contrast between clinical (*in vivo*) and *ex vivo* conditions can thus be attributed to changes in fluorophor concentration associated with tissue degradation.

7.4.2 Raw LIAF Intensity Ratios After Spectral Correction

Absorption features noticed in the LIAF spectra of tissues at 545 and 575 nm are attributed to the presence of HbO_2 in the cells (Subhash et al., 2006; Zonious et al., 1999; Mourant et al., 1995). It was noticed that HbO_2 absorption under *in vivo* is larger in the dorsal tongue, buccal mucosa, alveolus and gingiva as compared other anatomical sites of oral cavity (See chapter 5, session 5.3.1). Therefore, these absorption anomalies in autofluorescence spectrum have the potential to affect the classification process, especially at locations where hemoglobin absorption is large. It was also reported that utilization of diffuse reflecta-nce features in the classification algorithm reduces the influence of variations in blood content and keratinisation (Zaak et al., 2001). Therefore, these absorption anomalies were removed from raw LIAF spectra using equation 7.1 before computation of LIAF ratios, and the results can be visualized in Fig. 7.1.

Zheng et al (2002) had used red-to-blue fluorescence image intensity ratios (Ir/Ib) to discriminate malignant oral cavity mucosa from normal. They reported that the mean intensity ratio (Ir/Ib) of dysplastic tissue (1.1±0.28) is 43.6% higher than the mean value of normal tissue (0.62±0.09). Similar studies were carried out by Zaak et al. to discriminate malignant

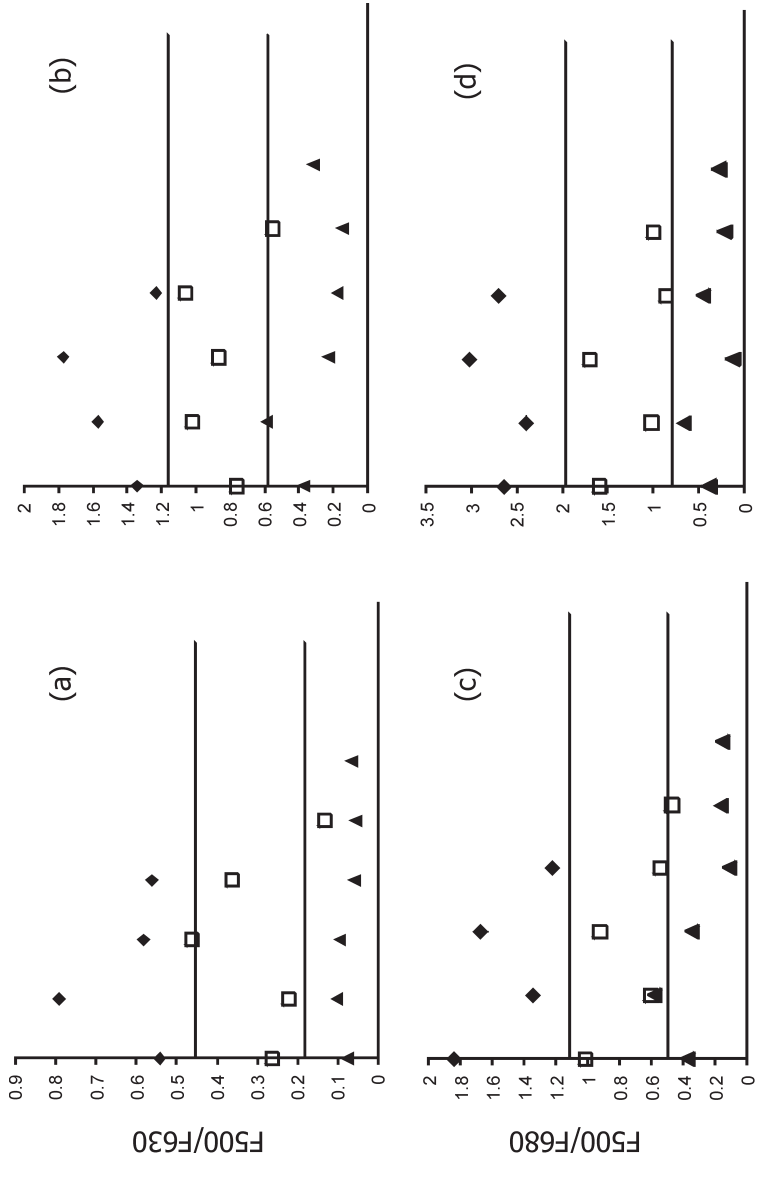

Fig. 7.6 Discrimination scatter plots of **(a)** Gaussian amplitude F500/F630 ratios **(b)** Gaussian area F500/F630 ratio **(c)** Gaussian amplitude F500/F680 ratio **(d)** Gaussian area F500/F680 ratio, in a population of 15 patients.

bladder tissues from benign, with lower false-positive rates (Wang et al., 1999). Scott et al (2000) proposed the use of red to green fluorescence imaging ratios for diagnosis, with blue light excitation, and found good contrast enhancement between control and malignant samples. After 4h of application of 5-ALA, they observed that Ir/Ig values of normal and dysplastic tissues show a variation of 71%. In comparison, it was noticed that even without the use of any photosensitizer, the raw LIAF ratios, F500/F630 and F500/680, were effective in tissue classification (Table 7.3). The percentage variation of these ratios between normal and cancerous lesions depends up on the grade of malignancy. The amount of decrease in raw LIAF ratios for F500/F630 and F500/F680 different grades of SCC under *ex vivo* and *in vivo* conditions can be notoced in Table 7.3. As the tissue grade changes from WDSCC to PDSCC, the F500/F630 and F500/F680 ratios of *in vivo* tissues decreased by 73% and 76%, respe-ctively, whereas the variations between WDSCC and MDSCC lesions were 56% and 48%, respectively.

7.4.3 Curve-fitted Ratios in Tissue Grading

7.4.3.1 Ex vivo Studies

In *ex vivo* normal tissues, with curve-fitting, two peaks were observed at 496.46 and 544.1 nm in the corrected autofluo-rescence spectra whereas in a typical malignant lesion (WDSCC) five peaks are seen at 435.7, 497.8, 549.3, 632.5 and 680.3 nm. Since the correlation coefficients of fitting were of the order of 0.99 (Table 7.1) and the residuals of fitting were few and scattered uniformly over the fitted curve, it is to be assumed that the peak wavelength positions identified by the curve-fitting algorithm are fairly accurate, for all the categories. Further, an additional peak at 435.7 nm was noticed in malignant tissues, which was found to be red-shifted at higher grades of malignancy. Similar red-shifts were noticed in the other peaks at 496.42 and 544.14 nm. These peak shifts could be due to changes in fluorophore concentration with malignancy and/or due to tissue degradation. Nevertheless, these peak shifts can also be serve as indicators of the extent and stage of malignancy.

The fluorescence ratios (F500/F630 and F500/680) derived from 500, 630 and 680 nm the Gaussian peak amplitude and Gaussian curve area of the bands showed improved sensitivities in the grading of SCC as compared to the raw spectral ratios (Table 7.3). A variation of *ca.* 90% was observed in the curve-fitted F500/F630 area ratio as compared to 88% variation observed in the curve-fitted amplitude ratio during tissue transformation from WDSCC to PDSCC.

7.4.3.2 Clinical In Vivo *Studies*

Curve-fitting of the *in vivo* autofluorescence emission from the oral mucosa of healthy volunteers has shown two peaks at 500.5 and 549.5 nm that were red-shifted by about 5 nm as compared to the peaks observed in the *ex vivo* spectra of tissues from margin areas. During *in vivo* clinical studies in a group of 15 patients, the WDSCC and MDSCC lesions

Table 7.3 LIAF spectral ratios derived from Gaussian curve area, amplitude and raw spectral intensities under *ex vivo* and *in vivo* environments

Type	LIAF Ratios	Curve fitted LIAF Amplitude			% of variation between WDSCC to PDSCC	Curve fitted LIAF Area			% of variation between WDSCC to PDSCC	Raw LIAF Amplitude			% of variation from WDSCC to PDSCC
		WDSCC	MDSCC	PDSCC		WDSCC	MDSCC	PDSCC		WDSCC	MDSCC	PDSCC	
Ex-vivo	F500/F630	4.7±1.3	2.3±0.7	0.6±0	88	11.0±1.6	4.5±1.0	1.1±0	90	3.7±1.0	2.0±0.5	0.75±0	80
	F500/F680	10.3±2.0	5.2±1.3	1.3±0	87	11.7±1.9	7.5±1.1	1.6±0	86	7.5±1. 6	2.6±0.8	1.28±0	83
In-vivo	F500/F630	0.5±0.1	0.3±0.1	0.07±0.02	86	1.5±0.2	0.9±0.2	0.3±0.2	82	0.9±0.3	0.4±0.1	0.2±0.1	73
	F500/F680	1.5±0.3	0.8±0.2	0.2±0.2	87	2.0±0.3	1.3±0.4	0.3±0.2	84	2.7±0.5	1.4±0.3	0.8±0.3	76

In *ex vivo* studies number of sites n= 3, 3, 1 for WDSCC, MDSCC, PDSCC respectively.
In *in vivo* studies number of sites n= 4, 5, 6 for WDSCC, MDSCC, PDSCC respectively.

showed four peaks on curve-fitting. However, the 435.7 nm peak observed in excised malignant tissues with curve-fitting was absent in the *in vivo* case. This peak could be attributed to some newly formed fluorophores associated with the degradation of surgically excised malignant tissues. In PDSCC lesions, an additional peak at 705.2 nm was observed *in vivo* along with the other four peaks observed in the lower grades of cancer. During tissue progression from normal to PDSCC, the 500.5 nm peak undergoes a red-shift of 10 nm; nevertheless, a large shift of 72 nm was observed for the 549.5 nm peak. In addition, the Gaussian curve area of the peaks showed substantial variations with increasing grades of the malignancy. For example, the Gaussian curve area of the 500 nm peak decreased markedly by 96% and the area of 630 and 680 nm peaks increased by 98% and 97%, respectively, during transformation from WDSCC to PDSCC. The variation in the Gaussian amplitude of the 500 nm peak with tissue transformation from normal to PDSCC was 98%. The Gaussian peak amplitude and curve area ratios, F500/F630 and F500/F680, follow the same trend as observed during *ex vivo* studies and show better detection and grading accuracy than raw LIAF ratios (Table 7.3, Fig. 7.5).

7.4.4 Pre-malignancy Detection

As mentioned earlier, the real challenge for a diagnostic system is to detect early tissue transformations, *i.e.* the ability to discriminate pre-malignant lesions from clinically similar hyperplasias. In this context, of the application of curve-fitting on the mean corrected spectra of 7 dysplastic and 8 hyperplastic lesions has shown interesting

results.

As can be seen in Table 7.2, hyperplastic tissues have two peaks at 501.02 and 549 nm, while dysplastic lesions have four peaks centred at 507.95, 587.26, 633.70 and 682.72 nm. During tissue transformation from hyperplastic to dysplastic, the amplitude and area of the 500.69 nm peak decreases substantially by 37% and 19%, respectively. Corresponding decrease in the amplitude and area of this peak in dysplastic lesions with respect to normal healthy mucosa is 69% and 24%, respectively. Also, a peak shift of *ca.* 7 nm is noticed in the 501 nm peak for dysplastic tissue spectra with respect to hyperplastic spectra. The curve fitted area ratio, F500/F630, for dysplastic lesions is 268% higher than that of WDSCC lesions, whereas the amplitude ratio is higher by 213%. Fig. 7.5 represents variation of F500/F630 and F500/F680 amplitude and area ratios, with their standard deviations, for the different tissue types studied.

7.4.5 Diagnostic Accuaracies

The diagnostic accuracies, ie., the sensitivity and specificity, of measurement were determined by validation with the gold standard. Since Gaussian amplitude and area ratios (F500/F630 and F500/F680) are more accurate, were used scatter plots of these ratios for grading different classes of SCC by correlation with pathological results (Fig. 7.6). The cut-off lines separating different categories were drawn at values that correspond to the mean ratio value of the respective groups as described in chapter 6. As the number of samples during *ex vivo* studies was less, the diagnostic accuracieswere determined only for *in vivo* studies.

Table 7.4 illustrates the sensitivity, specificity, PPV and NPV determined from the diagnostic scatter plots. The analysis has produced the same specificity and sensitivity of 100% for both the area ratios to discriminate pre-malignant dysplasia from WDSCC with a PPV and NPV of 1. The F500/F630 ratio have achieved a sensitivity of 80% and specificity of 100% with a corresponding PPV and NPV values of 1 and 0.86 respectively. Whereas, for F500/F680 amplitude ratio the corresponding diagnostic accuracies are 100%, 100%, 1, and 1, respectively. The F500/F630 area ratio and the F500/F680 amplitude ratios have shown a sensitivity and specificity of 100% to discriminate WDSCC from MDSCC with PPV and NPV of 1. Conversely, the F500/F680 area ratio shows 100% sensitivity and specificity to discriminate MDSCC from PDSCC, with NPV and PPV of 1. The unpaired Student's t-test value of $p<0.003$ for all categories reveals the level of accuracy and the statistical reliability of the classification technique.

In comparison, Wang et al (1999) reported a sensitivity of 81% and a specificity of 96% using partial least-squares and artificial neural network, while Heintzleman et al (2000) obtained a sensitivity of 90% and a specificity of 100% for distinguishing abnormal pre-malignant and malignant lesions from normal (healthy) benign mucosa. Further, Muller et al (2003) achieved an over all sensitivity of 96% and a specificity of 96%, by a combination

Table 7.4 Relative diagnostic accuracies of LIAF Gaussian curve area ratios, F500/F630 and F500/F680, in discriminating different tissue types *in vivo*

Gaussian Parameters	Relative Diagnostic Accuracies (%)	Gaussian LIAF Ratios	Dysplasia (7) Vs WDSCC (4)	WDSCC (4) Vs MDSCC (5)	MDSCC (5) Vs PDSCC(6)
Area	**Sensitivity (PPV)**	F500/F630	100 (1)	100 (1)	83 (0.83)
		F500/F680	100 (1)	100 (1)	100 (1)
	Specificity (NPV)	F500/F630	100 (1)	100 (1)	80 (0.80)
		F500/F680	100 (1)	100 (1)	100 (1)
Amplitude	**Sensitivity (PPV)**	F500/F630	80 (1)	75 (1)	100 (0.86)
		F500/F680	100 (1)	100 (1)	83 (0.83)
	Specificity (NPV)	F500/F630	100 (0.86)	100 (0.80)	80 (1)
		F500/F680	100 (1)	100 (1)	80 (0.83)

The value in parenthesis shows number of sites measured

of tissue autofluorescence, diffuse reflectance and scattering measurements for distinguishing abnormal (cancerous and dysplastic) from normal tissues. However, they were able to classify dysplastic tissues from cancerous with a sensitivity of 64% and specificity of 100% only.

7.5 Conclusions

The results of this study elucidate the potential of using corrected fluorescence spectroscopy alongside curve-fitting to track tissue progression towards malignancy and to grade them accordingly. The study has shown that tissue alterations not only affect the fluorescence spectral intensities, but also alter the spectral shapeor profile as evidenced by the appearence of new peaks, peak shifts, and variations in curve-fitted peak area, intensity and bandwidth. Further, by use of curve-fitting with Gaussian spectral functions, it was possible to locate the exact peak position, area under each peak, and amplitude of the constituent peaks in the LIAF spectra recorded from different types of oral mucosa under *ex vivo* and *in vivo* environments and use these parameters to distinguish different grades of oral cancer. Even though the curve-fitted Gaussian area and amplitude ratios, F500/F630 and F500/F680, were sensitive to tissue alterations under both environments, it was seen that under *in vivo* conditions the changes in these fluorescence intensity ratios were much more robust and distinct. Moreover, the ratios determined from curve-fitted spectral parameters showed better sensitivity and specificity to tissue transformations as compared to the ratios derived from raw spectral data. Among the two spectral ratios studied the

F500/F630 Gaussian curve area ratio was found to have more diagnostic accuracy. It may be noted that a distinction between pre-malignant dysplastic lesions and WDSCC was achieved in this clinical trials with 100% sensitivity and 86% specificity by tracking changes in the curve-fitted F500/F630 area and amplitude ratio.

Chapter 8

5-ALA Induced PpIX Fluorescence in Oral Cancer Detection *In Vivo*

This work is to be submitted to:

Lasers in Surgery and Medicine (Wiley-Blackwell), 2008.

5-ALA Induced PpIX Fluorescence in Oral Cancer Detection *In Vivo*

8

8.1 Introduction

5-ALAor ALA, is an endogenous molecule involved in Heme synthesis, which gets converted intracellularly into the fluorescing compound PpIX. ALA has been studied extensively as a photosensitizer for PDD and in PDT both in animal models (Sorensen et al., 1999; van der Veen et al., 1996; Peng et al., 1995) and in humans (Messman et al., 2003, 2000; af Klitenberg et al., 1999). However, the temporal evolution of PpIX fluorescence kinetics in different anatomical sites of human oral mucosa has not been well understood. ALA penetrates into the superficial mucosal cells when applied topically (de Rosa et al., 2000; van den Akker et al., 2000). Topical application is generally treated to be a good route of administration as it avoids systemic side effects and induces only local photosensitization. The objective of the current study is to find the optimal accumulation time of 5-ALA induced PpIX at different anatomical sites in healthy oral mucosa and in different grades of abnormal mucosa. The assumption is that since the oral cavity contains different types of mucosa, which differ in histology and keratin content, this could alter the penetration time of 5-ALA, accumulation rate in tissues and efficiency of conversion to PpIX. A proper understanding of the optimum accumulation time of 5-ALA in oral mucosa would definitely help to increase the accuracy of cancer diagnosis. This chapter presents the results of *ex vivo* and *in vivo* fluorescence measurements of carried out at various anatomical locations of the oral cavity after topical administration of 5-ALA.

8.2 Materials and Methods

8.2.1 Subjects and Study Protocol

5-ALA was selected for the study, as it is endogenous in nature and gets excreted from the body in less than 24 hours, eliminating side effects due to skin photosensitivity (Riedl et al., 2001; Messmann, 2000). ALA for topical application was prepared by mixing 20%bby wt. of 5-ALA (Medac, Germany) in an oil-in water cream (Johnsons & Johnsons baby cream). This freshly prepared cream was applied on *ex vivo* tissues collected immediatley following surgery. Fluorescence spectral measurements were conducted using the LIFRS system with nitrogen pumped dye laser(405 nm), at various intervals of time, viz. 90, 120, 150, 180, 210 and 240 mins., after topical application of 5-ALA in normal and malignant tissue samples.

The i*n vivo* uptake of 5-ALA and the accumulation of ensuing PpIX are studied at13 anatomical sites of oral cavity, in a population of 11 healthy volunteers and 15 patients. Prior to application of 5-ALA, the oral cavity was cleaned with isotonic saline and

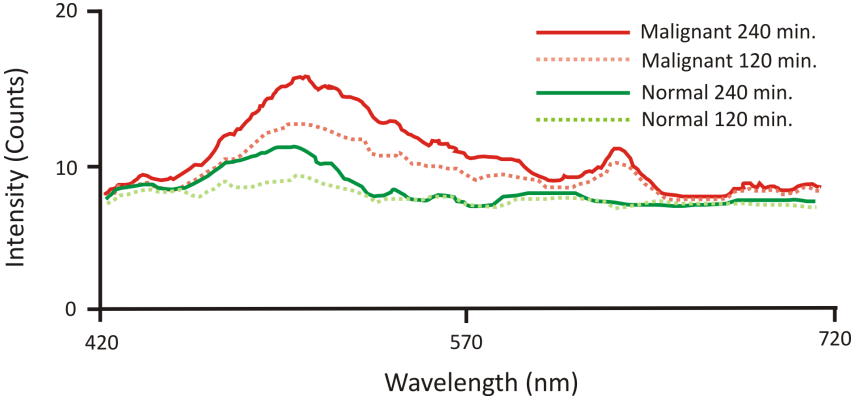

Fig. 8.1 Relative intensity of the ex vivo fluorescence spectra of a normal and cancerous buccal tissue after 120 minutes and 240 minutes of application of 5-ALA cream.

autofluorescence measurements were carried out at the normal and suspicious sites selected by the physician examining the patients. The photosensitisation of the oral mucosa was carried out by directing the patients and/or healthy volunteers to hold/rinse 0.4% solution of 5-ALA for 15 min. within the oral cavity. The measurements on patients were carried out in a dark room to avoid direct exposure to external light. Since the excitation power of the diode laser(405 nm) was very low (142 mW/cm^2), skin photosensitization or side effects were not observed in any of the subjects. The *in vivo* measurements were performed at time intervals of 90, 120, 150 and 210 mins. after topical application of 0.4% 5-ALA solution. The optimum accumulation times for different healthy anatomical sites and abnormal tissues were determined by tracking temporal variation in intensity of the PpIX fluorescence emission.

8.3 Results & Discussion

8.3.1 *Ex vivo* Studies

Fig. 8.1 shows a typical fluorescence spectra from the malignant buccalmucosa of the oral cavity diagnosed as high-grade squamous cell carcinoma and that of an adjoining normal tissue recorded using the LIFRS system. With excitation at 405 nm from the nitrogen laser pumped dye laser, the LIAF spectra shows a broad band at 500 nm and the PpIX bands at 635 and 705nm in malignant lesions, whereas, normal tissues the PpIX peaks are absent. It is obvious that the intensity of 5-ALA induced PpIX peaks in malignant tissues attains a maximum intensity after 120 minutes of application, which was found to decrease thereafter. Porphyrins are thought to be continuously created and expelled by the cancerous tissue as metabolites. After the removal of the cancerous tissue, the porphyrin band intensities

Table 8.1 Maximum accumulation time of ALA induced PpIX in different anatomical sites of oral cavity determined by monitoring temporal variation of the 500 nm normalized porphyrin intensities at 635, 685 an 705 nm after topical application of 0.4% 5-ALA solution

Site	Max. accumulation time PpIX	Intensity at 635nm	Intensity at 685nm	Intensity at 705nm
Alveolus	90	0.27±0.15	0.08±0.02	0.07±0.02
Buccal Mucosa	90	0.23±012	0.08±0.03	0.07±0.01
DST	150	2.98±0.34	1.20±0.23	0.84±0.21
LST	150	1.56±0.22	0.49±0.10	0.43±0.09
Ventral Tongue	90	0.39±0.06	0.11±0.02	0.10±0.03
Hardpalate	90	0.29±0.10	0.12±0.03	0.11±0.04
Softpalate	90	0.27±0.09	0.14±0.06	0.12±0.05
Floor of mouth	90	0.26±0.13	0.08±0.06	0.07±0.01
TFM	90	0.27±0.08	0.08±0.05	0.07±0.03
Inner Lip	90	0.37±0.05	0.11±0.03	0.11±0.03
VBL	150	0.38±0.04	0.10±0.03	0.09±0.05
Gingiva	90	0.31±0.06	0.12±0.04	0.11±0.04

of resected tissues decrease. This could be explained by the assumption that the rate production of porphyrins in the cancerous tissues before excision may be higher than that of excretion (Inaguma M and Hashimoto K, 1999).

Further, during *ex vivo* studies, the spectrum showed high noise due to lower laser power, which affected the signal to noise ratio of the detection system. In order to enhance the spectral quality of the signal, a diode laser of 50 mw output power was used to replace the nitrogen pumped dye laser (see chapter3) during the clinical studies.

8.3.2 *In vivo* Studies

8.3.2.1 Optimum Accumulation Time for 5-ALA Induced PpIX in Healthy Oral Mucosa

The uptake of 5-ALA and corresponding accumulation of PpIX at different anatomical sites of the oral cavity was studied by monitoring the LIF spectral changes over a period of 210 minutes after topical application of ALA. With 5-ALA application, it was seen that the autofluorescence intensity around 500 nm decreases while the PpIX emission at 635 and 705 nm gets enhanced. An additional peak at 685 nm was observed in the LIAF spectra (origin of this emission is discussed in the chapter 6), which helps in broadening the 705

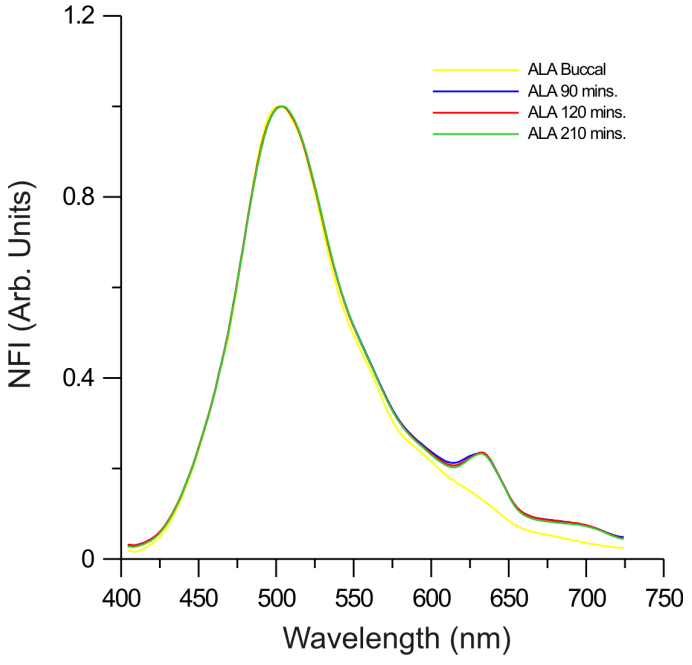

Fig. 8.2 Temporal variation in the normalized variation of LIF spectra from the buccal mucosa of the healthy volunteers before and after topical application of 0.4% 5-ALA solution for 15 minutes.

nm. Fig. 8.2 and Fig. 8.3 show the mean LIF spectra normalized to the intensity of the autofluorescence 500 nm peak, at different time periods after topical application of 5-ALA on the buccal mucosa and at the DST, respectively, in healthy volunteers. Changes due to PpIX accumulation in spectral emission start showing usually after 60 minutes of 5-ALA application. By tracking the 5-ALA induced PpIX peak intensities the optimum time for maximum accumulation can be determined for different sites. Table 8.1 lists the time at which ALA-induced PpIX accumalates maximum in different anatomical sites of oral cavity.

In anatomical locations such as masticatory mucosa (the gingiva, the hardpalate) and all the lining mucosa (the inner lip, the softpalate, the floor of mouth, the transition to floor mouth, the alveolus, the LST and the ventral tongue), by normalizing the LIF spectrum to the intensity of autofluorescence band at 500nm, it is observed that maximum enhancement in intensity of the porphyrin emissions at 635, 705 and 685 nm occurs around 90 minutes of 5-ALA application. This could be considered as the optimum time for the accumulation of PpIX in these types of mucosa. Also, intensities of the three peaks for these mucosa fall in same range (Table 8.1). However, in the case of VBL, LST and DST mucosa the maximum enhancement was seen only after 150 minutes of 5-ALA application. The DST and the LST sites have larger variations in the normalized spectral peak intensities as compared to all

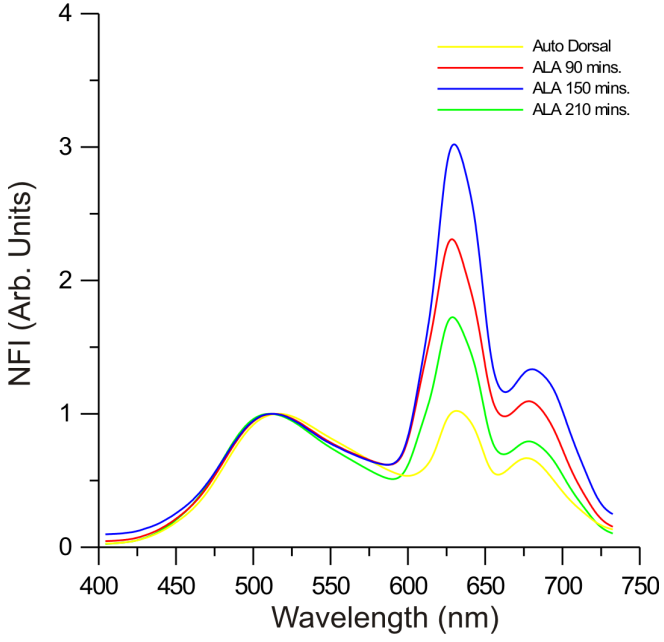

Fig. 8.3 Temporal variation in the normalized LIF spectra from the DST mucosa of the healthy volunteers before and after topical application of 0.4% 5-ALA solution for 15 minutes.

other anatomical sites; they are also unique due to higher accumulation time of PpIX. However, for VBL sites the accumulation time is same as that of VBL and LST, but the intensity variation is similar to those of other sites. These results indicate that for all anatomical locations, excluding DST, LST and VBL, the normalized intensities are interchangeable for diagnostic purposes using 5-ALA induced porphyrin fluorescence. After this optimal accumulation time, alll three intensities found to be decrease depends on the tissue type. In buccal mucosa these decrease are very small with time, whereas the corresponding decrease in DRS are much faster.

It's known that PpIX selectively accumulates in the abnormal tissues due to the reduced activity levels of the enzymes in the heme biosynthetic pathway (see chapter 2 and 6). The accumulation and expulsion of PpIX within normal cells can be explained on the basis of synthesis pathway as follows:

In every metabolic pathway there is at least one reaction that, in the cell, is far from equilibrium because of the relatively low activity of the enzyme that catalyzes it. The rate of this reaction is not limited by substrate availability, but only by the activity of this enzyme. The reaction is therefore said to be *enzyme-limited,* and because its rate limits the rate of

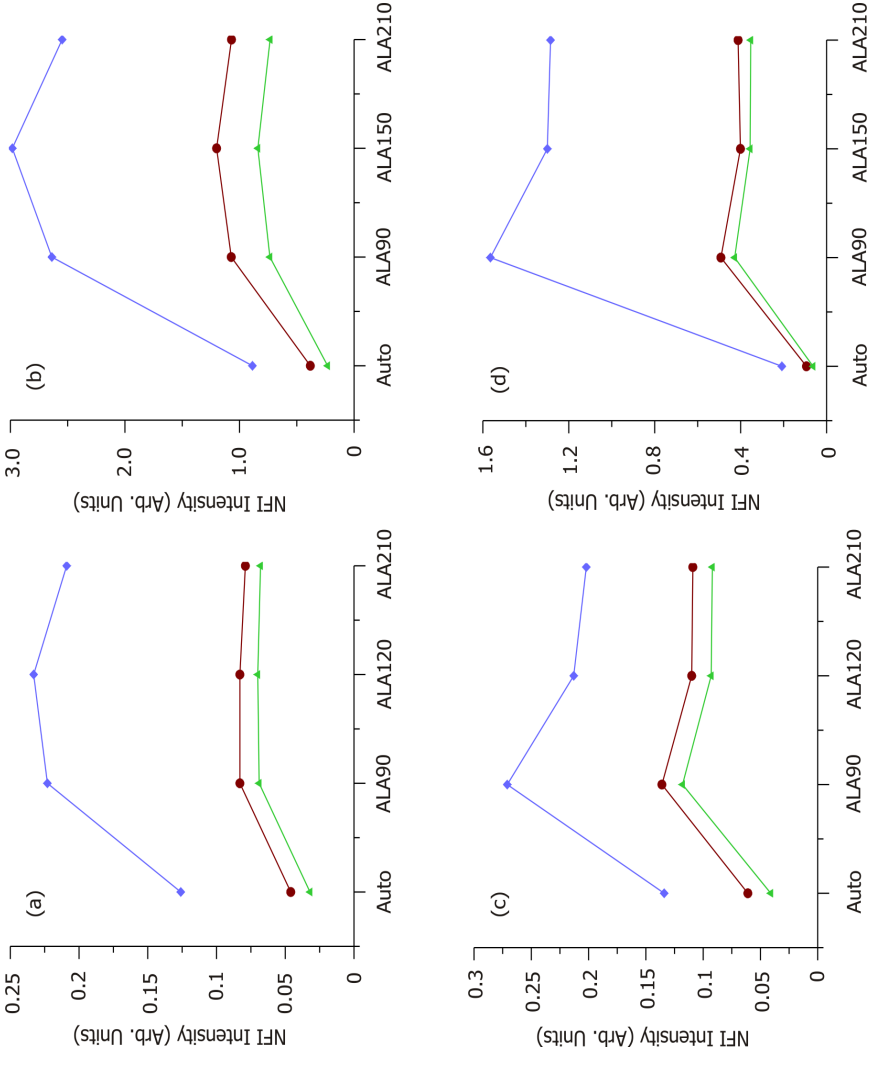

Fig. 8.4 Temporal variation in the mean normalized intensities at 635, 685 and 705nm of **(a)** buccal mucosa **(b)** DST **(c)** softpalate **(d)** LST mucosa after the topical application 0.4% solution of 5- ALA.

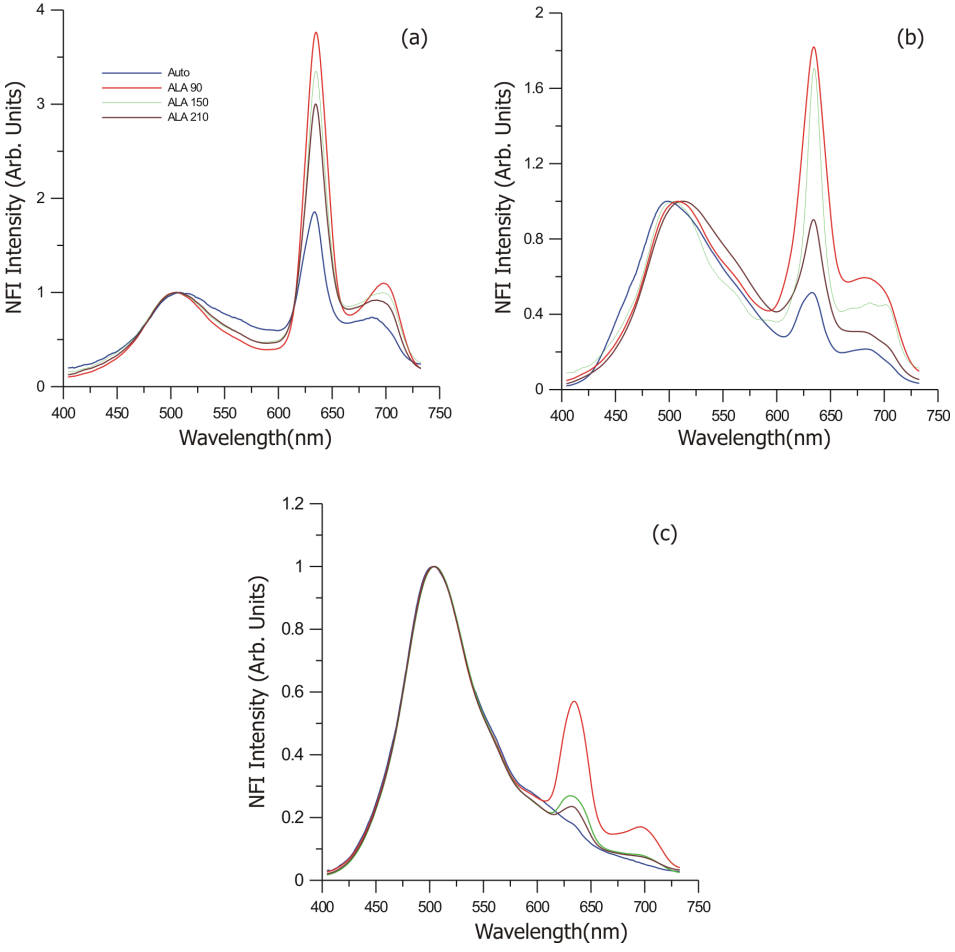

Fig. 8.5 Temporal variation of LIF spectra normalized to the autofluorescence at 500 nm for **(a)** SCC [n=5] **(b)** dysplasia [n=5] and **(c)** hyperplasia [n=6] of group I mucosa for different time periods after the topical application 0.4% solution of 5-ALA for 15 minutes.

the whole reaction sequence, the step is called the *rate-limiting step* in the pathway. In this context, the various biochemical steps in the heme cycle are rate limiting, particularly the last three steps. When 5-ALA is given in excess exogenously, the activity of the enzymes gets limited, because of high exogenous input of the substrate, and resulting accumulation

of PpIX and its precursors. However in healthy cells, this accumulation is no longer permanent and slowly gets washed out by conversion to PpIX and then to heme with time.

Eventhough the epithelium is stratified throughout the oral cavity, the mucous membrane differs in morphology at different sites. This definitely affects the diffusion of 5-ALA into the

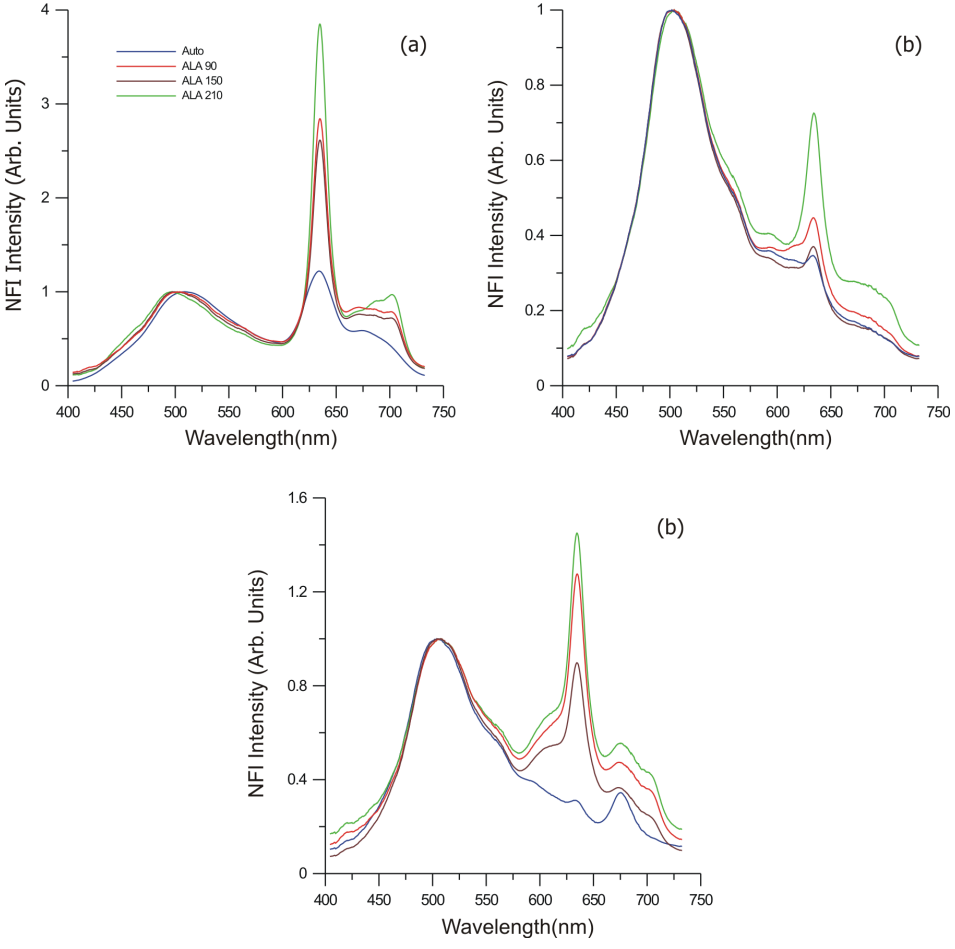

Fig. 8.6 Temporal variation of LIF spectra normalized to the autofluorescence at 500 nm for **(a)** SCC [n=7] **(b)** dysplasia [n=2] and **(c)** hyperplasia [n=3] of group II mucosa for different time periods after the topical application 0.4% solution of 5-ALA for 15 minutes.

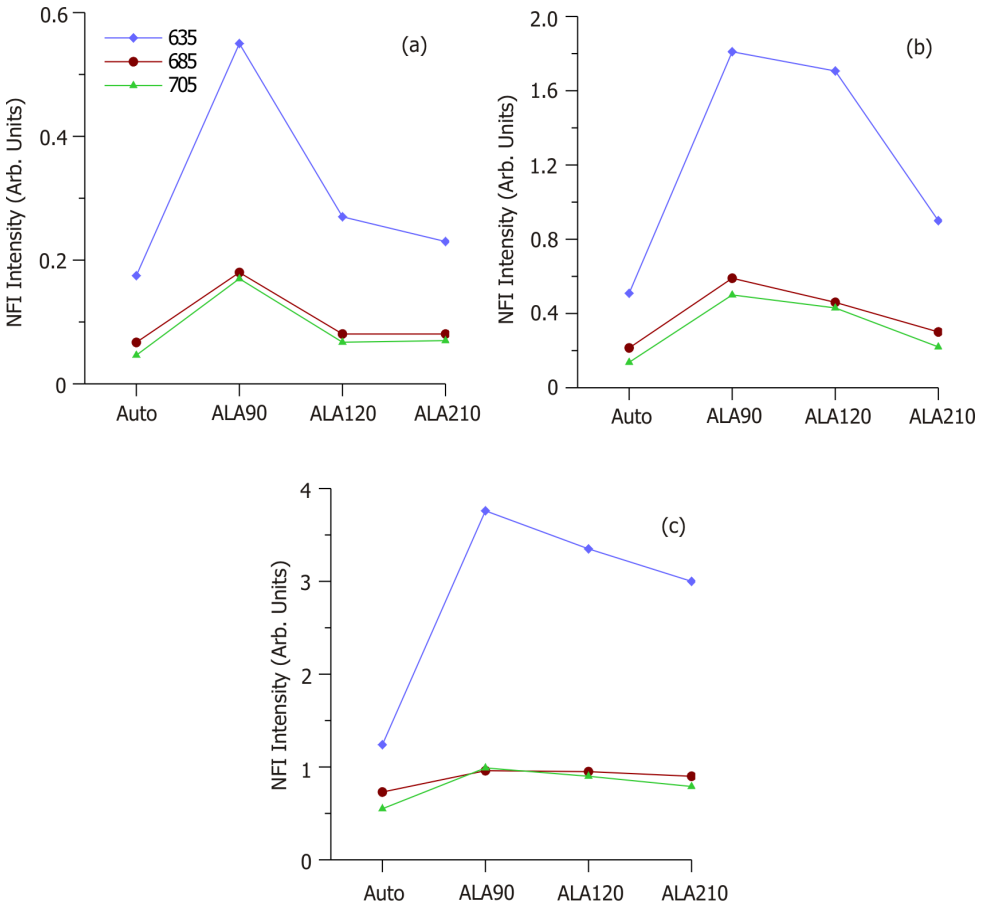

Fig. 8.7 Temporal variation in the mean normalized porphyrin intensities at 635, 685 and 705nm in group I **(a)** hyperplasia **(b)** dysplasia and **(c)** SCC mucosa after the topical application 0.4% solution of 5-ALA for 15 minutes.

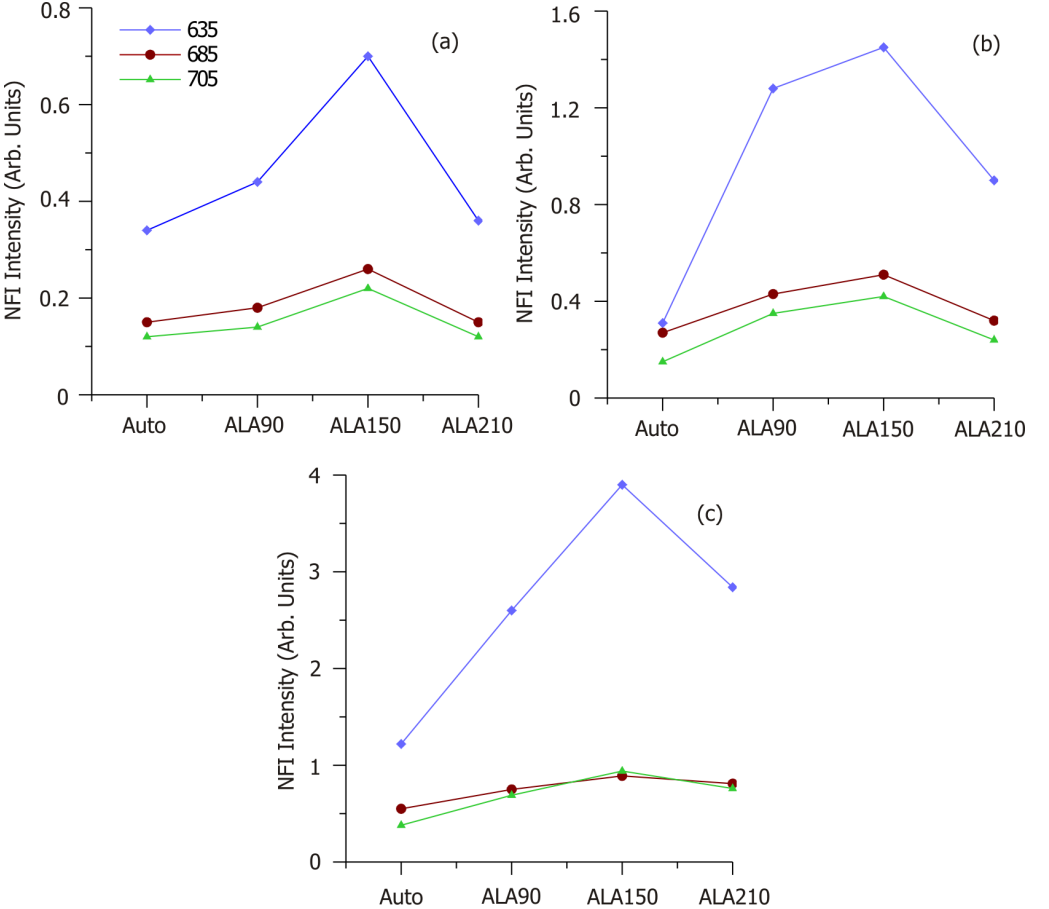

Fig. 8.8 Temporal variation in the mean normalized porphyrin intensities at 635, 685 and 705nm in group II **(a)** hyperplasia **(b)** dysplasia and **(c)** SCC mucosa after the topical application 0.4% solution of 5-ALA for 15 minutes.

cells during topical application. Particularly, in the case of DST and LST, the papillary structure of the mucosa, which allow the deposition of ALA solution increases the accumulation time leading to larger PpIX intensities. Similar results were observed in a model study on nude mouse skin using 10% (w/w) 5-ALA and ALA hexyl esters (ALAHE) (van den Akker et al., 2000) wherein the 635 intensity increased to its maximum with increasing administration time. Further, it was noticed that with increase in administration time the optimum accumulation time was also increased. However, in flat non-papillary structures associated with other lining types mucosa the deposition possibility is very feeble.

The superficial layer of the epidermis, reduces the diffusion rate of 5-ALA across the stratum corneum (van den Akker et al., 2000). Therefore, the thicker lingual structure and superficial keratin layer of DST and LST sites results in slower uptake. On the other hand, VBL, which is the transitional zone between the lip skin and the mucous membrane of the lip is covered by a moderately thick keratinized epithelium with a rather thick stratum corneum. The presence of these two layers together slows down the uptake of the 5-ALA as compared to inner lip or other lining mucosa. For all healthy anatomical sites, the intensity of PpIX emission decreases with time showing the temporal elimination of 5-ALA from the body. Fig. 8.4 shows the temporal variation in the mean normalized intensities at 635, 685 and 705nm at different time periods for buccal and DST, LST, soft palate respectively after application of 5-ALA.

8.3.2.2 Optimum Accumulation Time for PpIX in Diseased Mucosa and Diagnosis based on 5-ALA Induced PpIX Fluorescence

The anatomical sites are categorized into two groups; one with an optimum accumulation time of 90 mins. (group I), which represents average of the all the anatomical sites except the DST, LST and VBL and two, that with an accumulation time of 150 mins. (group II) representing the average of the three sites viz. DST, LST and VBL.

Table 8.2 Variation in 5-AlA induced PpIX intensities at 635, 685 and 705 nm with tissue alterations at optimum accumulation time (%variation from lower grade is shown in parenthesis)

Type	NFI	Healthy	Hyperplasia	Dysplasia	SCC
	635	0.29	0.55(89.6)	1.85(236)	3.76(103)
Group I	685	0.1	0.18(80)	0.59(227)	0.95(61)
	705	0.09	0.17(89)	0.5(194)	0.99(98)
	635	0.76	0.7(-8)	1.45(107)	3.9(169)
Group II	685	0.59	0.26(-56)	0.51(96)	0.89(75)
	705	0.45	0.22(-51)	0.42(91)	0.94(124)

The group I of the patient population involves diverse grade lesions of the alveolus, the buccal and the FM mucosa, whereas, group II consists of LST and DST mucosa. As seen in the case of healthy mucosa, in group I tissues maximum accumulation of PpIX in abnormal tissue types was observed at 90 mins. Further, after 90 minutes of application, SCC tissues garner 5-ALA induced PpIX to the maximum, and this accumulation is reflected in the peak intensities of 635, 685 and 705 nm as shown in Fig. 8.5 (a-c). Similarly, in the case of group II diseased mucosa, peak accumulation time for different tissue grades was observed at 150 min., as shown in Fig. 8.6(a-c).

In normal tissues, the superficial stratum corneum layer is the main barrier against the diffusion of 5-ALA (van den Akker et al., 2000). The stratum corneum consists of keratin layers (corneocytes) embedded in a lipid matrix. There are two ways for diffusion through the stratum corneum; across the corneocytes (trancellular) or via lipid matrix (intercellular) (Landmann, 1988; Menton and Eisen, 1971). The latter route is believed to be the principal pathway and thus, the major barrier for permeation (Williams and Barry, 1992; Suhonen et al., 1999). Since pre-malignant and malignant lesions usually associate with hyperkeratosis, higher optimum time periods could be expected in these lesions. However, similar optimal times observed in the pre-malignant and malignant lesions could be explained as due to the cutaneous stratum corneum. Eventhough thicker hyperkeratic layer limits the diffusion, at the same time, the disorder produced in the lipids within the intercellular space permits the diffusion through stratum corneum. After reaching the optimal accumulation period in both groups I and II, the PpIX intensity shows a decreasing or constant trend indicating the clearance of the 5-ALA induced PpIX from the system. Figs. 8.7 (a-c) and Figs. 8.8 (a-c) represent the temporal variation of PpIX intensities in different tissue types.

During the optimal period of 90 minutes in group I tissues, the enhancement in average normalized intensity at 635 nm with respect to the autofluorescence intensity was 126.4% in healthy volunteers, whereas in lesions diagnosed as hyperplastic, dysplastic and SCC, the corresponding variations were 223%, 254% and 203%, respectively. Similar trend was observed at the other two peaks at 685 nm and 705 nm. Thus, with ALA application, PpIX emission at 635, 685 and 705 nm gets enhanced both in abnormal and normal mucosa and higher % variations in intensities indicate higher accumulation of ALA in the abnormal tissues.

Conversely, for the group II mucosa, the intensity variations with respect to autofluorescence emission at the optimal time are 285%, 105%, 367% and 220% for healthy, hyperplasia, dysplasia and SCC, respectively. It may be noted that in this case, contrary to group I, normal mucosa shows higher intensity variations comparable with or even higher than that of benign and abnormal mucosa. This problem arises mainly due to the presence of PpIX like emission in healthy tissues due to bacterial presence. The intensity enhancements could be much larger if constituents of group II, particularly DST and LST, are considered separately.

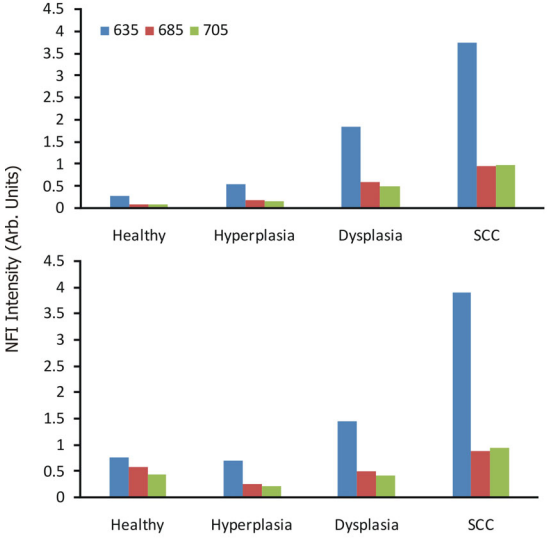

Fig. 8.9 Histogram showing variation in average normalized porphyrin fluorescence intensities at 635, 685 and 705 nm **(a)** group I and **(b)** group II, at optimal accumulation time after application of 5-ALA for 15 minutes.

Intrestingly, this intensity variation of PpIX in group I tissues (Fig. 8.9 a) can be utilized in diagnosis and grading of tissues. Although the intensity of the three peaks observed varies with tissue alteration towards malignancy, the changes are more prominent in the case of F635. Zeng et al (2002) has used the red-blue intensity ratio to differentiate different grades oral tissues using an endoscopic imaging system after topical application of 0.4% solution of 5-ALA. The malignant lesions (includes CIS and SCC) show the maximum variation of 294%, while pre-malignant dysplasia and benign hyperplasia/inflammatory mucosa show variations of 200% and 100%, respectively from normal values in 4 hours of ALA application. In contrast, the corresponding variations are very much higher at 1196%, 537% and 89.6% respectively in this study.

Thus, by tracking the intensity of these three peaks it is possible to discriminate malignant, pre-malignant, benign from normal tissues. Thus, with this technique one could differentiate different grades of tissue without any comparison with the normal tissues of the same patient and avoid the possibility of misclassification due to wrong selection of the control site. Table 8.2 lists the relative normalized intensities of the F635, F685 and F705 nm peaks, with their % variation with respect to the control values at the optimum accumulation time.

For group II, the intensities of the major emission bands at F635, F685 and F705 were found to increase in abnormal tissues. In this group also, the intensity variations at F635 were prominent, with SCC and dysplasia showing variations of 413 % and 91% respectively. As against the inceasing trend seen in group I mucosa, there is a decreasing trend during transition from normal to hyperplastic in group II (Table. 8.2). In other words, group II tissues that were pathologically identified as hyperplastic were indistinguishable from normal by obesrvation of fluorescence intensity variations.

8.4 Conclusions

Optimum accumulation time was determined for 5-ALA induced PpIX in different anatomical sites of the oral cavity in healthy population and in different grades of abnormal oral *ex vivo* and *in vivo* tissues by tracking the emssion peak intensities F635, F685 and F705 in the LIF spectra normalized to the intensity of autofluorescence peak at 500 nm. These normalized PpIX fluorescence intensities were found to maximize within 90 to 150 minutes of administration depending on the anatomical location, both in healthy and abnormal *in vivo* tissues. In group I, which involves all anatomical sites excepting the DST, LST and VBL, the intensities F635, F685 and F705 show an increasing trend during tissue transformation from healthy to SCC. Among the three peak intensities studied, the F635 was found to be more sensitive to tissue characteristics. In the group II mucosa consisting of DST, LST and VBL, the normalized intensities of the three peaks increased according to the grade of abnormal tissue. In this group, however, there was decreasing trend in these intensities during transformation to hyperplasia. This trend reversal in healthy tissues lead to a misclassification of normal tissues as benign hyperplasia, abnormal dysplasia or even as SCC, particularly in the case of DST and LST where these emissions are more prominent than in VBL. This also would also increase the number of false positives and tends to decrease the specificity of the diagnostic technique. Thus, the results of this pilot study suggest that, direct visualization of *in vivo* fluorescence at the optimum accumulation time, after topical application of 5-ALA, improves the capability for early detection and grading of oral cancer. The knowledge of the optimum accumulation time and high tissue selectivity of PpIX in abnormal tissues offers opportunities for therapeutic approach using PDT in future. Towards discrimination of cancers affecting the DST, LST and VBL, other methodologies such as those based on RSS or DRS could be utilized with better accuracies. In the following chapter, the results of using DRS to detect tongue cancer are presented.

Chapter 9

Diffuse Reflectance Spectral Features: An Adjunct to Tongue Cancer Diagnosis by Autofluorescence

This work is to be submitted to:

Applied Spectroscopy (SAS), 2008.

Diffuse Reflectance Spectral Features: An Adjunct to Tongue Cancer Diagnosis by Autofluorescence

9

9.1 Introduction

Autofluorescence spectroscopy is a non-invasive optical tool for early detection of oral cavity cancer at various anatomical sites and has shown its potential to discriminate different tissue types using SRRS (See Chapter 6). However, certain anatomical sites such as DST, LST and VBL were excluded from this study due to the ambiguity associated with the presence of similar spectral features in normal and abnormal tissues (Fig. 6.1). This study is an extension of the results presented in chapters 6 and 7 to develop a criterion for early detection of cancer affecting DST sites. Efforts are made initially to develop a site-specific SRRS for these sites using the three spectral intensity ratios. Toward this, a separate reference standard (SRRS) was developed for the DST, where a large number of the lesions were observed in clinical trials after buccal mucosa. This reference database involves 29 DST sites from 15 patients and 36 DST sites from healthy volunteers. But, it was seen that none of the these three scatter plots could discriminate different grades of dorsal tongue malignancy as in the case of buccal and other anatomical sites owing to the overlap of different grades that resulted in very poor diagnostic accuracies. This particular flaw in cancer diagnosis involving DST fluorescence is overcome by using DRS spectral features of tissue. In other words, this chapter explores the applicability of site-specific diffuse reflectance spectral intensity ratio (R545/R575) of the oxygenated haemoglobin bands to classify different dorsal tongue mucosa, where LIAF has poor reliability.

9.2 Materials and Methods

Spectral data from the DST recorded earlier from 35 healthy volunteers are used as control (See chapter 6). Clinical trials were conducted in 13 patients at 24 DST lesions with differing grades of malignancy. LIAF and DR spectral data acquisition and analysis were carried out as described before (section 3.3) using the LIFRS system . Study protocol and subject handling were the same as explained in the section 6.1.

9.3 Results and discussion

9.3.1 Fluorescence SRRS for DST Tissue Grading

Fig. 9.1 represents the normalized LIAF spectra recorded from different anatomical sites of oral cavity. The porphyrin like emission are quite prominent in the DST healthy tissues as compared to LST and VBL. These emissions are from the bacterial colonization, within the lingual papillary structure of the DST tissues, as discribed earlier (See chapter 6). In such histological structures the changes for deposition and retention of food particles

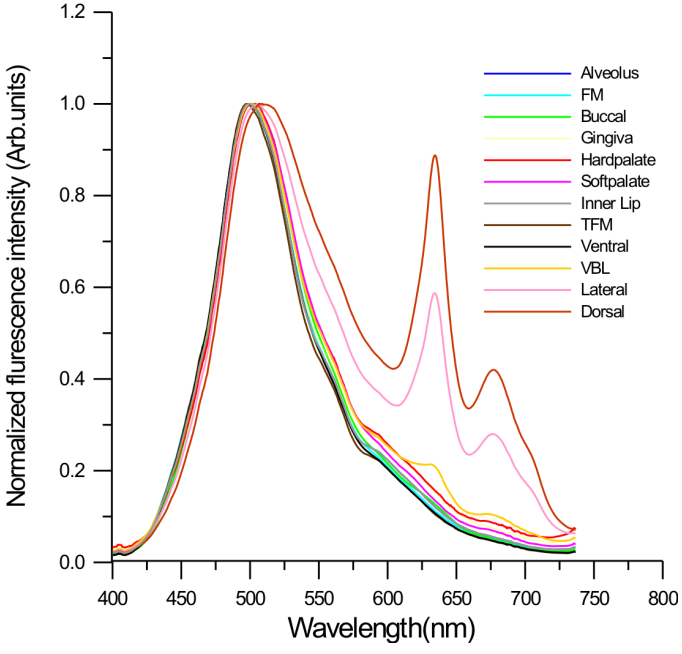

Fig. 9.1 Mean LIAF spectra from different anatomical sites of oral cavity normalized to the autofluorescence intensity at 500 nm. Each averaged spectra shown represent the mean of 15 measurements in 35 volunteers.

is enormous, making the ground fertile for bacterial colonization *(de Veld et al., 2003)*. Fig. 9.2 represents different grades of dorsal tongue tissues viz. healthy, hyperplastic, dysplastic and SCC. Surprisingly, it was seen that the porphyrin like emission peaks in the red region at 635, 685 and 705 nm for the healthy tissues are more prominent than those observed in the case of SCC. However, the emissions from abnormal tissues were found to vary according to the grade of the tissue abnormality, as observed at buccal and other sites of oral cavity (Fig. 6.3).

Earlier studies have shown LIAF spectral intensity ratios to be highly sensitive and specific to discriminate different mucosal variations and to screen early stages of tissue progression towards malignancy for all the anatomical sites other than the dorsal tongue, the lateral tongue and the vermillion border of lip (See Chapter 6). As described in the section 6.3.3, SRRS scatter plots for DST sites were drawn using the three spectral intensity ratios F500/F635, F500/F685 and F500/F705 from 24 sites in 13 patients, comprising of hyperplasia, dysplasia and SCC. To avoid the erroneous diagnosis the mean ratios from the DSt sites of 21 healthy volunteers were used as normal for comparison. The average

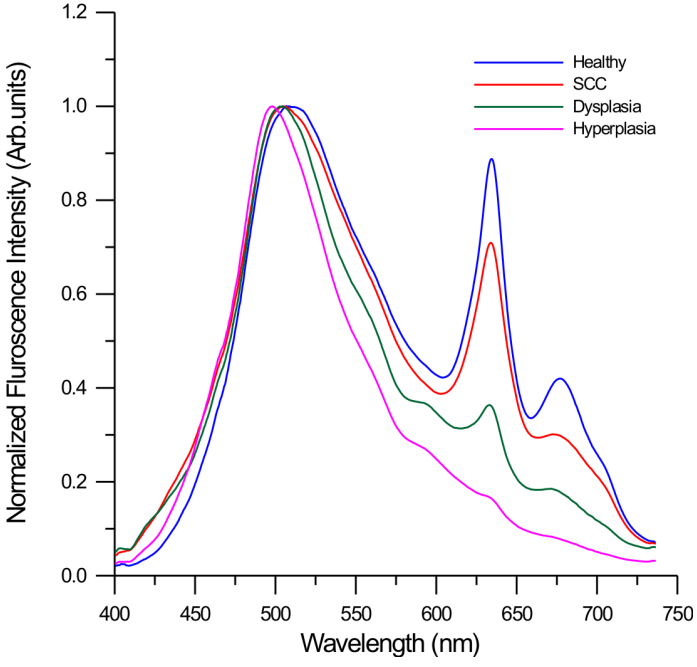

Fig. 9.2 Mean LIAF spectra from different grades of dorsal tongue tissues normalized to the autofluorescence intensity at 500 nm. Healthy spectra is the average of 36 volunteers, hyperplastic spectra is average of 4, dyspastic spectra is the average of 7, and SCC spectra is average of 13 lesions. Each spectrum shown is the average of 15 measurements.

fluroscence intensity ratios (F500/F635, F500/F705 and F500/F685) determined from the autofluorescenec spectra of study population along with the results of histology, visual impression and spectral impression for each ratios studied are shown in Table 9.1.

Fig. 9.3(a-c) shows the standard reference scatter plots for the three autofluorescence intensity ratios, which discriminates normal, hyperplastic, dysplastic and malignant dorsal tissues from one another. Discrimination lines were drawn between the normal and hyperplastic, hyperplastic and dysplastic, dysplastic and malignant at values that correspond to the average ratio values of the respective groups. For example, in the case of healthy tissues, the average F500/F635, F500/F685 and F500/F705 ratio values were 1.48, 3.24 and 4.8, respectively. The cut-off lines for discriminating the normal from hyperplastic were drawn at values corresponding to the mean of the normal ratios and those from the hyperplastic mucosa at 3.95, 7.87 and 13.95, respectively in patients.

The sensitivity and specificity were assessed by validation with the gold standard. Cut-off values in the reference scatter plots Fig. 9.3(a-c) of the autofluorescence intensity ratios (F500/F635, F500/F685 and F500/F705) were used in the determination of the dagnostic accuracies viz. sensitivity, specificity, PPV and NPV. Table 9.1 lists the diagnostic accuracies in discriminating normal tissues from hyperplastic, hyperplastic from dysplastic and dysplastic from SCC lesions for all the 23 dorsal sites in 13 patients. For the F500/F635 ratio a sensitivity of 100% and specificity of 75% was obtained to discriminate, by selecting cut-off at the mean (4.85) of dysplastic and hyperplastic values with a PPV and NPV of 0.80 and 1.0 respectively. In the same plot, cut-off line drawn at 2.61 discriminates pre-malignant dysplastic tissues from malignant SCC with a sensitivity of 77% and specificity of 86%, with NPV of 0.91 and 0.67 respectively. Using the information provided by the three SRRS plots, an overall sensitivity of 95% and specificity of 75% with a PPV of 0.85 and NPV of 0.92 was achieved in distinguishing dysplastic from hyperplasia, whereas dysplasias could be discriminated from SCC with a overall sensitivity of 67% and specificity of 77%, with a PPV of 0.84 and 0.56 respectively. Nevertheless, these figures are lower than the diagnostic accuracies attained for other anatomical sites using LIAF-SRRS (See chapter 6).

It is to be noted that in all the three discrimination scatter plots most of the normal tissue values were occupying the position meant for SCC, which means all the true negatives were wrongly identified as true positives. This indicates the incapability of the SRRS technique to differentiate normal oral mucosa from abnormal. In the past, many researchers (Betz et al., 1999; Dhingra et al., 1998, 1996; Gillenwater et al., 1998) reported very low specificities with high sensitivities to detect abnormal tissue sites in the oral cavity using blue light for excitation of endogenous porphyrin fluorescence. These lower specificities reported might

Table 9.1 Comparison of sensitivities and specificities of different LIAF and DR ratios in discriminating different tissue types of DST *in vivo.* Corresponding PPV and NPV values are shown in paranthesis, respectively.

Diagnostic Accuracies	Ratios	Normal Vs Hyperplasia	Hyperplasia Vs Dysplasia	Dysplasia Vs SCC
Sensitivity (%)	F500/F635	-	100 (0.80)	77 (0.91)
(PPV)	F500/F685	-	100 (0.88)	69 (0.90)
	F500/F705	-	86 (0.86)	54 (0.70)
	R545/R575	75 (1.00)	86 (0.86)	85 (0.92)
Specificity (%)	F500/F635	-	75 (1.00)	86 (0.67)
(NPV)	F500/F685	-	75 (1.00)	86 (0.60)
	F500/F705	-	75 (0.75)	58 (0.40)
	R545/R575	100 (0.97)	75 (0.75)	86 (0.75)

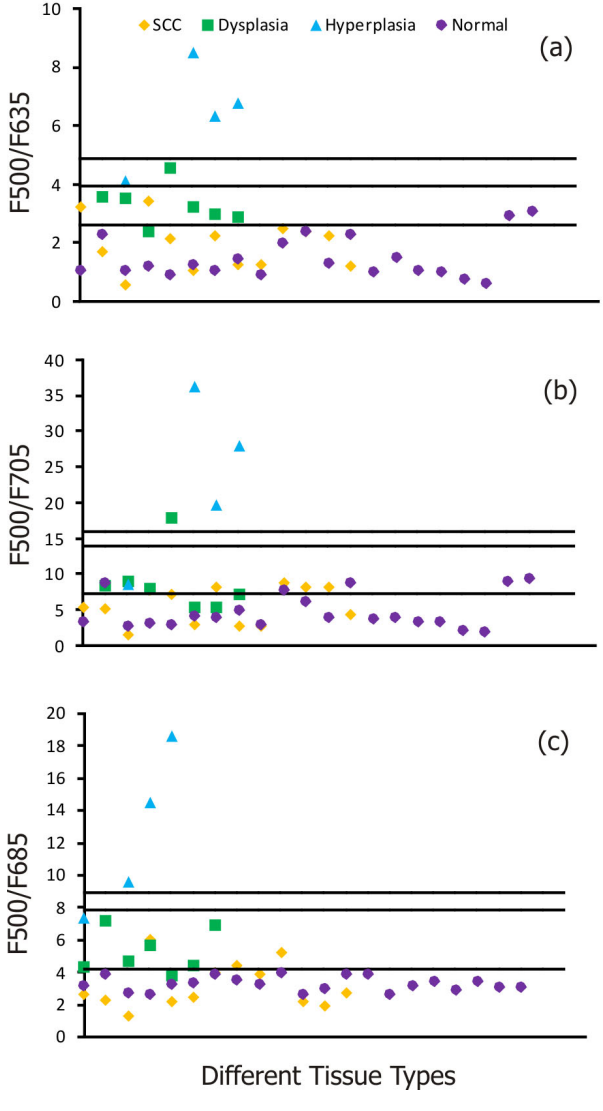

Fig. 9.3 Site-specific spectral ratio reference standard (SRRS) developed using the fluorescence intensity ratios **(a)** F500/F635 **(b)** F500/F685 **(c)** F500/F705 from the dorsal tongue in 21 healthy population and from 24 sites in 13 patients.

Table 9.1 Comparison of spectral impressions achieved using fluorescence intensity ratios (F500/F635, F500/F705 and F500/F685) and DR ratio R545/R575 of patients with corresponding histological and visual impresssions for DST.

P#	Histological Impression	Visual Impression	R545/R575	Spectral Impression	F500/F635	Spectral Impression	F500/F705	Spectral Impression	F500/F685	Spectral Impression
1	SCC	Ulcerative growth	0.865	SCC	3.22	Dysplasia	5.43	SCC	2.57	SCC
	Dysplasia	Proliferative growth	0.843	Dysplasia	3.56	Dysplasia	8.45	Dysplasia	4.33	Dysplasia
2	SCC	Ulcero proliferative lesion	0.867	SCC	1.70	SCC	5.23	SCC	2.27	SCC
	Hyperplasia	Normal	0.789	Normal	4.12	Dysplasia	8.53	Dysplasia	7.37	Dysplasia
3	SCC	Lesion	0.876	SCC	0.57	SCC	1.51	SCC	1.27	SCC
	Dysplasia	Normal	0.822	Dysplasia	3.50	Dysplasia	8.97	Dysplasia	7.15	Dysplasia
4	SCC	Ulcero proliferative lesion	0.874	SCC	3.43	Dysplasia	7.87	Dysplasia	5.99	Dysplasia
	SCC	Proliferative growth	0.855	SCC	2.15	SCC	7.21	Dysplasia	2.20	SCC
5	Dysplasia	Verrucous carcinoma	0.815	Hyperplasia	2.37	SCC	8.04	Dysplasia	4.64	Dysplasia
	Dysplasia	Verrucous carcinoma	0.832	Dysplasia	4.54	Dysplasia	17.81	Hyperplasia	5.66	Dysplasia
6	SCC	Lesion	0.856	SCC	1.07	SCC	2.91	SCC	2.39	SCC
	Hyperplasia	Normal	0.812	Hyperplasia	8.48	Hyperplasia	36.16	Hyperplasia	9.56	Hyperplasia
7	SCC	Lesion	0.859	SCC	2.24	SCC	8.26	Dysplasia	3.99	SCC
	SCC	Superficial growth	0.880	SCC	1.25	SCC	2.86	SCC	4.40	Dysplasia
8	SCC	Superficial growth	0.876	SCC	1.25	SCC	2.86	SCC	3.86	SCC
	Dysplasia	Leukoplakia	0.847	SCC	3.22	Dysplasia	5.43	SCC	3.75	SCC
9	SCC	Homogenous leukoplakia	0.840	Dysplasia	2.50	SCC	8.88	Dysplasia	5.21	Dysplasia
	Dysplasia	Erytroplakia	0.835	Dysplasia	2.97	Dysplasia	5.31	SCC	4.37	Dysplasia
10	Hyperplasia	Normal	0.836	Dysplasia	6.33	Hyperplasia	19.69	Hyperplasia	14.45	Dysplasia
	SCC	Homogenous leukoplakia	0.852	SCC	2.37	SCC	8.16	Dysplasia	2.19	SCC
11	SCC	Lesion	0.840	Dysplasia	2.24	SCC	8.26	Dysplasia	1.92	SCC
	Hyperplasia	Normal	0.817	Hyperplasia	6.75	Hyperplasia	27.92	Hyperplasia	18.60	Hyperplasia
12	Dysplasia	Superficial growth	0.840	Dysplasia	2.88	Dysplasia	7.26	Dysplasia	6.87	Dysplasia
13	SCC	Ulcero proliferative growth	0.869	SCC	1.18	SCC	4.45	SCC	2.72	SCC

Misclassifications are underlined

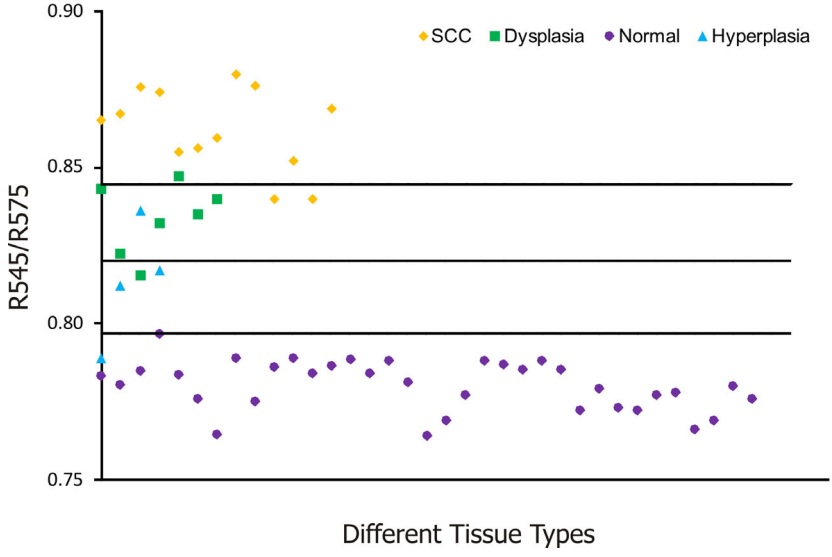

Fig. 9.4 Site-specific DR spectral ratio (R545/R575) scatter plot developed for discriminating different grades of DST tissues *in vivo*. The data shown relate to 24 DST sites in 13 patients and DST sites in35 healthy volunteers.

be due to the inclusion of tongue tissues in their algorithms, where the possibility of false positives is too high to affect the overall diagnostic capability of the fluorescence technique.

9.3.2 DRS-SRRS in Tissue Grading of DST

In order to overcome the flaws associated with LIAF in DST tissue grading, DR spectral spectral features of these tissue were studied. Fig. 9.4 shows the site-specific SRRS scatter plot of the oxygenated hemoglobin (R545/R575) ratio derived from DRS for discriminating hyperplastic, dysplastic and malignant tissues of the DST in the same set of 13 patients studied earlier using autofluorescence (Fig. 9.3a-c). Discrimination lines are drawn between the normal and hyperplasic, hyperplastic and dysplastic, dysplastic and SCC, at values that correspond to the average ratio value of the respective groups, as described in Chapter 5 (See section 5.3.4).

For example, the cut-off line discriminating the normal from hyperplastic was drawn at 0.789 that corresponds to the mean of healthy volunteer R545/R575 ratio (0.78) and the hyperplastic mucosa ratio (0.816) of patients. Similarly, the other two cut-off lines discriminating hyperplasia with dysplasia and dysplasia with SCC were drawn at their

respective mean values and each ratio was assigned a spectral impression based on their position in the scatter plot (see section 5.3.4).

Contrary to LIAF scatter plots (Fig. 9.3a-c), the R545/R575 ratio for normal tissues in Fig 9.4 occupies their designated area without any displacement to other areas and the ratio values were found to increase according to the progression of tissues towards malignancy. The classification sensitivity, specificity, PPV and NPV for discriminating each of these categories were determined based on the discrimination threshold values, by validation with the gold standard as before (Table 9.1).

The sensitivity and specificity for discrimination of hyperplastic DST tissues from normal were 75% and 100%, respectively, with a positive predictive value of 1.00 and negative predictive value of 0.97 using DRS technique. However, for discriminating pre-cancerous (dysplastic) DST mucosa from hyperplastic tissues, a sensitivity of 86% and specificity of 75% was achieved, with a positive predictive value of 0.86 and a negative predictive value of 0.75. On the other hand, dysplastic lesions were distinguishable from SCC with a sensitivity of 85% and specificity of 86%, with a corresponding PPV of 0.92 and NPV of 0.75.

The average DRS ratio R545/R575 determined from the DR spectra and their spectral impression is given Table 9.2 along with the three LIAF spectral ratios (F500/F635, F500/F685 and F500/F705) with corresponding histology and visual impression of each site. Spectral impressions given in Table 9.2 for each site are based on the spectral ratios of scatter plots shown in (Fig 9.3 and Fig 9.4). Visuallly, it is not possible to differentiate between various tissue types what a clinician can do is to discriminate normal from abnormal mucosa. But, results of the present study show that in some lesions, paticularly sites around the lesions which are histologicaly proven hyperplasia (Patient # 6, 11 and 10, in Table 9.2) and dysplasia (Patient #3), get misclassifiied by the clinician as normal. This shows that abnormal tissues need not necessarily present visual impresson to a clinician eventhough abnormality may be present in it microscopically. Further, it was noticed that DRS scatter plot accurately categorizes most of these sites as abnormal. In one case (Patient #10), the tissue which was identified clinically as homogenous leukoplakia was found to be SCC on histological analysis and also with the spectral impression based on the R545/R575 ratio SRRS and also with F500/F635, F500/F685 and F500/F705 ratio SRRS.

As can be seen from Table 9.2, among the LIAF scatter plots developed, F500/F705 scatter plot had the maximum number of misclassifications (8 out 24), while F500/F635 scatter plot produced the best classification (4 out of 24). In comparison, the R545/R575 SRRS produced a classification accuaracy 6 out of 24. However, in the DRS scatter plot (Fig. 9.4), it is seen that in only 1out of 38 cases there were misclassifications between normal and hyperplasia. This shows that DRS R545/R575 ratio scatter plot provides good potential to discriminate between normal and hyperplastic tissues. Whereas, LIAF ratio scatterplots (Fig 9.3a-c) have comparitively lesser ability to discriminate these tissue types, since most of the normal values were seen occupied in the region designated for SCC.

Thus, spectral approach using DRS appear to be an indispensable adjunct to LIAF in tongue cancer detection.

9.4 Conclusion

The results of the comparitive study between LIAF and DRShave shown that cancers affecting the tongue are always difficult to diagnose and be graded using tissue autofluorescence owing to the presence of porphyrin like fluorescence in normal tissues. Eventhough LIAF-SRRS developed can distingush between different abnormal tissues, the misclassification of normal tissues as SCC shows its frailty. This predicament in DST tissue grading using LIAF-SRRS was resolved to a great extent using the SRRS of oxygenated hemoglobin ratio (R545/R575) in an *in vivo* clinical experiment. Further, from the avilable results, it can be concluded that DRS-SRRS can differentiate different DST tissue typesin particular hyperplastic from normal with a sensitivity of 75% and specificity of and 100% respectively. Nonetheless, owing to the limited number of patients studied, the sensitivities and specificities shown may not be representative; however it shows the authenticity and potential of DRS ratio in discriminating tongue cancer.

Chapter 10

Conclusions and Future Perspectives

Conclusions and Future Perspectives

10

This final chapter critiques the entire study and compares the diagnostic accuracies of LIAF and DR modalities with results of different international groups working in this field. It also summarizes the advantages of these techniques and their limitations, major issues to be taken into consideration with regard to the application of these optical methodologies in oral cancer diagnosis and tissue grading. Future perspectives and directions for research and development in optical techniques for non-invasive detection oral pre-cancer are presented in the light of the present work.

Oral cancer is one of the most common cancers in India. Early diagnosis and treatment of cancer, helps in reducing mortality rates and in improving the quality of life of patients. More than 85% of cancers, like those affecting the oral cavity and cervix, are of epithelial origin. The vast majority of these epithelial cancers are preceded by cancerous changes that affect both the surface epithelium and deeper stroma. Biochemical and morphological changes associated with pre-cancer perturb tissue absorption, scattering and fluorescence properties. Therefore, optical spectroscopy is most suited for probing pre-cancerous changes in epithelial tissues (Chapter 1).

When light impinges on tissue, it is elastically scattered, following which absorption and fluorescence can occur, before the light leaves the tissue surface. Pre-cancers are accompanied by local metabolic and architectural changes in the nuclear-to-cytoplasmic ratio of cells, and changes in chromatin texture that affect the elastic scattering properties of tissue. Pre-cancers are characterized by increased metabolic activity that affects mitochondrial flurophores like NADH, FAD and selective accumulation of the PpIX and its pre-cursors thereby changing the autofluorescence spectral characteristics of the mucosa (Chapter 2).

Several point monitoring and imaging systems have been developed and some of these have turned into commercial products. A portable and compact laser-induced fluorescence and reflectance spectroscopy (LIFRS) system has been developed as part of this work for point monitoring of cancers affecting the mucosal tissues of the oral cavity and other superficial epithelial tissues. The LIFRS system uses a diode laser emitting at 405 nm for excitation of fluorescence and a tungsten halogen lamp for diffuse reflectance measurements from the oral cavity tissues. Optical radiation is taken out and guided to the tissues using optical fibers. The fiber-optic probe LIFRS system can easily be sterilized and is useful for measurements under normal room light. Tissue AF, DR and ALA-induced PpIX fluorescence spectra were recorded on a miniature fiber optic spectrometer, controlled by a laptop computer (Chapter 3).

Extensive *ex vivo* spectral measurements were carried out in surgically excised tissue samples before the LIFRS system was tested on human beings. Clearance from the Ethics Committee of the Regional Cancer Center, Trivandrum was obtained prior to initiation of clinical trials. During these clinical trials, tissue autofluorescence and fluorescence induced by topical application of 5-ALA were measured along with the diffuse reflectance spectra from different types of the oral lesions, within the lesion margin or apparently normal tissues of patients. Tissue biopsies were taken from the measurement sites for pathological confirmation of diagnosis. Fluorescence characteristics of healthy volunteers measured from the various anatomical sites of the oral cavity were utilized as control during data analysis.

Fluorescence diagnostics has been attracting a great deal of interest both in the research and clinical levels. It may be noted that field cancerization is a real problem and that oral carcinogenesis is regarded as a field effect and the surrounding mucosa is not genetically normal. Other hurdle is that most of the patients who participated in our study had smoking, chewing or alcohol consumption habits that could affect the adjoining and contra lateral tissue structure. To overcome this problem a clinical study in 36 healthy volunteers and 37 patients was conducted to develop a spectral reference standard to discriminate oral malignant squamous cell carcinoma (SCC) from dysplasia and hyperplasia using the spectral data of healthy population as control. The results of this study confirm that the distinction between the normal and diseased tissues within a patient is visually/clinically difficult and could lead to false classification or low specificities, as the tissues surrounding the lesion show varying degrees of dysplasia or atypia, in most of the cases.

It was observed that the fluorescence intensity of the 635, 685 and 705 nm bands in the autofluorescence spectra normalized to the 500nm peak has great value in the grading of oral cancer. LIAF studies in all anatomical mucosal sites of oral cavity, excluding DST, LST, VBT, have shown that these normalized fluorescence intensities increase with increasing grades of malignancy. The enhancement in these autofluorescence peak intensities, in particular at 635 nm, seen in the normalized fluorescence spectra was found to be most sensitive for detection of early tissue transformations and grading of oral mucosal malignancy.

LIAF intensity ratios F500/F635, F500/F685 and F500/F705 measured from different anatomical locations of the oral cavity have shown that usage of site specific ratios of healthy volunteers as control, instead of apparently normal tissues of patient, could improve the sensitivity and specificity in grading of oral SCC. Also, it was seen that all the 11 anatomical sites of the oral cavity, except DST, LST and VBT, have similar spectral features that led us to infer that the intensity ratios from these three sites are interchangeable. In this study, using spectral data from 40 sites of 37 patients and 36x11 sites of 36 healthy population, three spectral ratio reference standard (SRRS) scatter plots that correspond to F500/F635, F500/705 and F500/F685 ratios were created to discriminate malignant SCC from pre-malignant dysplasia, dysplasia from benign hyperplasia and hyperplasia from healthy tissues. The SRRS scatter plots developed shows improved sensitivity and specificity as compared to the clinical impressions and matches well with the gold standard. Among these three

Table 10.1 A comparison of the diagnostic accuracy of the present study using fluorescence spectral criteria with that of different research groups to distinguish in vivo hyperplasia (benign) from pre-malignant dysplasia

Research Group	Spectroscopy/ Methodology	Study site, population	Sensitivity (%)	Specificity (%)
de Veld et al., 2005	LIAF and DRS, PCA with various classifiers	Oral, 115 lesions	77	76
Nordstrom et al., 2001	DRS and UV excited fluorescence, Multivariate algorithm	Cervical, 120 lesions	77	76
Rupananda et al., 2008 (Present study, Chapter- 6)	LIAFS, Spectral ratio reference standard (SRRS) using scatter plots	Oral, 61 lesions	100	96
(Present study, Chapter-7)	Curve-fitted Gaussian area and intensity ratios of corrected LIAF spectra using DR spectra	Oral, 30 lesions	94	100

LIAFS – Laser Induced Autofluorescence Spectroscopy
ESS – Elastic Scattering Spectroscopy
DRS – Diffuse Reflectance Spectroscopy

SRRS plots, the F500/F685 SRRS appears more suited to identify tissue progression from normal to pre-malignant and malignant. Also, the blind-test conducted in a population of 17 patients confirmed the reliability of the SRRS criteria in discerning different tissue categories with good sensitivity and specificity. The advantage of using ratios over peak intensity method is that it eliminates errors in the system due to changes in excitation energy/ incident light levels, spectral response of the detection system, etc. (Chapter 6).

Dips were noticed in the autofluorescence spectra of tissues owing to the absorption from oxygenated hemoglobin. These absorption effects in the autofluorescence were filtered out or corrected with help of diffuse reflectance spectra from the same site. During tissue progression towards malignancy, the autofluorescence peak was seen red-shifted in the abnormal tissue and to locate the exact peak position of the constituent bands and their relative contributions in the overall spectra, the intrinsic LIAF spectrum was curve-fitted using Gaussian spectral functions. The ratios derived from curve-fitted Gaussian band intensities and areas showed higher contrast between different grades of tissues, as compared to raw LIAF ratios both under *ex vivo* and clinical environments (Chapter 7).

Measurements carried out in combination with the administration of fluorescent markers

or pre-cursors of fluorescent markers is also a practical and promising tool for tissue characterization. The uptake of 5-ALA by oral tissues was studied by monitoring the LIAF spectral variations over a three period. Towards this, the spectra of ALA induced porphyrin peaks were measured after topical application of 0.4% ALA solution in 11 healthy volunteers and in malignant and apparently normal (marginal) tissues of 15 patients.

The complex anatomy of oral cavity with differences in histology, keratin content and surface features, makes it distinctive from other organs. Eventhough, the type of epithelium is stratified throughout; the mucous membrane of the oral cavity is different for different sites. The mucosal lining of the buccal, the soft palate, the floor of mouth and the inner lip are non-keratinized, while those of lateral and dorsal tongue are keratinized. On the other hand, the gingival and the hard palate masticatory mucosa consist of a superficial keratin layer along with densely packed collagen fiber network beneath. These factors would jointly or severally be responsible for the observed changes in penetration or accumulation time of 5-ALA for different anatomical sites of the oral cavity. The knowledge of the optimum time for accumulation of ALA induced PpIX at different anatomical sites.would go a long way in improving the detection accuarcy.

The fluorescence intensities at 635, 685 and 705 nm measured from the LIAF spectra, normalized to the autofluorescence peak at 500 nm, studied and compared with the corresponding autofluorescence spectral data from the same set of patients (Chapter 8). The future directions in this field are promising particularly from the prospect of using endogenous sensitizers as compared to different exogenous contrast agents for cancer diagnosis. A proper understanding of accumulation rate of PpIX will also permit one to decide on the optimal time for therapeutic approaches like PDT.

The ratio (R545/R575) of the oxygenated hemoglobin absorption peaks at 542 and 577 nm present in the diffuse reflectance spectra is proposed for the first time to grade different stages of oral cancer, both under *ex vivo* and clinical conditions (Chapter 4 & 5). A sensitivity of 100% and specificity of 86% were achieved for discriminating pre-malignant tissues from benign tissues. Based on the results of autofluorescence studies presented, it can be presumed that the LIAF-SRRS criteria have low specificity in detecting abnormalities of three oral anatomical sites viz. DDT, LST and VBL, due to the presence of porphyrin peaks in healthy tissues. However, from the available results, it is seen that the DRS methodology using oxygenated HbO_2 has the potential to diagnose pre-cancer of the tongue (Chapter 9) with relatively better accuracies.

Majority of studies were undertaken to distinguish normal (a group of healthy and benign) from abnormal (a group of dysplastic and malignant) tissues (Volynskaya et al., 2008; Zhu et al., 2006; Muller et al., 2003; Mourant et al., 1996) or dysplastic from malignant lesions (de Veld et al., 2005; Muller et al., 2003; Mourant et al., 1996) or normal from malignant lesions (Anjan dhar et al., 2006; Muller et al., 2003; Bigio et al., 2000) or cancerous and high grade dysplasia from low grade, benign and normal (Park et al., 2008). The real

challenge for a diagnostic system lies in its ability to track malignancy in the premature stages, i.e. to distinguish hyperplastic (benign) from dysplastic (pre-malignant) lesions. As a consequence, the relevant question is not to be whether the suspicious tissue or lesion is normal or abnormal, because it has already been established as abnormal from its appearance by the clinician. The relevant question here should instead be whether the visible tissue alterations are of a benign or a pre-malignant nature, and the modality used would facilitate detection of the cancer in its incipient stage. Further, this is the most relevant question in the classification of visible lesions, the answer to which is crucial for treatment planning.

Consequently, detection of dysplasia is the critical element in determining therapy; but is extremely challenging. Many novel optical techniques are developed to address this problem. Some of these modalities show great promise as stand-alone techniques but, only few have solved this pivotal challenge to the point of clinical adoption to discriminate hyperplastic (benign) from dysplastic with good enough sensitivity and specificity. Tables 10.1 and 10.2 give a comparison of the diagnostic accuracies of the fluorescence and diffuse reflectance studies presented in this thesis with the results obtained by other groups for distinguishing hyperplastic from dysplastic tissues *in vivo*.

Since scanning of the entire oral cavity with a fiber-optic probe is impractical, in practice, the measurement probe is usually targetted at lesions that have already been found suspicious by visual inspection, and this tends to give good figures for diagnostic accuracies. However, in the current study, although the sites from the margin areas were often seen clinically as normal, both LIAF and DRS were able to identify them correctly as hyperplasia or dysplasia and these findings were well substantiated by histological reports. Further, in some cases, clinically misclassified leukoplakias were shown as SCC, which were again confirmed histologically as SCC. Results indicate that these techniques have immense potential to provide quantitative information about tissue transformation during experimental drug therapy and in the investigation of disease progression prior to the appearence of visible changes, suggesting the potential for these techniques to be used as complementary to clinical assessment.

In order to check which methodology is superior for discrimination of hyperplasia versus dysplasia ROC- curve analysis was performed on the three LIAF intensity ratios and DR oxygenated hemoglobin ratio using SPSS (Version 10) software. This software automatically calculates the sensitivity and specificity of given input ratio values and plots the ROC curves, with sensitivity values against the values of 1-specificity. We compared the area under different curves (AUC) to check the efficacy of different methodologies without being constricted to single values of sensitivity and specificity, which largely depend on the threshold or cut-off values chosen (Metz, 1978). For both LIAF and DRS, the classification of these lesions were successful with very good values of ROC-AUC. Figs 10.1 (a-d) show ROC-curve plotted using sensitivity and specificity values obtained for LIAF ratios F500/F635, F500/F685, and F500/F705 (See chapter 6) and DR HbO_2 ratio R545/R575 (See chapter 5) to discriminate different grades oral mucosa. Discrimination of different tissue types are possible

Table 10.2 Comparison of the diagnostic accuracies of the present study with ESS/DRS spectral criteria of different international groups to distinguish in vivo hyperplasia (benign) from pre-malignant dysplasia

Research Group	Methodology	Study site, population	Sensitivity (%)	Specificity (%)
Lovat et al., 2006	ESS, Classification by leave one out and block validation statistical approach.	Oesophagous 181 lesions	79	79
Anjan Dhar et al., 2006	ESS, Statistically validated model using PCA and linear discriminant analysis (LDA).	Colon, 138 lesions	85	88
de Veld et al., 2005	LIAF and DRS, PCA with various classifiers	Oral, 115 lesions	77	76
Nordstrom et al., 2001	DRS and UV excited fluorescence, Multivariate algorithm	Cervical, 120 lesions	77	76
Ge et al., 1998	DRS, Pattern recognition algorithms including multiple linear regression (MLR), LDA.	Colon, 76 lesions	85	81
Ge et al., 1998	DRS, Pattern recognition algorithms including back-propogating neural network (BNN).	Colon, 76 lesions	82	82
Nieman et al., 2008	Oblique polarized reflectance spectroscopy (OPRS), LDA.	Oral, 57 lesions	96	77
Rupananda et al., 2008 (present study, chapter-5)	DRS, HbO_2 absorption intensity ratios,	Oral, 49 lesions	100	86
Present study, chapter-7	Curve-fitted Gaussian area and intensity ratios of corrected LIAF spectra using DR spectra	Oral, 30 lesions	94	100

LIAFS – Laser Induced Autofluorescence Spectroscopy
ESS – Elastic Scattering Spectroscopy
DRS – Diffuse Reflectance Spectroscopy

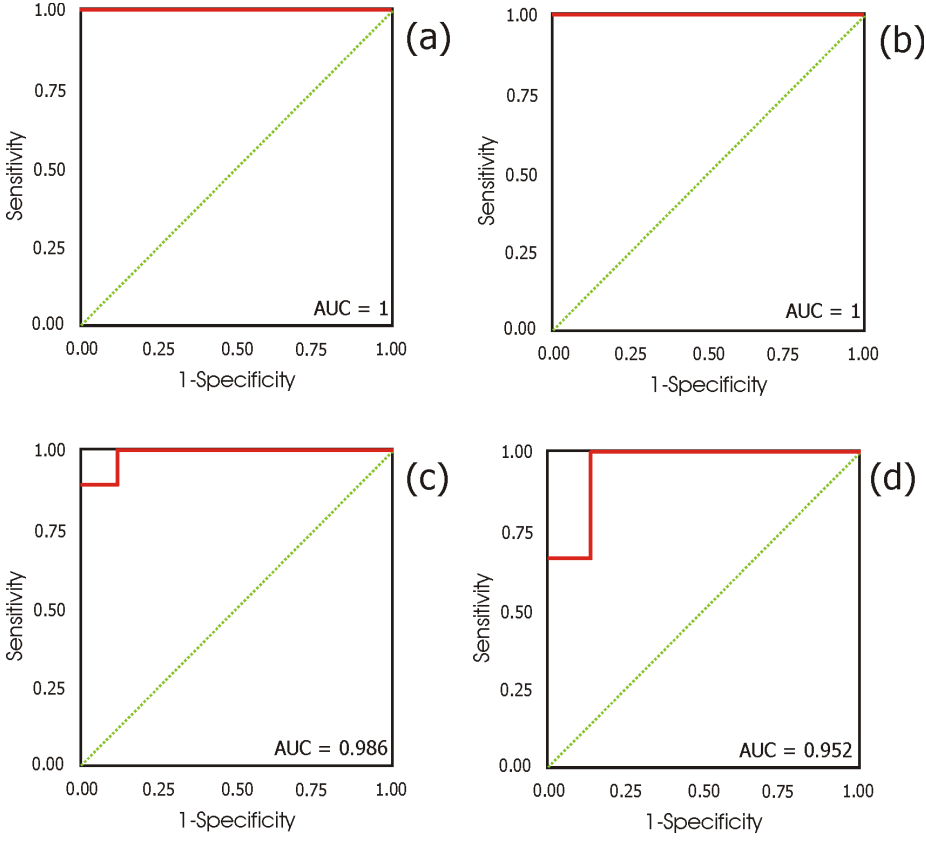

Fig. 10.1 ROC curve and area for four different intensity ratios **(a)** F500/F635 **(b)** F500/F685 **(c)** F500/F705 **(d)** R545/R575, for classifying hyperplastic from dysplastic tissues. (a-c) represent the mean *in vivo* LIAF ratio values from all sites of 43 patients except DST, LST and VBL (See chapter 6) whereas (d) relate to the mean *in vivo* DR ratio from all the sites studied in 29 patients (See chapter 5).

with ROC-AUC in the range 0.9-1. However, for the relevant clinical challenge, of discriminating hyperplastic from dysplastic lesions using F500/F635 and F500/F685 LIAF ratios ROC-AUC values were 1, while for the F500/F705 ratio it was a less at 0.986. In another study, using a different combination of normalization methods and classifiers de veld et al (2005) has obtained ROC-AUC <0.65 to differentiate hyperplastic tissues from dysplastic tissues for different excitation wavelengths, which are well below the values achieved in this study using LIAF spectral ratios. In the same study, by applying the same procedure to DRS spectra they have achieved a better ROC-AUC in the range 0.70-0.77. In comparison, the

DR ratio R545/R575 has produced a ROC-AUC value of 0.952 to discriminate hyperplastic from dysplastic tissues. Therefore is the AUC value shown by the R545/R575 ratio is of great significance since the variation in the HbO_2 ratio values with tissue transformation are often occur in the last two decimals and the good ROC-AUC value od 0.952 shows the adequacy of the DRS-SRRS developed. However, the results of the ROC curve analysis shows that LIAF-SRRS is a better diagnostic technique as compared to DRS-SRRS.

In conclusion, it is evident that the LIFRS system developed has the capability to sequentially measure autofluorescence and diffuse reflectance spectra from target tissues and be utilized as a non-invasive tool for oral cancer diagnosis. This study has clearly shown that the methodology developed could act as an auxiliary adjunct to the clinicians in tissue differentiation and facilitate speedy diagnosis at the clinic to arrive at appropriate follow-up decisions, ensuing in treatment or surgery. Further, application of this this point monitoring system is extendable for detection of other epithelial cancers of the cervix or skin and has the potential to aid in demarcating malignant lesions during surgical interventions. It can also be adapted to detect superficial tumors of internal organs by coupling to an endoscope. Neverthless, the diffuse reflectance ratio technique by virtue of its low cost, high sensitivity and specificity could turn out to be a viable alternative for *in vivo* cancer screening. Thus, it can be concluded that findings of the current study demonstrate that information provided by non-invasive DR, LIAF and LIPSIF spectroscopyalong with suitable analytical methods has immense potential to diagnose oral cancer in its early stages.

Eventhough, there is no thumb rule regarding study population, the basic constraint of this study was with respect to the patient population, especially as lesions were divided into different categories for classification. Another limitation associated with point monitoring is that it takes a few minutes to scan the entire lesion surface and to identify pre-malignant changes. This can be overcome with the use of multi-spectral imaging systems based on intensified CCD (ICCD) or EMCCD cameras that can gather fluorescence/reflectance images of the suspicious sites at specified wavelengths regions with use of proper interference filters or liquid crystal tunable filters in a fast and sensitive manner. The lateral spread of malignancy as well as early tissue transformations could be assessed from fluorescence image intensities at 635, 685 and 705 nm, or from the F500/F635, F500/F685 and F500/F705 image ratios or with the use of the diffuse reflectance image ratio (R545/R575) with white light illumination. Such imaging systems could be operated even by low-skilled persons for tissue grading and would be very useful in the community extension centers for mass screening of suspicious lesions.

Bibliography

af Klitenberg C, Charlotta L, Wang I, Vaitkuviene A, Svanberg K, Laser-induced fluorescence studies of premalignant and benign lesions in female genital tract. In: Bigio IJ, Svanberg K, Sehncekenberger H, Salik J, Viallet PM, eds., Optical biopsies and microscopic techniques II, Proc. SPIE vol.3197, 34-40, 1997.

af Klinteberg C, Enejedar AMK, Wang I, Andersson-Engels S, Svanberg S, Svanberg K, Kinetic fluorescence studies of 5-ALA induced protoporphyrin IX accumulation in basal cell carcinomas, *J Photochem Photobiol B* 49:120-128, 1999.

Alberts B, Johnson A, Lewis J, Alberts, Raff M, Roberts K, Walter P, Molecular biology of the cell, Garland Science, Newyork (2002).

Amelink A, Sterenborg HJCM, Bard MPL, Burgers SA, *In vivo* measurement of the local optical properties of tissue by use of differential path-length spectroscopy, *Opt Letters* 29(10):1087-1089, 2004.

Andersson RR and Parrish JA, Optical properties od human skin, In: The science of photomedicine, eds., Regan JD and Parrish JA, pp. 147-194, Plenum press, Newyork, 1982.

Andersson-Engels S, Baeret L, Berg R, D'Hallewin MA, Johansson J, Stenram U, Svanber K, Svanberg S, Fluorescence charecteristics of human atherosclerotic plaque and malignant tumors, In: Dougherty TJ, ed., Optical methods for tumor treatment and early diagnosis mechanism and techniques, Proc. SPIE vol. 1426, 31-43, 1991.

Andersson-Engels S and Wilson BC, *In vivo* fluorescence in clinical oncology: fundamental and practical issues, *J Cell Pharmacol* 3:48-61, 1992.

Andersson-Engels S, Johansson J, Svanberg S, Medical diagnostic system based on simultaneous multispectral fluorescence imaging, *Appl Opt* 33:8022-8029, 1994.

Andersson-Engels S, af Klinteberg C, Svanberg K, Svanberg S, *In vivo* fluorescence imaging for tissue diagnostics, *Phys Med Biol* 42:815–24, 1997.

Anjan Dhar DM, Johnson KS, Novelli MR, Bown SG, Bigio IJ, Lovat LB, Bloom SL, Elastic scattering spectroscopy for the diagnosis of colonic lesions: initial results of a novel optical biopsy technique, *Gastrointestinal Endoscopy* 63(2):257-261, 2006.

Araki K, Ariji E, Shimizu M, Kanda S, Ozeki S, Shinohara M, Ariji Y, Computed tomography of carcinoma of the upper gingiva and hardpalate: correlation with the surgical and histopathological findings, *Dentomaxillofac Radiol* 26(3):177-182, 1997.

Backman V, Wallace M, Perelman LT, Arendt JT, Gurjar R, Müller MG, Zhang Q, Zonios G, Kline E, McGillican T, Shapshay S, Valdez T, Badizadegan K, Crawford JM, Fitzmaurice M, Kabani S, Levin HS, Seiler M, Dasari RR, Itzkan I, Van Dam J, Feld MS, Detection of pre-invasive cancer cells, *Nature* 406:35-36, 2000.

Backman V, Gurjar R, Badizadegan R, Dasari R, Itzkan L, Perelman LT, Feld MS, Polarized ligh scattering

spectroscopy for quantitative measurment of epithelial cellular structures *in situ*, *IEEE J Sel Top Quant Elect* 5:1019-1027, 1999.

Bakker STC, Witjes MJ, Sterenborg HJCM, Speelman OC, Roodenburg JL, Marple ET, Bruining HA, Puppels GJ, *In vivo* detection of dysplastic tissue by Raman Spectroscopy, *Anal Chem* 72:6010-6018, 2000.

Baumgartner R, Huber RM, Schulz H, Stepp H, Rick K, Gamarra F, Leberig A, Roth C, Inhalation of 5-aminolevulinic acid: a new technique for fluorescence detection of early stage lung cancer, *J Photochem Photobiol B* 36(2):169-174, 1996.

Beauvoit B, Kitai T, Chance B, Contribution of the mitochondrial compartment to the optical properties of the rat liver: a theoretical and practical approach, *Biophys J* 67: 2501-2510, 1994.

Benson RC, Meyer RA, Zaruba ME, McKhann GM, Cellular autofluorescence-is it due to flavins?, *J Histochem Cytochem* 27:44-48, 1979.

Betz CS, Mehlmann M, Rick K, Stepp H, Grevers G, Baumgartner R, Leunig A, Autofluorescence imaging and spectroscopy of normal and malignant mucosa in patients with head and neck cancer, *Lasers Surg Med* 25:323-334, 1999.

Betz CS, Stepp H, Janda P, Arbogast S, Grevers G, Baumgartner R, Leunig A, A comparative study of normal inspection, autofluorescence and 5-ALA-induced PpIX fluorescence for oral cancer diagnosis, *Int J Cancer* 97:245-252, 2002.

Beuthan J, Minet O, Helfmann J, Herrig M, Müller G, The spatial variation of the refractive index in biological cells, *Phys Med Biol* 41:369-382, 1996.

Bigio IJ, Bown SG, Briggs G, Kelley C, Lakshmi S, Pickard D, Ripley PM, Rose IG, Saunders C, Diagnosis of breast cancer using elastic-scattering spectroscopy: Preliminary clinical trials, *J Biomed Opt* 5(2):221-228, 2000.

Blair EA and Callendar DL, Head and neck cancer-the problem, *Clin Plast Surg* 21:1-7, 1994.

Boggards A, Aalders MCG, Jongen AJL, Dekker E, Sterenborg HJCM, Double ratio fluorescence imaging for early detection of superficial cancers - Design, construction and performance of a clinical prototype, *Rev Sci Instrum* 72(10):3956-3961, 2002a.

Boggards A, Aalders MCG, Zeyl CC, Blok S, Dannecker C, Hillemanns P, Stepp H, Sterenborg HJCM, Localisation and staging of cervical intraepithelial neoplasia using double ratio fluorescence imaging, *J Biomed Opt* 7(2):215-220, 2002b.

Bolin FP, Preuss LE, Taylor RC, Ference RJ, Refractive index of some mammalian tissue using a fiber optic cladding method, *Appl Opt* 28:2297-2303, 1989.

Bonnett R, Berenbaum M, Porphyrins as photosensitizers, In: Photosensitizing Compounds: their Chemistry, Biology and Clinical Use, eds., Bock G and Harnett S, pp. 40-59, John Wiley & Sons Ltd, Chichester, UK, 1989.

Boone C, Bacus JW, Bacus JV, Steele VE, Kelloff GJ, Properties of intraepithelial neoplasia relevant to cancer chemopreventation and the development of surrogate for clinical trial, *Proc Soc Exp Biol Med* 216:151-165, 1997.

Boring CC, Squires TS, Tong T, Montgomery S, Cancer statistics, *CA Cancer J Clin* 44:7-26, 1994.

Bottiroli G, Roce AC, Locatelli D, Marchesini E, Pignoli E, Tomatis S, Cuzzoni C, Dipalma S, Dalfante M, Spinelli P, Natural fluorescence a of normal and neoplastic humon colonm: A comparitive *ex-vivo* study, *Lasers Surg Med* 16:48-60, 1995.

Bottomley SS and Muller-Eberhard U, Pathophysiology of heme synthesis, *Semin Hematol 25:*282-302, 1988.

Boulnois JL, Photophysical processes in recent medical laser developments: a review, *Lasers Med Sci* 1:47-66, 1986.

Carvalho AL, Nishimoto IN, Califano JA, and Kowalski LP, Trends in incidence and prognosis for head and neck cancer in the United States: a site-specific analysis of the SEER database, *Int J Cancer* 114:806-816, 2005.

Cerussi AE, Jakubowski D, Shah N, Bevilacqua F, Lanning R, Berger AJ, Hsiang D, Butler J, Holcombe RF, Tromberg BJ, Spectroscopy enhances the information content of optical mammography, *J Biomed Opt* 7:60-71, 2002.

Charlotta E, Optical characterization of tissue for medical diagnostics, Ph. D Thesis, Department of Physics, Lund Institute of Technology, Lund, Sweeden, 1999.

Chance B and Schoener B, Fluorometric studies of flavin component of respiratory chain, In: Flavins and flavoproteins, ed., Slater EC, pp. 510-519, Elsevier Publishing Comp, New York, USA, 1966.

Charoenbanpachon S, Krasieva T, Ebihara A, Psann K, Wilder-Simth P, Acceleration of ALA-induced PpIX fluorescence development in Oral Mucosa, *Lasers Surg Med* 32(3):185-188, 2003.

Coremans JMCC, Ince C , Bruining HA, Puppels J, Semi-quantitative analysis of reduced nicotinamide adenine di-nucleotide fluorescence images of blood-perfused rat heart, *Biophy J* 72:1849-1860, 1997.

DaCosta RS, Wilson BC, Marcon NE, Photodiagnostic techniques for the endoscopic detection of premalignant gastrointestinal lesions, *Digestive Endoscopy* 15:153-173, 2003.

Da Costa RS, Anderson H and Wilson B, Molecular Fluorescence excitation-emission matrices relevant to tissue spectroscopy, *Photochem Photobiol* 78:384-392, 2003.

Dailey HA and Smith A, Differential interaction of porphyrins used in photoradiation therapy with ferrochelatase, *Biochem J* 223:441-445, 1984.

Daniell MD, Hill JS, A history of photodynamic therapy, *Aust N Z J Surg* 61:340-348, 1991.

de Rosa FS, Marchetti JM, Thomazini JA, Tedesco AC, Bentley MVLB, A vehicle for photodynamic therapy of skin cancer: influence of dimethylsulfoxide on 5-ALA in vitro cutaneous permeation and in vivo PpIX accumulation determined by confocal microscopy, *J Control Release* 65:359-366, 2000.

de Veld DCG, Skurichina M, Witjes MJH, Duin RPW, Sterenborg HJCM, Roodenburg JLN, Autofluorescence and diffuse reflectance spectroscopy for oral oncology, *Lasers Surg Med* 36(5):356-364, 2005a.

de Veld DCG, Witjes MJH, Strenborg HJCM, Roodenburg JLN, The status of in vivo autofluorescence and imaging for oral oncology, *Oral Oncology* 41:117-131, 2005b.

de Veld DC, Skurichina M, Witjes MJH, Duin RPW, Sterenborg HJCM, Clinical study for classification of benign, dysplastic and malignant oral lesions using autofluorescence spectroscopy, *J Biomed Opt* 9(5):940-950, 2004.

de Veld DCG, Skurichina M, Witijes MJH, Duin RPW, Sterenborg HJCM, Star WM, Roodenburg JLN, Autofluorescence characteristics of healthy oral mucosa at different anatomical sites, *Lasers Surg Med* 23:367-376, 2003.

Dhingra JK, Perrault DF jr, McMillan K et al, Early diagnosis of upper aerodigestive tract cancer by autofluorescence, *Arch Otolaryngol Head Neck Surg* 122:1181-1186, 1996.

Diamond KR, Farrell TJ, Patterson MS, Measurement of fluorophore concentrations and fluorescence quantum yield in tissue-simulating phantoms using three diffusion models of steady-state spatially resolved fluorescence, *Phys Med Biol* 48(24):4135-4149, 2003.

Dougherty TJ, Henderson BW, Schwartz S, Winkelman JW, Lipson RL, Historical perspective, In: Photodynamic therapy, eds., Henderson BW and Dougherty TJ, pp. 1-15, Marcel Dekker, New York, 1992.

Drezek R, Guillaud M, Collier T, Boiko I, Nalpica A, Macaulay C, Follen M, Richards-kortum R, Light scattering from cervicall cells throughout neoplastic progression: Influence of nuclear morpholpgy, DNA content, and chromatin texture, *J Biomed Opt* 8:7-16, 2003.

Drezek R, Sokolov K, Utzinger U, Boiko I, Malpica A, Follen M, Richards-Kortum R, Understanding the contributions of NADH and collagen to cervical tissue fluorescence spectra:modeling, measurements and implications, *J Biomed Opt* 6:385-396, 2001.

Eker C, Rydell R, Svanberg k, Andersson-Engels S, Multivariate analysis of laryngeal fluorescence spectra recorded *in vivo*, *Lasers Surg Med* 28:259-266, 2001.

El-Sharabasy MMH, El-Waseef AM, Hafez MM, Salim SA, Porphyrin metabolism in some malignant diseases, *Br J Cancer* 65**:**409-412, 1992.

Epstein JB, Feldman R, Dolor RJ, Porter SR, The utility of tolonium chloride rinse in the diagnosis of recurrent or second primary cancers in patients with prior upper aerodigestive tract cancer, *Head Neck* 25:911-921, 2003.

Epstein JM, Phototherapy and Photochemotherapy, *N Engl J Med* 32:1149-1151, 1990.

Evan GI and Vousden KH, Proliferation, cell cycle and apoptosis in cancer, *Nature* 411:342-348, 2001.

Fantini S, Walker S, Franceschini MA, Kaschke M, Schlag PM and Moesta KT, Assessment of size, position and optical properties of breast tumors *in vivo* by noninvasive optical methods, *Appl Opt* 37:1982-1989, 1998.

Farrell TJ, Patterson MS, Wilson B, Diffusion theory model of spatially resolved, steady-state diffuse reflectance for non-invasive determination of tissue optical properties *in vivo*, *Med Phys* 19:879-888, 1992.

Feld MS, Spectral pathology using reflected light, In: *Biomedical* nuclear morphology, *Opt Express* 5:302-317, 1999.

Feld MS. Spectral pathology using reflected light, In: Biomedical Optical Spectroscopy and Diagnostics, Technical Digest, pp. 2/BMA 1-1, Optical Society of America, Washington DC, 1998.

Figge FHJ, Weiland GS, The affinity of neoplastic, embryonic, and traumatized tissue for porphyrins and metalloporphyrins, *Anat Rec* 100:659-659, 1948.

Filbeck T, Roessler W, Knuechel R, Straub M, Kiel HJ, Wieland WF, Clinical results of the transurethreal resection and evaluation of superficial bladder carcinomas by means of fluorescence diagnosis after intravesical instillation of 5-aminolevulinic acid, *J Endourol* 13, 117-121, 1999.

Finlay CJ, Reflectance and fluorescence spectroscopies in Photodynamic therapy, PhD thesis, Department of Physics and Astronomy, The college Arts and Sciences, Rochester University, NY, USA 2003.

Finsen NR, Phototherapy, Edward Arnold, London, England, 1901.

Fitzpatrick TB and Pathak MA, Historical aspects of methoxsalen and other furocoumarins, *J Inest Dermatol* 23:229-232, 1959.

Forlay J, Parking DM, Pissani P, Globscan 2002: Cancer incidence mortality and prevalence worldwide, Lyon IARC publication, 2007.

Friesen SA, Hjortland GO, Madsen SJ, Hirscheberg H, Engebraten O, Nesland JM and Peng Q, 5-Aminolevulinic acid-based photodynamic detection and therapy of brain tumors, *Int J Oncol* 21:577-582, 2002.

Ge Z, Schomacker KT, Nishioka NS, Identification of colonic dysplasia and neoplasia by diffuse reflectance and pattern recognition technique, *Appl Spectrosc* 52:833-845, 1998.

Ghadially FN, Neish WJP, Dawkins HC, Mechanisms involved in the production of red fluorescence of human experimental tumors, *J Pathol Bact* 83:77-92, 1963.

Gillenwater A, Jacob R, Ganeshappa R, Kemp B, El-Naggar AK, Palmer JL, Clayman G, Mitchell MF, Richards-Kortum R, Noninvasive diagnosis of oral neoplasia based on fluorescence spectroscopy and native tissue autofluorescence, *Arch Otolaryngol Head Neck Surg* 124:1251-1258, 1998a.

Gillenwater A, Jacob R, Richards-Kortum R, Fluorescence spectroscopy: A technique with potential to improve the early detection of aerodigestive tract neoplasia, *Head Neck* 20: 556-562, 1998b.

Gillies R, Zonios G, Anderson RR, Kollias N, Fluorescence excitation spectroscopy provides information about human skin *in vivo*, *J Invest Dermatol* 115:704-707, 2000.

Godavarty A, Zhang C, Eppstein MJ, Sevick-Muraca EM, Fluorescence-enhanced optical imaging of large phantoms using single and simultaneous dual point illumination geometries, *Med Phys* 31:183-190, 2004.

Goergakoudi I, Jacobson BC, Muller MG, Sheets EE, Badizadegan K, Carr-Locke DL, Crum CP, Boone CW, Dasari RR, Dam JV, Feld MS, NAD(P)H and collagen as *in vivo* quantitative fluorescent biomarkers of epithelial precancerous changes, *J Cancer Res* 62:682-687, 2002.

Goergakoudi I, Jacobson BC, Dam JV, Backman V, Wallace MB, Muller MG, Zhang Q, Badizadegan K, Sun D, Thomas GA, Perelmann LT, Feld MS, Fluorescence, Reflectance and light-scattering for evaluating dysplasia in patients with Barrett's esophagus, *Gastroenterology* 120(7):1620-1629, 2001.

Griner PF, Mayewski RJ, Mushlin AI, Greenland P, Selection and interpretation of diagnostic tests and procedures, *Annals Int Med* 94:555-600, 1981.

Grosenick D, Moesta KT, Wabnitz H, Mucke J, Stroszczynski C, Macdonald R, Schlag PM, Rinneberg H, Time-domain optical mammography: initial clinical results on detection and characterization of breast tumors, *Appl Opt* 42:3170–3186, 2003.

Gupta PK, Majumdar SK, Uppal A, Breast cancer diagnostics using N_2 laser excited autofluorescence spectroscopy, *Lasers in Surg Med* 21:417-422, 1997.

Harris ML, Lam S, MacAulay C, Qu J, Palcic B, Diagnostic imaging of the larynx: autofluorescence of laryngeal tumours using helium-cadmium laser, *J Laryngeal Otol* 109(2):108-110, 1995.

Hebden JC, Veenstra H, Dehghani H, Hillman EM, Schweiger M, Arridge SR, Delpy DT, Three-dimensional time-resolved optical tomography of a conical breast phantom, *Appl Opt* 40:3278-3285, 2001.

Heintzelman DL, Utzinger U, Fuchs H, Zuluaga A, Gossage K, Gillenwater AM, Jacob R, Kemp B, Richards-Kortum R, Optimal excitation wavelengths for in vivo detection of oral neoplasia using fluorescence spectroscopy, *Photochem Photobiol* 72:103-113, 2000.

Hewett J, Nadeau V, Feguson J, Moseley H, Ibbotson S, Allen JW, Sibbett W, Padgett M, The application of a compact multispectral imaging system with integrated excitation source to *in vivo* monitoring of fluorescence during topical photodynamic therapy of superficial skin cancers, *Photochem Photobiol* 73(3):278, 2001.

Heyerdahl H, Wang I, Liu DL, Berg R, Andersson-Engels S, Peng Q, Moan J, Svanberg S, Svanberg K, Pharmacokinetic studies on 5-aminolevulinic acid-induced protoporphyrin IX accumulation in tumours and normal tissues, *Cancer Lett* 112:225-231, 1997.

Hillegersberg R, van den Berg JWO, Kort WJ, Terpstra OT, Wilson JHP, Selective accumulation of endogenously produced porphyrins in a liver metastasis model in rats, *Gastroenterology* 103:647-651, 1992.

Hillemanns P, Weingandt H, Baumgartner R, Diebold J, Xiang W, Stepp H, Photo detection of cervical intraepithelial neoplasia using 5-aminolevulinic acid-induced porphyrin fluorescence, *Cancer* 88:2275-2282, 2000.

Hinnen P, de Rooij FWM, van Velthuysen MLF, Edixhoven A, van Hillegersberg R, Tilanus HW, Wilson JHP, Siersema PD, Biochemical basis of 5-aminolaevulinic acid-induced protoporphyrin IX accumulation: a study in patients with pre-malignant lesions of the oesophagus, *Br J Cancer* 78:679-682, 1998.

Huang Z, Zheng W, Xie S, Chen R, Mclean DF, Lui H, Zeng H, Laser-induced autofluorescence microscopy of normal and tumor human colonic tissue, *Int J Oncol* 24:59-63, 2004.

Hung J, Lam S, LeRiche JC, Palcic B, Autofluorescence of normal and malignant bronchial tissue, *Lasers Surg Med* 11:99-105, 1991.

Hyde N, and Hopper C, Oral cancer: The importance of early referral, *Practitioner* 243 (1603):756-761, 1999.

Inaguma M and Hashimoto K, Phorphyin-like fluorescence in oral cancer: *in vivo* fluorescence spectral characterization of lesions by use of a near ultravioler excited autofluorescence diagnosis system and separation of fluorescent extracts by capillary electrophoresis, *Cancer* 86(11): 2202-2211, 1999.

Ingrams DR, Dingra JK, Roy K, Perault DF, Bottrill ID, Kabani S, Rebeiz EE, Pankratov MM, Shapshay SM, Manoharan R, Itzkan I, Feld MS, Autofluorescence characteristics of oral mucosa, *Head Neck* 19:27-32, 1997.

Irving JB, Stephen GB, Spectroscopic sensing of cancer and cancer therapy, *Cancer Bio Therapy* 3(3):259-267, 2004.

Jain B, Majumdar SK, Gupta PK, Time resolved and steady state autofluorescence spectroscopy of normal and malignant human breast tissue, *Lasers in Life Sci* 8:163-173, 1998.

Jain RK, Determinants of tumour blood flow: a review, *Cancer Res* 48:2641-2658, 1988.

Jayachandran B, Ge J, Regalado S, Godavarty A, Design and development of a hand-held optical probe toward fluorescence diagnostic imaging, *J Biomed Opt* 12(5):054014, 1-10, 2007.

Jiang H, Iftimia NV, Xu Y, Eggert JA, Fajardo LL, Klove KL, Near-infrared optical imaging of the breast with model-based reconstruction, *Acad Radiol* 9:186-98, 2002.

Johnson NW, Warnakulsuriya KAAS, Langdon JD, Oral Cancer: a serious and growing problem, *Ann R Cell Surg Eng* 77:321-322, 1995.

Katzir A, Application of lasers in therapy and diagnosis, In: *Lasers and Optical Fibers in Medicine*, pp. 83-87, Academic Press, London,UK, 1993.

Kennedy JC, Marcus SL, Pottier RH, Photodynamic therapy (PDT) and photodiagnosis (PD) using endogenous photosensitisation induced by 5-aminolevulinic acid (ALA): mechanisms and clinical results, *J Clin Laser Med Surg* 14(5):289-304, 1996.

Kennedy JC, Pottier RH, Endogenous protoporphyrin IX, a clinically useful photosensitizer for photodynamic therapy, *J. Photochem Photobiol B* 14:275-292, 1992.

Koenig F, Larne R, Enquist H, McGovern FJ, Schomacker KT, Kollias N, Deutsh TF, Spectroscopic measurement of diffuse reflectance for enhanced detection of bladder carcinoma, *Urol* 51:342-345, 1998.

Kollias N and Stamatas GN, Optical non-invasive approaches to diagnosis of skin diseases, *J Investigat Dermatol* 7:64-75, 2002a.

Kollias N, Zonios G, Stamatas G, Fluorescence spectroscopy of skin, *Vib Spectrosc* 28:17-23, 2002b.

Kollias N, Gillies R, Moran M, Kochevar I, Anderson R, Endogenous skin fluorescence includes bands that may serve as quantitative markers of aging and photoaging, *J Investigat Dermatol* 111:776-780, 1998.

Kondo M, Hirota N, Takaoka T, Kajiwara M, Heme-biosynthetic enzyme activities and porphyrin accumulation in normal liver and hepatoma cell lines of rat, *Cell Biol Toxicol* 9:95-105, 1993.

Kortum G, Reflectance Spectroscopy, Springer, New York, 1969.

Kozikowski S, Wolfram L, Alfano R, Fluorescence spectroscopy of eumelanins, *IEEE J Quantum Electron* 20:1379-1382, 1984.

Kriegmair M, Baumgartner R, Knuchel R, Stepp H, Hofsadter F, Hofstetter A, Detection of early bladder cancer by 5-aminolevulinic acid induced porphyrin fluorescence, *J Urol* 155:105-110, 1996.

Kubler A, Haase T, Rheinwald M, Barth T, Muhling J, Treatment of oral leukoplakia by topical application of 5-aminolevulinic acid, *Int J Oral Maxillofac Surg* 27:466-469, 1998.

Lam S, MacAulay C, Palcic B, Detection and localization of early lung cancer by imaging techniques, *Chest(S)* 103:12-14, 1993.

Lane PM, Gilhuly T, Whitehead P, Zeng H, Simple device for the direct visualization of oral-cavity tissue fluorescence. *J Biomed Opt* 11(2):024006(1-7), 2006.

Landmann L, The epidermal permeability barrier, *Anat Embryol* 178:1-13, 1988.

Leibovici L, Schoenfeld NILI,. Yehoshua HA, Mamet R, Rakowski R, Shindel A, Atsmon A, Activity of porphobilinogen deaminase in peripheral blood mononuclear cells of patients with metastatic cancer, *Cancer* 62:2297-2300, 1988.

Leunig A, Rick K, Stepp H, Gutmann RT, Alwin G, Baumgartner R et al. Fluorescence imaging and spectroscopy of 5-aminolevulinic acid induced protoporphrin IX for the detection of neoplastic lesions in the oral cavity. *Am J Surg* 172:674–677, 1996.

Li A, Miller EL, Kilmer ME, Brukilacchio TJ,Chaves T, Stott J, ZhangQ, Wu T,Chorlton MA, Moore RH, Kopans DB, Boas DA, Tomographic optical breast imaging guided by three-dimensional mammography, *Appl Opt* 42(25):5181-90, 2003.

Li B and Xie S, Autofluorescence excitation-emission matrices for diagnosis of colonic cancer, *Word J Gastroenterol* 11(25):3931-3934, 2005.

Lin WC, Toms SA, Johnson M, Jansen ED, Mahadevan JA, *Photochem Phtotobiol* 73(4):396-402, 2001.

Lipson RL, Baldes EJ, Olsen AM, Hematoporphyrin derivative: A new aid for endoscopic detection of malignant disease, *J Thorac Cardiovasc Surg* 42:623-629, 1961.

Lovat LB, Johnson K, Mackenzie GD, Clark BR, Novelli MR, Davies S, O'Donovan M, Selvasekar C, Thorpe SM, Pickard D, Fitzgerald R, Fearn T, Bigio IJ, Bown SG, Elastic scattering spectroscopy accurately detects high grade dysplasia and cancer in Barrett's Oesophagus, *Gut* 55:1078-1083, 2006.

Mahadevan-Jansen A, Mitchell MF, Silva S, Thomsen S, Richards-Kortum R, Study of the fluorescence properties of normal and neoplastic human cervical tissue, *Lasers Surg Med* 13:647-655, 1993.

Mahadevan-Jansen A and Richards-Kortum R, Raman spectroscopy for detection of cancers and precancers, *J Biomed Opt* 1:31-70, 1996.

Mahadevan A, Mitchell MF, Thomsen S, Silva E, Richards-Kortum R, Study of the fluorescence properties of normal and neoplastic human cervical tissue, *Lasers Surg Med* 13:647-655, 1993.

Majumder SK, Ghosh N, Kataria S, Gupta PK, Nonlinear pattern recognition for laser-induced fluorescence diagnosis of cancer, *Lasers Surg Med*, 33(1):48-56, 2003.

Majumder SK, Gupta PK, Uppal A, Autofluorescence spectroscopy of tissues from human oral cavity for discriminating malignant from normal, *Lasers in Life Sci* 8:211-227, 1999.

Majumder SK, Uppal A, Gupta PK, Autofluorescence spectroscopy of oral mucosa, Porc. of SPIE Conf on Ooptical Diagnostics of Biological Fluids III, San Jose, CA, USA, pp. 158-168, 1998.

Majumder SK, Ghosh N, Kataria S, Gupta PK, Nonlinear pattern recognition for laser-induced fluorescence diagnosis of cancer, *Lasers Sur Med* 33:48-56, 2003.

Mayinger B, Jordan M, Horner P, Gerlach C, Muehldorfer S, Bittorf BR, Matzel KE, Hohenberger W, Hahn EG, Guenther K, Endoscopic light induced autofluorescence spectroscopy for the diagnosis of colorectal cancer and adenoma, *J Photochem Photobiol B* 70(1):13-20, 2003.

McKechnie T, Jahan A, Cuschieri A, Sibbett W, Padgett M J, Optical system for the early detection of cancer, IEEE CLEO-Europe, pp. 118, 1998a.

McKechnie T, Jahan A, Tait I, Cuschieri A, Sibbett W, Padgett M J, An optical system for the early detection of cancers of the GI tract, *Rev Sci Instr* 69:2521-2523, 1998b.

Messmann H, 5-ALA induced PpIX for the detection of gastrointestinal dysplasia, *Gastrointest Endosc Clin N Am* 10:497-512, 2000.

Messmann H, Endlicher E, Freunek G, Rummele P, Scholmerich J, Kruchel R, Fluorescence endoscopy for the detection of low and high grade dysplasia in ulcerative colitis using systemic or local 5-ALA sensitization, *Gut* 52:1003-1007, 2003.

Metz CE, Basic principles of ROC curve analysis, *Semin Nucl Med* 8(4):283-298, 1978.

Mirabal YN, Chang SK, Atkinson EN, Malpica A, Follen M, Richards-Kortum R, Reflectance spectroscopy for *in vivo* detection of cervical pre-cancer, *J Biomed Opt* 7(4):587-594, 2002.

Moesta KT, Bernd E, Tim H, Dirk N, Christian N, Wolfgang EH, Ravindra KP, Thomas JD, Herbert R, Peter MS, Protoporphyrin IX occurs naturally in Colorectal cancers and their metastases, *Cancer Research* 61:991-999, 2001.

Mohanty SK, Gosh N, Majumdar SK, Gupta PK, Depolarisation of autofluorescence from malignant and normal human breast tissue, *Appl Opt* 40:1-8, 2001.

Menton DN, Eisen AZ, Structure and organisation of mammalian stratum corneum, *J Ultrastruct Res* 35:247-264, 1971.

Mourant JR, Gibson RR, Johnson TM, carpenter S, Short KW, Yamada YR, Freyer JP, Methods for measuring the infrared spectra of biological cells, *Phys Med Biol* 48:243-257, 2003.

Mourant JR, Canpolat M, Brocker C, Esponda-Ramos, Johnson TM, Matanock A, Stetter K, Freyer JP, Light scattering from cell: the contribution of the nucleous and effect of proliferative status, *J Biomed Opt* 5(2):131-137, 2000.

Mourant JR, Bigio IJ, Boyer J, Johnson TM, Lacey J, Bohorfoush AG, Mellow M, Elastic scattering spectroscopy as a diagnostic tool for differentiating pathologies in the gastrointestinal tract: Preliminary testing, *J Biomed Opt* 1(2):192-199, 1996.

Mourant JR, Bigio IJ, Boyer J, Conn RL, Johnson T, Shimada T, Spectroscopic diagnosis of bladder cancer with elastic light scattering, *Lasers Surg Med* 17: 350-357, 1995

Mueller GJ and Sliney DH(eds.), Dosimetry of laser radiation in medicine and biology, SPIE, Bellingham, WA, 1989.

Muller MG, Georgakoudi I, Zhang Q, Wu J,Feld MS, Intrinsic fluorescence spectroscopy in turbid media: disentangling effects of scattering and absorption, *Appl Opt-OT* 40(25):4633-4646, 2001.

Muller MG, Valdez TA, Georgakoudi I, Backman V, Kabani C, Laver N, Wang Z, Boone CW, Dasari RR, Shapshay SM, Feld MS, Spectroscopic detection and evaluation of morphologic and biochemical changes in early human oral carcinoma, *Cancer* 97(7):1681-1692, 2003.

Ng SH, Yen TC, Liao CT, Chang JTC, Chan SC, Ko SF, Wang HM, Wong HF, 18F-FDG PET and CT/MRI in oral cavity squamous cell carcinoma: a prospective study of 124 patients with histologic correlation, *J Nucl Med* 46(7):1136-1143, 2005.

Nicholas MG, Hall EL, Foster TH, Design and testing of white-light, steady state diffuse reflectance spectrometer for determination of optical properties of highly scattering systems, *Appl Opt* 36:93-104, 1997.

Niedorf F, Jungmann H, Kietzmann M, Non-invasive reflection spectra provide quantitative information about the spatial distribution of skin chromophores, *Med Phys* 32:1297-1307, 2005.

Nieman LT, Kan C-W, Gillenwater A, Markey MK, Sokolov K, Probing local tissue changes in the oral cavity for early detection of cancer using oblique polarized reflectance spectroscopy: a pilot clinical trial, *J Biomed Opt* 13(2):024011, 2008.

Nordstorm RJ, Burke L, Niloff JM, Myrtle JF, Identification of cervical intraepithelial neoplasia (CIN) using UV-excited fluorescence and diffuse reflectance tissue spectroscopy, *Lasers Surg Med* 29(2):118-127, 2001.

Novo M, Hüttmann G, Diddens H, Chemical instability of 5-aminolevulinic acid used in the fluorescence diagnosis of bladder tumors, *J Photochem Photobiol B* 34:143-148, 1996.

Onofre MA, Sposto MR, Navarro CM, Reliability of toluidine blue application in the detection of oral epithelial dysplasia and in situ and invasive squamous cell carcinomas. *Oral Surg Oral Med Oral PatholOral Radiol Endod* 91(5):535-540, 2001.

Palmer GM, Marshek CL, Vrotsos KM, Ramanujam N, Optimal methods for fluorescence and diffuse reflectance of tissue biopsy samples, *Lasers Surg Med* 30:191-200, 2002.

Park SY, Follen M, Milbourne A, Rhodes H, Malpica A, MacKinnon N, MacAulay C, Markey MK, Richards-Kortum R, Automated image analysis of digital colposcopy for the detection of cervical neoplasia, *J Biomed Opt* 13(1):014029(1-10), 2008.

Parking DM, Whelan SL, Ferlay J, Raymond L, Young J, Cancer incidence in five continents, Lyon IARC Sci. publication, Lyon, France, 1997.

Patton LL, The effectiveness of community-based visual screening and utility of adjunctive diagnostic aids in the early detection of oral cancer, *Oral Oncology* 37:708-723, 2003.

Peng Q, Warloe T, Moan J, Heyerdahk H, Steen HB, Nesland JM, Giereksky K E, Distribution of 5-ALA induced porphyrins in nodulo-ulcerative basal cell carcinoma, *Photochem Photobiol* 62:906-913, 1995.

Perelmann LT, Backman V, Wallace M, Zonious G, Manoharan R, Nusrat A, Sheilds S, Seiler M, Lima C, Hamano T, Itzkan I, Dam JV, Crawford JM, Feld MS, Observation of periodic fine structure in reflectance from biological tissue: a new techniquefor measuring nuclear size distribution, *Phys Rev Lett* 80:627-630, 1998.

Pifferi A, Taroni P, Torricelli A, Messina F, Cubeddu R, Danesini G, Four-wavelength time-resolved optical mammography in the 680–980-nm range, *Opt Lett* 28:1138-1140, 2003.

Pogue BW, Poplack SP, McBride TO, Wells WA, Osterman KS, Osterberg UL, Paulsen KD, Quantitative hemoglobin tomography with diffuse near-infrared spectroscopy: pilot results in the breast, *Radiology* 218**:**261-266, 2001.

Pretty IA and Gerando M, A closer look at diagnosis in clinical dental practice: Part1. Reliability, validity, specififcity and sensitivity of diagnostic procedures, *J Canadian Dental Assoc* 70(4):251-255, 2004a.

Pretty IA and Gerando M, A closer look at diagnosis in clinical dental practice: Part 2. Using predictive values and receiver operating characteristics in assessing diagnostic accuaracy, *J Canadian Dental Assoc* 70(4):313-316, 2004b.

Profio AE, Balchum OJ, Fluorescence diagnosis of cancer, *Adv Exp Med Biol* 193:43-50, 1985.

Prosst RL, Gahlen J, Fluorescence diagnosis of colorectal neoplasms: a review of clinical applications, *Int J Colorectal Dis* 17:1-10, 2002.

Qu JY, Wing P, Huang Z, Kwong D, Sham J, Lung LS, Kuen HW, Wei WI, Preliminary study of *in vivo* autofluorescence of nasopharyngeal carcinoma and normal tissue, *Lasers Surg Med* 26:432-440, 2000.

Ramanujam N, Fluorescence spectroscopy *in vivo*, In: Encyclopaedia of analytical chemistry Biomedical Spectroscopy Section I, ed., Meyers R, pp. 20-56, John Wiley & Sons Ltd, Chichester, UK, 2000.

Ramanujan N, Mitchell MF, Mahadeven A, Thomsen S, Malpica A, Wright T, Atkinson N, Richard-Kortum R, Spectroscopic diagnosis of cervical intraepithelial neoplasia (CIN) in vivo using laser induced fluorescence spectra at multiple excitation wavelength, *Lasers Surg Med* 19:63-74, 1996.

Ramanujam N, Mitchell MF, Mahadevan A, Warren S, Thomsen S, Silva E, Richards-Kortum R, *In vivo* diagnosis of cervical intraepithelial neoplasia using 337-nm-excited laser induced fluorescence, *Proc Nat Acas Sci USA* 91(21):10193-10197, 1994.

Rava RP, Richards-Kortum R, Fitzmaurice M, Cothren RM, Petras RE, Sivak MV, Levin H, Feld MS, Early detection of dysplasia in colon and bladder tissue using laser induced fluorescence, In:

Dougherty TJ, ed., Optical methods for tumor treatment and early diagnosis : Mechanism and techniques, Proc. SPIE vol. 1426, 68-78, 1991.

Regula J, MacRobert AJ, Gorchein A, Buonaccorsi GA, Thorpe SM, Spencer GM, Hatfield AR, Bown SG, Photosensitisation and photodynamic therapy of oesophageal, duodenal and colorectal tumours using 5-aminolaevulinic acid induced protoporphyrin IX - a pilot study, *Gut* 36:67-75, 1995.

Richards-Kortum R, Sevick-Muraca E, Quantitative optical spectroscopy for tissue diagnosis, *Ann Rev Phys Chem* 7: 555-606, 1996.

Richards-Kortum R, Rava RP, Petras RE, Fitzmaurice M, Sivak MV, Levin H, Feld MS, Spectroscopic diagnosis of colonic dysplasia, *Photochem Photobiol* 53:777-786, 1991.

Richards-Kortum R, Mehta A, Kolubayev T, Hoyt C, Cothren R, Sacks B, Kittrell C,. Feld MS, Ratliff NB, Kjellstrom T, Bord-agaray G, Fitzmaurice M, Kramer J, Spectroscopic diagnosis for control of laser treatment of atherosclerosis, In: *Laser Spectroscopy VIII,* eds., Persson W and Svanberg S, pp. 366-369, Springer Ver-lag, Berlin, Heidelberg, Germany, 1987.

Riedl CR, Daniltchenko D, Koenig F, Simak R, Koening SA, Pflueger H, Flurescence endoscopy with 5-ALA reduced early recurrence rate in superficial bladder cancer, *J Urol* 165:1121-1123, 2001.

Ries LAG, Kosary CL, Hankey BF, Miller BA, Harras A, Edwards BK (eds.), *SEER cancer statistics review, 1973-1994*, National Cancer Institute, NIH pub. No.97-2789, Bethesda, MD, 1997.

Rokahr I, Andersson-Engels S, Svanberg S, D'Hallewin MA, Baert L, Wang I and Svanberg K, Optical detection of human urinary bladder carcinoma utilising tissue autofluorescence and protoporphyrin IX-induced fluorescence following low-dose ALA instillation, In: Cubeddu R,. Mordon SR and Svanberg K, eds., Optical Biopsies, Proc. SPIE vol. 2627, 2-12, 1995.

Roy K, Ingrams D, Pankratov M, Rebeiz E, Woo P, Kabani S, Shapshay SM, Manoharan R, Itzkan I, Feld MS, Diagnostic fluorescence spectroscopy of oral mucosa. In: Anderson R, ed., Lasers in surgery: Advance characterization, therapeutics and systems V, Proc. SPIE vol. 2395:135-142, 1995.

Rupananda JM, Subhash N, Thomas S, Kumar R, Mathews A, Madhavan J, Sebastian P, Oral pre-malignancy detection using autofluorescence spectral ratios, *Oral Oncol(S)* 2(1):209-210, 2007.

Rupananda JM, Subhash N, Shiny ST, Rejnish Kumar R, Anitha M, Jaipraksh M, Paul S, Laser induced autofluorescence spectral ratio standard for early detection of oral cancer, *Cancer 112(7):1503-12,* 2008.

Rupananda JM, Shiny ST, Anitha M, Paul S, Jayaprakash M, Subhash N, Oxygented hemoglobin diffuse reflectance ratio for in vivo detection of oral pre-cancer, *J Biomed Opt* 13(4):041306, 2008.

Savage H, Kolli V, Ansley J, Chandawarkar R, Alfano R, and Schantz S, Innate tissue fluorescence of the oral mucosa of controls and head and neck cancer patients. In: Alfano RR, ed., Advances in lasers and light spectroscopy to diagnose cancer and other diseases II, Proc. SPIE vol. 2387:2-14, 1995.

Schantz SP, Kolli V, Savage HE,Yu G, Shah JP, Harris DE, Katz A, Alfano RR, Huvos AG , *In vivo* native cellular fluorescence and histological characteristics of head and neck cancer, *Clin Cancer Res* 4(5):1177-1182, 1998.

Schomacker KT, Fusoli JK, Compton CC, Flotte TJ, Richter JM, Nishioka NS, Deutsch TF, Ultraviolet laser induced fluorescence of colonic tissue: basic biology and diagnosis potential, *Lasers Surg Med* 12(1):63-78, 1992.

Scott MA, Hopper C, Sahota A, Springett R, Mcllroy BW, Bown SG, Mac Robert AJ, Fluorescence photodiagnostics and photobleaching studies of cancerous lesions using ratio imaging and spectroscopic techniques, *Lasers Med Sci* 15:63-72, 2000.

Setlow RB, Grist E, Thompson K, Woodhead AD, Wavelengths effective in induction of malignant melanoma, *Proc Natl Acad Sci USA* 90:6666-6670, 1993.

Shafer WG and Waldron CA, Erythroplakia of the oral cavity, *Cancer* 36:1021-1028, 1975.

Shah N, Cerussi A, Eker C, Espinoza J, Butler J, Fishkin J, Hornung R, Tromberg B, Noninvasive functional optical spectroscopy of human breast tissue, *Proc Natl Acad Sci* 98:4420-4425, 2001.

Shetty KV, Johnson NW, Attitude and beliefs of adult south asians living in London regarding risk factors and signs for oral cancer, *Community Dental Health* 16:227-231, 1999.

Silverman S, Early diagnosis of oral cancer, *Cancer*, 62(8)(S): 796-1799, 1988.

Skala MC, Palmer GM., Vrotsos KM, Fitzpatrick AG, Ramanujam N, Comparison of a physical model and principal component analysis for the diagnosis of epithelial neoplasia *in vivo* using diffuse reflectance spectroscopy, *Optics Express* 15(12):7863-7875, 2007.

Slaughter D, Southwick H, Smejkal W, Field cancerization in oral stratified squamous epithelium, *Cancer* 6:963-968, 1953.

Soklov K, Drezek R, Gossage K, Richards-Kortum R, Reflectance spectroscopy with polarized light: is it sensitive to cellular and nuclear morphology, *Opt Express* 5:302-317, 1999.

Sorensen R, Juzenas P, Iani V, Moan J, Formation of PpIX in mouse skin after topical application of 5-ALA and its methyl ester, In: Photochemotherapy of cancer and other diseases, Proc. SPIE vol. 3563, 77-81, 1999.

Spikes JD, The historical development of ideas on applications of photosensitized reactions in health sciences,In: Primary photoprocess in Biology and Medicine, eds., Bergasson RV, Jori G, Land EJ, Truscott TG, pp. 209-227,Plennum Press, New York, 1985.

Stamatas GN, Estanislao RB, Suero M, Rivera ZS, Li J, Khaiat A, Kollias N, Facial skin fluorescence as a marker of the skin's response to chronic environmental insults and its dependence on age, *Br J Dermatol* 154:125-132, 2006.

Sterenborg HJCM, Motamedi M, Wagner JRF, Duvic M,Thomsen S, Jacques SL, *In vivo* fluorescence spectroscopy and imaging of human skin tumours, *Lasers Med Sci* 9:191-201, 1994.

Stokes GG, Uber die Anderung der Brechbarkeit des litche, *Phil Tranact* 107:11-11, 1852.

Stubel H, Die Fluoreszenz tierischer Gewebe in ultravioletten Light, *Pflugers Arch* 142: 1-1, 1911.

Suarez P, Batsakis JG, el-Naggar AK, Leukoplakia: still a gallimaufry or is progress being made?- A review, *Adv Anat Pathol* 5:137-155, 1998.

Subhash N, Mohanan CN, Curve-fit analysis of chlorophyll fluorescence spectra: Application to nutrient stress detection in sunflower, *Remote Sens Environ* 60:347-356, 1997.

Subhash N, Rupananda MJ, Shiny ST, Anitha M, Paul S, Madhavan J, Oral cancer detection using diffuse reflectance spectral ratio R540/R575 of oxygenated hemoglobin bands, *J Biomed Opt* 11(1): 014018(1-6), 2006.

Subhash N, Shiny ST, Rupananda JM, Mini J, Tooth caries detection by curvefitting of laser-induced fluorescence emissiom: A comparative evaluation with reflectance spectroscopy, *Lasers Surg Med* 37:320-328, 2005.

Suhonen ATM, Bouwstra JA, Urtti A, Chemical enhancement of precutaneous absorption in reation to stratum corneum structural alterations, *J Controlled Release* 59:149-161, 1999.

Svanberg S, Svanberg K, Fluorescence diagnostics and kinetic studies in the head and neck region utilising low-dose d-aminolevulinic acid sensitisation, Cancer Lett 135:11-19, 1999.

Svanberg K, Wang I, Colleen S, Idvall I, Ingvar C, Rydell R, Jocham D, Diddens H, Brown S, Gregory G, Montan S, Andersson-Engels S, Svanberg S, Clinical multicolour fluorescence imaging of malignant tumours-initial experience, *Acta Radiol* 39:2-9, 1998.

Svanberg K, Andersson T, Killander D, Wang I, Stenram U, Andersson-Engels S, Johansson J, Svanberg S, Photodynamic therapy of non-melanoma malignant tumours of the skin using topical-amino levulinic acid sensitisation and laser irradiation, *Br J Dermatol* 130:743-751, 1994.

Svirsky JA, Burns JC, Carpenter WM, Comparison of computer-assisted brush biopsy results with follow up scapel biopsy and histology, Gen Dent 50(6):500-503, 2002.

Svistum E, Alizedeh-Naderi R, El-Naggar A, Jacob R, Gillenwater A, Richards-Kortum R, Vision enhancement system for detection of oral cavity neoplasia based on autofluorescence, *Head Neck* 26(3):205-215, 2004.

Tearney GJ, Brezinski ME, Southern JF, Bouma BE, Hee MR, Fujimoto JG, Detrmination of the refractive index of highly scattering human tissue by optical coherence tomography, *Opt Lett* 20:2258-2260, 1995.

Teuchner K, Mueller S, Freyer W, Leupold D, Altmeyer P, Stucker M, Hoffmann K, Femto second two-photon excited fluorescence of melanin, In: Belfield KD, Caracci SJ, Kajzar F, Lawson CM, Yeates AT, eds., Multi photon absorption and nonlinear transmission processes: materials, theory, and applications, SPIE vol. 4797:211-219, 2003.

Thomsen S and Tatman D, Physiological and pathological factors of human breast disease that can influence optical diagnosis, *Ann New York Acad Sci* 838**:**171-193, 1998.

Tromberg BJ, Coquoz O, Fishkin JB, Pham T, Anderson ER, Butler J, Cahn M, Gross JD, Venugopalan V, Pham D, Non-invasive measurements of breast tissue optical properties using frequency-domain photon migration, *Phil Trans R Soc Lond B* 352:661-668, 1997.

Tsai T, Chen H, Wnag C, Tsai J, Chen C and Chiang C, *In vivo* autofluorescence spectroscopy of oral

premalignant and lesions: Distortion of fluorescence intensity by submucous fibrosis, *Lasers Surg Med* 33:40-47, 2003.

Tsuchida M, Miura T, Aibara K, Lipofuscin and lipofuscin-like substances, *Chemistry and Physics of Lipids* 44:297-325, 1987.

Tuchin VV, Light scattering methods and instruments for medical diagnostic, In: Tissue optics, SPIE, Bellingham, 2007.

Tuchin VV, Selected papers on tissue optics: Applications in medical diagnostic and therapy, SPIE, Bellingham, WA, 1994.

Tuchin VV, Laser and fiber optics in biomedicine, *Laser Phy* 3:767-820; 925-950, 1993.

Utzinger U, Brewer M, Silva E, Gershenson D, Blast Jr RC, Follen M, Richards-Kortum R, Reflectance spectroscopy for *in vivo* characterization of ovarian tissue, *Lasers Surg Med* 28:56-66, 2001.

van den Akker JTHM, Iani V, Star WM, Sterenborg HJCM, Moan J, Topical application of 5-aminolevulinic acid hexyl ester and 5-aminolevulinic acid to normal nude mouse skin: differences in PpIX fluorescence kinetics and the role of the stratum corneum, *Photochem Photbiol* 72:681-689, 2000.

van der Breggen, EWJ, Rem AI, Christian MM, Yang CJ, Calhoun KH, Sterenborg, HJCM, Motamedi M, Spectroscopic detection of oral and skin tissue transformation in a model for squamous cell carcinoma: autofluorescence versus systemic aminolevulinic acid-induced fluorescence, In: Selected Topics in Quantum Electronics, IEEE vol. 2(4), 997-1007, 1996.

van der Veen N, de Bruijn HS, Berg RJW, Star WM, Kinetics and localization of PpIX fluorescence after topical and systemic ALA application, observed in skin and skin tumors of UVB-treated mice, *Br J Cancer* 73:925-930, 1996.

van Staveren HJ, Van Veen RL, Speelman OC, Witjes MJH, Star WM, Roodenburg JLN, Classification of clinical autofluorescence spectra of oral leukoplakia using an artificial neural network: A pilot study, *Oral Oncol* 3:286-293, 2000.

van Veen RLP, Amelink A, Menke-Pluymers M, van der Pol C, Sterenborg HJCM, Optical biopsy of breast tissue using differential path-length spectroscopy, Phy Med Biol 50:2573-2581, 2005.

van Zijlstra WG, Buursma A, Meeuwsen-van der Roest P, Absorption spectra of human fetal and adult oxyhemoglobin, deoxyhemoglobin, carboxy hemoglobin and methemoglobin, *Clin Chem* 37:1633-1638, 1991.

Vaupel P, Oxygen transport in tumours: characteristics and clinical implications, *Adv Exp Med Biol* 388:341-351, 1996.

Volynskaya Z, Haka AS, Bechtel KL, Fitzmaurice M, Shenk R, Wang N, Nazemi J, Dasari RR, Feld MS, Diagnosing breast cancer using diffuse reflectance spectroscopy and intrinsic fluorescence spectroscopy, *J Biomed optics* 13(2):024012, 2008.

Wagnieres GA, Star W, Wilson BC. *In vivo* fluorescence spectroscopy and imaging for oncological applications, *Photochem Photobiol* 68:603-32, 1998.

Wang CY, Tsai T, Chen HM, Chen CT, Chiang CP, PLS-ANN based classification model for oral

submucous fibrosis and oral carcinogenesis, *Lasers Surg Med* 32(4):318-326, 2003.

Wang CY, Chiang HK, Chen CT, Chiang CP, Kuo YS, Chow SN, Diagnosis of oral cancer by light induced autofluorescence spectroscopy using double excitation wavelength, *Oral Oncol* 35:144-150, 1999.

Wang I, Photodynamic therapy and laser-based diagnostic studies of malignant tumors, Ph. D Thesis, Department of Oncology, The Jubileum Institute, Lund University Hospital, Lund, Sweeden, 1999.

Wang TD, Crawford JM, Feld MS, Wang Y, Itzkan I, Van Dam J, *In vivo* identification of colonic dysplasia using fluorescence endoscopic imaging, *Gastro Endoscopy* 49:447-455, 1999.

Weersink RA, Hayward JE, Diamond KR, Paterson MD, Accuracy of non-invasive *in vivo* measurements of photosensitizer uptake based on a diffusion model of reflectance spectroscopy, *Photochem Photobiol* 66:326-335, 1997.

Wendlandt WW and Hencht HG, Reflectance Spectroscopy, John Wiley and Sons, New York, 1966.

Wiener E, Pautke C, Link TM, Neff A, Kolk Andreas, Comparison of 16-slice MSCT and MRI in the assessment of squamous cell carcinoma of the oral cavity, *Eur J Radiol* 58(1):113-8, 2005.

William AC and Barry BW, Skin absorption enhancers, *Crit Rev Ther Drug carrier Syst* 9(3,4):305-353, 1992.

Wingo PA, Tong T, Bolden S, Cancer statistics, *CA Cancer J Clin* 45:8-30, 1995.

Wu T, Qu JY, Cheung TH, Lo W-KK, Yu M-Y, Preliminary study of detecting neoplastic growths in vivo with real-time calibrated autofluorescence imaging, *Optic Exp* 11(4):291-298, 2003.

Yen TC, Chang JTC, Ng SH, Chang YC, Chan SC, Wang HM, See LC, Chen TM, Kang CJ, Wu YF, Lin KJ, Liao CT, Staging of untreated squamous cell carcinoma of buccal mucosa with 18F-FDG PET: comparison with head and neck CT/MRI and histopathology, *J Nucl Med* 46(5):775-781,2005.

Young AR, Chromophores in human skin, *Phys Med Biol* 42:789-802, 1997.

Zaak D, Frimberger D, Steep H, Wagner S, Baumgartner R, Schneede P, Siebels M, Knuchel R, Kriegmair M, Hofstetter A, Quantification of 5-ALA induced fluorescence improves the specificity of bladder cancer detection, *J Urol* 166:1665-1669, 2001.

Zang Q, Muller MG, Wu J Feld MS, Turbidity -free fluorescence spectroscopy of biological tissues, *Opt Lett* 25:1451-1453, 2000.

Zheng W, Khee CS, Ranjiv S, Malini O, Detection of neoplasms in the oral cavity by digitized endoscopic imaging of 5-aminolevulinic acid-induced protoporphyrin IX fluorescence, *Int J Oral Onc* 21:763-768, 2002.

Zhu C, Palmer GM, Breslin TM, Harter J, Ramanujam N, Diagnosis of breast cancer using diffuse reflectance spectroscopy: Comparison of a Monte Carlo versus partial least squares analysis based feature extraction technique, *Lasers Surg Med* 38:714-724, 2006.

Zonios G, Perelmann LT, Bacjmann V, Manoharan R, Fitzmaurice M, Dam JV, Feld MS, Diffuse reflectance spectroscopy of human adenomatous colon polyps *in vivo*, *Appl Opt* 38:6628-6637, 1999.

Zweig MH and Campbell G, Receiver-operating characteristic (ROC) plots; a fundamental evaluation tool in clinical medicine, *Clin Chem* 39:561-577, 1993.